Synthesis of Tripeptides, Pd(II) and Ni(II) Complexes and their Potential Use in Activation of Small Molecules

Lindsey Jean Monger

Faculty of Physical Sciences
University of Iceland
2021

Synthesis of Tripeptides, Pd(II) and Ni(II) Complexes and their Potential Use in Activation of Small Molecules

Lindsey Jean Monger

Dissertation submitted in partial fulfillment of a
Philosophiae Doctor degree in Chemistry

Advisor
Prof. Sigríður G. Suman

PhD Committee
Prof. Krishna K. Damodaran
Dr. Stefán Jónsson

Opponents
Prof. Elzbieta Gumienna-Kontecka
University of Wroclaw
Prof. Marc Devocelle
Royal College of Surgeons

Faculty of Physical Sciences
School of Engineering and Natural Sciences
University of Iceland
Reykjavik, May 2021

Synthesis of Tripeptides, Pd(II) and Ni(II) Complexes and their Potential Use in Activation of Small Molecules
Dissertation submitted in partial fulfillment of a *Philosophiae Doctor* degree in Chemistry

Faculty of Physical Sciences
School of Engineering and Natural Sciences
University of Iceland
Dunhagi 3
107, Reykjavik
Iceland

Telephone: 525 4000

Bibliographic information:
Lindsey Jean Monger, 2021, *Synthesis of Tripeptides, Pd(II) and Ni(II) Complexes and their Potential Use in Activation of Small Molecules*, PhD dissertation, Faculty of Chemistry, University of Iceland, 177 pp.

ISBN: 978-9935-9564-4-6

Author ORCID: 0000-0003-2269-080X
Printing: Háskólaprent
Reykjavik, Iceland, May 2021

Abstract

The use of protecting groups on amino acid and peptides affords opportunities to change preferred coordination behaviors to metal centers. Alkylating the C-terminus carboxylate allows directed tripeptide coordination, forming tetradentate $\kappa^4[NH_2,N,N,=O]$ complexes. Changing tripeptide composition enables the formation of chelates of various ring sizes, and depending on the N-terminus side chains, tetradentate $\kappa^4[n,5,5]$ (where n = 5, 6, 7, or 8 membered rings) coordination geometries can be achieved.

The alkylated tripeptide compounds α-Asp(O^{t}Bu)AlaGly(OMe), β-Asp(O^{t}Bu)AlaGly(OMe), TrpAlaGly(OMe), HisAlaGly(OMe), and γ-Glu(OMe)Cys(SMe)Gly(OMe) were synthesized as ligands to coordinate to palladium and nickel to form neutral tetradentate complexes. The coordination of select alkylated tripeptides to palladium was first established by potentiometric and NMR spectroscopic data. pH-dependent complexation was analyzed and coordination properties to $[Pd(en)(H_2O)_2]^{2+}$ were inferred from their NMR spectra. Building on aqueous NMR studies, Pd(II) complexes with the tripeptides α-Asp(O^{t}Bu)AlaGly(OMe), β-Asp(O^{t}Bu)AlaGly(OMe), and TrpAlaGly(OMe) were synthesized and characterized. The ligands form tri- and tetradentate complexes with Pd(II). For tridentate coordination complexes, ligand exchange reactions, occupying the fourth coordination sphere, showed that sufficiently labile ligands may be removed to form the tetradentate coordination mode, which adopt a square planar geometry with tetradentated ligands. The complex coordination geometry was established using ^{1}H and ^{13}C NMR, and infrared spectroscopy, and supported using DFT calculations. Reactivity of palladium tripeptide complexes with small molecules such as ethylene, acids, CO and formates, and episulfides were investigated. Complexes were found to be rather inert towards ethylene coordination and decompose in acid and under acidic conditions; in the presence of ethylene, acetaldehyde was formed only after complex decomposition. Reactivity with CO and CO surrogates such as formates results in the dissociation of the ligand and reduces the metal to Pd(0). Pd(II) is a soft Lewis acid and thiophilic; when reacted with thiirenes, Pd-tripeptide complexes abstracted sulfur from the episulfide at modest catalytic rates.

Ni(II) complexes with the ligands, α-Asp(O^{t}Bu)AlaGly, β-Asp(O^{t}Bu)AlaGly, and TrpAlaGly were synthesized and characterized using infrared and ^{1}H, ^{13}C NMR spectroscopy, mass spectrometry and elemental analysis. The complexes were predicted using DFT calculations to have square planar geometries. The esters of these ligands proved highly pH sensitive and hydrolyze fully at moderately basic conditions. The electrochemistry of the complexes was investigated in water to reveal irreversible redox behavior of all three complexes.

Útdráttur

Notkun verndarhópa á virka hópa aminosýra í litlum peptíðum gefur tækifæri til að breyta girðieiginleikum viðkomandi peptíðs við málmjónir. Alkýlun á karboxýlhóp C-enda peptíðsins beinir girðingu málmjónarinnar í fjórgirta $\kappa^4[NH_2,N,N,=O]$ komplexa. Með stýringu á samsetningu peptíðsins er hægt að mynda kelaða hringi umhverfis málmjónina í misstórum hringjastærðum; Hægt er að mynda fjórgirðandi peptíð, $\kappa^4[n,5,5]$ (þar sem n = 5, 6, 7, eða 8 atóm) með misstórum hringjum á hliðarkeðju N-endans sem leiðir til mismunandi rúmfræðilegrar girðingar málmsins og væntanlega breytilegra efnaeiginleika. Fjögur trípeptíð með alkýlaða karboxylhópa voru smíðuð, α-Asp(O^{t}Bu)AlaGly(OMe), β-Asp(O^{t}Bu)AlaGly(OMe), TrpAlaGly(OMe), HisAlaGly(OMe), og γ-Glu(OMe)Cys(SMe)-Gly(OMe) til þess að mynda palladium og nickel komplexa í fjórgirtu umhverfi.

Girðieiginleikar alkýleraðra trípeptíða voru rannsakaðir með spennutítrunum og NMR mælingum í vatni. Sýrustigsháð girðing tenglanna við $[Pd(en)(H_2O)_2]^{2+}$ var greind og myndaðir komplexar staðfestir með NMR greiningum. Út frá þessum niðurstöðum voru tilraunir hannaðar til að smíða Pd(II) komplexa með trípeptíðunum α-Asp(O^{t}Bu)AlaGly(OMe), β-Asp(O^{t}Bu)AlaGly(OMe), og TrpAlaGly(OMe). Þessir komplexar voru einangraðir og greindir að fullu. Tenglarnir mynda þrí- og fjórgirta komplexa með Pd(II). Þrígirtu komplexarnir höfðu fjórða tengilinn frá upphafsefninu. Skiptihvörf á þessum fjórða tengli sýndu að hægt væri að fjarlægja rétt valinn tengil og trípeptíðið myndaði þá fjórgirt lokaefni með ferningslaga byggingu. Byggingar komplexanna voru reiknaðar með DFT reikningum þar sem kristalbyggingar fengust ekki. Hvarfgirni með litlum sameindum eins og ethylen, sýrum, formati, og episúlfíði var skoðuð, en komplexarnir hvörfuðust ekki við ethylene. Þeir brotna niður í sýru og við súrar aðstæður. Asetaldehýð myndaðist í hvarfi við ethylene við súrar aðstæður. Pd(II) er mjúk Lewis sýra og myndar auðveldlega súlfíð; Pd-trípeptíð komplexarnir tóku auðveldlega brennistein frá episúlfíði og mynduðu alken við hvötunaraðstæður. Hvarf við format leiddi til rof málmsins frá tenglinum og afoxun í Pd(0).

Ni(II) komplexar með tenglunum, α-Asp(O^{t}Bu)AlaGly(OMe), β-Asp(O^{t}Bu)AlaGly(Ome), og TrpAlaGly(OMe) voru smíðaðir og greindir með litrófsgreiningum, frumefna og massagreiningum. Komplexarnir hafa bjagaða ferningslaga byggingu samkvæmt DFT reikningum. Alkýlhópar tenglanna reyndust viðkvæmari fyir sýrustigi í hvörfum með Ni(II) en með Pd(II) og C-endi trípeptíðsins gekkst undir vatnsrof við mildar aðstæður. Rafefnafræði komplexanna var mæld í vatni og sýndi óafturkræfa hegðun fyrir alla þrjá komplexa.

Thank you, Ragnar

~ I could have never done this without you.

Table of Contents

List of Figures ..... **x**

List of Schemes ..... **xi**

List of Tables ..... **xii**

List of Publications ..... **xiii**

Abbreviations ..... **xv**

Acknowledgements ..... **xvii**

1 Introduction **1**
1.1 Activation of Small Molecules with Palladium(II) and Nickel(II) Complexes 1
1.1.1 Olefin Activation, and Homo- and Copolymerization. 1
1.1.2 CO_2 Activation 2
1.2 Synthesis of Peptides 3
1.2.1 Protecting Groups 3
1.2.2 Coupling Reagents 5
1.3 Palladium(II) and Nickel(II) Peptide Complexes 6
1.4 Aim of This Work 6

2 Synthesis, Characterization & Aqueous Coordination Studies of Tripeptides: α-Asp(O^{t}Bu)AlaGly(OMe), β-Asp(O^{t}Bu)AlaGly(OMe), HisAlaGly(OMe), and TrpAlaGly(OMe) **9**
2.1 Synthetic Methodology 9
2.1.1 Coupling 9
2.1.2 Deprotection and Purification 10
2.2 Characterization 11
2.2.1 ^{1}H- And ^{13}C-NMR Spectroscopy 11
2.2.2 Infrared Spectroscopy 11
2.2.3 UV-Vis Spectroscopy 12
2.2.4 Mass Spectrometry 12
2.2.5 Optical Rotation 12
2.3 Aqueous Coordination Properties 13
2.3.1 pH-Dependent Coordination of $[Pd(en)(H_2O)_2]^{2+}$ with **1** 13
2.3.2 pH-Dependent Coordination of $[Pd(en)(H_2O)_2]^{2+}$ with **2** 14
2.3.3 pH-Dependent Coordination of $[Pd(en)(H_2O)_2]^{2+}$ with **3** 15
2.3.4 Mass Spectrometry of Pd(II) Complexes with **1**-**3** 16
2.4 Conclusions 17
2.5 Experimental 18
2.5.1 Physical Methods 18
2.5.2 Materials 19
2.5.3 Synthesis 19

3 Synthesis and Characterization of Palladium Tripeptide Complexes 27
3.1 Synthetic Methodology 27
3.1.1 Aqueous Synthesis 27
3.1.2 Non-Aqueous Synthesis 29
3.1.3 Base Effects 31
3.1.4 Metal Salt Effects 31
3.2 Calculations 31
3.3 Characterization 32
3.3.1 ^{1}H- And ^{13}C-NMR Spectroscopy 32
3.3.2 Infrared Spectroscopy 35
3.3.3 UV-Vis Spectroscopy 37
3.3.4 Mass Spectrometry 38
3.4 Conclusions 38
3.5 Experimental 39
3.5.1 Physical Methods 39
3.5.2 Materials 39
3.5.3 Synthesis 39

4 Synthesis and Characterization of Nickel Tripeptide Complexes 43
4.1 Synthetic Methodology 43
4.1.1 Aqueous Synthesis 43
4.1.2 Metal Salt Effects 43
4.1.3 Non-Aqueous Synthesis 45
4.2 Calculations 45
4.3 Characterization 46
4.3.1 ^{1}H- And ^{13}C-NMR Spectroscopy 46
4.3.2 Infrared Spectroscopy 48
4.3.3 UV-Vis Spectroscopy 49
4.3.4 Mass Spectrometry 50
4.4 Electrochemistry 50
4.5 Conclusions 51
4.6 Experimental 51
4.6.1 Physical Methods 51
4.6.2 Materials 52
4.6.3 Synthesis 52

5 Reactivity Studies of Ni(II) and Pd(II) Tripeptide Complexes with Small Molecules 55
5.1 Palladium 55
5.1.1 Olefins 55
5.1.2 Derivatives of CO_2 and CO 57
5.1.3 Sulfur Reagents 58
5.2 Nickel 59
5.2.1 CO_2 Activation 59
5.3 Conclusions 60
5.4 Experimental 60
5.4.1 Physical Methods 60
5.4.2 Materials 62

6 Conclusions 63

References **65**

Appendix **77**

Article 1 ..... **81**

Article 2 ..... **107**

Article 3 ..... **137**

List of Figures

Figure 2.1 Infrared spectra for **1**-**4** 11

Figure 2.2. UV-Vis Spectra **1**-**4** 12

Figure 2.3. Percent ester hydrolysis as a function of pH..... 17

Figure 3.1. DFT optimized structures of Pd(II) complexes **5**, **7**-**10**. 31

Figure 3.2. Progression of select ^{1}H NMR resonances of **1** to **5**, **7**, and **8** 33

Figure 3.3. IR spectra for **1**, **5**, and **7**-**8**. 36

Figure 3.4. UV-Vis spectra **8**-**10** in DMSO 38

Figure 4.1. DFT optimized structures of complexes **13**-**15**..... 46

Figure 4.2. UV-Vis spectra **13**-**15** in H_2O.. 49

Figure 4.3. Electrochemical CV traces of Ni(II) complexes and ligands in water. 50

Figure 5.1. Percent catalytic conversion of cyclohexene sulfide to cyclohexene with complexes **8** (3 mol %) and **9** (3 mol %), monitored via ^{1}H NMR. 58

Figure 5.2. DFT optimized for Ni(I)**13** and Ni(I)(cyclam) 59

Appendix Figure 1. Stacked ^{1}H NMR spectra of **8** with ethylene 79

Appendix Figure 2. Stacked ^{13}C NMR spectra of **8** with ethylene 80

List of Schemes

Scheme 1-1. Possible binding modes of CO_2 to Ni(I) 3

Scheme 1-2. Coupling reaction isomerization pathways 4

Scheme 1-3. Coupling reaction with carbodiimide and triazole (HOBt) additive. 5

Scheme 2-1. Ligand synthetic pathway 10

Scheme 2-2. Possible coordination geometries of **1** with $[Pd(en)(H_2O)_2]^{2+}$ 13

Scheme 2-3. Possible coordination geometries of **2** with $[Pd(en)(H_2O)_2]^{2+}$ 14

Scheme 2-4. Possible coordination geometries of **3** with $[Pd(en)(H_2O)_2]^{2+}$ 15

Scheme 3-1. Formation of $\kappa^3[NH_2,N,N]$ species **Pd-1A** 27

Scheme 3-2. Synthetic routes to form charged and neutral Pd(II) complexes 28

Scheme 3-3. Formation of $\kappa^2[NH_2,O]$ species **Pd-2B** 30

Scheme 3-4. Formation of $\kappa^3[NH_{indol},N,N]$ species **Pd-3B** 30

Scheme 4-1. Synthetic route to form isomers **11** and **12** 44

Scheme 4-2. Synthetic route to form mono-anionic complexes **13-15**. 45

Scheme 5-1. Oxidation of ethylene to form acetaldehyde catalyzed by Pd(II) 55

Scheme 5-2. Spontaneous reaction between trifluoromethanesulfonate and ethylene to form ethyl trifluoromethanesulfonate 56

Scheme 5-3. Catalytic homopolymerization of ethylene to polyethylene. 56

Scheme 5-4. Coordination of CO to Pd(II) to **5** and **6** complexes. 57

Scheme 5-5. Catalytic copolymerization of CO and styrene to form polyketones. 57

Scheme 5-6. Catalytic conversion of cyclohexene sulfide cyclohexene. 58

Scheme 5-7. Catalytic cycle for palladium oxidation of alkenes to aldehydes. 60

List of Tables

Table 2-1. Optical rotation for compounds **1-4** in DMSO 13

Table 2-2. Possible coordination geometries of **1** with $[Pd(en)(H_2O)_2]^{2+}$ 14

Table 2-3. Possible coordination geometries of **2** with $[Pd(en)(H_2O)_2]^{2+}$ 15

Table 2-4. Possible coordination geometries of **3** with $[Pd(en)(H_2O)_2]^{2+}$ 16

Table 2-5. Mass spectra of **1-3** with $[Pd(en)(H_2O)_2]^{2+}$ at pH of ~10.5. 16

Table 3-1. ^{1}H NMR data for Pd(II) **5-10**. 32

Table 3-2. Assigned ^{13}C NMR resonance for complexes **5**,**7-10**. 34

Table 3-3. ^{13}C NMR resonance for complexes **5**,**7-10** compared to calculated values..... 35

Table 3-4. Infrared data for Pd(II) complexes **5**, **7-10**. 36

Table 3-5. Comparative values for ν(C=O) vibrational modes observed versus DFT calculated for **5**, **7-10** 37

Table 4-1. ^{1}H NMR data in D_2O for **11a-14** in D_2O 44

Table 4-2. ^{1}H NMR data for complexes **13-15** in DMSO-d_6. 47

Table 4-3. ^{13}C NMR resonance for complexes **13-15** in DMSO-d_6..... 47

Table 4-4. Infrared vibrations for complexes **11-15** 48

Table 4-5. Comparative values for ν(C=O) vibrational modes observed vs. calculated for **11-15**. 49

Table 4-6. List of potentials and peak currents for Cyclic Voltammetry experiments in aqueous solution with 0.25 M KNO_3 vs. Ag/AgCl. 51

Appendix Table 1. ^{1}H NMR data of **1-3** in DMSO-d_6 77

Appendix Table 2. ^{1}H NMR data of **1-3** in D_2O 77

Appendix Table 3. ^{13}C NMR data of **1-3** in DMSO-d_6 78

Appendix Table 4. Summary of infrared data for **1-4** 78

Appendix Table 5 Comparative values for ν(C=O) vibrational modes observed versus DFT calculated for **1-3**. 79

List of Publications

Publications included in the thesis

- *Article 1*

  Lindsey J. Monger, Gerdur R. Runarsdottir, Sigridur G Suman

  Directed coordination study of $[Pd(en)(H_2O)_2]^{2+}$ with hetero-tripeptides containing C-terminus methyl esters employing NMR spectroscopy. JBIC Journal of Biological Inorganic Chemistry, 2020 vol. 25 (5), 8 pp. 811-825.
  https://doi.org/10.1007/s00775-020-01804-0

  Declaration of Contribution: The research presented in this paper is Lindsey's original work. Gerdur contributed the synthesis of β-Asp(O^{t}Bu)AlaGly(OMe) and γ-Glu(OMe)Cys(SMe)Gly(OMe) used in this paper and conducted preliminary NMR investigations with $[Pd(en)(H_2O)_2]^{2+}$and γ-Glu(OMe)Cys(SMe)Gly(OMe). Lindsey synthesized the other two compounds and performed the NMR and potentiometric experiments. Lindsey and Sigridur wrote the article together.

- *Article 2*

  Lindsey J. Monger, Dmitrii Razinkov, Ragnar Bjornsson, Sigridur G. Suman. Synthesis, Characterization, And Reaction Studies Of Novel Palladium Tripeptide Complexes, *Manuscript In Preparation.*

  Declaration of Contribution: The research presented in this paper is Lindsey's original work. She performed all of the synthesis and characterization and completed reaction studies for olefins. Dmitrii completed sulfur transfer NMR based experiments. Ragnar contributed DFT calculations. Lindsey and Sigridur wrote the article together.

- *Article 3*

  Lindsey J. Monger, Ragnar Bjornsson, Sigridur G. Suman. Synthesis, Characterization, and Electrochemistry of Ni(II) Tripeptide Complexes. *Manuscript In Preparation.*

  Declaration of Contribution: The research presented in this paper is Lindsey's original work. She performed all of the synthesis and characterization and completed electrochemistry. Ragnar contributed DFT calculations. Lindsey and Sigridur wrote the article together.

Publications not included in the thesis

- *Article 4*

  Benedikt O Birgisson, Lindsey J Monger, Krishna K Damodaran, and Sigridur G Suman. Synthesis and characterization of asymmetric $[Mo_2O_2(\mu\text{-}S)_2(S_2)(L)]$ complexes (L = bipy, en, dien) and their heterogeneous reaction with propylene sulfide. Inorganica Chimica Acta, 501 (2020) 119272. doi:10.1016/j.ica.2019.119272 https://doi.org/10.1016/j.ica.2019.119272

  Declaration of Contribution: Benedikt completed all the synthesis and calculations for this work and ran most of the NMR based catalytic experiments. Krishna performed crystallographic analysis. Lindsey provided additional NMR experiments. Benedikt and Sigridur wrote the article together.

Abbreviations

AA	Amino Acid
Ala (A)	Alanine
Ar	Argon gas
Asp (D)	Aspartic acid
$CDCl_3$	Deuterated
Cys (C)	Cysteine
CBZ (Z)	Benzyl carbamate
CODHs	Carbon monoxide dehydrogenases
COO^-	Carboxylate ion
COSY	Correlation spectroscopy
DCC	Dicyclohexylcarbodiimide
DFT	Density functional theory
DMF	Dimethylformamide
DMSO	Dimethyl sulfoxide
DMSO-d_6	Deuterated dimethyl sulfoxide
D_2O	Deuterium oxide
EDC	N-ethyl-N'-(3-dimethylaminopropyl)carbodiimide
en	Ethylenediamine
ESI-MS	Electrospray ionization mass spectrometry
Fmoc	Fluorenylmethoxycarbonyl
Glu (E)	Glutamic acid
Gly (G)	Glycine
GSH	Glutathione

GSMe	S-methylated glutathione
His (H)	Histidine
HOBt	Hydroxybenzyltriazole
HSQC	Heteronuclear single quantum coherence spectroscopy
IR	Infrared
K^+	Potassium ion
KBr	Potassium Bromide
Lu	2,6-Lutidine
N_2	Nitrogen gas
Na^+	Sodium ion
NaOH	Sodium hydroxide
Ni^{2+}	Nickel ion
NMR	Nuclear magnetic resonance
Pd^{2+}	Palladium ion
Py	Pyridine
SPPS	Solid phase peptide synthesis
TEA	Triethylamine
Trp (W)	Tryptophan
Trt	Triphenylmethyl
UV-Vis	Ultraviolet-Visible

Acknowledgements

I would like to begin by expressing my deepest gratitude to my advisor Prof. Sigríður G. Suman for her patient guidance and enthusiastic encouragement during my Ph.D. studies. I value the knowledge, time, and funding that she has shared with me throughout the years. I genuinely respect her extensive knowledge of chemistry and her contributions to the field, both for research and teaching. A truly great advisor, I am eternally grateful to her for this opportunity.

I wish to extend a special thanks to Prof. Barbara Milani at the University of Trieste for inviting me to participate in a scientific exchange in her group. Applying the skills and techniques acquired while in Italy has enriched my studies.

I would also like to thank my committee members, Prof. Krishna Damodaran and Dr. Stefán Jónsson for their guidance, advice and helpful discussions. Thank you for considering my work worthy of a doctoral degree.

Thank you to my opponents, Professor Elzbieta Gumienna-Kontecka at the University of Wroclaw, and Professor Marc Devocelle, at the Royal College of Surgeons for the value of their time in evaluating this work.

To all past and present members of the Suman Group, thank you for the helpful discussions and support. A special thanks is due to Dmitrii, Andres, Johanna, Linda, and Hafdís for their friendship and shenanigans, which helped make even difficult days enjoyable.

My gratitude to Dr. Ragnar Björnsson at the Max Planck Institute for Chemical Energy Conversion for the DFT calculations and for the great chemistry discussions over the years.

I wish to recognize and thank Dr. Sigríður Jónsdóttir for the many NMR and MS measurement throughout the years, and for being available when help is needed. Thank you to Sverrir Guðmundsson, Svana H. Stefánsdóttir, and Óskar Kettler for their continued support.

I gratefully acknowledge The Icelandic Centre of Research (Grant #152323) and the University of Iceland Teaching Assistantship Grant for funding. I also thank COST Action CM1105 for funding the STSM in Trieste and HÍ travel grants for the opportunities to attend international conferences.

Finally, I would like to thank my family, especially my husband. Thank you for the support, I would not have been able to do this without you.

1 Introduction

1.1 Activation of Small Molecules with Palladium(II) and Nickel(II) Complexes

1.1.1 Olefin Activation, and Homo- and Copolymerization.

Polyolefins are polymers derived from an olefin monomer; these monomers are usually inexpensive short chain alkenes. [1] Industrially, polyolefins are produced catalytically using a transition metal catalyst. [1] The ability of transition metal complexes to activate ethylene and other olefins in homo- and co-polymerization reactions has widespread applications and has been studied extensively. [1-10] Ethylene polymerization with early transition metals exhibit oxophilicity and are deactivated by polar monomers, [11] but in the mid 1990's, Brookhart developed palladium and nickel centered α-diimine complexes that not only catalyzed the polymerization of ethylene and olefins but were stable around polar monomers. [12,13]

The production of polyethylene from ethylene with highly branched structures by α-diimine Pd(II) and Ni(II) catalysts is widely studied. [14,15] The mechanism responsible for branching is known as "chain walking" polymerization, and is summarized into three steps, propagation, chain transfer, and chain isomerization. [16,17] Chain walking is a distinguishing feature of this classification of catalyst, because late transition metals are uniquely apt to chain walking owing to their tendency toward β-hydride elimination and reinsertion. [15] There are key differences to the behaviors of Ni(II) *versus* Pd(II) catalysts. The Ni-based catalysts generate polymers with low or moderate branching, due to the less favorable β-hydride elimination, but are generally more active, whereas the Pd achieves shorter chain branches but higher chain branching density. [18] Further developments of palladium- and nickel-based catalysts with α-diimine type ligands were able to produce polyolefins with high molecular weights, which depending on ligand environment, temperature and ethylene pressure [19] now catalyze many different polymerization reactions between olefins and polar monomers. [20,21] The ligand structure affects the polymerization reactions profoundly, including factors such as steric tuning, electronic perturbation, and backbone composition. [3,21-23] Nickel-based catalysts developed by Grubbs, with salicylaldimine ligands were also shown to tolerate heteroatoms. [24] Activation and polymerization of ethylene with bidentate imine carboxylate ligand has also been reported, however, low polymer weight attributed to β-hydride. [25]

Salens are Schiff-type ligands that form bis diimine-tetradentate square planar coordinated complexes. These complexes are well studied for their catalytic features. [26-28] The catalytic polymerization of styrene to form polystyrene is among the many applications of salen complexes. [29] More recently, attention has refocused on salen derivatives known as salans. Salans are diamine complex derived from imide reduction of salen complexes. Secondary amines in salan complexes are more basic than the imide counterparts and less

susceptible to hydrolysis and therefore more suitable for reactions in aqueous medium. [30] Pd(II) and Ni(II) salan complexes have shown mild success in hydrogenation/redox isomerization of allylic alcohols. [31] Metal-salan complexes of Titanium, Zirconium, and Vanadium have also been applied to polymerization reactions. [32,33]

Polymerization of olefins is a vast field and continues to grow. [19] Many studies into new ligands and catalysts may initially be motivated by application in olefin polymerization, but ultimately lead to other areas of catalysis such as ring-opening polymerization, [34,35] radical polymerizations, [36] cross-coupling reactions and carbon-carbon bond [37] formation to name a few. [19]

1.1.2 CO_2 Activation

The need for an efficient means of carbon dioxide activation is a pressing present-day issue, but the challenges that arise from CO_2 reduction are considerable. Single electron reduction of CO_2 to $CO_2^{\bullet-}$ occurs at E^0 = -1.90 V (vs. NHE), which is due to a large reorganizational energy between the linear molecule and bent radical anion. [38] This large potential can be avoided with a suitable catalyst, where addition of two protons and two electrons reduce CO_2 to CO and H2O, which has the potential of -0.53 V (vs. NHE). [38] Redox-active catalysts such as transition metal complexes often display high turnover numbers; common products of this reaction are CO, formate, oxalate. [39] As more protons and electrons are added to the system, higher value-added products, such as methane and alcohols are can be produced. [40] Current advances in CO_2 reduction involve electrochemical homogeneous and heterogeneous catalysts, [40-46] Photochemical reduction, [47,48] and biochemical transformation of CO_2 into value-added products. [49]

The most effective systems for the catalytic reduction of CO_2 are found in nature and are performed by a group of enzymes known as carbon monoxide dehydrogenases (CODHs). CODHs are grouped into two classes based on the metal found in the activation site: Ni-Fe-S and Mo-S-Cu. [38,50,51] In the Ni-Fe-S cluster, activation of the CO_2 is accomplished by coordination to the Ni and Fe simultaneously, where the Ni acts as a Lewis base, and the Fe acts as a Lewis acid. [51] The CO_2 is coordinated to the fourth position of the Ni but has minimal effect on the coordination geometry. This Ni-Fe-S cluster has inspired Ni based catalysts for activation of CO_2. [50,52]

The first transition metal complexes to report high efficiencies for electrocatalytic reduction of CO_2 to CO were N,N,N,N-tetradentate Ni and Co macrocycles (cyclam). These complexes were able to perform this reduction at potentials between -1.3 and -1.6 V (vs. SCE). The Ni(II) cyclam complexes have become widely studied and have achieved highly selective Faradaic efficiencies in the production of CO at -0.86 V (vs. SCE), even in aqueous conditions and are still widely studied today. [53-62] The mechanism for the CO_2 activation on Ni(cyclam) is believed to start with reduction of Ni(II) to Ni(I), from there CO_2 is believed to coordinate to the metal center via the carbon, activating CO_2. [60,63-65] A detailed DFT study of Ni(cyclam) investigated the coordination modes of CO_2 to the metal and found that η^1- CO_2 (see Scheme 1-1) is the most thermodynamically stable. Upon protonation this forms bound COOH and oxidizes the metal to Ni(III); addition of another proton and electron releases H_2O and reduces the complex back to Ni(II). This is followed by CO cleavage. [60]

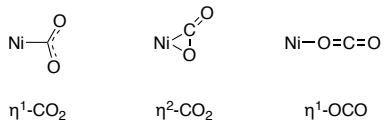

Scheme 1-1. Possible binding modes of CO_2 to Ni(I)

Nickel salen complexes have recently shown the ability to electrocatalytically reduce CO_2 to ethanol through 12-e- transfer reaction. Another currently explored area is using CO_2 as a one carbon building block for organic synthesis, [49,66-69] including the catalytic production of acrylate from CO_2 and ethylene coupling, [70] which proceeds in a one-pot reaction with bidentate diphosphine ligands and either Ni(II) [71,72] or Pd(II) [73-75] complexes.

1.2 Synthesis of Peptides

Amino acids are organic compounds that consist of an amine, a carboxylic acid and various side chain moieties. The composition of the side chain determines whether an amino acid is acidic, basic, polar, or non-polar. When amino acids are coupled together, they become di-, tri-, etc. peptides, and fewer than 20 chained amino acids are classified as oligopeptides. Proteins are large biomolecules that consist of more than ~50 amino acids and are ubiquitous in nature, performing all manner of functions. There are 20 different naturally occurring amino acids found in nature and as a consequence all combinations of tripeptides can be found in nature. [76]

Coupling reactions are needed in order to form peptides from amino acids; if a coupling reaction is performed without the use of protecting groups on either the C or N terminus of the acid a myriad of coupling combinations could occur. In order to purposefully synthesize long chains of amino acids, protection groups are employed. There are a variety of groups and combinations used to serve this purpose. One of the most important features of protecting group combinations is orthogonality. Since the formation of peptide chains involves repetitive coupling, usually in C-terminus to N-terminus direction, directed cleavage of the N-terminus protection group, while preserving semi-permanent side chain and C-terminus groups is imperative. The role of the protection groups can vary widely depending on reagents and synthetic design. [76, 83]

Coupling reactions also require activation of the carboxy group, which is usually performed *in situ* with the formation of an electron withdrawing group. This step unfortunately carries with it the potential loss of stereochemistry. Two main pathways exist through which racemization can occur, keto-enol tautomerization and oxazolone formation (Scheme 1-2). Traditionally, this is minimized with the addition of coupling reagents that protect against racemization. Carbodiimides are among the most widely used coupling reagents, in conjunction with N-hydroxy derivatives, which increase the efficiency of carbodiimide mediated coupling reactions. [77]

1.2.1 Protecting Groups

In order to avoid self-condensation during in situ activation of the carboxy group, semi-permanent protection of the C-terminus carboxylate is needed. Depending on the need,

different esters can be used, this includes esters that can be cleaved with acids (Boc and t-butyl), bases (Fmoc and methyl), or by hydrogenation (Z and benzyl). [78] Amino acid methyl esters are generally the HCl salt and must be deprotonated before coupling. This is usually performed in situ with the aid of a tertiary amine, which must be carefully controlled in order to avoid side reactions such as aspartimide formation or racemization of the activated carboxy-residues. [76] Methyl esters are stable to catalytic hydrogenation and acidolysis but are cleaved in basic conditions. [78] The longer the peptide chain, the harsher the conditions for cleavage become, but for short chain peptide this is accomplish easily. Employing t-butyl esters is widely used because they are stable to catalytic hydrogenation and bases and are particularly suited to be used in combination with Fmoc and Z groups. [76,78] Steric effects of the t-butyl groups afford some protections against ester carbonyl substitutions, but prolonged exposure to extremely basic conditions can hydrolyze the ester. [78]

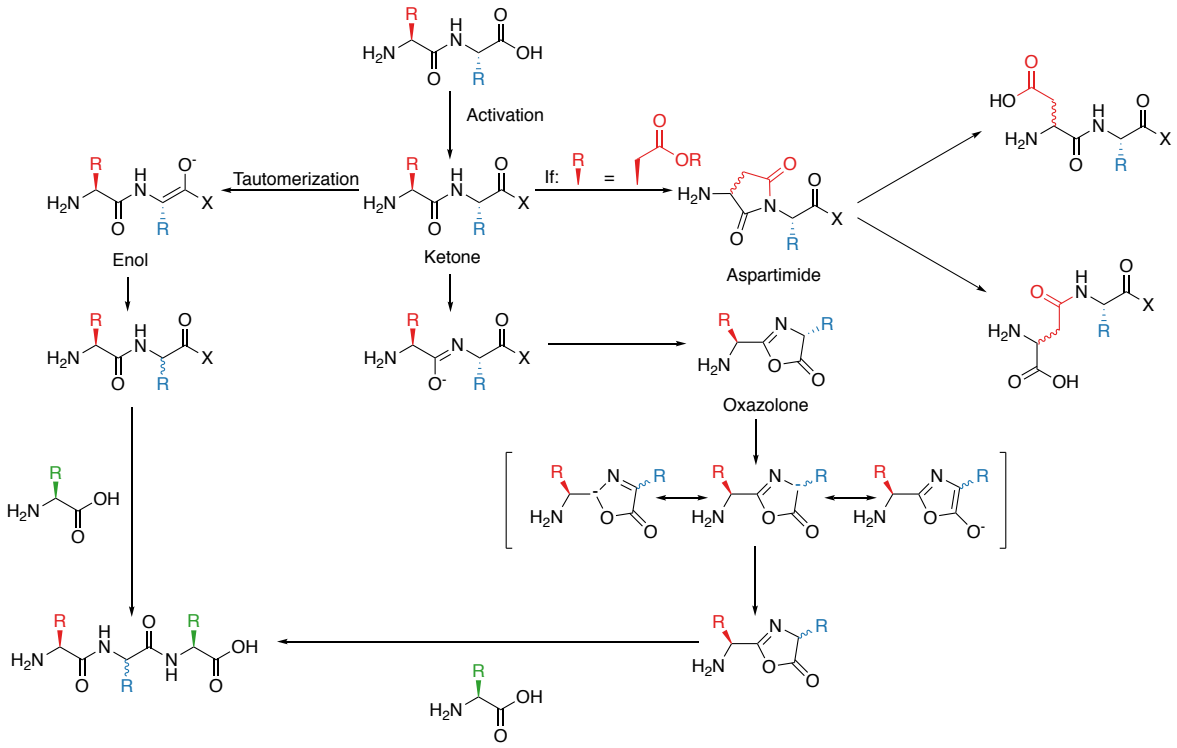

Scheme 1-2. Coupling reaction isomerization pathways

Protection of the α-amino group is required to reduce nucleophilicity of the functional group. Ideally, N-terminus amino protecting groups should be easily cleaved in mild conditions. These groups fall into two broad categories, urethane and non-urethane derivatives. Non-urethane type groups are not as widely used but are more important for peptidomimetic synthesis. [76] Urethane based protection groups are widely used in both solution and solid-phase peptide synthesis (SPPS) and include carbamates and alkyloxycarbonyl groups. [76] Urethane protected amino acids are also less prone to racemization than acyl-based groups. The first and still widely employed group in this category is benzyloxycarbonyl (Cbz or Z), which has the advantage of being cleaved via catalytic hydrogenation and is stable in most coupling reaction conditions. [76,78,79] The Z group is preferably employed for solution phase synthesis because it is easily cleaved, and its side product (benzene) is easily removed. Another frequently employed N-terminus protecting group is 9-Fluorenylmethoxycarbonyl

(Fmoc). This group undergoes base catalyzed cleavage but is stable in acidic conditions and is resistant to catalytic hydrogenations. [78-80] The Fmoc group is widely used in peptide synthesis and is particularly popular in SPPS. The side product during cleavage is dibenzofulvene and is known to participate in side-reactions. Typically, a scavenger agent is used in order to avoid the formation of unwanted cyclic peptides. [81]

1.2.2 Coupling Reagents

Carbodiimides, are used in coupling reactions to activate the acid and form O-acyl*iso*urea intermediates, which in the presence of an amine will undergo aminolysis to form a peptide bond. This active species can however cyclize and form the oxazolone, which removes the chiral center (Scheme 1-2); N-hydroxy derivatives (often triazoles) are added in order to avoid this species. These additives form the active ester and decrease the degree of racemization. Carbodiimides are converted to their urea derivatives during coupling reactions. [76]

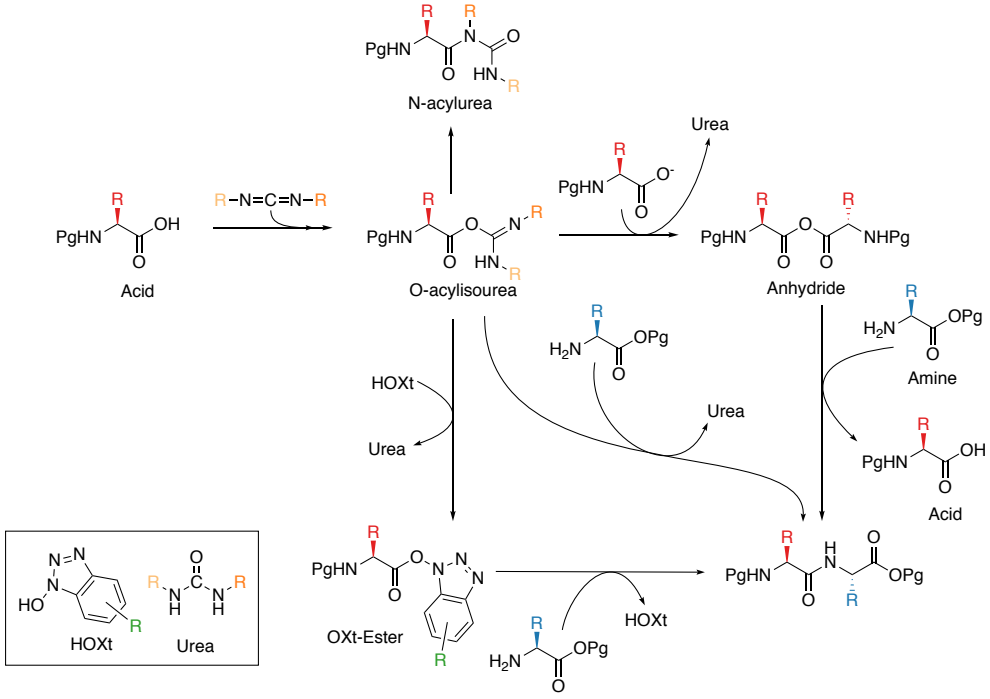

Scheme 1-3. Coupling reaction with carbodiimide and triazole (HOBt) additive.

One of the most common carbodiimides is dicyclohexylcarbodiimide (DCC); the urea (DCU) of DCC is highly insoluble and can be separated out with filtration, however traces of DCU are difficult to remove. [80,82] For this reason, other carbodiimides have be adopted as standards in coupling reactions, one example is N-ethyl-N'-(3-dimethylaminopropyl) carbodiimide (EDC). [76,82,83] The resulting urea (EDU) is water soluble and can be removed from the reaction mixture with simple aqueous work-up.

Once the carboxylic acid has been activated a number of undesirable side reaction can occur. [78-80] The efficiency of carbodiimide mediated reactions is increased with the addition N-hydroxy derivatives. This class of additives protonates and replaces the O-acylisourea to form the OXt-ester, thus preventing the intermolecular rearrangement leading to the formation of N-acylurea.

1.3 Palladium(II) and Nickel(II) Peptide Complexes

The complexation of biological peptides with various transition metal ions has been studied for many decades, specifically in the context of metallodrugs and metal toxicity. [84-88] Generally when complexed, peptides form stable 5- or 6-membered ring chelates through the amino, amide backbone or the carboxylate moiety. [89] The formation of metal amide bonds requires the presence of a primary ligating group, or "anchor group". For simple oligopeptides this is the N-terminus amine, and once amine coordination takes place, the amide coordination is facilitated. [89-92]

Palladium(II) and nickel(II) ions have a high affinity for nitrogen and soft sulfur donor atoms found in various organic ligands. [93-98] One characteristic feature found in the complexation of Pd(II) and Ni(II) with small peptides is their ability to induce deprotonation of the amides. [99,100] Nickel is able to induce deprotonation and coordination at pH values around 8, whereas in the absence of coordinating anions like chloride, the chelation of amides to palladium is complete at pH values below 2. [99]

Strong ligating side chain moieties also serve as anchor groups; histidine is a well-studied example. [101-103] The so-called ATCUN-motif (Amino Terminal Cu and Ni) forms strong coordinating ligands with histidine in the third amino residue for the N-terminus. Innumerable possibilities of side chain combinations and modification allow a variety of metal complexes to be synthesized with tunable geometries and electronic properties. [90,92,102,104-111]

1.4 Aim of This Work

The aim of this Ph.D. work was to synthesize and characterize new nickel and palladium complexes intended for CO_2 activation. In order for CO_2 activation to be achieved, strong sigma donors are needed to create an electron rich metal center. Tripeptides are ideal for such ligand design, but the 5 membered chelates were thought to be unreactive. Altering the N-terminus amino acid affords ligands designed with comparable donor sets, but with variable flexibility and reactivity. The resulting complexes can achieve κ^4[n,5,5] (where n = 5, 6, 7, or 8 membered rings) coordination geometries. Commercially available tripeptides with analogs that fit these criteria were not available, and thus had to be synthesized. Drawing inspiration from salen and salan ligands, tripeptide complexes should form stable tetradentate square planar geometries. In order to form neutral complexes, the C-terminus carboxylate was alkylated, and a synthetic technique was developed which prevents ester hydrolysis and coordination via the carbonyl oxygen occurs. This weak bonding would then allow for labile interactions of the carbonyl to act as an "on-off" switch, providing stability during catalysis. Palladium readily forms this coordination mode; however, nickel was not able to coordinate in this fashion. Pd(II) and Ni(II) complexes were synthesized and then surveyed for small molecule activation.

The content in Chapter 2 describes the synthesis and characterization of four new tripeptides to be used as ligands. The synthesis of these tripeptides was achieved using solution phase peptide synthesis. The design of the tripeptides was intended to maximize organosolubility

after complexation by employing small side chain moieties. Alkylating the C-terminus ester would direct coordination to the N-donor atoms, and potentially serve as a non-rigid donor. The N-terminus side chain analogs provide variable ring sizes, electronic properties, and lability if coordinated via side chain functional groups, either equatorially or axially in a pendent-type fashion. The intent is that lability would translate to different catalytic properties. The aqueous coordination properties of **1-3** were investigated in order to determine preferred complex coordination geometries.

Chapter 3 describes the synthesis of new tripeptide palladium(II) complexes and is divided into aqueous and non-aqueous synthesis. The effects of starting materials, such as base, and starting palladium complex are discussed. The synthetic effort focused on the synthesis of a neutral complex with Pd(II) to maximize organosolubility, as solvation properties are important in complex reactions with various small molecules.

In Chapter 4 the synthesis of new nickel tripeptide complexes is described. For nickel the isolated products were highly dependent on starting materials, and several combinations of Ni(II) salts, bases and solvent systems were attempted for synthesis of Ni(II) complexes. Nickel is known to promote the deprotonation and coordination of amides at pH values ~8-9, [109] and methyl ester is labile under basic conditions. [112] Considering this, hydrolysis of the methyl ester upon nickel complexation was expected owing to elevated pH values required for amide chelation.

Chapter 5 provides a summary of the reactivity studies for the synthesized palladium(II) and nickel(II) complexes. Palladium was reacted with ethylene and other olefins in order to establish whether catalytic polymerization could proceed. Supposition based on comparative calculations suggests nickel tripeptide complexes are worth exploring for the electrocatalytic reduction of CO_2 to CO. Summary, outlook, and potential future applications are discussed in Chapter 6.

2 Synthesis, Characterization & Aqueous Coordination Studies of Tripeptides: α-Asp(O^{t}Bu)AlaGly(OMe), β-Asp(O^{t}Bu)AlaGly(OMe), HisAlaGly(OMe), and TrpAlaGly(OMe)

2.1 Synthetic Methodology

The content of this chapter describes the synthesis and characterization of four new tripeptides to be used as ligands. Although the parent tripeptides have been identified as fragments in protein digestion, [113-115] the tripeptides **1**-**4** were not synthesized previously. Using the aa-AlaGly(OMe) framework allowed distinctive NMR resonances for the alanyl and glycyl residues to be identified and interpreted, while avoiding hydrophobicity introduced by larger side chains. Alkylation of the C-terminus both increases non-aqueous solubility and directs coordination to the N-donors, with the goal of increased organosolubility after complexation. Additionally, a weaker ester donor group potentially serves as a non-rigid donor. While the N-terminus side chain would provide variable ring sizes with additional lability, if coordinated either equatorially or axially in a pendant type fashion. The intent is that lability that would translate to different catalytic properties. The synthesis of theses tripeptides was achieved using solution phase peptide synthesis, which has many benefits for short peptide synthesis, including easy scale-up and less consumption of materials. [77,79,83] All tripeptides were fully characterized using ^{1}H, ^{13}C, COSY, and HSQC NMR spectroscopy, as well as ESI-MS, IR, UV-vis, and elemental analysis. The aqueous coordination properties of **1**-**3** were investigated in order to determine their preferred complex coordination geometries.

2.1.1 Coupling

The choice to use both the methyl ester and *t*-butyl ester on **1** and **2** presented itself with a variety of challenges in the synthesis. The *t*-butyl ester was selected as a commercially available protection on the Fmoc-protected aspartic acid, and the methyl ester protection was chosen over the *t*-butyl or ethyl because of facile completion of the esterification reaction for the methyl ester with quantitative yields, whereas *t*-butyl or ethyl esters required long reaction times which resulted in incomplete esterification, and yield loss in conducted experiments. Both Fmoc- and CBZ-protected amino acid were used as starting materials, based on availability and cost. The reaction pathway is shown in Scheme 2-1 with

intermediates listed in the legend. First, the dipeptide AlaGly was alkylated to form AlaGly(OMe)-HCl, which was then coupled with either CBZ-(**1a**, **3a**, **4a**) or Fmoc-(**1b**, **2b**, **4b**) protected amino acid intermediates. The coupling reactions were fairly straightforward and produced pure products in high yields. The exception was CBZ-His, which exhibited low solubility which resulted in low yields. This was improved by changing the coupling solution solvent to DMF; however high yields could not be achieved for this reaction. The coupling agent selected was EDC, as the resulting urea is highly water soluble which allowed for facile aqueous workup. Hydroxybenzyltriazole (HOBt) was added to decrease racemization.

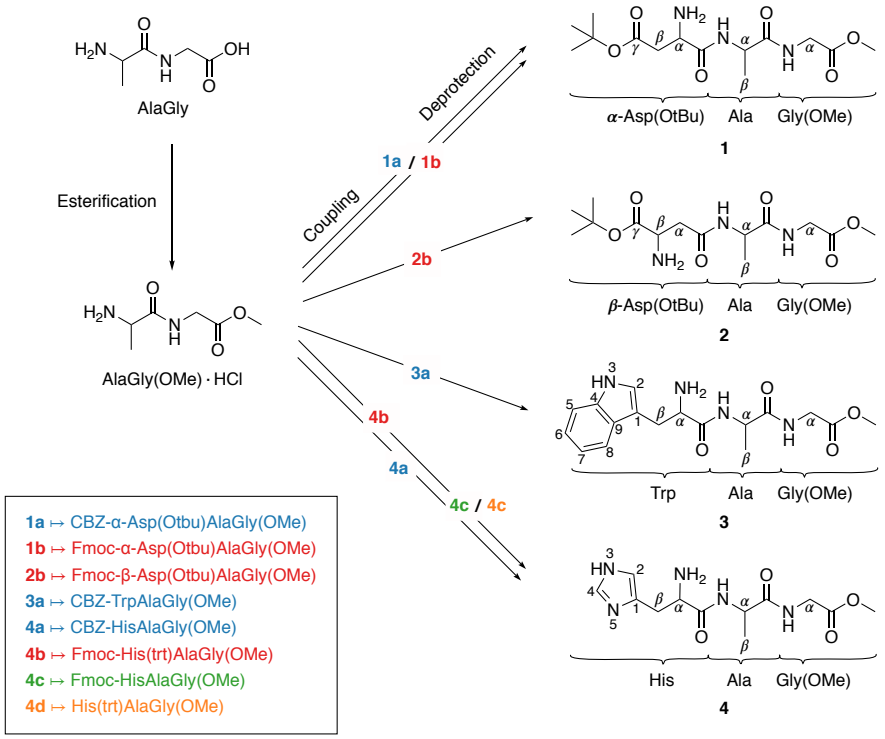

Scheme 2-1. Ligand synthetic pathway

2.1.2 Deprotection and Purification

Challenges presented themselves in the selection of a deprotection method for the Fmoc or Z and work-up procedures to obtain pure compounds. Methyl ester hydrolysis is catalyzed by basic conditions above a pH of 10, whereas *t*-butyl esters are catalytically hydrolyzed in acidic conditions below a pH of 2 and is more sensitive to heating. [112] Attempted deprotection of Fmoc-Asp(O^{t}Bu)AlaGly(OMe) and Fmoc-β-Asp(O^{t}Bu)AlaGly(OMe) using standard basic conditions resulted in the formation of aspartimide, and thus could not be employed. Complications arose due to the common solubilities of the product and side products, making separation difficult, this was solved through the selection of DMF to mediate Fmoc cleavage. [81] This selection worked well, although residual DMF content likely contributed to very hygroscopic behavior of the crude compounds. Analytically pure compounds were isolated by washing them thoroughly with dry solvent after flash chromatography. Attempts to precipitate out the HCl salt of **1** and **2** produced the partially hydrolyzed *t*-butyl ester species, but anaerobic reaction conditions using dry ethereal hydrogen chloride solution, precipitated pure amine hydrochloride salts. Attempts to reform

the free amine using zinc dust [116] left residual chloride. Synthesis and purification of **3** was straightforward using standard methods employed for CBZ amine protecting group. [117] Difficulties arose during the synthesis and isolation of **4**, partially related to solubility issues. Fmoc-His(Trt) requires two sequential deprotection steps; either Fmoc is cleaved in basic conditions first then the Trt group is removed with acid, or vice versa. Low yields for Trt cleavage led to selection of Z-His as starting material. Standard methods were again employed for CBZ deprotection with good yields. After isolation and purification all compounds were stored under nitrogen in the freezer.

2.2 Characterization

2.2.1 ^{1}H- And ^{13}C-NMR Spectroscopy

^{1}H and ^{13}C spectra of **1**-**4** and their precursors were obtained, and the resonances were assigned with the aid of COSY and HSQC measurements. The spectra were collected in D_2O, $CDCl_3$ and DMSO-d_6. Hydrochloride salt products of **1** and **2** were obtained. Their spectra reflected the difference between the free base and the salt, which shifts the resonances of all protons in the spectra. Values reported in the experimental section at the end of this chapter are in $CDCl_3$ and are for the free base. The spectra for **1**-**3** is tabulated in Appendix Table 1 for DMSO-d_6 and Appendix Table 2 for D_2O.

2.2.2 Infrared Spectroscopy

The infrared spectra of **1**-**4** were recorded as KBr pellets and are shown in Figure 2.1. The observed peaks were assigned using the comparative spectra of the free amino acids. Notable functional groups have been assigned and listed in the synthesis section. The *t*-butyl and methyl ester carbonyl stretching frequencies are observed between ~1760 and 1725 cm^{-1} and the Amide I and Amide II bands are observed at ~1660 cm^{-1} and ~1540 cm^{-1}, respectively.

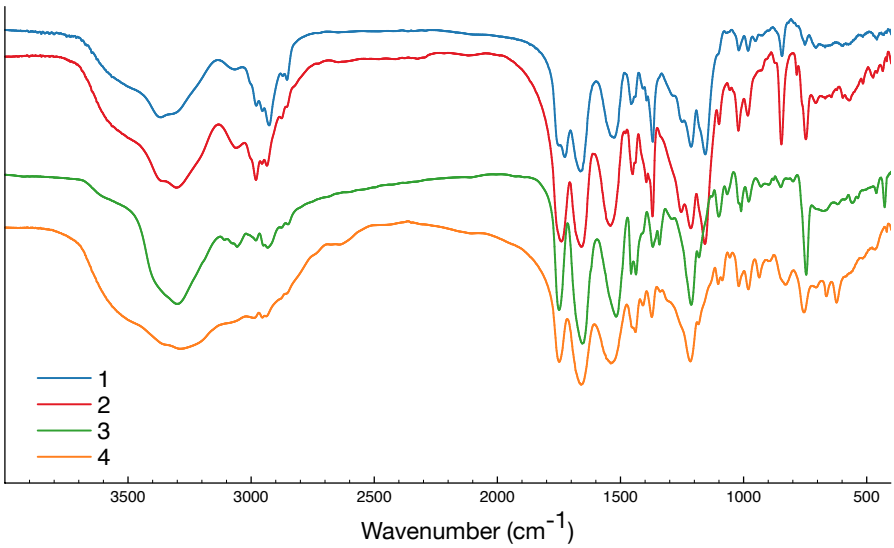

*Figure 2.1 Infrared spectra for **1-4***

2.2.3 UV-Vis Spectroscopy

The electronic spectra of **1-4** in H_2O are shown in Figure 2.2. The carbonyl n → π^* bands are observed at 280 and 275 nm for **1-3**. These transitions are forbidden and have low intensity; compound **4** has $\varepsilon_{280} = 20M^{-1}\ cm^{-1}$. The indole of **3** shows intense $\pi \rightarrow \pi^*$ bands between 260 - 290 nm, and the absorption coefficient of Trp in proteins is 5500 at 280 nm and can also be used as a quantitative measurement for peptide size when composition is known. [118,119]

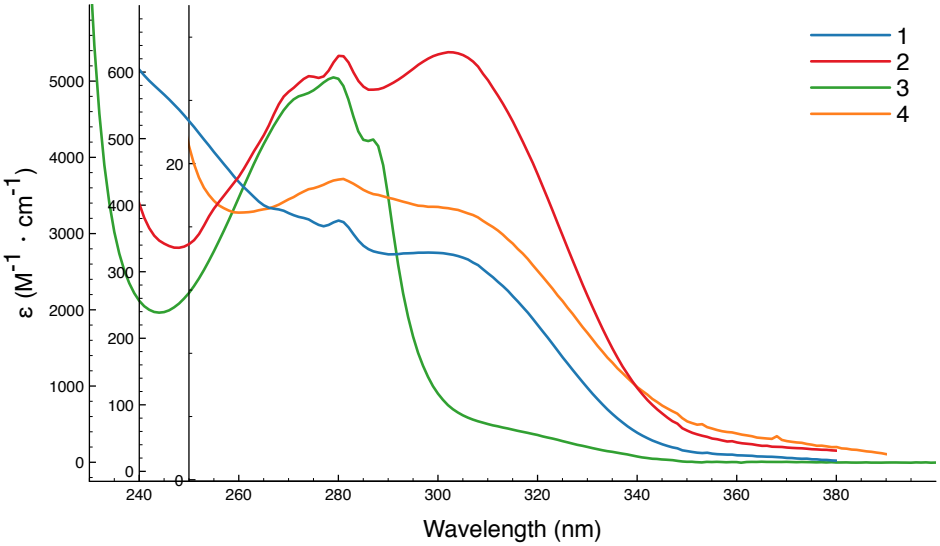

*Figure 2.2. UV-Vis Spectra **1-4***

2.2.4 Mass Spectrometry

Mass spectra were obtained using electrospray ionization mass spectrometry (ESI-MS) in the negative ion scan for anions and the positive ion scan for neutral or positive ions. The found ion peaks were simulated with expected isotope patterns to confirm the composition of the compound found compared to the expected composition. The isolated compounds showed an excellent match with less than 2 ppm variation in simulated vs found values.

2.2.5 Optical Rotation

Optical activity is a measurement of the degree of rotation of a plane of polarized light that passes through an analyte solution and only occurs in molecules with chiral centers. Optical activity can only be observed if a solution of the analyte contains one or mostly one stereoisomer. If there is a mixture of enantiomers in equal portion, optical activity will not be observed. By using HOBt in the coupling reactions, racemization in minimized. Optical activity is physical property, individualistic to each compound and is not additive. Optical rotation measurements are useful in determining consistency between multiple preparations of a compound. Optical rotation was measured for pure ligands by dissolving 25 mg of sample in 1 mL of DMSO. The results are reported in Table 2-1.

*Table 2-1. Optical rotation for compounds **1-4** measured with 25mg of sample in 1mL DMSO*

1	2	3	4
-1.4	+6.9	-18.8	-25.6

2.3 Aqueous Coordination Properties

Aqueous coordination properties of tripeptides **1-3** to a palladium(II) complex were studied. Tripeptide **4** was not included in this study because of low solubility in D_2O. It was of interest to establish the coordination behavior of these ligands and confirm the different chelate ring sizes formed at the N-terminus rather than the C-terminus. [102,103] In order to study the initial formations of the Pd complexes, ideally the starting complex would have easily exchangeable ligands that would also prevent dimerization of the metal ion. For these reasons, $[Pd(en)(H_2O)_2](NO_3)_2$ was selected. [120] pH-dependent coordination was analyzed by NMR spectroscopy and the coordination to the alkylated tripeptides at selected pH values inferred from their NMR spectra and reported literature, and the molecular ions of the formed complexes were identified in mass spectra.

The tripeptides with N-terminus α-Asp(O^{t}Bu) and β-Asp(O^{t}Bu) (**1** and **2**, respectively allow for a direct comparison of chemical reactivities based on the five versus six membered chelates; both have five coordination sites possible: the amine, two amide groups, and the two esters. Compound **3** has seven possible coordination sites; in addition to the backbone amino and carbonyl functional groups of the peptide, indole complexation has been reported through the secondary amine, [121] the C2 carbon, [122,123] and the C3 carbon, which would form chelates larger than six. [124]

2.3.1 pH-Dependent Coordination of $[Pd(en)(H_2O)_2]^{2+}$ with 1

A mixture of $[Pd(en)(H_2O)_2]^{2+}$ with **1** at a pD of 3.77 did not result in complexation and is consistent with reports stating that amine coordination to the $[Pd(en)]^{2+}$ fragment does not take place until a pH of 4 due to its competitive binding of Cl^-. [99]

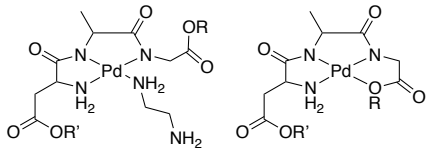

*Scheme 2-2. Possible coordination geometries of **1** with $[Pd(en)(H_2O)_2]^{2+}$*

At a pD of 4.71 the formation of a new species, **Pd-1A** (Scheme 2-2) was observed. The tripeptide formed a tridentate species with Pd(II) that has a mono-coordinated ethylenediamine occupying the fourth coordination site. Free tripeptide **1** was still present amounting to about ~50% based on integrations as seen in Table 2-2. Convergence of the NMR resonances at pD of 7.34 is evidence that coordination geometry **Pd-1A** becomes the major species. At this pD the methyl ester starts hydrolyzing, and after 8h about 35% of the ester has been hydrolyzed. Palladium catalyzed hydrolysis of methyl esters for alanylglycine is known to occur at a pH of 4-5, [125,126] however base catalyzed hydrolysis of methyl

esters tends to start at pH values greater than 10, [112] indicating observed ester hydrolysis is Pd(II) catalyzed. After raising the pD to 11.20, the formation of tetradentate species **Pd-1B** is observed. At this pD, the *t*-butyl ester was ~30% hydrolyzed, while the methyl ester was completely hydrolyzed after 8h.

*Table 2-2. Possible coordination geometries of **1** with $[Pd(en)(H_2O)_2]^{2+}$ at varying pD values with hydrolysis values present after 1 hour.*

pD	Species present		% Ester Hydrolysis R (OMe)	% Ester Hydrolysis R' (O^{t}Bu)
3.77	**1** ~100%	—	~0	~0
4.71	A ~55%	**1** ~ 45%	~12	~5
7.34	A ~100%	—	~35	~5
11.20	B ~100%	—	100	~30

2.3.2 pH-Dependent Coordination of $[Pd(en)(H_2O)_2]^{2+}$ with 2

Initial pD of the $[Pd(en)(H_2O)_2]^{2+}$ and **2** was 5.01, and observed coordination geometries are shown in Scheme 2-3. Complexation was seen immediately with mono-coordination geometry shown in **Pd-2A**. However, some methyl ester hydrolysis (10%) and *t*-butyl hydrolysis (< 8%) is also occurring. No evidence of bidentate coordination of the peptide was observed at this pD.

However, two species appear to be present at pD 6.93, both with the coordination geometry **Pd-2B**; the majority showing probable $\kappa^2[NH_2,O^tBu]$ binding and the minor showing $\kappa^2[NH_2,O^-]$ binding accompanied by *t*-butyl ester hydrolysis (Table 2-3). Hydrolysis of the methyl and *t*-butyl esters reaches ~20% as indicated by growing MeOH and ^{t}BuOH signals however, no evidence of amide chelation was present.

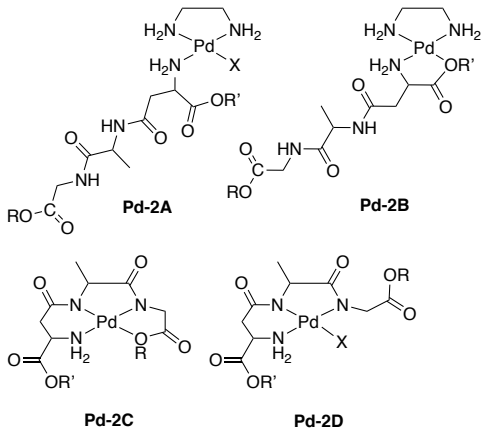

*Scheme 2-3. Possible coordination geometries of **2** with $[Pd(en)(H_2O)_2]^{2+}$*

As many as 4 isomers were present at pD 9.61 due to varying degrees of hydrolysis of the methyl and *t*-butyl esters, but the coordination geometry of all of the isomers is represented by **Pd-2C** with $\kappa^4[NH_2,N,N,O]$. Methyl and *t*-butyl ester hydrolysis was estimated to be

~65%/35% respectively, where the *t*-butyl ester hydrolysis was likely Pd-catalyzed, induced by the proximity of the ester to the Pd-NH_2 group. At highly basic conditions complete hydrolysis of the methyl ester was observed, and *t*-butyl ester hydrolysis was ~70%, while the major species maintained the coordination geometry shown as **Pd-2C**. Another minor species was observed as probable formation of a Pd-hydroxo species, as suggested by coordination geometry **Pd-2D**. [127] At basic pH values, the fourth coordination site in Pd(II) peptides complexes has been reported as occupied by hydroxide ions. [99,128,129]

*Table 2-3. Possible coordination geometries of **2** with $[Pd(en)(H_2O)_2]^{2+}$ at varying pD values with hydrolysis values present after 1 hour.*

pD	Species present		% Ester Hydrolysis R (OMe)	% Ester Hydrolysis R' (O^tBu)
5.01	A ~100%	—	~10	~8
6.93	B ~100%	—	~20	~20
9.21	C ~100%	—	~65	~35
11.06	C ~70%	D ~30%	100	~70

2.3.3 pH-Dependent Coordination of $[Pd(en)(H_2O)_2]^{2+}$ with 3.

The initial mixture of $[Pd(en)(H_2O)_2]^{2+}$ and **3** resulted in the formation of two metal complex isomers in approximately 1:1 ratio (Scheme 2-4). One isomer has the proposed bidentate coordination **Pd-3A** with $\kappa^2[NH_2,N]$ chelation, with en group still present. The second isomer present at pD 4.76 has a mono-coordinated ethylenediamine [130] and indole amine-amide coordination corresponding to the **Pd-3B** geometry. Support for this assignment is observed by all resonances for the indole moiety doubling.

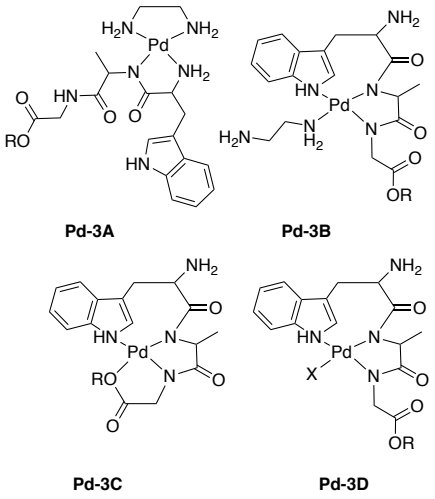

*Scheme 2-4. Possible coordination geometries of **3** with $[Pd(en)(H_2O)_2]^{2+}$*

As the pD is increased to 6.52, **Pd-3B** is the only isomer present in the NMR spectrum (Scheme 2-4); whereas a further increase to pD 7.92 results in complete dissociation of en, leading to carboxylate ligation, which suggests coordination mode **Pd-3C**, with ~75%

methyl ester hydrolysis is the best model at moderate pH values. At extremely basic pD conditions, the methyl ester is completely hydrolyzed and a new minor species appears (**Pd-3D**), tentatively assigned as hydrolyzed Pd(II), i.e. containing a coordinated hydroxo group rather than the carboxylate group. [127]

*Table 2-4. Possible coordination geometries of **3** with $[Pd(en)(H_2O)_2]^{2+}$ at varying pD values with hydrolysis values present after 1 hour.*

pD	Species present		% Ester Hydrolysis R (OMe)	% Ester Hydrolysis R' (O'Bu)
4.76	A ~50%	B ~50%	~10	—
6.52	B ~100%	—	~19	—
7.92	C ~100%	—	~75	—
11.54	C ~75%	D ~25%	100	—

2.3.4 Mass Spectrometry of Pd(II) Complexes with 1-3.

The complexes were not amenable to isolation from aqueous solutions because multiple species present in solution proved separation of products a serious challenge. As identification of the species present, mass spectra were obtained; the results summarized in Table 2-5. A pH of 10.5 was chosen assuming that molecular peaks of the expected complexes could be identified in the mass spectrum. At high pH it is expected to see the carboxylate of the C-terminus amino acid as the fourth donor to Pd(II) or alternatively, either Cl^- or OH^- from the solution mixture. Molecular ion peaks in the mass spectrum corresponded to complexes predicted by NMR.

*Table 2-5. Summary of expected and found molecular ion peaks in the mass spectra of **1-3** with $[Pd(en)(H_2O)_2]^{2+}$ at pH of ~10.5.*

Ligand	Species expected by NMR			Species found by MS		
1	**Pd-1B** *major*	—	—	**Pd-1B** *major*	**Pd-1A**† *minor*	—
2	**Pd-2C** *major*	**Pd-2D** *minor*	—	**Pd-2C** *major*	**Pd-2D** *minor*	—
3	**Pd-3C** *major*	**Pd-3D** *minor*	—	**Pd-3C** *major*	**Pd-3D** *minor*	**Pd-3B*** *minor*

*Hydrolyzed methyl ester. †With and without ester hydrolysis

The methyl ester hydrolysis is rapid and only ligand **3** showed peaks with the methyl ester intact. The *t*-butyl ester was observed in spectra of **1** and **2**. Ligands **1** and **3** showed presence of ethylene diamine in minor peaks that could be caused by incomplete removal of free ethylene diamine during sample preparation.

2.4 Conclusions

Four new alkylated tripeptides **1-4** were synthesized and characterized fully using solution phase synthesis in high yields. The coordination preferences of **1-3** were explored as ligands for Pd(II) in water at different pH values using $[Pd(en)(H_2O)_2]^{2+}$ to explore stepwise coordination and draw out differences in ligand properties.

Coordination of $[Pd(en)(H_2O)_2]^{2+}$ with **3** through the indole nitrogen led to an unusual 8 membered chelate, although 8-membered chelates are rare. [131] Formation of an initial 5-membered ring via the α-amine and the Ala amide was observed at the lowest pH (Scheme 2-4, **Pd-3A**), in a similar fashion to the five membered chelate coordination of Pd(II) and Pt(II) bis-tryptophan complexes, in which coordination proceeds through the amine N, and carboxyl O. [132,133] Additionally, five membered chelate coordination of Trp coordination with the $[Pd(en)]^{2+}$ fragment from the indole C3 to the carboxyl O has been reported. [124]

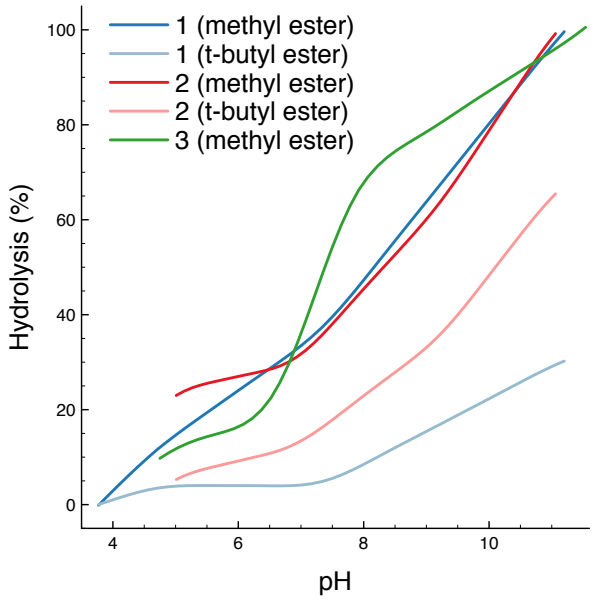

Figure 2.3. Percent ester hydrolysis as a function of pH.

The indole C2 proton is the most acidic proton and is most likely to leave when interacting with a Lewis acid, [122] where C2-indole coordination together with Ala amide would lead to a less-strained 7-membered ring. Palladacycles with indoles have been reported, where the Pd(II) center is sigma bonded to the C2 carbon and the indole nitrogen is functionalized to form a 6-membered chelate with the palladium. [123] Another possibility is an 8-membered ring with the indole nitrogen and the nearest amide. Examples of η^1 coordination of Ru(II) with indole nitrogen show that it is not deprotonated [121] in such coordination, and is in that way comparable to amine coordination. The pK_a of the indole proton in $[(cymene)Ru(\eta^1\text{-indoline})(CH_3CN)_2]^{2+}$ was determined to be 5.2 or much lower than for free indole. [134] An NMR spectrum of **3** and Pd(II) mixed with two equivalences of base in DMSO-d_6 confirmed the loss of the amide resonances, but the N1 proton was still present. The presence of the C2 proton in the NMR spectrum of **3** with $[Pd(en)(H_2O)_2]^{2+}$ leads to the conclusion that κ^4[8,5,5] coordination is present in the mixture at all pH values, albeit a minor species at low pH values. An interesting result here is that the indole nitrogen is a

strong donor for the Pd(II) center competing efficiently with the normally dominant α-amine donor group in peptide coordination.

Ligands **1** and **2** were expected to form respective five and six membered chelates with the amine and the nearest amide. This was achieved, but in an unpredictable manner. Ligand **2** coordination is more strongly pH driven, where at moderate pH values **2** preferred a 5-membered chelate with the amine and the side-chain ester carbonyl oxygen, (Scheme 2-3, **Pd-2B**) promoting *t*-butyl ester hydrolysis. [93,94] This coordination type (N,O) is well known for simple amino acids [135] and prevails until the pH was sufficiently high enough to deprotonate the amides leading to tetradentate κ^4[6,5,5] complexation. This suggests that 5-membered chelate stability is more important than the amine/amide coordination even for a soft ion such as Pd(II). Ligand **1** forms a conventional κ^4[5,5,5] chelate in basic conditions, completely dissociating the en. Ligand **1** shows significantly less Pd^{2+} promoted *t*-butyl ester hydrolysis, however **1** shows multiple isomers that represent various forms of hydrolyzed ester combinations. (Figure 2.3) Despite ester hydrolysis the study successfully drew out interesting differences in the coordination of these ligands and site directed coordination geometries using pH manipulations.

Comparable studies were carried out for the alkylated biological tripeptide glutathione. Although the alkylated glutathione was able to form a stable 7-membered ring, this was a minor product. Through these studies it was concluded that the presence of the thioether, along with uncontrollable reaction products, glutathione was deemed not amenable to continued work. [136] The tripeptides chosen exhibited their maximum expected chelating ring sizes at the N terminus and confirmed it is possible to form complexes with κ^4[n,5,5] (n = 8,6,5) chelates that may be employed to adjust ligand frameworks for bioinspired catalyst design in future work.

2.5 Experimental

2.5.1 Physical Methods

Infrared spectra were recorded on a Nicolet Avatar 360 FT-IR (E.S.P.) spectrophotometer using KBr pellets. ^{1}H, COSY, and ^{13}C nuclear magnetic resonance spectra were recorded at ambient temperature on a Bruker Avance 400 MHz spectrometer at 400 and 101 MHz, respectively. Solvents used were D_2O, DMSO-d_6, and $CDCl_3$. Electronic spectra were obtained using either Varian Cary 100 Bio spectrophotometer or Perkin Elmer Lambda 25 UV/Vis spectrophotometer. Mass spectra were recorded on a micrOTOF-Q spectrometer, equipped with E-spray atmospheric pressure ionization chamber (ESI). Elemental Analyses were obtained from Midwest Microlab, IN, USA.

pH-dependent NMR studies were performed in D_2O. A stock solution of the ligands (**1**-**3**) (0.020M) and a stock solution of the Pd(II) (0.040M) complex were mixed in a 1:1 ratio, for final concentrations of 5.0×10^{-3} M. The ionic concentration was increased to 0.100 M with KCl and the pH adjusted with NaOD. The reaction mixture was monitored over a 48 h period using NMR spectroscopy.

The pH potentiometric titrations were carried out in 15 ml samples using four different metal to ligand ratios (0:1, 1:1, 2:1, 4:1). During titration argon was bubbled through the samples

to prevent oxygen and carbon dioxide and to prevent aggregation of the samples. The concentration of the ligand was fixed at ~$3.2x10^{-3}$ M and the metal concentration adjusted to fit desired ratios. The ionic strength of the samples was adjusted with KCl to 0.2 M in a 60-fold excess to suppress complex formation due to competitive binding of the Cl^-. The titrations were carried out at constant temperature (298 K). The use of acid to lower the pH before titration was omitted because the *t*-butyl ester is subject to acid catalyzed hydrolysis. The analytes were titrated with standardized potassium hydroxide and 30 to 40 data points were obtained for each titration curve. The apparent equilibrium constants were evaluated from the titration data as defined by Equations 1 and 2, using the evaluation function on the Excel sheet CurTiPot, developed by Prof. Gutz, [137] where M, L and H represent $[Pd(en)(H_2O)_2]^{2+}$ ion, the ligand and protons, respectively:

$$\boldsymbol{pM + qL = rH \leftrightharpoons MpLqHr} \quad (1)$$

$$\boldsymbol{\beta_{pqr} = \frac{M_p L_q H_r}{[M]^q [L]^q [H]^r}} \quad (2)$$

2.5.2 Materials

Reagents used were purchased from Sigma Aldrich and used without further purification unless otherwise stated. Alanylglycine, Z-Asp(O^{t}Bu)-OH, Fmoc-Asp(O^{t}Bu)-OH, Fmoc-Asp(OH)-O^{t}Bu, Z-Trp, Z-His, Fmoc-His(Trt), and EDC-Cl use in peptide coupling were purchased from Bachem. Solvents were purchased from Sigma Aldrich and were distilled under nitrogen and dried using standard methods. [138] Alanylglycine esterification was completed by reacting it with trimethylchlorosilane. [139]

2.5.3 Synthesis

Coupling reactions were executed by adding N-protected amino acids to Hydroxyl-benzotriazole (HOBt) and stirring in chloroform or DMF at 0 °C. Once the solution cooled, 1-Ethyl-3-(3-dimethylaminopropyl) carbodiimide (EDC-HCl) was added and stirred for 30 min, after which AlaGly(OMe)-HCl was added, followed by addition of triethylamine (TEA). The solution was stirred under slight N_2 flow at ambient temperature for 24 h. [140] If $CHCl_3$ was used as solvent, product was simply washed with water, dried with $MgSO_4$, and $CHCl_3$ removed *in vacuo*. The product was then washed with ether and dried in a vacuum desiccator to obtain clean product. If DMF was used, the DMF was removed *in vacuo* with elevated heat and azeotropic distillation with toluene.

Cleavage of the Fmoc protecting group was executed by dissolving in DMF and stirring at 110 °C for ~50 min using an oil bath. [81] After cooling water was added, and the product washed with ether and hexane. Water and DMF were removed *in vacuo* with elevated heat and azeotropic distillation with toluene.

The CBZ protecting group was removed by adding Z-protected amine and 10% catalyst loaded Pd/C (10% wt.) together and evacuating the flask, backfilling with argon. Dry methanol (50 mL) was syringed in. A balloon filled with H_2, attached to a needle, was inserted into the top of the flask via septum, the N_2 was then flushed out of the flask and replaced with H_2. [117] (Care must be taken because Pd/C is pyrophoric and can cause organic solvents to ignite when air is present) The reaction mixture was stirred overnight with the H_2 balloon attached. When finished, the H_2 is flushed out by argon and the product

is filtered through Celite on a fritted filter and washed with an additional 20 mL of methanol. Methanol was removed under reduced pressure with slight heat.

AlaGly(OMe)-HCl

(*Modified from established procedure*) Esterification of the glycine carboxylate was completed by adding 1.7 mL (13.685 mmol) trimethylchlorosilane to a 20 mL methanolic solution of AlaGly (1.000 g, 6.843 mmol) and allowing to stir for at least 24 hrs. [139] The dipeptide was isolated by removing the methanol under reduced pressure (1.393 g). The percent yield was 100%. Product was isolated as a hydrochloric salt. ^{1}H NMR (400 MHz, Deuterium Oxide) δ 4.16 – 4.06 (m, 1H, α-C_{Ala}), 4.04 (d, J = 2.0 Hz, 2H, α-C_{Gly}), 3.72 (s, 3H), 1.52 (d, J = 7.1 Hz, 3H, β-C_{Ala}). IR (KBr) cm^{-1}: 3360, 3235 (b, ν(N—H)), 1755 (sh, ν(C=O)), 1670 (s, Amide I), 1568 (s, Amide II), 1212 (s, ν(C—O)), 1114 (s, ν(C—O)). MS (ESI/Positive) MW: ($C_{14}H_{25}N_3O_6$) = 160.1730, M/Z found(calc) = 161.0920(161.0921) [M+H$^+$].

Z-α-Asp(O^{t}Bu)AlaGly(OMe) (**1a**)

Coupling reaction was executed using coupling procedure. Reactant amounts are as follows. Z-Asp(O^{t}Bu)-OH (1.102 g, 3.407 mmol), HOBt (0.460 g, 3.407 mmol), EDC-HCl (0.719 g, 3.748 mmol), AlaGly(OMe)-HCl (0.670 g, 3.407 mmol), TEA (0.5 mL, 3.588 mmol) in 50 mL of chloroform. The yield was 1.515 g (95.5%). ^{1}H NMR (400 MHz, Chloroform-d) δ: 7.34 (q, J = 3.1 Hz, 5H, Ar_{CBZ}), 7.02 (d, J = 9.2 Hz, 2H, NH_{Ala}, NH_{Gly}), 5.94 (d, J = 7.1 Hz, 1H, NH_{Asp}), 5.11 (s, 2H, $CH_{2\ CBZ}$), 4.60 – 4.47 (m, 2H, α-H_{Asp}, α-H_{Ala}), 4.10 – 3.90 (m, 2H, α-H_{Gly}), 3.71 (d, J = 1.8 Hz, 3H, $OCH_{3\ Gly}$), 2.89 – 2.64 (m, 2H, β-H_{Asp}), 1.40 (s, 8H, $OC(CH_3)_{3\ Asp}$), 1.37 (d, J = 7.6 Hz, 5H, β-H_{Ala}). ^{13}C NMR (101 MHz, $CDCl_3$) δ: 172.12 (C=O_{Asp}), 170.94 (C=O_{Ala}), 170.67 (γ-C=O_{Asp}), 170.10 (C=O_{Gly}), 156.10 (C=O_{CBZ}), 135.97 (Ar_{CBZ}), 128.57 (Ar_{CBZ}), 128.49 (Ar_{CBZ}), 128.31 (Ar_{CBZ}), 128.17 (Ar_{CBZ}), 128.11 (Ar_{CBZ}), 82.02 ($OC(CH_3)_{3\ Asp}$), 77.16 ($CDCl_3$), 67.34 ($CH_{2\ CBZ}$), 52.29 ($OCH_{3\ Gly}$), 51.40 (α-C_{Asp}), 49.00 (α-C_{Ala}), 41.12 (α-C_{Gly}), 37.36 (β-C_{Asp}), 27.98 ($OC(CH_3)_{3\ Asp}$), 17.66 (β-C_{Ala}). IR (KBr, cm^{-1}) 3367, 3234 (s, ν(N—H)), 1754 (sh, ν(C=O)), 1728 (s, ν(C=O)), 1657 (s, Amide I), 1543 (s, Amide II), 1246 (sh, ν(C—O)), 1216 (s, ν(C—O)), 1153 (s, ν(C—O)). MS (ESI/Positive) MW: ($C_{22}H_{31}N_3O_8$) = 465.5030, M/Z found(calc) = 488.1991(488.2003) [M+Na$^+$]

Fmoc-α-Asp(O^{t}Bu)AlaGly(OMe) (**1b**)

Coupling reaction was executed using coupling procedure. Reactant amounts are as follows. Fmoc-Asp(O^{t}Bu)-OH (1.406 g, 3.418 mmol), HOBt (0.462 g, 3.418 mmol), EDC-HCl (0.462 g, 3.418 mmol), AlaGly(OMe)-HCl (0.672 g, 3.418 mmol), TEA (0.5 mL, 3.588 mmol). The yield was 1.807 g (95.3%). ^{1}H NMR (400 MHz, $CDCl_3$) δ 7.85 – 7.69 (m, 2H), 7.66 – 7.51 (m, 2H), 7.40 (td, J = 7.6, 1.1 Hz, 2H), 7.31 (td, J = 7.5, 1.2 Hz, 2H), 6.89 (s, 2H), 5.88 (d, J = 8.3 Hz, 1H), 4.51 (p, J = 7.0 Hz, 1H), 4.43 (d, J = 7.0 Hz, 1H), 4.22 (t, J = 6.9 Hz, 1H), 4.12 – 3.89 (m, 2H), 3.72 (s, 3H), 2.94 – 2.66 (m, 2H), 1.52 – 1.32 (m, 11H). ^{13}C NMR (101 MHz, $CDCl_3$) δ 172.09 (C=O_{Asp}), 171.24 (C=O_{Ala}), 170.75 (γ-C=O_{Asp}), 170.20 (C=O_{Gly}), 143.83 (C=O_{Fmoc}), 143.76 (Ar_{Fmoc}), 141.45 (Ar_{Fmoc}), 127.94 (Ar_{Fmoc}), 127.24 (Ar_{Fmoc}), 125.15 (Ar_{Fmoc}), 120.18 (Ar_{Fmoc}), 82.30 ($OC(CH_3)_{3Asp}$), 67.48 ($CH_{2\ Fmoc}$), 52.47 ($OCH_{3\ Gly}$), 51.50 (α-C_{Ala}), 49.20 (α-C_{Asp}), 47.24 (CH_{Fmoc}), 41.28 (α-C_{Gly}), 37.53 (β-C_{Asp}), 28.17 ($OC(CH_3)_{3\ Asp}$), 17.73 (β-C_{Ala}). IR (KBr, cm^{-1}) 3380, 3231 (s, ν(N—H)), 1754 (sh, ν(C=O)), 1732 (s, ν(C=O)), 1654 (s, Amide I), 1533 (s, Amide II), 1246 (sh, ν(C—O)),

1216 (s, ν(C—O)), 1158 (s, ν(C—O)). MS (ESI/Positive) M ($C_{29}H_{35}N_3O_8$) = 553.6120, M/Z found(calc) = 576.2316(576.2313) [$M+Na^+$]

α-Asp(O^{t}Bu)AlaGly(OMe) (**1**)

The protecting group Fmoc was removed using the procedure detailed above. **1b** (2.453 g, 4.443 mmol), 10 mL DMF. The yield was 82%. ^{1}H NMR (400 MHz, $CDCl_3$) δ 8.39 – 8.29 (d, J = 6.7 Hz, 1H, NH_{Ala}), 7.87 (t, J = 5.9 Hz, 1H, NH_{Gly}), 7.26 ($CDCl_3$), 4.58 (p, J = 7.0 Hz, 1H, α-H_{Ala}), 4.50 (d, J = 6.2 Hz, 1H, α-H_{Asp}), 3.98 (qd, J = 17.8, 5.6 Hz, 2H, α-H_{Gly}), 3.71 (s, 3H, $OCH_{3\ Gly}$), 3.11 (t, J = 6.6 Hz, 2H, β-H_{Asp}), 1.42 (d, J = 4.1 Hz, 13H, $O(CH_3)_{3\ Asp}$, β-H_{Ala}). ^{13}C NMR (101 MHz, $CDCl_3$) δ 172.75 (C=O_{Asp}), 170.77 (C=O_{Ala}), 170.24 (γ-C=O_{Asp}), 168.44 (C=O_{Gly}), 82.93 ($O\underline{C}(CH_3)_{3\ Asp}$), 52.30 ($OCH_{3\ Gly}$), 50.23 (α-$C_{Asp}$), 49.95 (α-$C_{Ala}$), 41.04 (α-$C_{Gly}$), 36.23 (β-$C_{Asp}$), 28.00 ($OC(\underline{C}H_3)_{3\ Asp}$), 17.59 (β-$C_{Ala}$). IR (KBr, cm^{-1}) 3360 (b, N-H, N-H_2), 3235 (b, ν(N—H)), 1755 (sh, ν(C=O)), 1728 (s, ν(C=O)), 1670 (s, Amide I), 1545 (s, Amide II), 1249 (s, ν(C—O)), 1214 (s, ν(C—O)), 1158 (s, ν(C—O)). UVVis ($CHCl_3$), ε_{286} = 157.97 L/mol·cm. Specific rotation [α] = -1.4° (2.5g/100mL, DMSO). MS (ESI/Positive) MW ($C_{14}H_{25}N_3O_6$) = 331.368, M/Z found(calc) = 332.1816(332.1816) [$M+H^+$]. CHN ($C_{14}H_{25}N_3O_6$)·1/2 H_2O found(calc) %, C: 49.60(49.40), H: 7.58(7.70), N: 12.31(12.35).

CBZ group was remove as described above with following amounts. **1a** (1.515 g, 3.255 mmol), 10% catalyst loaded Pd/C (150 mg) Yield was 0.525 g (65%) ^{1}H NMR (400 MHz, Chloroform-d) δ 8.39 – 8.29 (d, J = 6.7 Hz, 1H, NH_{Ala}), 7.87 (t, J = 5.9 Hz, 1H, NH_{Gly}), 7.26 ($CDCl_3$), 4.58 (p, J = 7.0 Hz, 1H, α-H_{Ala}), 4.50 (d, J = 6.2 Hz, 1H, α-H_{Asp}), 3.98 (qd, J = 17.8, 5.6 Hz, 2H, α-H_{Gly}), 3.71 (s, 3H, $OCH_{3\ Gly}$), 3.11 (t, J = 6.6 Hz, 2H, β-H_{Asp}), 1.42 (d, J = 4.1 Hz, 13H, $O(CH_3)_{3\ Asp}$, β-H_{Ala}). ^{13}C NMR (101 MHz, $CDCl_3$) δ 172.75 (C=O_{Asp}), 170.77 (C=O_{Ala}), 170.24 (γ-C=O_{Asp}), 168.44 (C=O_{Gly}), 82.93 ($O\underline{C}(CH_3)_{3\ Asp}$), 52.30 ($OCH_{3\ Gly}$), 50.23 (α-$C_{Ala}$), 49.95 (α-$C_{Asp}$), 41.04 (α-$C_{Gly}$), 36.23 (β-$C_{Asp}$), 28.00 ($OC(\underline{C}H_3)_{3\ Asp}$), 17.59 (β-$C_{Ala}$). IR (KBr, cm-1) 3360, 3235(b, ν(N—H)), 1755 (sh, ν(C=O)), 1728 (s, ν(C=O)), 1670 (s, Amide I), 1545 (s, Amide II), 1249 (s, ν(C—O)), 1214 (s, ν(C—O)), 1158 (s, ν(C—O)). MS (ESI/Positive) MW ($C_{14}H_{25}N_3O_6$) = 331.368, M/Z found(calc) = 332.1816(332.1816) [$M+H^+$]. CHN ($C_{14}H_{25}N_3O_6$) found(calc) %, C: 49.60(50.75), H: 7.58(7.60), N: 12.31(12.86). UVVis (H_2O): ε_{281} = 377, ε_{299} = 330 L/mol·cm. Specific rotation [α] = -1.4°(2.5mg/100mL, DMSO)

Fmoc-β-Asp(O^{t}Bu)AlaGly(OMe) (**2b**)

Coupling reaction was executed using coupling procedure. Fmoc-Asp-O^{t}Bu (2.783 g, 6.764 mmol), HOBt (0.914 g, 6.764), EDC-HCl (1.426 g, 7.440 mmol), AlaGly(OMe)-HCl (1.330 g, 6.764) and TEA (0.99 mL, 7.102 mmol). The yield was 3.682 g (98.3%). ^{1}H NMR (400 MHz, $CDCl_3$) δ 7.77 (d, *J* = 7.5 Hz, 2H, Ar_{Fmoc}), 7.63 (d, *J* = 7.6 Hz, 2H, Ar_{Fmoc}), 7.41 (t, *J* = 7.5 Hz, 2H, Ar_{Fmoc}), 7.37 – 7.31 (m, 2H, Ar_{Fmoc}), 7.11 (d, *J* = 5.7 Hz, 1H, NH_{Gly}), 6.61 (d, *J* = 7.5 Hz, 1H, NH_{Ala}), 6.20 (d, *J* = 8.3 Hz, 1H, NH_{Asp}), 4.67 (h, *J* = 7.3 Hz, 1H, α-H_{Ala}), 4.54 (dt, *J* = 9.1, 4.7 Hz, 1H, α-H_{Asp}), 4.36 (q, *J* = 10.4, 9.1 Hz, 2H, $CH_{2\ Fmoc}$), 4.23 (t, *J* = 7.2 Hz, 1H, CH_{Fmoc}), 4.18 – 3.97 (m, 2H, α-H_{Gly}), 3.71 (s, 3H, $OCH_{3\ Gly}$), 2.99 – 2.76 (m, 2H, β-H_{Asp}), 1.49 (s, 9H, $OC(CH_3)_{3\ Asp}$), 1.42 (d, *J* = 7.0 Hz, 3H, β-H_{Ala}). ^{13}C NMR (101 MHz, $CDCl_3$) δ 172.56 (C=O_{Asp}), 170.43 (C=O_{Ala}), 170.16 (γ-C=O_{Asp}), 169.96 (C=O_{Gly}), 156.36 (C=O_{Fmoc}), 143.99 (Ar_{Fmoc}), 141.37 (Ar_{Fmoc}), 127.80 (Ar_{Fmoc}), 127.19 (Ar_{Fmoc}), 125.33 (Ar_{Fmoc}), 120.05 (Ar_{Fmoc}), 82.51 ($O\underline{C}(CH_3)_{3\ Asp}$), 67.31 ($CH_{Fmoc}$), 52.48 ($OCH_{3\ Gly}$), 51.53 (α-$C_{Ala}$), 48.83 (α-$C_{Asp}$), 47.26 ($CH_{2\ Fmoc}$), 41.23 (α-$C_{Gly}$), 38.31 (β-$C_{Asp}$), 28.06 ($OC(\underline{C}H_3)_{3\ Asp}$), 18.60 (β-$C_{Ala}$). IR (KBr, cm^{-1}) 3300 (s, ν(N—H)), 1744 (s, ν(C=O)), 1730

(sh, ν(C=O)), 1693 (s, Amide I), 1539 (s, Amide II), 1249 (sh, ν(C—O)), 1220 (s, ν(C—O)), 1158 (s, ν(C—O)). MS (ESI/Positive) MW ($C_{29}H_{35}N_3O_8$) = 553.6120, M/Z found(calc) = 576.2318(576.2316) [M+Na^+]

β-Asp(O^{t}Bu)AlaGly(OMe) (**2**)

The protecting group Fmoc was removed by above procedure. **2b** (3.778 g, 6.764 mmol) in 10 mL of DMF. Yield for this reaction was 2.120 g (94%) ^{1}H NMR (400 MHz, $CDCl_3$) δ 8.20 (d, J = 6.3 Hz,1H, NH_{Ala}),8.03(d,J=7.2Hz,1H, NH_{Gly}),4.63(q,J=7.2Hz,1H, α-H_{Ala}), 4.38 (d, J = 6.9 Hz, 1H, α-H_{Asp}), 4.05 (qd, J = 17.6, 5.5 Hz, 2H, α-H_{Gly}), 3.75 (d, J = 5.7 Hz, 3H, $OCH_{3\ Gly}$), 3.26 (ddd, J = 72.9, 17.2, 4.4 Hz, 2H, β-H_{Asp}), 1.51 (s, 9H, $O(CH_3)_3$), 1.47 (d, J = 7.1 Hz, 3H, β-H_{Ala}). ^{13}C NMR (101 MHz, $CDCl_3$) δ 172.86 (C=O_{Asp}), 171.90 (C=O_{Ala}), 170.60 (γ-C=O_{Asp}), 170.49 (C=O_{Gly}), 82.83 ($O\underline{C}(CH_3)_{3\ Asp}$), 52.46 ($OCH_{3\ Gly}$), 51.68 (α-$C_{Asp}$), 49.12 (α-$C_{Ala}$), 41.20 (α-$C_{Gly}$), 38.51 (β-$C_{Asp}$), 28.05 ($OC(\underline{C}H_3)_{3Asp}$), 17.76 (β-$C_{Ala}$). IR (KBr, cm^{-1}) 3385, 3307 (b, ν(N—H)), 1743 (sh, ν(C=O)), 1728 (s, ν(C=O)), 1653 (s, Amide I), 1541 (s, Amide II), 1254 (s, ν(C—O)), 1210 (s, ν(C—O)), 1155 (s ν(C—O)). UVVis ($CHCl_3$), ε_{281} = 625, ε_{302} = 630 L/mol·cm. Specific rotation $[\alpha]_D$ = +6.9 ° (2.5g/100mL, DMSO). MS (ESI/Positive) M ($C_{14}H_{25}N_3O_6$) = 331.368, M/Z found(calc) = 354.1633(354.1636) [M+Na^+]. CHN: ($C_{14}H_{25}N_3O_6$) found(calc) %, C: 50.28(50.75), H: 7.11(7.60), N: 13.86(12.68).

Z-TrpAlaGly(OMe) (**3a**)

Coupling reaction was executed using coupling procedure with 50 ml of $CHCl_3$. Z-Trp (1.153 g, 3.407 mmol), HOBt (0.460 g, 3.407 mmol), EDC-HCl (0.719 g, 3.748 mmol), AlaGly(OMe)-HCl (0.670 g, 3.407 mmol), and TEA (0.50 mL, 3.578 mmol). The yield was 1.607 g (98.1%). ^{1}H NMR (400 MHz, $CDCl_3$) δ 8.42 (s, 1H, NH_{indole}), 7.61 (d, J = 7.9 Hz, 1H, $H_{indole\text{-}C5}$), 7.32 (p, J = 3.9, 2.9 Hz, 6H, Ar_{CBZ}), 7.29 (d, J = 8.1 Hz, 2H, $H_{indole\text{-}C8}$), 7.20 – 7.12 (t, J = 7.5 Hz, 1H, $H_{indole\text{-}C7}$), 7.07 (t, J = 7.5 Hz, 1H, $H_{indole\text{-}C6}$), 7.03 – 6.99 (m, 1H, $H_{indole\text{-}C2}$), 6.77 (d, J = 5.6 Hz, 1H, NH_{Gly}), 6.61 (s, 1H, NH_{Ala}), 5.78 – 5.71 (m, 1H, NH_{Asp}), 5.16 – 5.03 (m, 2H, $CH_{2\text{-}CBZ}$), 4.56 (d, J = 6.9 Hz, 1H, α-H_{Asp}), 4.46 (q, J = 7.2 Hz, 1H, α-H_{Ala}), 3.85 (dd, J = 18.1, 5.6 Hz, 1H, α-H_{Gly}), 3.77 – 3.64 (m, 1H, α-H_{Gly}), 3.68 (s, 3H, $OCH_{3\ Gly}$), 3.24 (qd, J = 14.6, 6.4 Hz, 2H, β-H_{Trp}), 1.20 (d, J = 7.0 Hz, 3H, β-H_{Ala}). ^{13}C NMR (101 MHz, $CDCl_3$) δ 172.27 (C=O_{Trp}), 171.62 (C=O_{Ala}), 170.31 (C=O_{Gly}), 156.39 (C=O_{CBZ}), 136.34 ($C9_{indole}$), 136.23 (Ar_{CBZ}), 128.69 (Ar_{CBZ}), 128.63 (Ar_{CBZ}), 128.38 (Ar_{CBZ}), 128.26 (Ar_{CBZ}), 127.39 ($C4_{indole}$), 123.65($C2_{indole}$), 122.38 ($C7_{indole}$), 119.87 ($C6_{indole}$), 118.86 ($C5_{indole}$), 111.43 ($C3_{indole}$), 110.09 ($C8_{indole}$), 100.11 (Ar_{CBZ}), 77.16 ($CDCl_3$), 67.31 ($CH_{2\ CBZ}$), 55.92 (α-C_{Trp}), 52.43 ($OCH_{3\ Gly}$), 48.92 (α-C_{Ala}), 41.18 (α-C_{Gly}), 28.67 (β-C_{Trp}), 18.01 (β-C_{Ala}). IR (KBr, cm^{-1}) 3413, 3288 (s, ν(N—H)), 1747 (s, ν(C=O)), 1693 (s, ν(C=C)), 1645 (s, Amide I), 1535 (s, Amide II), 1249 (sh, ν(C—O)), 1220 (s, ν(C—O)). MS (ESI/Positive) MW ($C_{25}H_{28}N_4O_6$) = 480.5210, M/Z found(calc) = 503.1902(503.1901) [M+Na^+]

TrpAlaGly(OCH_3) (**3**)

The protecting group Z was removed as above with **3a** (1.515 g, 3.255 mmol) and 150 mg 10% catalyst loaded Pd/C. Yield was 0.912 g (85%) ^{1}H NMR (400 MHz, $CDCl_3$) δ 8.30 (s, 1H, NH_{indole}), 7.69 (d, J = 7.8 Hz, 1H, NH_{Ala}), 7.65 (dd, J = 7.9, 1.0 Hz, 1H, $H_{indole\text{-}C5}$), 7.36 (dt, J = 8.1, 1.0 Hz, 1H, $H_{indole\text{-}C8}$), 7.20 (ddd, J = 8.2, 7.0, 1.2 Hz, 1H, $H_{indole\text{-}C7}$), 7.11 (ddd, J = 8.0, 7.0, 1.1 Hz, 1H, $H_{indole\text{-}C6}$), 7.07 (d, J = 2.4 Hz, 1H, $H_{indole\text{-}C2}$), 6.99 (t, J = 5.4 Hz, 1H, NH_{Gly}), 4.51 (p, J = 7.2 Hz, 1H, α-H_{Ala}), 4.07 – 3.91 (m, 2H, α-H_{Gly}), 3.78 – 3.73 (m, 1H, α-H_{Asp}), 3.73 (s, 1H, $OCH_{3\ Gly}$), 3.35 (ddd, J = 14.5, 4.4, 0.9 Hz, 1H, β-H_{Trp}), 2.97 (dd, J = 14.5,

8.6 Hz, 1H, β-H_{Trp}), 1.72 – 1.65 (m, 2H, $NH_{2\ Trp}$), 1.31 (d, J = 7.0 Hz, 3H, β-H_{Ala}). ^{13}C NMR (101 MHz, $CDCl_3$) δ 175.44 (C=O_{Trp}), 172.66 (C=O_{Ala}), 170.35 (C=O_{Gly}), 136.53 ($C9_{indole}$), 127.56 ($C4_{indole}$), 123.29 ($C2_{indole}$), 122.45 ($C7_{indole}$), 119.79 ($C6_{indole}$), 119.03 ($C5_{indole}$), 111.51 ($C3_{indole}$), 111.42 ($C8_{indole}$), 55.45 (α-C_{Trp}), 52.48 ($OCH_{3\ Gly}$), 48.51 (α-C_{Ala}), 41.28 (α-C_{Gly}), 30.67 (β-C_{Trp}), 17.36 (β-C_{Ala}). IR (KBr, cm^{-1}) 3389, 3296 (sh, ν(N—H)), 3056 (m, aromatic ν(C—H)), 1749 (s, ν(C=O)), 1655 (s, Amide I), 1517 (s, Amide II), 1213 (s, ν(C—O)), 745 (s, aromatic δ(C—H)). UVVis($CHCl_3$), ε_{281} = 6114 L/mol·cm. Specific rotation $[\alpha]_D$ = -18.76° (2.5mg/100mL, DMSO). MS (ESI/Positive) MW ($C_{17}H_{22}N_4O_4$) = 346.164, M/Z found(calc) = 347.1714(347.1709) [$M+H^+$]. CHN: ($C_{17}H_{22}N_4O_4$) found(calc) %, C: 58.78(58.95), H: 6.38(6.40), N: 15.91(16.17).

Z-HisAlaGly(OCH_3) (**4a**)

Coupling reaction was executed using coupling procedure. Z-His (2.192 g, 7.578 mmol), HOBt (1.229 g, 9.093 mmol), EDC-HCl (1.598 g, 8.335 mmol), AlaGly(OMe)-HCl (1.490 g, 7.578 mmol), and TEA (2.6 mL, 18.944 mmol) in 75 ml of DMF. The product was purified by removing the DMF *in vacuo*, redissolving in ethyl acetate, washing with saturated sodium bicarbonate (3x20 mL), and extracting the sodium bicarbonate layer with two more portions of ethyl acetate (3x20 mL). The combined ethyl acetate layers were then washed with a brine solution, dried with $NaSO_4$, removing the solvent under reduced pressure. The yield was 1.800 g (55.1%). ^{1}H NMR (400 MHz, Chloroform-d) δ 7.99 (s, 1H, NH_{gly}), 7.59 (s, 1H, CH_{im}), 7.41 – 7.30 (m, 6H, Ar_{CBZ}), 7.18 (d, J = 7.5 Hz, 1H, NH_{Ala}), 6.85 (s, 1H, CH_{im}), 6.35 (d, J = 7.0 Hz, 1H, NH_{His}), 5.11 (s, 2H, $CH_{2\ CBZ}$), 4.53 – 4.44 (m, 2H, α-H_{Ala}, α-H_{His}), 4.01 (ddd, J = 73.7, 17.8, 5.6 Hz, 2H, α-H_{Gly}), 3.72 (s, 3H, $OCH_{3\ Gly}$), 3.16 – 3.02 (m, 2H, β-H_{His}), 1.34 (d, J = 7.2 Hz, 4H, β-H_{Ala}).^{13}C NMR (101 MHz, $CDCl_3$) δ 173.04 (C=O_{His}), 171.31 (C=O_{Ala}), 170.64 (C=O_{Gly}), 136.30 ($C2_{Im}$), 135.22 (Ar_{CBZ}), 128.70 (Ar_{CBZ}), 128.39 (Ar_{CBZ}), 128.20 (Ar_{CBZ}), 77.16($CDCl_3$), 67.27 ($CH_{2\ CBZ}$), 55.20 (α-C_{His}), 52.43 ($OCH_{3\ Gly}$), 49.31 (α-C_{Ala}), 41.25 (α-C_{Gly}), 30.11 (β-C_{His}), 17.78 (β-C_{Ala}). IR (KBr, cm^{-1}) 3296 (s, ν(N—H)), 1751 (s, ν(C=O)), 1708 (s, ν(C=C)), 1655 (s, Amide I), 1532 (s, Amide II), 1251 (sh, ν(C—O)), 1213 (s, ν(C—O)). MS (ESI/Positive) MW ($C_{20}H_{25}N_5O_6$) = 431.4490, M/Z found(calc) = 454.1708(454.1697) [$M+Na^+$]

Fmoc-His(Trt)AlaGly(OMe) (**4b**)

Coupling reaction was executed following coupling procedure. Fmoc-His(Trt)-OH (1.081 g, 1.744 mmol), HOBt (0.237 g, 1.744 mmol), EDC-HCl (0.368 g, 1.919 mmol), AlaGly(OMe)-HCl (0.343 g, 1.744 mmol) and TEA (0.26 mL, 1.832 mmol) The yield was 1.159 g (87%). ^{1}H NMR (400 MHz, Chloroform-*d*) δ 8.10 (s, 1H, NH_{Gly}), 7.75 (d, *J* = 7.6 Hz, 2H, Ar_{Fmoc}), 7.57 (dd, *J* = 7.6, 3.3 Hz, 2H, Ar_{Fmoc}), 7.39 – 7.38 (m, 2H, Ar_{Fmoc}), 7.37 (d, *J* = 7.5 Hz, 1H, $C2_{Im}$), 7.32 (dt, *J* = 4.0, 2.8 Hz, 9H, Ph_{Trt}), 7.28 (q, *J* = 1.4, 0.9 Hz, 2H, Ar_{Fmoc}), 7.16 – 7.06 (m, 6H, Ph_{Trt}), 7.03 (d, *J* = 8.1 Hz, 1H, NH_{Ala}), 6.70 (s, 1H, $C4_{im}$), 6.54 (d, *J* = 6.3 Hz, 1H, NH_{His}), 4.56 (dt, *J* = 15.6, 7.5 Hz, 1H, α-H_{Ala}), 4.44 (d, *J* = 5.9 Hz, 1H, α-H_{His}), 4.34 (dd, *J* = 12.8, 5.7 Hz, 1H, CH_{Fmoc}), 4.31 – 4.23 (m, 1H, $CH_{2\ Fmoc}$), 4.18 (t, *J* = 7.3 Hz, 1H, $CH_{2\ Fmoc}$), 4.10 (dd, *J* = 18.1, 5.7 Hz, 1H, α-H_{Gly}), 3.82 (dd, *J* = 17.6, 4.9 Hz, 1H, α-H_{Gly}), 3.62 (s, 3H, $OCH_{3\ Gly}$), 3.16 – 2.95 (m, 2H, β-H_{His}), 1.40 (d, *J* = 7.2 Hz, 3H, β-H_{Ala}). ^{13}C NMR (101 MHz, $CDCl_3$) δ 172.65 (C=O_{His}), 171.05 (C=O_{Ala}), 170.47 (C=O_{Gly}), 156.44 (C=O_{Fmoc}), 144.01 (Ar_{Fmoc}), 143.87 (Ar_{Fmoc}), 142.15 ($Ph_{3\ Trt}$), 141.39 ($C5_{Im}$), 138.58 ($C2_{Im}$), 129.81 ($Ph_{3\ Trt}$), 128.38 ($Ph_{3\ Trt}$), 128.29 ($Ph_{3\ Trt}$), 127.85 (Ar_{Fmoc}), 127.19 (Ar_{Fmoc}), 125.32 (Ar_{Fmoc}), 120.28 ($C4_{Im}$), 120.10 (Ar_{Fmoc}), 77.16 ($CDCl_3$), 75.77 ($\underline{C}Ph_{3\ Trt}$), 67.39 (CH_{Fmoc}), 55.39 (α-C_{His}), 52.23 ($OCH_{3\ Gly}$), 49.23 (α-C_{Ala}), 47.23 ($CH_{2\ Fmoc}$), 41.13 (α-C_{Gly}),

30.82 (β-C_{His}), 17.78 (β-C_{Ala}). IR (KBr, cm^{-1}) 3299 (s, ν(N—H)), 1751 (s, ν(C=O)), 1723 (s, ν(C=C)), 1667 (s, Amide I), 1518 (s, Amide II), 1236 (sh, ν(C—O)), 1208 (s, ν(C—O)). MS (ESI/Positive) MW ($C_{46}H_{43}N_5O_6$) = 761.8790, M/Z found(calc) = 784.3076(784.3016) [M+Na^+]

Fmoc-HisAlaGly(OMe) (**4c**)

The amino protecting group (Trt) was removed by dissolving **4b** (0.500 g, 0.656 mmol) in 40 mL of 50% aqueous acetic acid. The reaction was stirred in a steam bath for 15 min. The solution was then washed with 2 x 40 mL 1:1 Pet ether/ether solvent mixture. The water was then removed *in vacuo* and the product precipitated out with ether. The precipitate was filtered and wash with more ether then air dried. The yield was 65 g (24.5%) NMR. ^{1}H NMR (400 MHz, Chloroform-*d*) δ 7.92 (s, 1H, NH_{Gly}), 7.79 (s, 1H, NH_{Im}), 7.73 (d, *J* = 7.5 Hz, 2H, Ar_{Fmoc}), 7.61 – 7.48 (m, 2H, Ar_{Fmoc}), 7.37 (t, *J* = 7.3 Hz, 2H, Ar_{Fmoc}), 7.28 (d, *J* = 5.7 Hz, 2H, Ar_{Fmoc}), 7.27 (s, 1H, α-H_{Ala}), 6.90 (s, 1H, $C4_{im}$), 6.40 (s, 1H, α-H_{His}), 4.52 (m, 1H, α-H_{Ala}), 4.50 (s, 1H, α-H_{His}), 4.34 (m, 2H, $CH_{2\ Fmoc}$), 4.18 (q, *J* = 7.4 Hz, 2H, CH_{Fmoc}), 4.06 (m, 1H, α-H_{Gly}), 3.94 – 3.86 (m, 1H, α-H_{Gly}), 3.65 (d, *J* = 11.2 Hz, 3H, $OCH_{3\ Gly}$), 3.12 (s, 2H, β-H_{His}), 1.36 (d, *J* = 7.1 Hz, 3H, β-H_{Ala}). ^{13}C NMR (101 MHz, $CDCl_3$) δ 170.65 (C=O_{His}), 161.97 (C=O_{Fmoc}), 143.81(Ar_{Fmoc}), 127.92 (Ar_{Fmoc}), 127.24 (Ar_{Fmoc}), 125.22 (Ar_{Fmoc}), 124.30 (Ar_{Fmoc}), 120.16 ($C4_{Im}$), 100.13, 77.16 ($CDCl_3$),67.34 (CH_{Fmoc}), 52.45 ($OCH_{3\ Gly}$), 49.44 (α-C_{Ala}), 47.21 ($CH_{2\ Fmoc}$), 41.29 (α-C_{Gly}), 34.05 (β-C_{His}), 17.86 (β-C_{Ala}). IR (KBr, cm^{-1}) 3315 (s, ν(N—H)), 1752 (s, ν(C=O)), 1699 (s, ν(C=C)), 1661 (s, Amide I), 1531 (s, Amide II), 1246 (sh, ν(C—O)), 1209 (s, ν(C—O)). MS (ESI/Positive) MW ($C_{27}H_{29}N_5O_6$) = 519.5580, M/Z found(calc) = 542.2006(542.2010) [M+Na^+]

His(Trt)AlaGly(OMe) (**4d**)

The protecting group Fmoc was remove by stirring **4b** (1.937 g, 2.542 mmol) in 10 mL of DMF as outlined above. Yield was 52.2% (0.717 g). ^{1}H NMR (400 MHz, Chloroform-*d*) δ 7.79 (d, *J* = 7.7 Hz, 1H, α-H_{Ala}), 7.54 (d, *J* = 6.0 Hz, 1H, α-H_{Gly}), 7.35 (s, 1H, $C2_{Im}$), 7.34 – 7.28 (m, 9H, Ph_{Trt}), 7.12 – 7.05 (m, 6H, Ph_{Trt}), 6.70 – 6.60 (m, 1H, $C2_{Im}$), 4.46 (p, *J* = 7.1 Hz, 1H, α-H_{Ala}), 4.06 – 3.85 (m, 2H, α-H_{Gly}), 3.72 – 3.68 (m, 1H, α-H_{His}), 3.67 (s, 3H, $OCH_{3\ Gly}$), 3.03 (dd, *J* = 14.7, 4.6 Hz, 1H, β-H_{His}), 2.85 (dd, *J* = 14.6, 6.8 Hz, 1H, β-H_{His}), 1.36 (d, *J* = 7.1 Hz, 2H, β-H_{Ala}). ^{13}C NMR (101 MHz, $CDCl_3$) δ 172.72 (C=O_{His}), 170.44 (C=O_{Ala}), 170.42 (C=O_{Gly}), 142.43 ($Ph_{3\ Trt}$), 138.79 ($C2_{Im}$), 137.31 ($C5_{Im}$), 129.84 ($Ph_{3\ Trt}$), 128.29 ($Ph_{3\ Trt}$), 128.26 ($Ph_{3\ Trt}$), 128.22 ($Ph_{3\ Trt}$), 119.84 ($C4_{Im}$), 77.16 ($CDCl_3$), 75.50 ($\underline{C}Ph_{3\ Trt}$), 55.21 (α-C_{His}), 52.36 ($OCH_{3\ Gly}$), 48.81 (α-C_{Ala}), 41.21 (α-C_{Gly}), 32.79 (β-C_{His}), 17.35 (β-C_{Ala}). IR (KBr, cm^{-1}) 3291 (s, ν(N—H)), 1752 (s, ν(C=O)), 1662 (s, Amide I), 1517 (s, Amide II), 1234 (sh, ν(C—O)), 1206 (s, ν(C—O)). MS (ESI/Positive) MW ($C_{31}H_{33}N_5O_4$) = 539.6360, M/Z found(calc) = 562.2425(562.2425) [M+Na^+]

HisAlaGly(OMe) (**4**)

The protecting group Z was removed by adding **4a** (1.800 g, 4.172 mmol) and 180 mg 10% catalyst loaded Pd/C. Yield was 0.975 g (78.6%) NMR. ^{1}H NMR (400 MHz, Chloroform-*d*) δ 7.63 (d, *J* = 7.7 Hz, 1H, NH_{Ala}), 7.54 (d, *J* = 1.1 Hz, 1H, $C2_{im}$), 7.38 – 7.32 (m, 1H NH_{Gly}), 6.86 (d, *J* = 1.1 Hz, 1H, $C2_{im}$), 4.46 (p, *J* = 7.2 Hz, 1H, α-H_{Ala}), 4.10 – 3.93 (m, 2H, α-H_{Gly}), 3.74 (s, 3H, $OCH_{3\ Gly}$), 3.63 (t, *J* = 5.7 Hz, 1H, α-H_{His}), 3.00 (d, *J* = 5.6 Hz, 2H, β-H_{His}), 1.37 (d, *J* = 7.1 Hz, 3H, β-H_{Ala}). ^{13}C NMR (101 MHz, $CDCl_3$) δ 175.23 (C=O_{His}), 172.76 (C=O_{Ala}), 170.52 (C=O_{Gly}), 145.12 ($C2_{Im}$), 135.33 ($C5_{Im}$), 99.98 ($C4_{Im}$), 77.16 ($CDCl_3$), 55.08 (α-C_{His}), 52.4836 ($OCH_{3\ Gly}$), 48.89 (α-C_{Ala}), 41.28 (α-C_{Gly}), 32.25 (β-C_{His}),17.54 (β-

C_{Ala}). IR (KBr, cm^{-1}) 3345, 3288 (s, ν(N—H)), 1748 (s, ν(C=O)), 1659 (s, Amide I), 1538 (s, Amide II), 1251 (sh, ν(C—O)), 1216 (s, ν(C—O)). UVVis (H_2O), ε_{281} = 19 L/mol·cm. Specific rotation $[\alpha]_D$ = -25.6° (2.5mg/100mL, DMSO). MS (ESI/Positive) MW ($C_{12}H_{19}N_5O_4$) = 297.3150, M/Z found(calc) = 320.1328(320.1329) [$M+Na^+$] CHN: ($C_{12}H_{19}N_4O_4$)·H_2O found(calc) %, C: 46.69(45.71), H: 6.61(6.71), N: 22.37(22.21).

The protecting group Fmoc was removed by stirring **4c** (1.159 g, 1.521 mmol) in 10 mL of DMF as outlined above. Yield for this reaction was 92% (0.756 g). Spectroscopic data same as above.

3 Synthesis and Characterization of Palladium Tripeptide Complexes

3.1 Synthetic Methodology

This chapter describes the synthesis of new tripeptide palladium complexes based on the ligands described in the previous chapter. It is divided into aqueous and non-aqueous synthesis. The effects of starting materials, such as base, and starting palladium complex are discussed. The synthetic effort focused on the synthesis of a neutral complex with Pd(II) to maximize organosolubility, as solvation properties are important in complex reactions with various small molecules. Several different synthetic routes were attempted to achieve tetradentate neutral palladium tripeptide complexes. Initial experiments used ligand **1** because it is the most economic for synthetic optimization and the acid/base sensitivity of its protecting groups renders it a good model to develop a synthetic method that is reproducible for more expensive ligands **2-3**. A summary of the synthetic routes employed to synthesize neutral tripeptide complexes is shown in Scheme 3-2.

3.1.1 Aqueous Synthesis

Synthesis of Mono-Anionic Complex **5a**

Coordination of tripeptide **1** with Pd(II) and degree of hydrolysis are highly dependent on pH. [136] Having established that $\kappa^3[NH_2,N,N]$ chelation between **1** and Pd(II) occurs at a pH of ~7.35, even in the presence of the en ligand, (Scheme 3-1) and that methyl ester hydrolysis remains relatively low at ~35%, synthesis of a neutral tetradentate Pd(II) complex appeared feasible. Methods to establish an aqueous synthetic strategy in order to form such complex were explored. Using this strategy, K_2PdCl_4 was dissolved in water and added to an aqueous solution of **1**, and then the pH was adjusted to ~6.5. This resulted in the formation of two isomers, one major and one minor. The major product is the charged species K[Pd{α-Asp(O^{t}Bu)AlaGly(OMe)}Cl] (**5a**). The composition of **5a** was confirmed by mass spectrometry along with the presence of the Pd_2L_2Cl dimer. The coordination of **5a** is $\kappa^3[NH_2,N,N]$ and support for this coordination mode was determined by spectroscopic data.

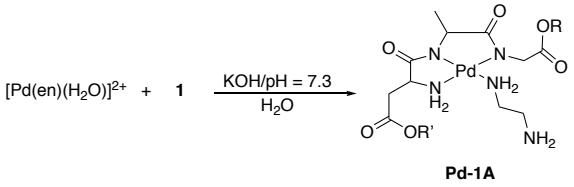

*Scheme 3-1. Formation of $\kappa^3[NH_2,N,N]$ species **Pd-1A** at pH 7.3 in aqueous solution studies. (Chapter 2.3.1)*

The aqueous synthesis strategy afforded the neutral tetradentate palladium complex **8**. This was accomplished by adding an aqueous solution of K_2PdCl_4 to an aqueous solution of the

ligand, adjusting the pH to 10 and then immediately removing the solvent. The NMR for this species matches the product formed by heating **7,** which aided in the identification of this product. This reaction was performed multiple times, but the outcome was difficult to control and usually resulted in multiple isomers. Here again the use of aqueous medium proved difficult to reproduce effectively for complex synthesis.

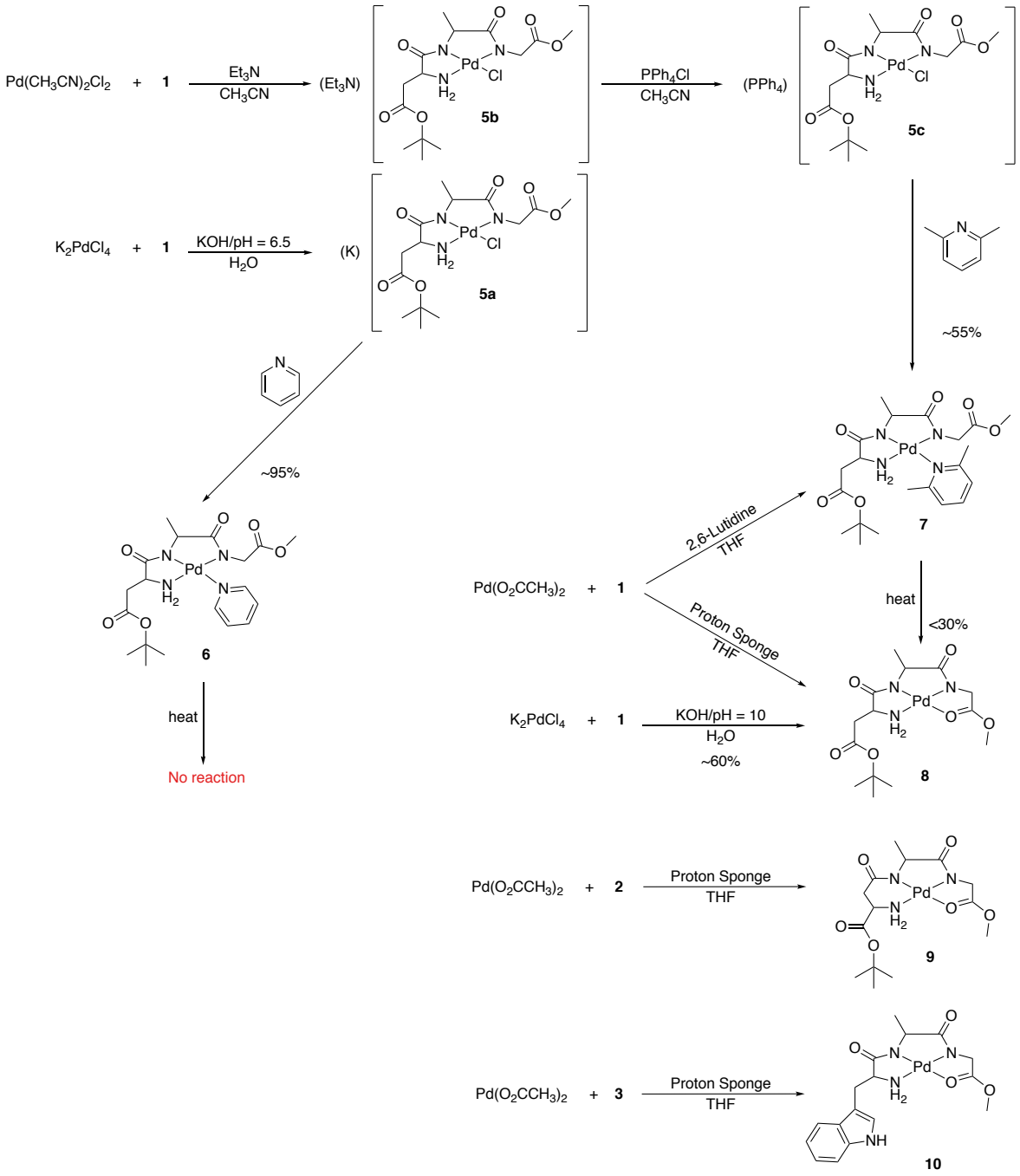

*Scheme 3-2. Attempted synthetic routes to form charged (**5a-5c**) and neutral (**6-10**) Pd(II) complexes.*

3.1.2 Non-Aqueous Synthesis

Synthesis of Mono-Anionic Complexes **5b**-**5c**

Complex **5a** was synthesized with improved control by transitioning into a non-aqueous environment. Using $Pd(CH_3CN)_2Cl_2$ as the starting complex and substituting KOH for two molar equivalents of triethylamine results in isolation of the complex (Et_3N)[Pd{α-Asp(O^{t}Bu)Ala-Gly(OMe)}Cl], **5b**. The composition of this product was also confirmed by mass spectrometry. The NMR resonances for different cationic salts **5a** and **5b** are identical, whereas the latter has an organic cation, which can be tracked in the NMR spectra. Excess Et_3N^+ proved difficult to remove, but this was resolved by cation exchange with PPh_4^+ to produced complex **5c**. The exchange did not noticeably affect the ligand NMR resonances however, this led to loss of yield and some decomposition. After the cation exchange, integration of the PPh_4^+ was ~1 mol equivalence, confirming **5a**-**5c** are mono-anionic. Although Et_3N^+ was able to form the mono-ionic complex, separation from the organic salts proved difficult.

Ligand Exchange Reactions to form **6** and **7**

In order to form the neutral complex, and increase organosolubility, attempts to exchange or remove the chloride were explored. To that effect, pyridine (Py) was added to the potassium salt **5a** and the results monitored with NMR (Table 3-1, **7**). The spectrum shows new peaks in the 7-8 ppm region indicating coordination of pyridine. Integrating these peaks showed the chloride was successfully replaced by the pyridine. When the pyridine complex **6** was heated at 110 ºC overnight, the pyridine remained coordinated. In a second reaction, 2,6-lutidine (Lu) was added to **5c** and the reaction monitored by NMR. Upon lutidine addition, integration of its peaks in the NMR showed incorporation of about 0.5-0.6 mol eq of lutidine for incomplete replacement of the chloride. Lutidine is a weaker nucleophile and is stericly more hindered than pyridine, which explains why lutidine incorporation was less than pyridine.

A neutral palladium complex with coordinated lutidine was synthesized directly using $Pd(OAc)_2$ and 2 equivalence of 2,6-lutidine in dry THF (Scheme 3-2, **7**). Upon heating **7** overnight at 110˚C, tracking this reaction via NMR, a minor species started to form. NMR integration suggests the new species is less than 30 % mol of the total yield. Table 3-1 highlights the changes to the resonances in the NMR of **7** with the addition of heat. Formation of free Lu was also observed, confirming that lutidine's labile coordination may be controlled with heat. This reaction was able to form the desired tetradentate complex Pd{α-Asp(O^{t}Bu)AlaGly(OMe)} (**8**).

Synthesis of Neutral Complexes **8**-**10**.

A novel non-aqueous strategy for the formation of **8** was developed, wherein **1**, along with Proton Sponge (1,8-Bis(dimethylamino)naphthalene) were dissolved in dry THF, $Pd(OAc)_2$ was added to the solution and the reaction stirred under Ar. The Proton Sponge is a non-nucleophilic base which allows the last coordination site on the Pd(II) to remain open for the C-terminal ester to bind. The coordination of this complex is κ^4[NH_2,N,N,=O] with coordinated C-terminus methyl ester carbonyl as shown in Scheme 3-2. Composition of **8** was confirmed by mass spectrometry as well as elemental analysis and the product fully characterized using NMR, IR and UV-Vis spectroscopy. This method established the

synthesis of neutral palladium tripeptide complexes and was then applied to other ligands in the series (Scheme 3-2, **10** and **11**).

The tripeptide **2** is an *iso*-peptide, meaning that it forms the peptide bond through the side chain carboxylic acid. When coordinated to a metal center via the N-terminal amine and the nearest amide, the peptide forms a 6-membered chelate. In aqueous medium at neutral pH this system presents a competing coordination to the side chain carbonyl forming the 5-membered chelate instead of the $\kappa^3[NH_2,N,N]$ amide backbone. (Scheme 3-3) The $\kappa^4[NH_2,N,N,O]$ chelated complex could be formed in basic aqueous conditions at a pH value of ~9. However, Pd(II) catalyzed hydrolysis at this pH value led to *t*-butyl and methyl ester hydrolysis of up to 35% and 65%. Compared to ligand **1**, which respectively only reached 5% and 35% hydrolysis at pH 7.3, aqueous synthesis using **2** was not a viable option. However, utilizing Proton Sponge as a base in dry THF yields the $\kappa^4[NH_2,N,N,=O]$ species, Pd{β-Asp(O^{t}Bu)AlaGly(OMe)} (**10**), in good yields. The composition of complex **10** was confirmed by mass spectrometry and elemental analysis and fully characterized using NMR, IR and UV-Vis spectroscopy.

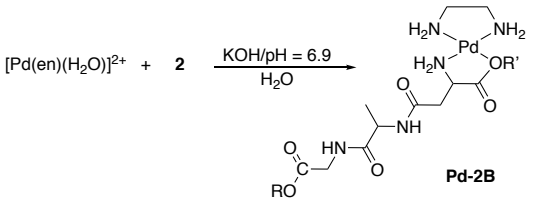

*Scheme 3-3. Formation of $\kappa^2[NH_2,O]$ species **Pd-2B** at pH 6.9 in aqueous solution. (Chapter 2.3.2)*

Aqueous coordination studies of **3** with $[Pd(en)(H_2O)_2]^{2+}$ revealed that the tryptophan indole participates in coordination. [136] The NMR study revealed that at low pH the NH_2 would coordinate as expected and chelation would continue to the Ala amide. However, as the pH was increased to ~8 the $\kappa^4[NH_{indole},N,N,O]$ isomer was detected, forming an 8 membered ring. (Scheme 3-4) This study also showed that the methyl ester is hydrolyzed up to 75% under these conditions. Utilizing this information, aqueous synthesis was not attempted and **3** was complexed to $Pd(OAc)_2$ in THF with Proton Sponge. This yields the isomer $\kappa^4[NH_2,N,N,=O]$ (Scheme 3-2, **10**). This complex was fully characterized using elemental analysis and NMR, IR, and mass spectrometry.

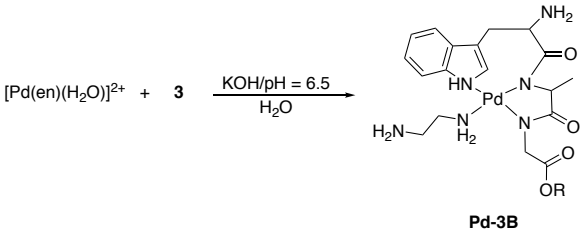

*Scheme 3-4. Formation of $\kappa^3[NH_{indol},N,N]$ species **Pd-3B** at pH 6.5 in aqueous solution. (Chapter 2.3.3)*

3.1.3 Base Effects

Several bases were used in attempt to form the neutral complex with tetradentate coordinated tripeptide ligands. The inorganic base KOH was used in aqueous preparations but could not be employed when switching to organic solvents. This is both because of solubility issues and hygroscopicity of KOH, which could contribute to hydrolysis. Using nucleophilic organic bases like pyridine and lutidine, while yielding neutral complexes, also coordinated to palladium and proved difficult to remove. Strong alkali metal alkoxide bases produced the desired product with a modicum of success but were accompanied with their own problems including solubility and transesterification. [141] The use of Proton Sponge proved to be the right balance between Brønsted base properties and sterically non-nucleophilic nature.

3.1.4 Metal Salt Effects

The starting palladium complex also had a significant role in which product would form. Namely, whether a chloride anion was present or not. When using a chlorinated starting complex, the chloride exhibited preferential coordination to the 4th coordination site over the ester carbonyl, and mass spectrometry data indicates that when chloride is present dimerization occurs, at least in solution. Chloride would effectively block the coordination of small molecules requiring complex activation before displaying reactivity. Palladium acetate was used successfully, in part because of its high solubility in organic solvents, and did not exhibit preferential coordination over the ester carbonyl.

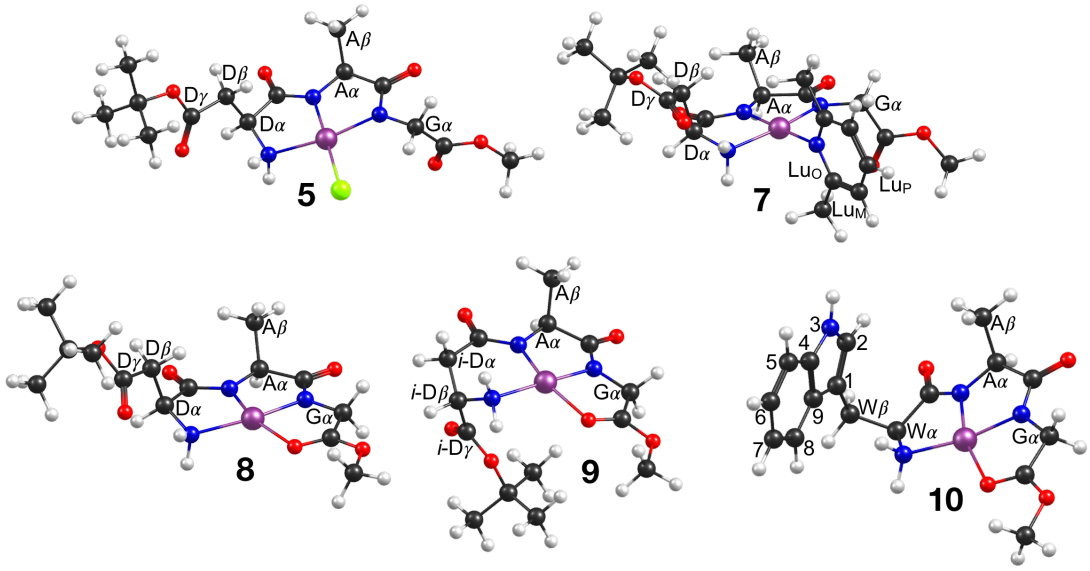

*Figure 3.1. DFT optimized structures of Pd(II) complexes **5**, **7-10**.*

3.2 Calculations

DFT calculations with a continuum solvation model were employed to determine the lowest energy structures in solution for complexes **5-10** which can be seen in Figure 3.1. Several different conformational possibilities were explored computationally. Due to the

conformational flexibility of the tripeptide ligand, a number of conformers for each complex are available (primarily due different orientations of the Asp or Trp sidechains) but only the lowest energy conformer was considered in the calculations of spectroscopic properties. As the Pd(II) peptide complexes are preferably square planar, [NH_2,N,N]-coordination was expected, and DFT results revealed this.

3.3 Characterization

Complexes **5**-**10** were characterized via NMR, IR, and UV-Vis spectroscopy, mass spectrometry and elemental analysis. Quantum chemical calculations at the DFT level used to aid the spectral interpretation. In order to correctly assign coordination geometries, similarities and differences in the complex NMR chemical shifts, and shifts in infrared frequencies of major bands were examined. Observed values were compared to calculated chemical shifts and vibrational frequencies of the DFT-optimized structural models.

3.3.1 ^{1}H- And ^{13}C-NMR Spectroscopy

^{1}H and ^{13}C spectra of **5**-**10** were obtained in DMSO-d_6 and the resonances were assigned with the aid of COSY and HSQC measurements. DMSO-d_6 was selected due to the low solubility of the complexes in organic and aqueous solvents.

*Table 3-1. Summary of NMR data from synthetic experiments to form neutral Pd(II) complexes, where **5** is the species K[Pd(**1**)Cl], **6** = Pd(**1**)Py, **7** = Pd(**1**)Lu, **8** = Pd(**1**), **9** = Pd(**2**), **10** = Pd(**3**).*

Chemical Shift (ppm)	**5**	**6**	**7**	**7** + *Δ**	**8**	**9**	**10**
Py *Ortho*	—	8.73	—	—	—	—	—
Py/Lu *Meta*	—	7.57	7.33	7.02	—	—	—
Py/Lu *Para*	—	7.99	7.78	7.54	—	—	—
N—H_2	4.20 3.86	4.96 4.38	4.76 4.15	5.03 4.54	5.04 4.55	4.63 4.48	4.96 4.24
α-C_{Ala}	3.54	3.66	3.66	3.68	3.68	3.89	3.78
α-C_{Gly}	3.64	3.52	3.14 2.91	3.86	3.87	3.62	3.96
α-$C_{Trp/Asp}$	3.40	3.44	3.54	3.53	3.52	2.33	3.40
$OCH_{3\ Gly}$	3.50	3.34	3.34	3.55	3.55	3.55	3.55
Lu CH_3	—	—	3.18	2.41	—	—	—
β-$C_{Trp/Asp}$	2.45 2.35	2.61 2.40	2.57 2.41	2.63 2.46	2.61 2.45	3.18	3.28 2.87
$OC(CH_3)_{3\ Asp}$	1.40	1.40	1.41	1.42	1.42	1.44	—
β-C_{Ala}	1.15	1.23	1.23	1.20	1.20	1.08	1.24

*Represents the minor species. Trp side chain listed in Experimental Section 3.5.3

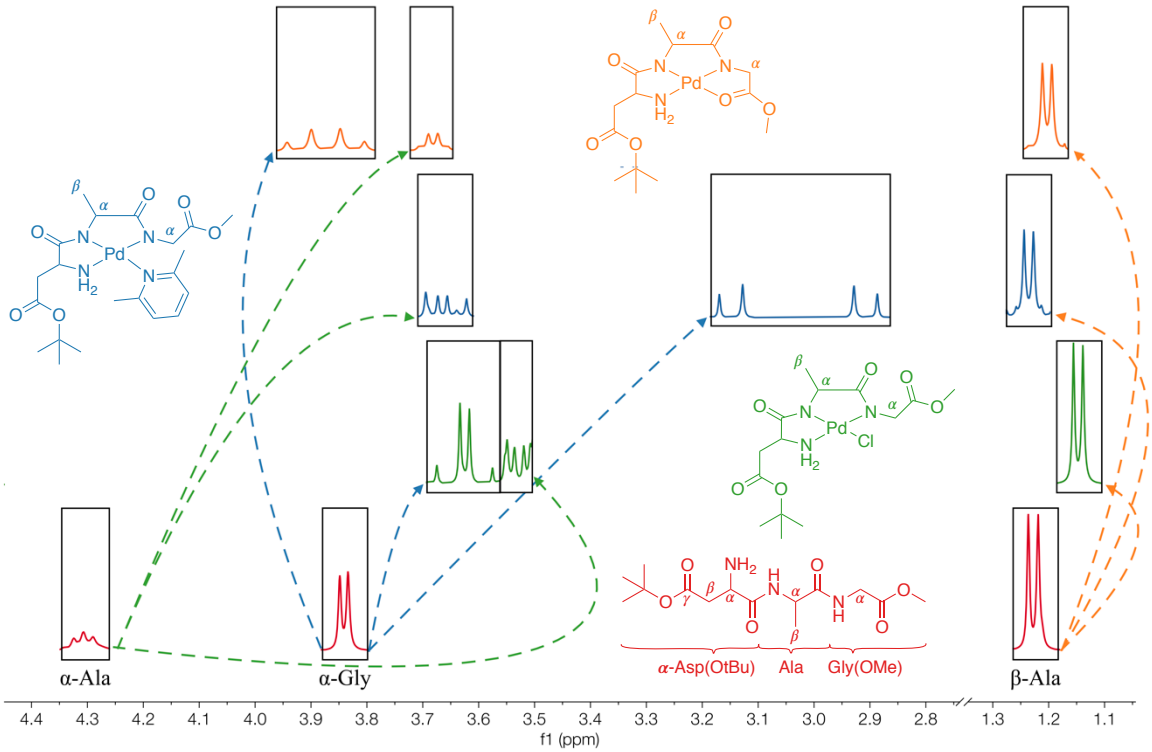

*Figure 3.2. Progression of select ^{1}H NMR resonances of **1** (red) to **5** (green), **7** (blue), and **8** (orange).*

^{1}H NMR Analysis.

The coordinated amine/amide backbone is a commonality of **5**-**10**; this coordination was established in the proton NMR (Table 3-1) with the appearance of amino protons as two triplets between ~5.0 and 3.8 ppm, while the amide protons, located ~8.40 – 8.10 ppm disappear. Generally, the α-C protons shift upfield, whereas Ala α-C protons tend to shift the most and have the largest shifting range, as seen in Figure 3.2. This behavior is expected considering the Asp amide is trans to the fourth coordination sphere, thus the magnetic environment of these protons changes more significantly.

The ^{1}H NMR resonances for **5**, generally shift upfield the most compared to **6**-**8**, presumably owing to the fact that this is the only negatively charged species in the series, and the chloride's π-donation to palladium effectively increases shielding around the ligand. Coordination of pyridine to **5** resulted in the amine, Asp and Ala α-C protons all shifting downfield, (Table 3-1, **6**) which is explained by pyridine π-back-bonding, resulting in metal deshielding. However, the Gly α-C and methyl ester protons shifted further upfield, one explanation for this is π-interactions with neighboring pyridine. Heating **6** overnight at 110 °C did not show any observable changes in the NMR. The complex with coordinated Lu (**7**) has slightly different spectroscopic behaviors compared to **6**. Notably, a large upfield shift of the NH_2 protons (0.20 and 0.23 ppm). In **7** the Gly protons experience the largest shielding effects of the series, appearing with a large coupling constant of ~ 96Hz with resonances at 3.14, and 2.91 ppm. (Figure 3.2) This is further evidence of π-interaction between the lutidine and the glycine moiety. Upon heating **7** overnight at 110 °C a new species is observed, where the Lu is no longer coordinated; the new species matches spectrum **8**.

Support for the coordination mode of **8** was established in part by examining the ^{1}H NMR. The appearance of the NH_2 protons at 4.76 and 5.03 ppm establish amine coordination. The Asp α-C proton appears at about the same resonances as in **1**. However, the Ala α-C protons experience a large upfield shift, supporting Asp amide coordination. The Gly protons only shift by 0.03 ppm compared to **1**, but the Gly coupling pattern changes from a doublet to a quadruplet, signifying Ala amide coordination as seen in Figure 3.2. The small change in resonances is explained with carbonyl oxygen coordination. Carbonyl is a π-acceptor ligand, deshielding the metal. An argument for a coordinated ester via carboxylate oxygen is not supported given the small change in the methyl ester chemical shift.

The NMR spectrum of **9** was poorly resolved owing to the lability of the 6-membered ring. However, important information regarding coordination geometry can still be gleaned from the 2D-NMR coupling patterns and discernible resonance positions and elevated temperature NMR experiments (330K) were performed to improve the spectral resolution. Coordination of the amine is evidenced by the NH_2 resonances at 4.63 and 4.48 ppm. Side chain methylene protons of the N-terminal amino acid (Asp or Trp) are a characteristic feature of the ligands **1**-**3**. These protons are distereotopic and, when recorded in DMSO-d_6, appear as a doublet of quadruplets, because they are in different magnetic environments with different vicinal coupling. For **5**-**8** these protons are outside a chelate ring and show similar coupling constants as the ligands. However, **9** encloses the methylene protons in a 6-membered ring and they become an apparent quadruplet (Figure 3.1). Additionally, a large upfield shift of the α-C protons for Asp (0.46 ppm), Ala (0.42 ppm), and Gly (0.21 ppm), confirms the amine/amide backbone chelation.

*Table 3-2. Assigned ^{13}C NMR resonance for complexes **5**,**7**-**10**.*

Chemical Shift (ppm)	**5**	**7***	**8**	**9**	**10**
$C{=}O_{Trp/Asp}$	170.14	169.93	169.79	170.75	172.93
$C{=}O_{Ala}$	185.17	185.45	177.03	176.26	178.24
γ-$C{=}O_{Asp}$	175.91	175.9	172.89	172.58	—
$C{=}O_{Gly}$	172.34	171.71	186.47	?	186.55
$O\underline{C}(CH_3)_{3\ Asp}$	79.93	80.14	80.47	82.32	—
$OCH_{3\ Gly}$	50.52	50.79	50.96	50.92	50.93
α-$C_{Trp/Asp}$	56.55	56.50	55.81	40.16	59.58
α-C_{Ala}	57.05	57.13	56.60	58.87	56.50
α-C_{Gly}	46.49	45.84	46.79	44.73	46.86
β-$C_{Trp/Asp}$	39.86	39.73	39.94	54.7	29.93
$OC(\underline{C}H_3)_{3\ Asp}$	27.79	27.79	27.79	27.58	—
β-C_{Ala}	19.43	19.78	19.80	20.64	19.92

Lutidine and Trp side chain listed in Experimental Section 3.5.3

In **10**, the appearance of the NH_2 protons at 4.96 and 4.24 ppm confirms N-terminus amine coordination, whereas the indole resonances are relatively unchanged suggesting N-terminal amine coordination rather than via indole amine. Ala (Δ0.56 ppm) and Trp (Δ0.11 ppm) α-C protons shift downfield and are in agreement with **8** and **9**.

^{13}C NMR Analysis.

The ^{13}C NMR spectrum collected for the ligands **1**-**3** (Appendix Table 3) and complexes **5**,**7**-**10** (Table 3-2) were tabulated and compared. Assignments for the carbon spectrum were aided by the 2D-NMR technique HSQC (which displays ^{13}C and ^{1}H homonuclear coupling). As expected, all α-carbons shifted downfield, while Ala α-carbons undergo the largest downfield shifts and have the broadest range.

The most significant and difficult ^{13}C assignments belonged to the carbonyl carbons. In order to confidently assign these signals, DFT calculations were used to elucidate coordination modes and to calculate the ^{13}C chemical shifts. These calculations are based on the optimized geometries found in Figure 3.1. Table 3-3 shows a comparison of observed and calculated carbonyl ^{13}C chemical shifts, which are adjusted for systematic differences in shielding values. For **5** and **7** there is decent agreement between the observed and calculated values for Gly and Asp esters, and Asp amides however, the Ala amide shows stronger deshielding then calculations suggest. Coordination of the ester carbonyl ($C{=}O_{Gly}$), seen in **8** and **10**, is accompanied by a large downfield shift from ~170 (**1**-**3**) to ~186 ppm which is consistent with reported values. [142] Due to the lability of **9**, this peak was not observed, even in the high temperature NMR experiment.

*Table 3-3. Assigned ^{13}C NMR resonance for complexes **5**,**7**-**10** compared to calculated values.*

Chemical Shift (ppm)	**5** (obs)	**5** (calc)	**7** (obs)	**7** (calc)	**8** (obs)	**8** (calc)	**9** (obs)	**9** (calc)	**10** (obs)	**10** (calc)
$C{=}O_{Trp/Asp}$	170.14	170.82	169.93	171.07	169.79	171.39	170.75	165.3	172.93	169.9
$C{=}O_{Ala}$	185.17	181.86	185.45	182.5	177.03	177.63	176.26	176.5	178.24	177.11
γ-$C{=}O_{Asp}$	175.91	171.72	175.9	174.71	172.89	172.31	172.58	172.4	—	—
$C{=}O_{Gly}$	172.34	171.34	171.71	173.3	186.47	186.23	?	187.8	186.55	185.82

3.3.2 Infrared Spectroscopy

Infrared spectroscopic data was collected and is detailed for ligands **1**-**3** in Appendix Table 4 and for complexes **5**,**7**-**10** in Table 3-4. For **5**,**7**-**10**, the low energy shift of symmetric and asymmetric stretching modes for NH_2 to energies typical of coordinated N_{amino}, ~3250 - 3100 cm^{-1}, [143] confirm amine coordination, and the Amide I bands, which are mostly ν(C-N) shift to low energy and combine with the Amide II bands; this supports amine/amide backbone chelation. Additionally, palladium to nitrogen vibrational energies appear and are consistent with reported values. [132,143-145]

Vibrational modes for the ligands and complexes were assigned with the aid of DFT calculations, based on relative value sets. Comparative values for observed and calculated carbonyl stretching bands for **8**-**10** are presented in Table 3-5.

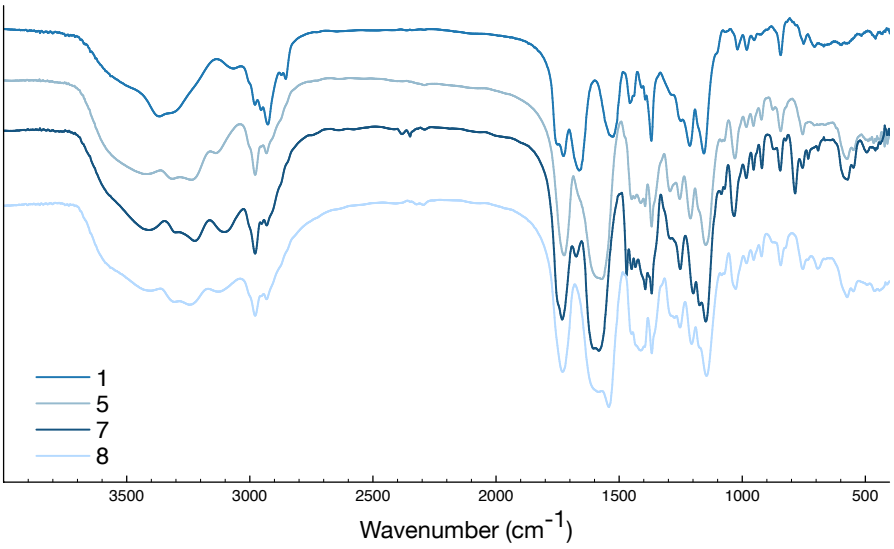

*Figure 3.3. IR spectra for **1**, **5**, and **7-8**.*

For **5**,**7-10**, the low energy shift of symmetric and asymmetric stretching modes for NH_2 to energies typical of coordinated N_{amino}, ~3250 - 3100 cm^{-1}, [143] confirm amine coordination, and the Amide I bands, which are mostly ν(C-N) shift to low energy and combine with the Amide II bands; this supports amine/amide backbone chelation. Additionally, palladium to nitrogen vibrational energies appear and are consistent with reported values. [132,143-145]

*Table 3-4. Summary of infrared data from synthetic experiments to form Pd(II) complexes **5**, **7-10**.*

Frequency (cm^{-1})	**5**	**7**	**8**	**9**	**10**
ν(N—H_2)	3234	3223	3245	3239	3286
ν(N—H)	3138	3100	3129	3121	3235
ν(C=O)					
O^{t}Bu	1723	1732	1729	1732	—
OMe	1748*	1750*	1541	1551	1554
Amide I	1585 1570	1604 1582	1608 1584	1590 1567	1598 1569
ν(C—O)					
O^{t}Bu	1254	1250	1253	1258	—
OMe	1210	1210	1205	1207	1207
ν(O—C)					
O^{t}Bu	1148	1147	1145	1155	—
ν(M—N)	573 548	568 548	573 548	573 533	568 534

*Denotes shoulder absorption.

For **5** and **7** the methyl ester carbonyl band is still present at ~1750 cm^{-1}, indicating that the carbonyl is uncoordinated. Lutidine coordination is confirmed for **7** with the appearance of an aromatic ν(C=C) band at 1471 cm^{-1} (free Lu 1481 cm^{-1}) and by the shift of the out-of-plane CH band to higher frequency (787 cm^{-1}) compared to that of the free ligand (770 cm^{-1}). [143] Unfortunately, Pd-Cl vibrations appear at far-IR frequencies and are not observable. Compared to **5** and **7**, the spectrum for **8** has a strong distinct band at 1541 cm^{-1}, as seen in Figure 3.3. Palladium complexes with similar ester coordination have been synthesized and report a large shift of the ester carbonyl stretching frequency to lower energies [146] upon coordination. This indicates that the methyl ester carbonyl oxygen is coordinated to Pd, resulting in a lower energy shift of ~200 cm^{-1}. This assignment is supported by the calculated relative vibrational frequencies for this complex; a similar band is present in the spectra collected for **9** and **10**, suggesting **8**-**10** have methyl ester carbonyl coordination. In addition, the methyl ester ν(C—O) for **8**-**10** appears to have the same low energy shift of ~ 7 cm^{-1}.

*Table 3-5. Comparative values for ν(C=O) vibrational modes observed versus DFT calculated for **5, 7-10.** The Δ values show the systematic error of the calculated DFT values.*

Complex	ν(C=O) O^{t}Bu	ν(C=O) OMe	ν(C=O) Amide I	ν(C=O) Amide I
5 Obs	1723	1748	1585	1570
DFT	1767	1782	1659	1639
Δ	*44*	*34*	*74*	*69*
7 Obs	1732	1750	1604	1582
DFT	1749	1790	1664	1642
Δ	*17*	*40*	*60*	*60*
8 Obs	1729	1541	1608	1584
DFT	1757	1677	1666	1652
Δ	*28*	*136*	*58*	*68*
9 Obs	1732	1551	1590	1567
DFT	1784	1674	1653	1653
Δ	*52*	*123*	*63*	*86*
10 Obs	—	1554	1598	1569
DFT	—	1652	1677	1662
Δ	—	*98*	*79*	*93*

3.3.3 UV-Vis Spectroscopy

The electronic spectra for complexes **8**-**10** are shown in Figure 3.4. The bathochromic shift of the ligand by ~50 nm is indicative of complexation and confirms coordination of the ligands to the metal, with the CT band at ~345 nm. [147] Strong concentrations are needed to observe the *d-d* transitions (inlay). For **8** this transition is at 450 with ε~184 nm, but was not observed for **9**, likely due to the structural distortion in solution for this complex. Complex **10** displays a large shoulder in this region which masks this transition.

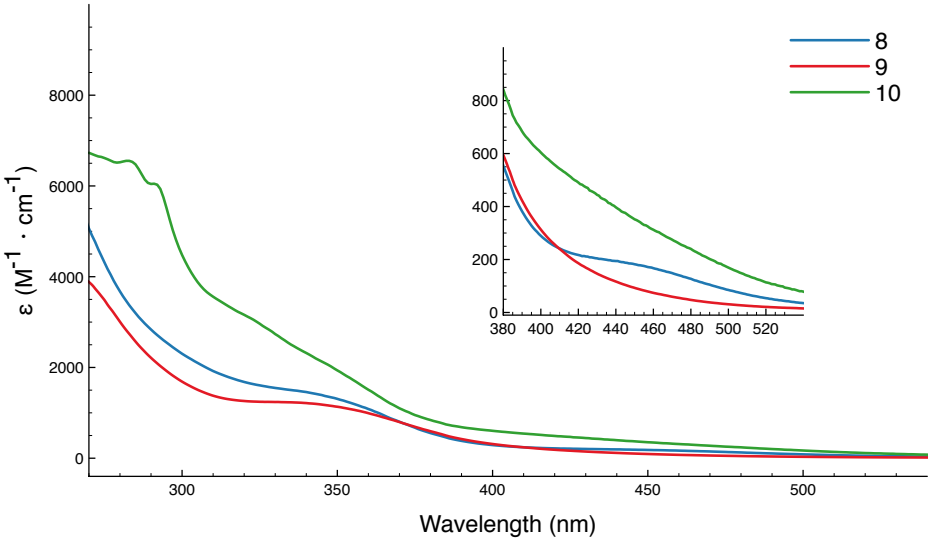

*Figure 3.4. UV-Vis spectra **8-10** (DMSO) taken at micromolar concentrations. Inlay is close up of spectra for **8-10** taken at millimolar concentrations*

3.3.4 Mass Spectrometry

MS spectra were obtained using ESI-MS in the negative ion scan for anions and the positive ion scan for neutral or positive ions. The found ion peaks were simulated with expected isotope patterns to confirm the composition of the compound found compared to the expected composition. Complexes **5a-5c** were obtained in the negative ion mode where the major isotope patterns observed was the [Pd{α-Asp(O^{t}Bu)AlaGly(OMe)}Cl]$^-$ ion, confirming these complexes are the anionic chloride species. The major isotope pattern for the neutral complexes was the M+Na$^+$ species. The isolated compounds showed an excellent match with less than 2 ppm variation in simulated vs found values.

3.4 Conclusions

The development of a non-aqueous synthesis strategy, using a non-nucleophilic base was instrumental in the formation of neutral tetradentate palladium complexes with κ^4[NH$_2$,N,N,=O] coordination. Charged ester carbonyl palladium complexes are reported in the literature, [146] but neutral complexes appear to be much rarer. This coordination mode forms weaker bonds which makes it inherently more difficult to form if more favorable ligands are present. The development of this class of complexes was meant to achieve maximum organosolubility, in order to carry out reactions in non-coordinating solvents. Despite **8** and **9** having multiple functional groups including the methyl and *t*-butyl esters, and an indole present **10**, these complexes are relatively insoluble. These complexes were soluble in DMSO and DMF but were also slightly soluble in acetonitrile and alcohols. However, they were insoluble in most other organic solvents. As a consequence, characterization and reaction studies were carried out in coordinating solvents. The use of this synthetic strategy offers the possibility to facilitate coordination of esters carbonyl oxygen to metals.

3.5 Experimental

3.5.1 Physical Methods

Instrumentation

Infrared spectra were recorded on a Nicolet Avatar 360 FT-IR (E.S.P.) spectrophotometer using KBr pellets. ^{1}H, COSY, and ^{13}C nuclear magnetic resonance spectra were recorded at ambient temperature on a Bruker Avance 400 MHz spectrometer at 400 and 101 MHz, respectively. Solvents used were D_2O, DMSO-d_6, and $CDCl_3$. Electronic spectra were obtained using either Varian Cary 100 Bio spectrophotometer or Perkin Elmer Lambda 25 UV/Vis spectrophotometer. Mass spectra were recorded on a micrOTOF-Q spectrometer, equipped with E-spray atmospheric pressure ionization chamber (ESI). Elemental Analyses were obtained from Midwest Microlab, IN, USA.

Quantum Chemical Calculations

Calculations were performed with a development version ORCA program. [148,149] The density functional theory based protocol consisted of the PBE0-D3BJ functional [150-152] (including the D3 dispersion correction by Grimme and coworkers [153,154]) and the triple-zeta basis set def2-TZVP. [155] The RIJCOSX [156,157] approximation was used to calculate Coulomb and Exchange integrals, using the def2/J auxiliary basis set by Weigend et al. [158] and the GridX5 (ORCA keyword) grid was used. Tighter grids for the exchange-correlation terms were also used (Grid5, FinalGrid6 keywords in ORCA). The CPCM solvation model [159-161] using a Gaussian pointcharge scheme and a scaled vdW surface was used to incorporate solvation effects. Vibrational frequencies were calculated analytically, as implemented in ORCA. [162,163] ^{13}C NMR shieldings were calculated using the same level of theory, except the pcSseg-2 basis sets [164] were utilized on carbon and hydrogen atoms. The calculated shieldings were converted into chemical shifts by calculating the shielding difference with respect to tetramethylsilane at the same level of theory. Chemical shifts were shifted by -15 ppm due to a systematic overestimation.

3.5.2 Materials

Reagents used were purchased from Sigma Aldrich and used without further purification unless otherwise stated. Solvents were purchased from Sigma Aldrich and were distilled under nitrogen and dried using standard methods. [138] $[Pd(CH_3CN)Cl_2]$ was prepared according to the published procedures. [165]

3.5.3 Synthesis

K[Pd{α-Asp(O^{t}Bu)AlaGly(OMe)}Cl] (**5a**):

K_2PdCl_4 (0.040 g, 0.136 mmol) and **1** (0.050 g, 0.136 mmol) were dissolved in H_2O (5 mL) and KOH was added until pH=6.5. Solution was stirred overnight under N_2. The H_2O was removed in vacuo and the product was isolated by dissolving in EtOH and filtering. ^{1}H NMR (400 MHz, DMSO-d_6) δ 4.20 (dd, 1H, NH_{Asp}), 3.84 (d, 1H, NH_{Asp}), 3.69 – 3.57 (m, 2H, α-H_{Gly}), 3.56 – 3.51 (m, 1H, α-H_{Ala}), 3.50 (s, 3H, -$OCH_{3\ Gly}$), 3.43 – 3.36 (m, 1H, α-H_{Asp}), 2.50 (DMSO), 2.48 – 2.42 (m, 1H, β-H_{Asp}), 2.35 – 2.29 (m, 1H, β-H_{Asp}), 1.40 (s, 9H, -$O(CH_3)_{3\ Asp}$), 1.15 (d, 3H, β-H_{Ala}). IR (KBr) cm^{-1}: 3315, 3234 (b, ν(N—H)), 1723 (s,

ν(C=O)), 1585 (s, ν(C=O)), 1570 (s, ν(C—N)), 1254 (s, ν(C—O)), 1210 (s, ν(C—O)), 1148 (s, ν(C—O)). UVVis (H_2O): ε_x MS (ESI/Negative) MW: ($C_{14}H_{23}N_3O_6PdCl$) = 471.2230, M/Z found(calc) = 472.0311(472.0313) [M^-].

(Et_3N)[Pd{α-Asp(O*t*Bu)AlaGly(OMe)}Cl] (**5b**):

$Pd(CH_3CN)_2Cl_2$ (0.076 g, 0.297 mmol) and **1** (0.097 g, 0.297 mmol) were dissolved in dry THF (~20 mL) and triethylamine (0.08 mL, 0.585 mmol) was added. The reaction was stirred overnight under Ar. Solution was filtered through celite and removed in vacuo. Excess yield due to Et_3NCl salt. ^{1}H NMR (400 MHz, DMSO-*d*$_6$) δ 4.21 (dd, 1H, NH_{Asp}), 3.85 (t, 1H, NH_{Asp}), 3.69 – 3.56 (m, 2H, α-H_{Gly}), 3.56 – 3.51 (m, 1H, α-H_{Ala}), 3.50 (s, 3H, -$OCH_{3\ Gly}$), 3.40 (d, 1H, α-H_{Asp}), 3.08 (q, 14H, -$CH_{2\ TEA}$), 2.50 (DMSO), 2.44 (d, 1H, β-H_{Asp}), 2.33 (dd, 1H, β-H_{Asp}), 1.40 (s, 9H, $O(CH_3)_{3\ Asp}$), 1.23 – 1.13 (m, 24H, $O(CH_3)_{3\ Asp}$,-$CH_{3\ TEA}$). IR (KBr) cm^{-1}: 3313, 3215 (b, ν(N—H)), 1750 (s, ν(C=O)), 1724 (s, ν(C=O)), 1601 (s, ν(C=O)), 1583 (s, ν(C—N)), 1250 (s, ν(C—O)), 1210 (s, ν(C—O)), 1148 (s, ν(C—O)).

(PPh_4)[Pd{α-Asp(O*t*Bu)AlaGly(OMe)}Cl] (**5c**):

PPh_4Cl (0.128 g, 0.293 mmol) and **5b** (0.220 g, 0.586 mmol) were dissolved in dry THF. The resulting precipitate was filtered. ^{1}H NMR (400 MHz, Chloroform-*d*) δ 7.98 – 7.91 (m, 4H, PPh_{para}), 7.81 (td, 8H, PPh_{meta}), 7.69 – 7.60 (m, 8H, PPh_{ortho}), 7.26($CDCl_3$), 4.01 – 3.85 (q, 2H, α-H_{Gly}), 3.96 (m, 1H, α-H_{Ala}), 3.64 (d, 1H, α-H_{Asp}), 3.58 (s, 3H, $OCH_{3\ Gly}$), 2.82 (d, 1H, β-H_{Asp}), 2.50 (dd, 1H, β-H_{Asp}), 1.42 (s, 9H, -$O(CH_3)_{3\ Asp}$), 1.35 (d, 3H, β-H_{Ala}). IR (KBr) cm^{-1}: 3314, 3215 (b, ν(N—H)), 1750 (s, ν(C=O)), 1724 (s, ν(C=O)), 1601 (s, ν(C=O)), 1583 (s, ν(C—N)), 1250 (s, ν(C—O)), 1194 (s, ν(C—O)), 1138 (s, ν(C—O))

Pd{D(O*t*Bu)AG(OMe)}(Lu) (**7**):

1 (0.097 g, 0.293 mmol) and 2,6-lutidine (0.064 mL, 0.585 mmol) were dissolved in THF (20 mL). $Pd(OAc)_2$ (0.066 g, 0.293 mmol) was added and the reaction stirred under Ar overnight. The solution was filtered, the volume reduced in vacuo and precipitated out and washed with Et_2O. ^{1}H NMR (400 MHz, DMSO-*d*$_6$) δ 7.78 (t, 1H, Lu$_{para}$), 7.33 (dd, 2H, Lu$_{meta}$), 4.76 (dd, 1H, NH_{Asp}), 4.15 (t, 1H, NH_{Asp}), 3.71 – 3.60 (m, 1H, α-H_{Ala}), 3.54 (q, 1H, α-H_{Asp}), 3.34 (s, 3H, -$OCH_{3\ Gly}$), 3.18 (s, 6H, Lu$_{CH3}$), 3.14 (d, 1H, α-H_{Gly}), 2.91 (d, 1H, α-H_{Gly}), 2.57 (dd, 1H, β-H_{Asp}), 2.50 (DMSO), 2.45 – 2.34 (m, 1H, β-H_{Asp}), 1.41 (s, 9H, -$O(CH_3)_{3\ Asp}$), 1.23(m, 3H, β-H_{Ala}). ^{13}C NMR (101 MHz, DMSO) δ 185.45 (C=O_{Asp}), 175.90 (C=O_{Ala}), 171.70 (C=O_{Gly}), 169.93 (γ-C=O_{Asp}), 160.12 (Lu$_{ortho}$), 159.69 (Lu$_{ortho}$), 139.08 (Lu$_{para}$), 122.72 (Lu$_{meta}$), 122.60 (Lu$_{meta}$), 80.14 (O<u>C</u>$(CH_3)_{3\ Asp}$), 57.13 ($OCH_{3\ Gly}$), 56.50 (α-C_{Asp}), 50.79 (α-C_{Ala}), 45.84 (α-C_{Gly}), 39.73 (β-C_{Asp}), 39.52(DMSO), 27.79 ((OC(<u>C</u>$H_3)_{3\ Asp}$), 25.86 (Lu$_{CH3}$), 25.77 (Lu$_{CH3}$), 19.78 (β-C_{Ala}). IR (KBr) cm^{-1}: 3303, 3223 (b, ν(N—H)), 1750 (s, ν(C=O)),1732 (s, ν(C=O)), 1604 (s, ν(C=O)), 1582 (s, ν(C—N)), 1250 (s, ν(C—O)), 1200 (s, ν(C—O)), 1147 (s, ν(C—O)). MS (ESI/Positive) MW: ($C_{21}H_{32}N_4O_6Pd$) = 542.9290, M/Z found(calc) = 565.1254(565.1257) [M+Na^+]

Pd{α-Asp(O*t*Bu)AlaGly(OMe)} (**8**):

1 (0.331 g, 1.000 mmol) and Proton Sponge (0.536 g, 2.500 mmol) were dissolved in THF (20 mL). $Pd(OAc)_2$ (0.224 g, 1.000 mmol) was added and the reaction stirred under Ar for 5 h. The solution was concentrated in vacuo and precipitated out with several additions of EtOAc and toluene. Product was recrystallize as a purple solid from acetonitrile and EtOAc (0.295 g, 67.7%) ^{1}H NMR (400 MHz, DMSO-*d*$_6$) δ 5.04 (t, 1H, NH_{Asp}), 4.55 (t, 1H, NH_{Asp}), 3.95 – 3.79 (m, 2H, α-H_{Gly}), 3.68 (q, 1H, α-H_{Ala}), 3.56 (s, 1H, α-H_{Asp}), 3.55 (s, 3H, -OCH_3

$_{Gly}$), 2.61 (dd, 1H, β-H_{Asp}), 2.50 (DMSO), 2.48 – 2.42 (m, 1H, β-H_{Asp}), 1.42 (s, 9H, -O(CH_3)$_{3\ Asp}$), 1.20 (d, 3H, β-H_{Ala}). ^{13}C NMR (101 MHz, DMSO) δ 177.03(C=O_{Asp}), 172.89(C=O_{Ala}), 169.79(γ-C=O_{Asp}), 99.49(C=O_{Gly}), 80.47(-O<u>C</u>(CH_3)$_{3\ Asp}$), 56.59($OCH_{3\ Gly}$), 55.80(α-C_{Asp}), 50.93(α-C_{Ala}), 46.79(α-C_{Gly}), 39.94(β-C_{Asp}), 39.52(DMSO), 27.79(-OC(<u>C</u>H_3)$_{3\ Asp}$), 19.80(β-C_{Ala}). IR (KBr) cm^{-1}: 3313, 3245 (b, ν(N—H)), 1731 (s, ν(C=O)), 1588 (s, ν(C=O)), 1541 (s, ν(C—N)), 1253 (s, ν(C—O)), 1206 (s, ν(C—O)), 1145 (s, ν(C—O)). UVVis (DMSO): ε_{335} = 1520 L/mol·cm MS (ESI/Positive) MW: ($C_{14}H_{25}N_3O_6Pd$) = 435.7730, M/Z found(calc) = 458.0515(458.0520) [M+Na^+]. CHN ($C_{14}H_{23}N_3O_6Pd$) found(calc) %: C: 38.36(38.59), H: 5.25(5.32), N: 9.64(9.64)

Route 2: α-D(O^{t}Bu)AG(OMe) (0.120 g, 0.362 mmol) dissolved in 10 ml H_2O was added to an aqueous solution of K_2PdCl_4 (0.146 g, 0.362 mmol) in 20 mL H_2O. The pH was increased to 10 with KOH and stir for 0.5 h. The water was removed, and the product was isolated by dissolving in acetonitrile and filtering. Presence of **8** was confirmed spectroscopically, but purification was unsuccessful.

Pd{β-Asp(O^{t}Bu)AlaGly(OMe)} (**9**):

2 (0.331 g, 1.000 mmol) and Proton Sponge (0.536 g, 2.500 mmol) were dissolved in THF (20 mL). $Pd(OAc)_2$ (0.224 g, 1.000 mmol) was added and the reaction stirred under Ar for 5 h. The solution was concentrated in vacuo and precipitated out with several additions of EtOAc and toluene. Product was recrystallize as a red-orange solid from acetonitrile and EtOAc (0.295 g, 67.7%) ^{1}H NMR (400 MHz, DMSO-d_6) δ 4.62 (m, 1H, NH_{Asp}), 4.48 (m, 1H, NH_{Asp}), 3.95 (m, 1H, α-H_{Ala}), 3.72 – 3.52 (m, 2H, α-H_{Gly}), 3.56 (s, 3H, -$OCH_{3\ Gly}$), 3.18 (s, 1H, α-H_{Asp}), 2.50 (DMSO), 2.44 – 2.22 (m, 2H, β-H_{Asp}), 1.44 (s, 9H, -O(CH_3)$_{3\ Asp}$), 1.08 (d, 3H, β-H_{Ala}). ^{13}C NMR (101 MHz, DMSO) δ 172.88(C=O_{Asp}), 171.14(C=O_{Ala}), 170.16 (γ-C=O_{Asp}), 99.49(C=O_{Gly}), 82.32 (O<u>C</u>(CH_3)$_{3\ Asp}$), 51.26 ($OCH_{3\ Gly}$), 54.70 (α-C_{Asp}), 59.14 (α-C_{Ala}), 46.20 (α-C_{Gly}), , 41.09 (β-C_{Asp}), 39.52(DMSO), 28.13 (OC(<u>C</u>H_3)$_{3\ Asp}$), 21.07 (β-C_{Ala}). IR (KBr) cm^{-1}: 3313, 3245 (b, ν(N—H)), 1731 (s, ν(C=O)), 1588 (s, ν(C=O)), 1541 (s, ν(C—N)), 1253 (s, ν(C—O)), 1206 (s, ν(C—O)), 1145 (s, ν(C—O)). UVVis (DMSO): ε_{333} = 1260 L/mol·cm MS (ESI/Positive) MW: ($C_{14}H_{25}N_3O_6Pd$) = 435.7730, M/Z found(calc) = 458.0515(458.0520) [M+Na^+]. CHN ($C_{14}H_{23}N_3O_6Pd$) C: 38.28(38.59), H: 5.24(5.32), N: 9.69(9.64)

Pd{TrpAlaGly(OMe)} (**10**)

3 (0.143 g, 0.413 mmol) and Proton Sponge (0.221 g, 1.032 mmol) were dissolved in THF (20 mL). $Pd(OAc)_2$ (0.093 g, 0.413 mmol) was added and the reaction stirred under Ar for 5 h. The solution was concentrated in vacuo and precipitated out with Et_2O. The orange solid was collected and washed with portions of EtOAc and Et_2O. Hot CH_3CN was used to redissolve the product, product was filtered and concentrated in vacuo. (0.169 g, 90.0%). ^{1}H NMR (400 MHz, DMSO-d_6) δ 10.90 (d, 1H, NH_{indole}), 7.55 (d, 1H, $H_{indole\text{-}C7}$), 7.37 (d, 2H, $H_{indole\text{-}C4}$), 7.27 (d, 2H, $H_{indole\text{-}C2}$), 7.09 (ddd, 1H, $_{indole\text{-}C5}$), 6.99 (ddd, 1H, $H_{indole\text{-}C6}$), 4.96 (t, 1H, NH_{Trp}), 4.24 (t, 1H, NH_{Trp}), 3.96 (d, 1H, α-H_{Gly}), 3.83 (d, 1H, α-H_{Gly}), 3.82 – 3.75 (m, 2H, α-H_{Ala}), 3.55 (s, 4H, $ROCH_{3\ Gly}$), 3.40 (dt, 2H, α-H_{Trp}), 3.28 (dd, 1H, β-H_{Trp}), 2.87 (dd, 2H, β-H_{Trp}), 1.24 (d, 3H, β-H_{Ala}). ^{13}C NMR (101 MHz, DMSO) δ 178.24(C=O_{Trp}), 172.93(C=O_{Ala}), 136.37($C3_{indole}$), 127.11($C8_{indole}$), 123.99($C2_{indole}$), 121.10($C5_{indole}$), 118.44($C6_{indole}$), 118.24($C7_{indole}$), 111.41($C4_{indole}$), 109.47($C1_{indole}$), 67.00, 59.58(α-C_{Gly}), 56.50($OCH_{3\ Gly}$), 50.93(α-C_{Ala}), 46.86(α-C_{Gly}), 39.52(DMSO), 29.93(β-C_{Trp}), 19.92(β-C_{Ala}). IR (KBr) cm^{-1}: 3370, 3286, 3235(b, ν(N—H)), 1741(s, ν(C=O)), 1569(sh)(s, ν(C=O)), 1543(ν(C—N)), 1333, 1070, 1010(ν(C—N)), 1105(sh), 1025, 981(ν(C—N)), 1207 (ν(C—

O)), 1178 (s, ν(C—O)). UVVis (DMSO): ε_{317} = 3239, ε_{344} = 2188 L/mol·cm MS (ESI/Positive) MW: ($C_{17}H_{20}N_4O_4Pd$) = 450.7910, M/Z found(calc) = 437.0417(437.0419) [M+Na^+]. CHN ($C_{17}H_{20}N_4O_4Pd$) found(calc) %: C: 44.51(43.55), H: 4.73(4.73), N: 11.47(11.95)

4 Synthesis and Characterization of Nickel Tripeptide Complexes

4.1 Synthetic Methodology

In this chapter the synthesis of new nickel tripeptide complexes is described. Isolated products obtained were highly dependent on starting materials, and several combinations of Ni(II) salts, bases and solvent systems were attempted for synthesis of Ni(II) complexes. Nickel is known to promote the deprotonation and coordination of amides at pH values ~8-9, [109] and methyl ester is labile under basic conditions. [112] Considering this, hydrolysis of the methyl ester upon nickel complexation was expected owing to elevated pH values required for aqueous synthesis. However, both ester protecting groups were shown to be susceptible to hydrolysis depending on synthetic conditions. Attempts to form neutral Ni(II) tripeptide complexes were unsuccessful. A summary of the synthetic routes employed to synthesize di-hydrolyzed tripeptide complexes is shown in Scheme 4-1; whereas the synthetic pathways towards mono-hydrolyzed complexes are found in Scheme 4-2.

4.1.1 Aqueous Synthesis

Using an aqueous synthesis strategy, *in situ* formation of $Ni(OH)_2$ was achieved by the addition of KOH and Ni(II) starting material. [166] The ligands **1-3** were dissolved in H_2O, and the Ni(II) hydroxide and tripeptide solutions were added together; the pH was increased to 10 with KOH, and the mixture stirred between 0.5-2 h. The reaction mixture was filtered, and the water removed. The product was isolated by dissolving it in alcohol, filtering, and precipitating from the filtrate by addition of ether. Several factors determined what product formed, including order of addition and the starting Ni(II) compound used.

4.1.2 Metal Salt Effects

Nickel Acetate as Starting Material

Complexing $Ni(CH_3CO_2)_2$ to **1** resulted in the di-hydrolyzed species $[Ni\{\alpha\text{-AspAlaGly}\}]^{2-}$, which was confirmed by mass spectrometry. However, different preparations revealed different ^1H NMR spectra (Table 4-1). When the Ni(II) solution was added to the aqueous solution of the ligand, the species generated in Table 4-1, **11a**, was observed; but in a reversed addition procedure, the product **11b** was formed. In both **11a** and **11b**, significant upfield shifts in the α-C protons, which are centralized between 3.50-3.30 ppm, were observed. This is a strong indication of coordination between nickel and the amine/amide nitrogens. C-terminus carboxylate coordination is well known in tripeptide coordination [90] and the emergence of a quadruplet pattern with a large coupling constant (~20 Hz), from loss of free rotation for the Gly α-C protons, suggests carboxylate coordination for both **11a** and **11b**. Applying these synthetic conditions by adding the Ni(II) solution to ligand **2**, the

di-hydrolyzed complex [Ni{β-AspAlaGly}]$^{2-}$ (**12a**) was formed, along with a minor isomeric product (<5%).

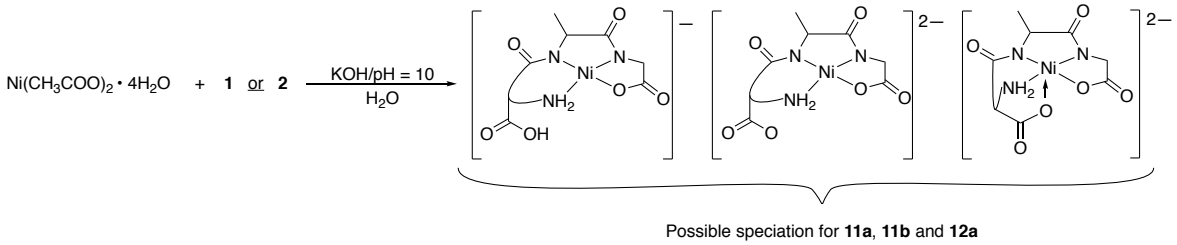

*Scheme 4-1. Synthetic route to form isomers **11** and **12**, where **11a**, **11b** and **12a** are possible isomers for the dianionic complexes formed from **1** and **2**.*

Examining the difference between **11a** *versus* **11b**, and **12a** *versus* its minor isomer, it is unclear what these structural isomers are. As these are di-hydrolyzed species in aqueous solutions, the coordination preference is not obvious. The resonances which experience the largest change were on the Asp α-C protons, which are closest to the carboxylate. These spectra were taken in D_2O which could mean pH-dependent resonance shifts. Less likely is the formation of a five-coordinate isomer with square pyramidal geometry. [167,168] Scheme 4-1 outlines possible isomers for the di-hydrolyzed anionic species **11a**, **11b** and **12a**. Due to the inconsistent behavior and difficulty in reproducing the synthesis of these species, other approaches were tested, and a method developed that consistently forms the monoanionic complexes.

*Table 4-1. ^{1}H NMR data in D_2O forming mono- and di-hydrolyzed Ni(II) complexes with **1** and **2**, where **11a** and **11b** are [Ni(α-AspAlaGly)]$^{2-}$, **12a** is [Ni(β-AspAlaGly)]$^{2-}$, **13** is K[Ni(α-Asp(O^{t}Bu)AlaGly)], and **14** is K[Ni(β-Asp(O^{t}Bu)AlaGly)]*

Chemical Shift (ppm)	**11a**	**11b**	**12a**	**13**	**14**
α-C_{Ala}	3.48	3.58	3.54	3.57	3.76
α-C_{Gly}	3.50-3.30	3.55-3.38	3.57-3.40	3.63-3.31	3.65-3.21
α-C_{Asp}	3.40	3.53	2.55 2.41	3.51	2.34 2.18
β-C_{Asp}	2.47 2.32	2.71	3.50	2.61	3.57
$OC(CH_3)_{3\ Asp}$	—	—	—	1.65	1.60
β-C_{Ala}	1.14	1.19	1.22	1.23	1.19

Nickel Chloride as Starting Material

Maintaining the same general procedure, but exchanging the metal starting material to $NiCl_2$, resulted in the mono-anionic species K[Ni{α-Asp(O^{t}Bu)AlaGly}] (**13**). Adding the Ni(II) solution to the ligand resulted in base catalyzed hydrolysis of the methyl ester but preserved the *t*-butyl ester, identified by mass spectrometry and ^{1}H NMR. (Table 4-1, **13**). *In situ* formation of the $Ni(OH)_2$ intermediate is dependent of the rate of dissociation for $NiCl_2$ *versus* $Ni(CH_3CO_2)_2$, where $NiCl_2$ dissociates faster and the slightly soluble $Ni(OH)_2$

precipitates more rapidly with excess base leading to the ligand experiencing base concentration dependent on the rate of $Ni(OH)_2$ formation.

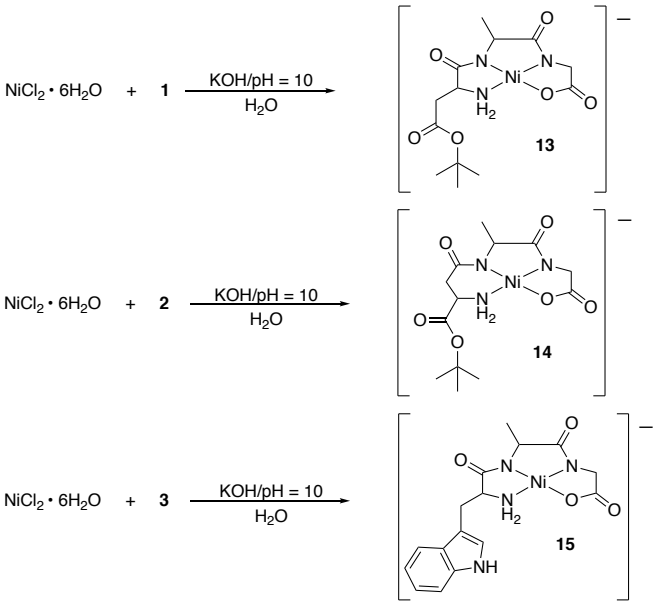

*Scheme 4-2. Synthetic route to form mono-anionic complexes **13-15**.*

The monoanionic species also has a large upfield shift in the α-C protons, and a large coupling constant for the Gly protons, indicating $\kappa^4[NH_2,N,N,O]$ chelation. The aqueous synthesis using $NiCl_2$ was then applied to ligands **2** and **3** to form the K[Ni{β-Asp(O^{t}Bu)AlaGly}] (**14**) and K[Ni{α-TrpAlaGly}] (**15**) (Scheme 4-2).

4.1.3 Non-Aqueous Synthesis

Attempts to form the neutral Ni-tripeptide complexes in non-aqueous conditions were unsuccessful. Various non-coordinating starting complexes were used including $Ni(F_3CSO_3)_2$ and $[Ni(CH_3CN)_6]^{2+}$. Using elevated temperatures and longer reaction times did not result in any single isolatable product. Several bases were also employed including "Proton Sponge", which was used to form the neutral palladium complexes **8**-**10**, but proved unsuccessful for nickel. It is believed that the weaker Lewis acid nature of nickel does not readily form metal carbonyl bonds, unlike palladium.

4.2 Calculations

DFT calculations with a continuum solvation model were employed to determine the lowest energy structures in solution for complexes **13**-**15** which can be seen in Figure 4.1. Several different conformational possibilities, including square pyramidal, were explored computationally. Both the mono- and di-hydrolyzed Ni(II) complexes are preferably square planar and $\kappa^4[NH_2,N,N,O]$ coordination was expected. DFT calculations were in agreement. Due to the conformational flexibility of the tripeptide ligand, a number of conformers for each complex are available (primarily due different orientations of the Asp or Trp

sidechains) but only the lowest energy conformer was considered in the calculations of spectroscopic properties.

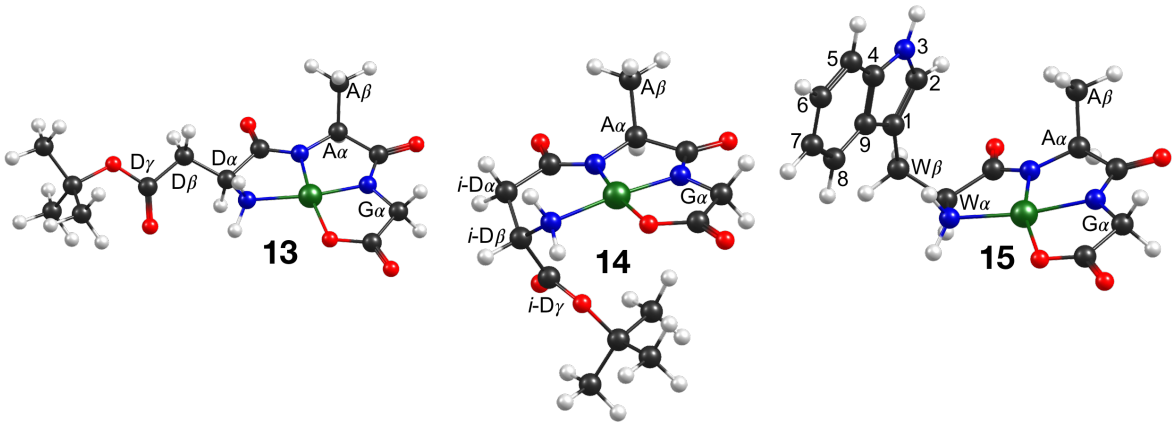

*Figure 4.1. DFT optimized structures of complexes **13-15***

4.3 Characterization

Complexes **11-15** were characterized via NMR, IR, and UV-Vis spectroscopy, mass spectrometry and elemental analysis. Quantum chemical calculations at the DFT level were used to aid the spectral interpretation. In order to correctly assign coordination geometries, similarities and differences in the complex NMR chemical shifts, and shifts in infrared frequencies of major bands were examined. Observed values were compared to calculated vibrational frequencies of the DFT-optimized structural models.

4.3.1 ^{1}H- And ^{13}C-NMR Spectroscopy

^{1}H NMR Analysis.

The coordinated amine/amide backbone is a commonality of **11-15**; this coordination is established in the proton NMR (Table 4-1(D_2O), & Table 4-2(DMSO-d_6)). Throughout the series **11-15** there is large upfield shift to all the side chain protons because the complexes are negatively charged and thus experience more shielding. This is in agreement with the reported behavior of Ni(II) tripeptide complexes. [111,169] The Ala α-C protons tend to shift the most and exhibit the largest ppm range, which is expected considering the Asp amide experience *trans*-influences from the carboxylate.

Examining the ^{1}H spectra for **13-15** in DMSO (Table 4-2), a better understanding of coordination geometries can be ascertained. The appearance of the NH_2 protons at ~3.60 - 2.20 ppm confirms amine coordination, while the Gly α-C protons all shift a comparative value and appear as a quadruplet with coupling constant of ~20 Hz, suggesting carbonyl coordination. However, there is very little shift related to the *t*-butyl ester. This suggests **13-15** have a common $\kappa^4[NH_2,N,N,O]$ coordination mode.

Complex **15** exhibits a unique upfield shift to one coordinated amine proton at 2.20 ppm; this strong shielding effect, coupled with a downfield shift of the indole C2 proton, is likely related to strong hydrogen bonding.

*Table 4-2. Assigned ^{1}H NMR data for complexes **13-15** in DMSO-d_6.*

Chemical Shift (ppm)	**13**	**14**	**15**
N—H_2	3.57 3.03	3.37 3.11	3.62 2.20
α-C_{Ala}	3.02	3.29	3.10
α-C_{Gly}	2.99	2.96	2.97
α-$C_{Trp/Asp}$	3.07	2.01 1.87	2.96
β-$C_{Trp/Asp}$	2.39 2.21	2.90	2.96 2.72
$OC(CH_3)_{3\ Asp}$	1.41	1.39	—
β-C_{Ala}	1.00	0.94	1.00

Trp side chain listed in Experimental Section 3.5.3

^{13}C NMR Analysis.

The ^{13}C NMR spectrum collected in DMSO-d_6 for the ligands **1-3** appears in Appendix Table 3 while tabulated data for complexes **13-15** in DMSO-d_6 can be seen in Table 4-3. Assignments for the carbon spectrum were aided by the 2D-NMR technique HSQC. As expected, all of the α-carbons shifted downfield, while the Ala α-carbons undergo the largest downfield shifts and display the broadest range. The Gly C=O signal for **14** only shifts downfield by ~ 1.5 ppm compared to the expected shifts of 5.5 and 7.0 ppm seen for **13** and **15**, respectively. [170] This is presumably related to the six-membered ring formed in complex **14**.

*Table 4-3. Assigned ^{13}C NMR resonance for complexes **13-15** in DMSO-d_6.*

Chemical Shift (ppm)	**13**	**14**	**15**
$C{=}O_{Trp/Asp}$	182.19	182.23	182.20
$C{=}O_{Ala}$	180.30	180.14	180.37
γ-$C{=}O_{Asp}$	170.17	170.61	—
$C{=}O_{Gly}$	175.71	171.02	177.09
$O\underline{C}(CH_3)_{3\ Asp}$	79.93	80.80	—
α-$C_{Trp/Asp}$	54.53	39.01	57.83
α-C_{Ala}	56.42	58.32	56.39
α-C_{Gly}	48.31	48.66	48.40
β-$C_{Trp/Asp}$	39.02	52.79	28.86
$OC(\underline{C}H_3)_{3\ Asp}$	27.77	27.61	—
β-C_{Ala}	18.65	19.66	18.63

Trp side chain listed in Experimental Section 3.5.3

4.3.2 Infrared Spectroscopy

The infrared spectra were taken as KBr pellets and analyzed in the range of 4000 cm^{-1} to 400 cm^{-1}. Shifts of key bands upon coordination to the Ni(II) were monitored; Table 4-4 shows positions found for these bands. Vibrational modes for the ligands and complexes were assigned with the aid of DFT calculations, based on relative value sets. Comparative values for observed and calculated carbonyl stretching bands for **11-15** are presented in Table 4-5.

In the electronic spectra a low energy shift of the symmetric and asymmetric stretching modes for NH_2 to energies typical for nickel coordinated N_{amino} functions, confirm amine coordination for **11-15**. Whereas support for amine/amide backbone chelation is found in the low energy shifts of the Amide I band by 50-100 cm^{-1}, which converges with the Amide II band. The ν(Ni—N) is observed at values consistent with literature values. [143]

Ester hydrolysis to an acid would result in a *t*-butyl ester band shifting to ~1730-1700 cm^{-1}. However, **11a** and **12a** shift further down into the strong Amide I band This is accompanied by a strong absorption at ~1400 cm^{-1}, which is characteristic of a carboxylate anion, Highly suggesting that the Asp side chain does not coordinate to the metal and remains deprotonated (represented as the isomer in the middle of Scheme 4-1).

*Table 4-4. Assigned Infrared vibrations for complexes **11-15***

Frequency (cm^{-1})	**11a**	**12a**	**13**	**14**	**15**
ν(N—H_2)	3411	3398	3401	3396	3396
ν(N—H)	3308	3246	3308	3257	3292
ν(C=O)					
O^{t}Bu	1595†	1602†	1722	1729	—
OMe	1653*†	1667*†	1653*†	1656*†	1651*†
Amide I	1595	1602 1560	1597	1600 1562	1593
ν(C—O)					
O^{t}Bu	1153	1156	1254 1146	1257 1155	—
OMe	1290	1292	1289	1282	1290
ν(M—N)	468	453	466	470	469

* denotes shoulder bands †- hydrolyzed acid

The ν(C=O) for the C-terminus carbonyl (OMe) shift to a lower energy to frequencies of ~1650 cm^{-1} upon hydrolysis and coordination. This is consistent with calculated values shown in Table 4-5. There is a systematic error value between the calculated and observed frequencies of ~60 cm^{-1}, and taking this into account, most carbonyl stretching frequencies are in good agreement with values calculated from the DFT optimized geometries shown in Figure 4.1.

*Table 4-5. Comparative values for ν(C=O) vibrational modes observed vs. calculated for **11-15**. The Δ values show the observed deviation between observed and calculated vibrational frequencies.*

Complex	ν(C=O) O^{t}Bu	ν(C=O) OMe	ν(C=O) Amide I	ν(C=O) Amide I
11a Obs	1595†	1653†	1595	1595
DFT	1657	1681	1654	1652
Δ	*62*	*28*	*59*	*57*
12a Obs	1602†	1648†	1602	1560
DFT	1654	1683	1655	1612
Δ	*52*	*35*	*53*	*52*
13 Obs	1724	1653†	1597	1597
DFT	1766	1684	1664	1656
Δ	*44*	*31*	*67*	*59*
14 Obs	1729	1656†	1600	1562
DFT	1780	1687	1657	1622
Δ	*51*	*31*	*57*	*60*
15 Obs	—	1651†	1593	1593
DFT	—	1674	1661	1654
Δ	—	*23*	*68*	*61*

†-Denotes the hydrolyzed acid.

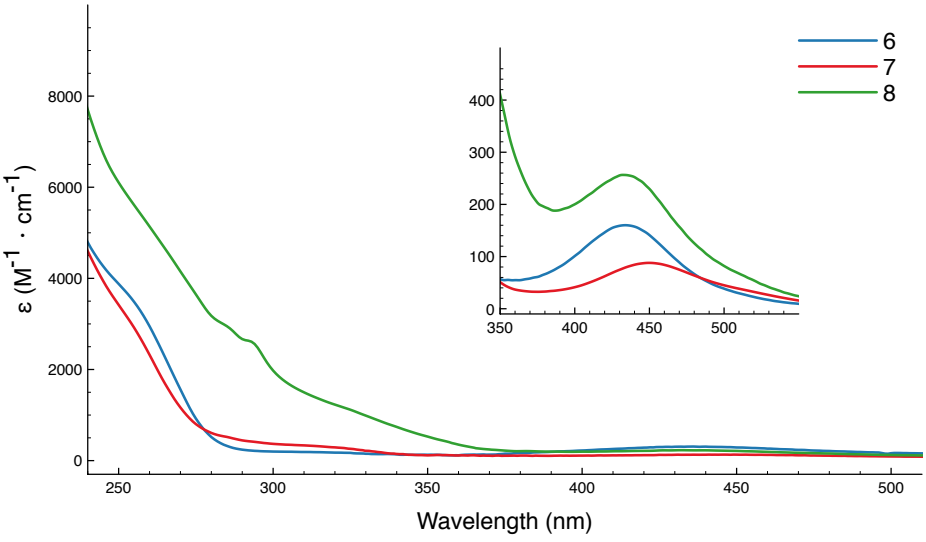

*Figure 4.2. UV-Vis spectra **13-15** in H_2O taken at micromolar concentrations. Inlay is close up of spectra for **13-15** taken at millimolar concentrations.*

4.3.3 UV-Vis Spectroscopy

The electronic spectra for complexes **13-15** are shown in Figure 4.2. The spectra display bands at ~255 nm that based on the molar extinction coefficient, are thought to be CT bands.

Strong concentrations are needed to observe the *d-d* transitions (inlay). The two complexes that have κ^4[5,5,5] chelation (**13** and **15**) show *d-d* transitions at 434 nm, but complex **14**, which has κ^4[6,5,5] chelation has a lower energy transition at 450 nm. This could be due to the added lability of the 6 membered ring distorting the square planar geometry.

4.3.4 Mass Spectrometry

Mass spectra were obtained using ESI-MS in the negative ion scan. The found ion peaks were simulated with expected isotope patterns to confirm the composition of the compound found compared to the expected composition. Mass spectrometry data for **11-15** is listed in the experimental section of this chapter. The isolated compounds showed an excellent match with less than 2 ppm variation in simulated *vs.* found values.

4.4 Electrochemistry

The electrochemistry of the complexes was explored in water. The cyclic voltammograms were run for 2 mM solutions of **11a**, **12a**, and **15** and 0.25 M in KNO_3 as supporting electrolyte, Ag/AgCl was used as the reference electrode. Both DFT calculations and IR spectroscopic data suggest that the mono- and di-anionic species have the same coordination geometry, thus the electrochemistry for the mono- and di-anionic complexes is assumed to be similar. The data are summarized in Table 4-6.

In general the redox behavior is irreversible. The ligands show strong irreversible reduction at values lower than -600 millivolts. Ligand **2** shows a single reduction wave at -616 mV while ligand **1** has two at -634 mV and at -940 mV. The data for ligand **3** was not obtained but complex **15** shows reduction similar to **11a** at -661 mV that is likely the ligand based reduction.

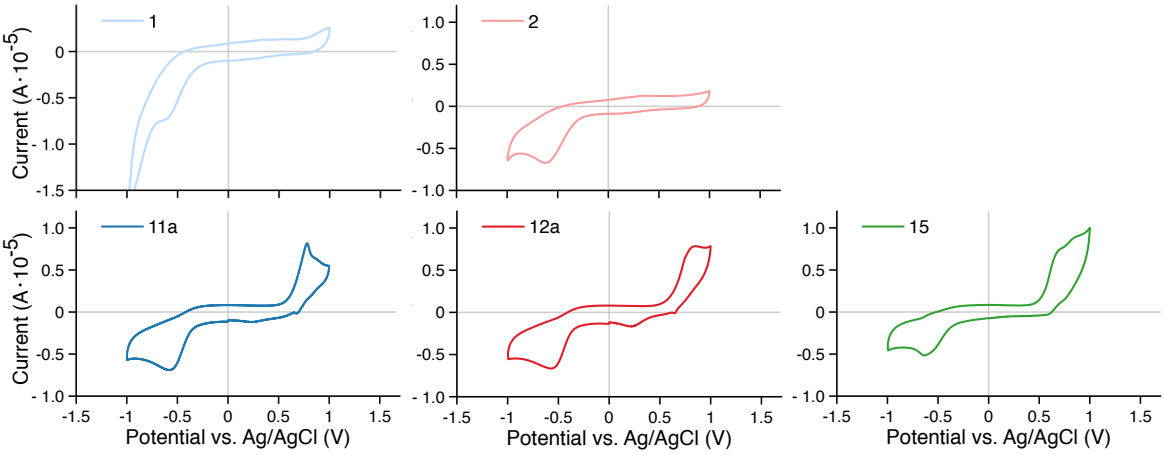

*Figure 4.3. Electrochemical CV traces of Ni(II) complexes **11a**, **12a**, and **15** and ligands **1-2** in water.*

Table 4-6. List of potentials and peak currents for Cyclic Voltammetry experiments in aqueous solution with 0.25 M KNO_3 vs. Ag/AgCl.

Complex	Potential, E (mV)	Current, I_p, Ax10^{-5}	Complex	Potential, E (mV)	Current, I_p, Ax10^{-5}	Complex	Potential, E (mV)	Current, I_p, Ax10^{-5}
11a	218	-0.118	**12a**	214	-0.166	**15**	794	0.828
	643	-0.0092		875	0.781		929	0.927
	794	0.787		607	-0.0046		691	0.092
	911	0.595		-571	-0.665		-661	-0.504
	-589	-0.689	**2**	-616	-0.672			
1	-634	-0.742						
	-940	-1.53						

The complexes show irreversible oxidations. Traces of **11a** and **12a** are very similar except the **11a** shows two irreversible oxidations and **12a** only one. The **11a** oxidations were observed at 794 and 911 mV, and **12a** oxidation wave was observed at 875 mV. The **11a** and **12a** show irreversible metal-based reduction at 218 and 214 mV respectively. Complex **15** exhibits two oxidation waves at 794 and 929 mV, and a weak irreversible reduction at 691 mV that is presumed metal based.

4.5 Conclusions

The synthesis of di- and mono- anionic nickel complexes based on the tripeptides α-Asp(O^{t}Bu)AlaGly(OMe), β-Asp(O^{t}Bu)AlaGly(OMe), and TrpAlaGly(OMe) were carried out in aqueous solutions by *in situ* formation of $Ni(OH)_2$. The complexes are air and water soluble. The starting material has a profound influence on the products formed. Complex **11**-**15** were isolated in the κ^4[NH_2,N,N,O] coordination mode with hydrolyzed ester carboxylate occupying the metal center 4th coordination site, and DFT calculations and IR data suggest that the mono- and di-anionic species have the same coordination geometry. Attempts to make the neutral nickel complexes were unsuccessful. Characterization of these complexes was aided by DFT calculations. Cyclic voltammograms of **11a** and **12a** show irreversible metal-based reduction at 218 and 214 mV respectively, while **15** exhibits a weak irreversible reduction at 691 mV that is presumed metal based.

4.6 Experimental

4.6.1 Physical Methods

Instrumentation

Infrared spectra were recorded on a Nicolet Ava- tar 360 FT-IR (E.S.P.) spectrophotometer using KBr pellets. ^{1}H, COSY, and ^{13}C nuclear magnetic resonance spectra were recorded at ambient temperature on a Bruker Avance 400 MHz spectrometer at 400 and 101 MHz, respectively. Solvents used were D_2O, DMSO-d_6, and $CDCl_3$. Electronic spectra were

obtained using either Varian Cary 100 Bio spectrophotometer or Perkin Elmer Lambda 25 UV/Vis spectrophotometer. Cyclic voltammetric measurements were recorded on EC Epsilon Eclipse™ Potentiostat/Galvanostat. Mass spectra were recorded on a micrOTOF-Q spectrometer, equipped with E-spray atmospheric pressure ionization chamber (ESI). Elemental Analyses were obtained from Midwest Microlab, IN, USA.

Quantum Chemical Calculations

Calculations were performed with a development version ORCA program. [148,149] The density functional theory based protocol consisted of the PBE0-D3BJ functional [150-152] (including the D3 dispersion correction by Grimme and coworkers[153,154]) and the triple-zeta basis set def2-TZVP. [155] The RIJCOSX [156,157] approximation was used to calculate Coulomb and Exchange integrals, using the def2/J auxiliary basis set by Weigend et al. [158] and the GridX5 (ORCA keyword) grid was used. Tighter grids for the exchange-correlation terms were also used (Grid5, FinalGrid6 keywords in ORCA). The CPCM solvation model [159-161] using a Gaussian pointcharge scheme and a scaled vdW surface was used to incorporate solvation effects. Vibrational frequencies were calculated analytically, as implemented in ORCA. [162,163] ^{13}C NMR shieldings were calculated using the same level of theory, except the pcSseg-2 basis sets [164] were utilized on carbon and hydrogen atoms. The calculated shieldings were converted into chemical shifts by calculating the shielding difference with respect to tetramethylsilane at the same level of theory. Chemical shifts were shifted by -15 ppm due to a systematic overestimation.

4.6.2 Materials

Reagents used were purchased from Sigma Aldrich and used without further purification unless otherwise stated. Solvents were purchased from Sigma Aldrich and were distilled under nitrogen and dried using standard methods. [138] $Ni(F_3CSO_3)_2$ and $[Ni(CH_3CN)_6]^{2+}$ were synthesized according to established procedure. [171,172]

4.6.3 Synthesis

[Ni{α-AspAlaGly}]$^{2-}$ (**11a**)

$Ni(OAc)_2{\cdot}6\ H_2O$ (0.250 g, 1.005 mmol) and KOH (0.085 g, 1.515 mmol) were dissolved in H_2O (5 mL) and added to a solution of **1** (0.150g, 0.452 mmol) in 5 mL H_2O. KOH was added until pH=10 and the solution was stirred for 0.5 h, then the H_2O was removed in vacuo and the product was isolated by dissolving in iso-propyl alcohol and filtering. ^1H NMR (400 MHz, Deuterium Oxide) δ 3.48 (s, 1H, α-H_{Ala}), 3.40 (d, 1H, α-H_{Asp}), 3.50 – 3.30 (m, 2H, α-H_{Gly}), 2.47 (dd, 1H, β-H_{Asp}), 2.32 (dd, 1H, β-H_{Asp}), 1.14 (d, 4H, β-H_{Ala}). IR (KBr) cm^{-1}: 3397, 3274 (b, ν(N—H)), 1651 (sh, ν(C=O)), 1593 (s, ν(C=O)), 1397 (s, ν(C—O)), 460 (w, ν(Ni—N)) MS (ESI/Negative) MW: ($C_9H_{12}N_3O_6Ni^-$) = 316.9034, M/Z found(calc) = 316.0096(316.0085) [M^-].

[Ni{β-AspAlaGly}]$^{2-}$ (**12a**)

$Ni(OAc)_2{\cdot}6H_2O$ (0.250 g, 1.005 mmol) and KOH (0.085 g, 1.515 mmol) were dissolved, and $Ni(OH)_2$ was formed *in situ*, **2** (0.179 g, 0.540 mmol) was dissolved in H_2O (5 mL) the Ni(II) solution was added to the ligand and the pH was increased with 1 M KOH until a pH of 10 was achieved. Solution was stirred for 2 h then the H_2O was removed in vacuo. The product was redissolved in iso-propyl alcohol and filtered. Product was precipitated out using a

combination of EtOH and EtOAc. (0.144 g, 65%) ^{1}H NMR (400 MHz, Deuterium Oxide) δ 3.89 – 3.73 (m, 1H, α-H_{Ala}), 3.69 (q, 1H, β-H_{Asp}), 3.66 – 3.39 (m, 2H, α-H_{Gly}), 2.55 (d, 1H, α-H_{Asp}), 2.41 (dd, 1H, , α-H_{Asp}), 1.42 (d, 3H, β-H_{Ala}). IR (KBr) cm^{-1}: 3404, 3272 (b, ν(N—H)), 1646 (sh, ν(C=O)), 1602 (s, ν(C=O)), 1561 (s, ν(C=O)), 1401 (s, ν(C—O)), 4657 (w, ν(Ni—N)) MS (ESI/Negative) MW: ($C_9H_{12}N_3O_6Ni^-$) = 316.9034, M/Z found(calc) = 316.0092(316.0085) [M$^-$].

K[Ni{α-Asp(O^{t}Bu)AlaGly}] (**13**)

$NiCl_2·6H_2O$ (0.250 g, 1.052 mmol) and KOH (0.100 g, 0.889 mmol) were dissolved in 20mL H_2O, **1**-HCl (0.231 g, 0.628 mmol) was dissolved in H_2O (5 mL) the Ni(II) solution was added to the ligand and the pH was increased with 1 M KOH until a pH of 10 was achieved. Solution was stirred for 2 h then the H_2O was removed in vacuo. The product was redissolved in iso-propyl alcohol. Product was precipitated out using a combination of EtOH and EtOAc . (0.203 g, 78%) ^{1}H NMR (400 MHz, DMSO-d_6) δ 3.57 (s, 1H, NH_{Asp}), 3.07 (d, 1H, α-H_{Asp}), 3.03 (s, 1H, NH_{Asp}), 3.02 (s, 1H, α-H_{Ala}), 2.99 (d, 2H, α-H_{Gly}), 2.50 (DMSO), 2.39 (dd, 1H,β-H_{Asp}), 2.21 (dd, 1H, β-H_{Asp}), 1.41 (s, 9H, -O(CH_3)$_{3\ Asp}$), 1.00 (d, 3H, β-H_{Ala}). ^{13}C NMR (101 MHz, DMSO) δ 182.19(C=O_{Asp}), 180.30(C=O_{Ala}), 175.71(C=O_{Gly}), 170.17(γ-C=O_{Asp}), 79.93 (-OC(CH_3)$_{3\ Asp}$), 56.42 (α-C_{Ala}), 54.53 (α-C_{Asp}), 48.31 (α-C_{Gly}), 39.52(DMSO), 39.02 (β-C_{Asp}), 27.77 (-OC(CH_3)$_{3\ Asp}$), 18.65 (β-C_{Ala}). IR (KBr) cm^{-1}: 3401, 3308 (b, ν(N—H)), 1722(s, ν(C=O)), 1642(sh, ν(C=O)), 1597(s, ν(C=O)), 1550(sh, ν(C=O)), 1254(s, ν(C—O)), 1289(s, ν(C—O)), 1146(s, ν(C—O)). 466(w, ν(Ni—N)). UV-Vis (H_2O): εx MS (ESI/Negative) ($C_{13}H_{20}N_3O_6Ni$) = 373.0114, M/Z found(calc) = 372.0716(372.0711) [M$^-$]. CHN ($C_{13}H_{20}N_3O_6Ni$)·H_2O found(calc) %: C: 36.97(36.30), H: 4.99(5.16), N: 9.89(9.77)

K[Ni{β-Asp(O^{t}Bu)AlaGly}] (**14**)

$NiCl_2·6H_2O$ (0.500 g, 2.104 mmol) and KOH (0.200 g, 1.779 mmol) were dissolved in 20mL H_2O, **2**-HCl (0.367 g, 1.000 mmol) was dissolved in 10 mL of H_2O. While monitoring pH add the Ni(II) solution to the ligand solution and adjust the pH to10 with 1M KOH solution, maintained a pH of 10 and stir for 2 hours. Excess $Ni(OH)_2$ was filtered off and the solvent removed in vacuo. The product was redissolved in iso-propyl alcohol. Product was precipitated out using a combination of EtOH and EtOAc. (0.168 g, 41%) ^{1}H NMR (400 MHz, DMSO-d_6) δ 3.37 (s, 7H, H_2O, NH_{Asp}), 3.29 (q, 1H, α-H_{Ala}), 3.16 – 3.05 (m, 1H, NH_{Asp}), 2.96 (q, 2H, α-H_{Gly}), 2.94 – 2.85 (m, 1H, β-H_{Asp}), 2.01 (dd, 1H, α-H_{Asp}), 1.87 (dt, 1H, α-H_{Asp}), 1.39 (s, 10H, -O(CH_3)$_{3\ Asp}$), 0.94 (d, 3H, β-H_{Ala}). ^{13}C NMR (101 MHz, DMSO) δ 182.23 (C=O_{Asp}), 180.14 (C=O_{Ala}), 171.02 (C=O_{Gly}), 170.61 (γ-C=O_{Asp}), 80.80 (-OC(CH_3)$_{3\ Asp}$), 58.32 (α-C_{Ala}), 52.79 (α-C_{Asp}), 48.66 (α-C_{Gly}), 39.52(DMSO), 39.01 (β-C_{Asp}), 27.61 (-OC(CH_3)$_{3\ Asp}$), 19.66 (β-C_{Ala}). IR (KBr) cm^{-1}: 3396, 3257(b, ν(N—H)), 1729(s, ν(C=O)), 1548(sh)(s, ν(C=O)), 1601(s, ν(C=O)), 1561(s, ν(C=O)), 1257(s, ν(C—O)), 1282(s, ν(C—O)), 1155(s, ν(C—O)), 470(w, ν(Ni—N)). UV-Vis (H_2O): ε_x MS (ESI/Negative) MW: ($C_{13}H_{20}N_3O_6Ni$) = 373.0114, M/Z found(calc) = 372.0713(372.0711) [M$^-$]. CHN ($C_{13}H_{20}N_3O_6Ni$)·H_2O found(calc) %: C: 35.91(36.30), H: 5.13(5.16), N: 9.63(9.77)

K[Ni{TrpAlaGly}] (**15**)

$NiCl_2·6H_2O$ (0.0.3 g, 1.262 mmol) and KOH (0.150 g, 1.334 mmol) were dissolved in 20 mL H_2O. **3** (0.346 g, 1.000 mmol) was dissolved in 10 mL of H_2O. While monitoring pH add the Ni(II) solution to the ligand solution and adjust the pH to10 with 1M KOH solution,

maintained a pH of 10 and stir for 2 hours. Excess $Ni(OH)_2$ was filtered off and the solvent removed in vacuo. The product was redissolved in iso-propyl alcohol and filtered. Product was precipitated out using a combination of EtOH and EtOAc. (0.206 g, 48%) ^{1}H NMR (400 MHz, DMSO-d_6) δ 10.89 (d, 1H, NH_{indole}), 7.48 (d, 1H, $H_{indole\text{-}C7}$), 7.34 (dt, 1H, $H_{indole\text{-}C4}$), 7.31 (d, 1H, $H_{indole\text{-}C2}$), 7.06 (ddd, 1H, $H_{indole\text{-}C5}$), 6.95 (ddd, 1H, $H_{indole\text{-}C6}$), 3.65 – 3.56 (m, 1H, NH_{Trp}), 3.10 (q, 1H, α-H_{Ala}), 3.01 (d, 2H, β-H_{Trp}), 2.96 (d, 1H, β-H_{Trp}), 3.07 – 2.87 (m, 2H, α-H_{Gly}), 2.72 (dd, 1H, β-H_{Trp}), 2.20 (dd, 1H, NH_{Trp}), 1.00 (d, 3H, β-H_{Ala}). ^{13}C NMR (101 MHz, DMSO) δ 182.20 ($C{=}O_{Trp}$), 180.37 ($C{=}O_{Ala}$), 177.09 ($C{=}O_{Gly}$), 136.29 ($C3_{indole}$), 127.39 ($C8_{indole}$), 123.87 ($C2_{indole}$), 120.91 ($C5_{indole}$), 118.38 ($C6_{indole}$), 118.23 ($C7_{indole}$), 111.28 ($C4_{indole}$), 110.06 ($C1_{indole}$), 57.83 (α-C_{Trp}), 56.39 (α-C_{Ala}), 48.40 (α-C_{Gly}), 39.52(DMSO), 28.86 (β-C_{Trp}), 18.63 (β-C_{Ala}). IR (KBr) cm^{-1}: 3396, 3292,(b, ν(N—H)), 1647(sh)(s, ν(C=O)), 1593(s, ν(C=O)), 1290(s, ν(C—O)), 469(w, ν(Ni—N)). UV-Vis (H_2O): ε_x MS (ESI/Positive) MW: ($C_{16}H_{17}KN_4O_4Ni$) = 426.0240, M/Z found(calc) = 387.0610(387.0609) [M^-]. CHN ($C_{16}H_{18}N_4O_4Ni$)·H_2O found(calc) %: C: 43.56(43.07), H: 4.88(4.52), N: 12.49(12.54)

5 Reactivity Studies of Ni(II) and Pd(II) Tripeptide Complexes with Small Molecules

5.1 Palladium

5.1.1 Olefins

Palladium is known to coordinate to ethylene in an η^2 fashion. The intention for the newly synthesized complexes outlined in this work was that, by either removing the chloride or lutidine ligand, or by opening the chelate on the C-terminus ester carbonyl, would allow access to the 4th coordination site, which would serve as a reaction site.

Ethylene Reactivity Studies

To examine whether these complexes are good candidates for catalysis, ethylene reactivity studies were performed and monitored with NMR spectroscopy. The general procedure was to dissolve the complexes in DMSO-d_6 and record the spectrum, bubble ethylene directly into the NMR tube and record the spectra again. The addition of ethylene produced a peak for the free ethylene resonance at 5.14 ppm, in DMSO-d_6 and no additional new resonances. It was concluded no reaction took place. It was surmised that the addition of an α-proton was needed in order to see reaction chemistry. Trifluoroacetic acid (TFA) and triflic acid (TFMS) were selected for study, because TFA is a weak acid and TFMS a strong acid, and neither have interfering proton resonances. Portions ranging from ~10 to 20-fold excess of TFA or TFMS were added to the complex and ethylene mixtures, and the spectra were recorded again. It was assumed that the palladium complexes would be fairly tolerant of acidic environment, considering Pd(II) can chelate peptide amide bonding at low pH values. [99]

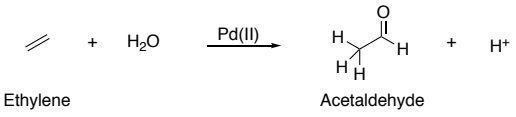

Scheme 5-1. Oxidation of ethylene to form acetaldehyde catalyzed by Pd(II)

The addition of increasing volumes of TFA to a solution of **8** and ethylene results in the demetallation of the ligand, where above ~15-fold excess, the spectra suggest complete demetallation and protonation of the N functional groups in the presence of acidic protons. This conclusion was based on observation of amide protons in the spectrum. In parallel, increased amounts of TFA resulted in oxidation of ethylene to form acetaldehyde (See Scheme 5-1). The formation of acetaldehyde increased proportionally with the quantity of TFA and appeared catalyzed by Pd(II) after dissociation of the ligand. With reversed order of addition, first TFA then ethylene, acetaldehyde only formed once both TFA and ethylene

were present. A blank spectrum of TFA and ethylene in DMSO confirmed that this is not a spontaneous reaction. The stacked spectra are found in Appendix Figure 1.

Triflic acid (TFMS) was substituted for TFA to determine if a different proton source produces the same product; unlike TFA, TFMS is non-coordinating. The addition of TFMS also resulted in demetallation of the ligand, and again oxidation of ethylene was observed by the formation of acetaldehyde signals. This reaction also formed a second product that is likely ethyl trifluoromethanesulfonate (Scheme 5-2), which is known to form from triflic acid in the presence of ethylene. [173,174]

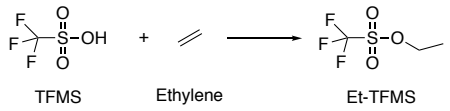

Scheme 5-2. Spontaneous reaction between trifluoromethanesulfonate and ethylene to form ethyl trifluoromethanesulfonate

The ^{13}C NMR for this experiment revealed that the addition of 20-30 µL TFA did not result in any significant changes to the signals of **8**; although this amounted to ~10 to 15-fold excess TFA, the signature quadruplets for TFA at ~158 and ~115 ppm were not present in the spectrum. This could be related to the volatility of this reagent and the length of ^{13}C experiments. When more TFA (40 µL) or TFMS (40 µL) is added, the ^{13}C signals were affected significantly. This supports the findings that demetallation has occurred. Confirmation of Et-TFMS formation is seen in the corresponding ^{13}C signals at 15.67 and 73.08 ppm, respectively. The formation of an aldehyde signal at 201.25 ppm and the appearance of a peak at 31.10 ppm supports the assertion that acetaldehyde was formed.

Complex **9**, with the more labile 6 membered ring, was also reacted with TFA and ethylene. It was expected in a direct comparison with **8**, complex **9** would show higher reactivity. Upon TFA addition to **9** the NMR changes dramatically. Again, partial demetallation and amide protonation occurred. However, a large shift in the Asp moiety, still coupled with the Asp NH_2, indicate that the amine is still coordinated. After the addition of ethylene, formation of acetaldehyde was observed in about ~10% quantitatively relative to the complex. The ^{13}C for this experiment was not informative due to the lability of the complex.

Having established that **8** was not reactive to ethylene alone, the catalytic ability of the **5a** to homopolymerize ethylene in trifluoroethanol was tested, (Scheme 5-3) believing that the acidic character of the solvent might be enough to activate the complex, without demetallizing the ligand. A reactor was charged with **5a**, along with trifluoroethanol at 35 °C. Ethylene was bubbled into the reactor and pressure kept at 2.5 bar and 35 °C for a total of 18 h. No noticeable color change was observed. Once the reaction was finished, the solvent was removed under reduced pressure, and the product dissolved in CD_3CN and a ^1H NMR spectrum was recorded. The NMR analysis confirmed no reaction took place and the MS analysis confirmed presence of the complex and absence of any small chain alkanes.

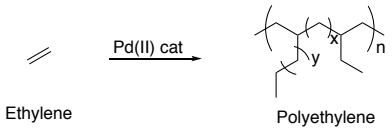

Scheme 5-3. Catalytic homopolymerization of ethylene to polyethylene.

5.1.2 Derivatives of CO_2 and CO

Carbonylation reactions are typically performed using CO in conjunction with various monomers, including olefins [175-177] and alcohols [178] under high pressure to yield various carboxylic acid derivatives. CO-surrogates can be used in order to avoid the use of carbon monoxide as C1-feedstock, which not only is toxic and difficult to transport, but also requires a reactor set-up. Chief among these alternatives are formic acid derivatives. [179]

In order to examine whether these complexes are candidates for carbonylation reactions, activation of methyl formate was investigated. A stock solution of methyl formate in DMF was added to solutions of **8**-**10** in a 1.1:1 ratio, with the intent of monitoring the electronic spectra. However, upon mixing, the formation and precipitation of Pd black occurred immediately.

To determine whether the formation of Pd black was related to the solvent, methyl formate or the neutral complexes, a solution of **5a** in CD_3OD was saturated with CO by bubbling into an NMR tube for 5 mins, hoping to see evidence of coordinated CO (Scheme 5-4). After 5 mins, a black precipitate started to form, and the color changed from light yellow to gray. The spectra revealed immediate appearance of at least 4 different unidentified species but were most likely decomposition products. After 1 day, most of the ligand had dissociated from the metal, leaving the free ligand intact. Next solutions of **6** in CD_3CN and CD_2Cl_2 were saturated with CO gas. After 5 mins, there was only a slight color change to gray but no changes in the NMR spectrum were observed in either of the solvents. This implies that in the absence of polar protic solvents, CO is not able to replace pyridine in the fourth coordination site.

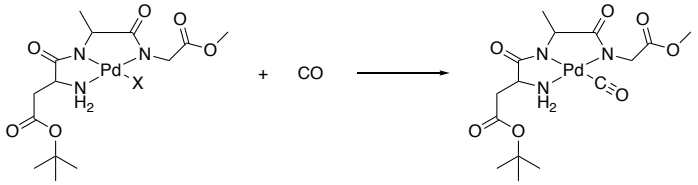

*Scheme 5-4. Coordination of CO to Pd(II) to **5** and **6** complexes.*

To test the catalytic ability of **5a** to copolymerize CO and styrene, (Scheme 5-5) a reactor was charged with complex **5a**, benzoquinone, and styrene in trifluoroethanol. Carbon monoxide was bubbled into the reactor for 10 min, then balloons filled with CO were attached to the system and it allowed to stir at 30 °C for 24 h. Palladium black started to appear after 2 hours of stirring. Analysis of the resulting green solution showed appearance of an unexpected product with resonances in the downfield region between δ =7-10 ppm. This product was not isolated or further identified but integrated to amounts sufficiently small to indicate a stoichiometric reaction.

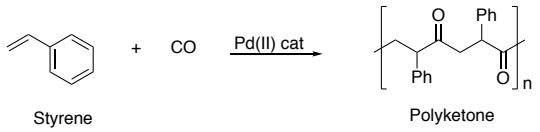

Scheme 5-5. Catalytic copolymerization of CO and styrene to form polyketones.

Following the same procedure, the catalytic ability of **6** to copolymerize CO and styrene were examined. Palladium black started to appear this time after 5 hours of stirring. Once the reaction was finished all the solvent was removed under reduced pressure. Again, the product was a green solution, and the same unidentified product was present as for the complex **5a**.

5.1.3 Sulfur Reagents

Palladium is a soft Lewis acid metal and is therefore thiophilic. Palladium is known to catalyze the thiocarbonylation of aromatic halide reagents this was done in the presence of CO and a protected cystinyl amino acid. [180] Fukuyama developed a chemoselective synthesis of ketones from thioesters. Reacting palladium tripeptide complexes with thiirenes could be a way to open coordination on the tetradentate complex and activate the metal. After sulfur coordination several outcomes are conceivably possible. Either (a) the thiirenes would coordinate and form palladium sulfur complexes, (b) Pd(II) would react with the sulfur substrates to catalytically transfer sulfur, or (c) a combination, where catalytic sulfur transfer would occur, expel sulfur as S_n and coordinate to the resulting olefin.

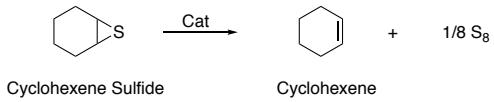

Scheme 5-6. Catalytic conversion of cyclohexene sulfide cyclohexene.

Cyclohexene sulfide was reacted with complex **8** and the results were monitored by NMR to determine conversion of thiirane to alkene in an overall reaction seen in Scheme 5-6. The spectrum showed quick conversion of cyclohexene sulfide to cyclohexene (Scheme 5-6) reaching up to 20%, then leveling out after ~30%. Deactivation of the catalyst occurred after ~30 hours. Figure 5.1 details the percent conversion as a function of time.

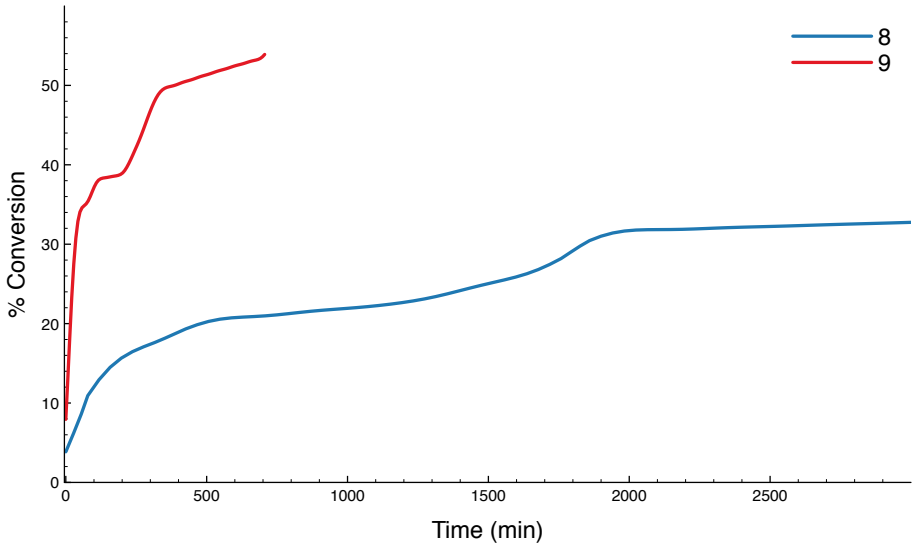

*Figure 5.1. Percent catalytic conversion of cyclohexene sulfide to cyclohexene with complexes **8** (3 mol %) and **9** (3 mol %), monitored via ^1H NMR*

Complex **9** showed much higher conversion of cyclohexene sulfide to cyclohexene, with conversion reaching >50% after 24 hours before deactivation of the catalyst. To ensure conversion was not spontaneous, a blank sample maintaining conditions but omitting the catalyst was run and showed no identifiable alkene formation for commensurate times as the catalytic runs.

5.2 Nickel

5.2.1 CO_2 Activation

Nickel complexes, especially with cyclams ligands, are well documented for their ability to electrocatalytically reduce CO_2. [54,58,61] The nickel tripeptide complexes **11-15** have design features similar to known active catalysts. In order to determine whether **13-15** would be suitable for electrochemical reduction of CO_2 to CO, DFT based calculations were first carried out. A model where forced CO_2 binding was applied to the Ni(II) state of the complex resulted in the dissociation of the CO_2 molecule. This was expected since a general consensus is that the first step for catalytic reduction of CO_2 to CO by Ni(cyclam) type complexes, is the reduction of Ni(II) to Ni(I). [60,63-65] Using a model starting with Ni(I) oxidation state, preliminary calculations indicate that CO_2 could bind to **13** and **14** in the reduced Ni(I) state. Applying the same level of theory, DFT optimized geometries of Ni(I)-**13**, Ni(I)-**14**, and Ni(I)(cyclam) were compared, with CO_2 attached axially as shown Figure 5.2. Assuming that the Ni(II) to Ni(I) reduction is at an accessible potential, DFT calculations thus suggest that complexes **13** and **14** would coordinate and activate CO_2. According to the calculations, CO_2 coordinates to Ni(I)-**13** and Ni(I)-**14** more strongly than to Ni(I)(cyclam), which is seen in the bond distance of 2.071 Å, and 2.082 Å *vs*. 2.087 Å, respectively. Calculations also suggest that CO_2 is more strongly activated by **13** because of the smaller O-C-O angle the coordinated CO_2 forms with **13**. For **13** and **14** it is 138º, whereas the Ni(cyclam)(CO_2) complex shows an angle of 142º. Preliminary cyclic voltammetry experiments indicate that there is an irreversible metal-based 1-electron reduction for **11a** and **12a** at 218 and 214 mV respectively. Future studies would need to explore whether **13-15** can electrochemically reduce CO_2 and if so, how selective and active these complexes are.

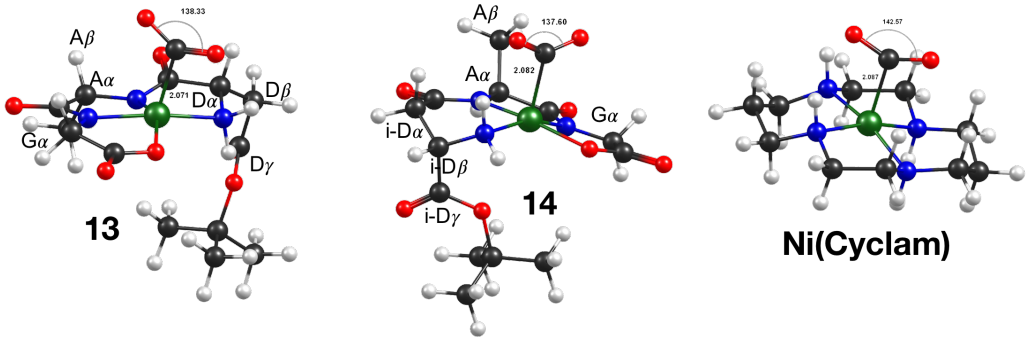

*Figure 5.2. DFT optimized for Ni(I)**13** and Ni(I)(cyclam)*

5.3 Conclusions

The reactivity studies of **8** and **9** with ethylene show activation of the ethylene group only with the addition of a proton source. Ethylene is oxidized to form the acetaldehyde in a well-known mechanism called the Wacker Process (WP). [181] In industrial applications, the WP converts olefins to aldehydes via catalytic oxidation, by first coordinating in a η^2-fashion followed by and external attack by an oxidizing agent (H_2O), then proton transfer, and finally dissociation. The WP reactions were stoichiometric when first studied, because of decomposition of $PdCl_2$ to Pd(0), but the addition of $CuCl_2$ to oxidize Pd(0) gave way for a bi-cyclic catalytic reaction with the overall reaction equation seen in Scheme 5-7.

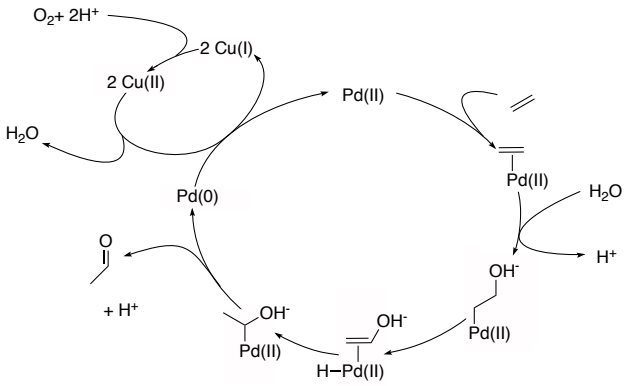

Scheme 5-7. Catalytic cycle for the palladium catalyzed oxidation of alkenes to aldehydes.

In the reaction studies carried out in this work, the acid causes demetallation after ~10-fold excess acid added. As more acid is added, the degree of demetallation increases, and the amount of converted acetaldehyde also increases. It is unclear if the formation of acetaldehyde is limited by the amount of acidic protons or oxidizing agent, namely water. Complexes **8** and **9** both exhibited a mild ability to convert ethylene to acetaldehyde, but it is unclear if this is due solely to ligand demetallation. Tripeptide palladium complexes synthesized in this work appear to be sensitive to reduction to Pd(0) in the presence of CO and CO surrogates. Both **8** and **9** are able to catalytically transfer sulfur atom however, where **9** outperforms **8** in terms of TOF before deactivation.

Tripeptide nickel complexes with coordinated CO_2 were explored with DFT calculations and compared to the known active CO_2 reduction catalyst, Ni(cyclam). DFT calculations suggest that nickel tripeptide complexes could active the electrocatalytic reduction of CO_2 to CO, assuming that the Ni(I) oxidation state is accessible.

5.4 Experimental

5.4.1 Physical Methods

Instrumentation

^1H, COSY, and ^{13}C nuclear magnetic resonance spectra were recorded at ambient temperature on a Bruker Avance 400 MHz spectrometer at 400 and 101 MHz, respectively. Solvents used were D_2O, DMSO-d_6, and $CDCl_3$. Electronic spectra were obtained using

either Varian Cary 100 Bio spectrophotometer or Perkin Elmer Lambda 25 UV/Vis spectrophotometer. Cyclic voltammetric measurements were recorded on EC Epsilon Eclipse^{TM} Potentiostat/Galvanostat. Mass spectra were recorded on a micrOTOF-Q spectrometer, equipped with E-spray atmospheric pressure ionization chamber (ESI).

Reagents used were purchased from Sigma Aldrich and used without further purification unless otherwise stated.

Quantum Chemical Calculations

Calculations were performed with a development version ORCA program. [148,149] The density functional theory based protocol consisted of the PBE0-D3BJ functional [150-152] (including the D3 dispersion correction by Grimme and coworkers[153,154]) and the triple-zeta basis set def2-TZVP. [155] The RIJCOSX [156,157] approximation was used to calculate Coulomb and Exchange integrals, using the def2/J auxiliary basis set by Weigend et al. [158] and the GridX5 (ORCA keyword) grid was used. Tighter grids for the exchange-correlation terms were also used (Grid5, FinalGrid6 keywords in ORCA). The CPCM solvation model [159-161] using a Gaussian pointcharge scheme and a scaled vdW surface was used to incorporate solvation effects. Vibrational frequencies were calculated analytically, as implemented in ORCA. [162,163] ^{13}C NMR shieldings were calculated using the same level of theory, except the pcSseg-2 basis sets [164] were utilized on carbon and hydrogen atoms. The calculated shieldings were converted into chemical shifts by calculating the shielding difference with respect to tetramethylsilane at the same level of theory. Chemical shifts were shifted by -15 ppm due to a systematic overestimation.

Ethylene Reaction Studies

NMR tube was charged with complex **8** or **9** (10.1 mg, 0.023 mmol) and dissolved in 650 μL of DMSO-d_6, the NMR recorded, then ethylene was bubbled in for 1 min, and the NMR recorded again (Appendix Figure 1). TFA (~20 μL, 0.128 mmol; ~30 μL, 0.192 mmol; ~40 μL (0.256 mmol) or TFMS (~40 μL, 0.443 mmol) was added to the NMR tube and the spectrum recorded again. Complex **8** (9.7 mg, 0.022 mmol) was dissolved in 650 μL of DMSO-d_6, then TFA (~ 20 μL, 0.128 mmol) was added and the spectrum recorded; Ethylene was bubbled in, and the NMR recorded again.

For catalytic reaction studies, the reactor was charged with 21 μmol of complex **5a** or **6**, along with 21 mL of trifluoroethanol and placed in an oil bath at 35 °C. Ethylene was bubbled into the reactor for 10 min, after the 10 min of bubbling the system closed off and charged with ethylene to 2.5 bar. The reactor was recharged to 2.5 bar every 15 min for the first two hours of the reaction, monitoring how much gas was consumed. After 45 min, the pressure stayed at 2.5 bar and no additional gas was consumed. After 2 hours, the ethylene was left open to the system and kept at 2.5 bar and 35 °C for total of 18 h.

CO Reaction Studies

The reactor was charged with **5a** or **6** (6.06 mg, (0.015% mol per mol styrene)), 4 mol eq. of benzoquinone and 10 mL of styrene in 20 mL of trifluoroethanol. Carbon monoxide was bubbled into the reactor for 10 min, after the 10 min of bubbling the system was attached to two 1-liter balloons filled with CO and allowed to stir at 30 °C for 24 h.

Sulfur Reaction Studies

Samples of **8** and **9** were prepared aerobically by adding cyclohexene sulfide (47 μL, 0.3833 mmol) to DMSO-d_6 (0.6 ml) in screw-cap NMR tub. Initial ^{1}H NMR spectrum were recorded at ambient temperature and pressure to obtain a blank spectrum. Complex **8** or **9** (5 mg, 0.0115 mmol) was added to NMR tube and ^{1}H NMR spectrum for recorded instantly. The progress of the reaction was monitored over the course of hours or days to determine conversion of thiirane to alkene. Maintaining conditions but omitting the catalyst showed no identifiable alkene formation over commensurate time periods as the catalytic runs.

5.4.2 Materials

Reagents used were purchased from Sigma Aldrich and used without further purification unless otherwise stated. Solvents were purchased from Sigma Aldrich and were distilled under nitrogen and dried using standard methods. [138]

6 Conclusions

The syntheses of alkylated tripeptides were carried out using solution phase synthesis and characterized fully. The coordination preferences of **1**-**3** were explored as ligands for Pd(II) in water at different pH values to explore stepwise coordination and draw out differences in ligand properties. The tripeptides chosen exhibited their maximum expected chelating ring sizes at the N terminus and confirmed it is possible to form complexes with κ^4[n,5,5] (n = 8,6,5) chelates that may be employed to adjust ligand frameworks for bioinspired catalyst design in future work. Despite ester hydrolysis the study successfully drew out interesting differences in the coordination of these ligands and site directed coordination geometries using pH manipulations were successfully carried out.

Combining spectroscopic data from ^{1}H and ^{13}C NMR, infrared, and mass spectrometry, the coordination geometry of six distinct palladium tripeptide complexes was elucidated. The complexes **5**-**10** have an amine/amide backbone coordination, and the 4th coordination site affects the spectroscopy. Coordinated chloride can be replaced by lutidine and pyridine. Complexes formed with pyridine and lutidine exhibited π-interaction with the glycine moiety and strong nitrogen to palladium coordination, proving difficult to remove. The development of a non-aqueous synthesis strategy, using a non-nucleophilic base was instrumental in the formation of neutral tetradentate palladium complexes with κ^4[NH_2,N,N,=O] coordination. Neutral palladium complexes with coordinated ester carbonyl are not common, and Sci-finder structure search did not identify another example of this coordination. This coordination mode forms weaker bonds which makes it inherently more difficult to form if more favorable ligands are present.

For ligand **3** there were distinct differences in the coordination behavior; In aqueous synthesis the indole amine competitively coordinated with metal, but in non-aqueous synthesis the N-terminal amine coordinated. The development of this class of complexes was meant to achieve maximum organosolubility, in order to carry out reactions in non-coordinating solvents. Despite **8** and **9** having multiple functional groups including the methyl and *t*-butyl esters, and an indole present **10**, these complexes are relatively insoluble. As a consequence, characterization and reaction studies were carried out in coordinating solvents. The use of this synthetic strategy offers the possibility to facilitate coordination of esters carbonyl oxygen to other metals.

In the ethylene reactivity studies with **8** and **9**, activation of the ethylene group was only achieved with the addition of an acidic proton source, that however caused demetallation after addition of about 10-fold excess of acid. Complexes **8** and **9** both exhibited a mild ability to convert ethylene to acetaldehyde, in parallel with ligand demetallation. As more acid was added, the degree of demetallation increased, and the amount of converted acetaldehyde also increased. Ethylene was oxidized by Pd(II) to form the acetaldehyde that is comparable to the well-known Wacker Process. The formation of acetaldehyde may be limited by the amount of acid or water present. Tripeptide palladium complexes synthesized in this work were sensitive to reduction to Pd(0) in the presence of CO and CO surrogates. Both **8** and **9** were able to catalytically transfer sulfur atom however, **9** outperforms **8** in terms of TOF before deactivating.

Synthesis of di- and monoanionic nickel complexes based on **1-3** were successful in aqueous solutions where the specific product was dependent on the starting complex. Complexes **11-15** were isolated in the $\kappa^4[NH_2,N,N,O]$ coordination mode with hydrolyzed ester carboxylate occupying the metal center 4^{th} coordination site. Characterization of these complexes was aided by DFT calculations. Cyclic voltammograms of **11a** and **12a** show irreversible metal-based reduction at 218 and 214 mV respectively, while **15** exhibits a weak irreversible reduction at 691 mV that is presumed metal based. DFT calculations were employed to optimize the geometry for the tripeptide nickel complexes with coordinated CO_2 and compared to known active CO_2 reduction catalyst, Ni(cyclam). Calculations suggested that reduced Ni(I) complexes of **13** and **14** could bind and activate CO_2, assuming an accessible Ni(I) reduction potential. Further CV studies may show these complexes useful for the electrochemical reduction of CO_2 to CO.

References

1 Kaiser, J. M. and Long, B. K. (2018) Recent developments in redox-active olefin polymerization catalysts, Elsevier B.V. 372, 141–152.

2 Chen, Z. and Brookhart, M. (2018) Exploring Ethylene/Polar Vinyl Monomer Copolymerizations Using Ni and Pd α-Diimine Catalysts. Acc. Chem. Res., American Chemical Society 51, 1831–1839.

3 Wang, J., Wang, L., Yu, H., Ullah, R. S., Haroon, M., Zain-ul-Abdin, Xia, X. and Khan, R. U. (2018) Recent Progress in Ethylene Polymerization Catalyzed by Ni and Pd Catalysts 2018, 1450–1468.

4 Dai, S., Sui, X. and Chen, C. (2015) Highly Robust Palladium(II) α-Diimine Catalysts for Slow-Chain-Walking Polymerization of Ethylene and Copolymerization with Methyl Acrylate. Angew. Chem. Int. Ed. 54, 9948–9953.

5 Coates, G. W. (2002) Polymerization catalysis at the millennium: frontiers in stereoselective, metal-catalyzed polymerization 467–475.

6 Nakamura, A., Ito, S. and Nozaki, K. (2009) Coordination−Insertion Copolymerization of Fundamental Polar Monomers. Chem. Rev. 109, 5215–5244.

7 Coates, G. W. (2000) Precise Control of Polyolefin Stereochemistry Using Single-Site Metal Catalysts. Chem. Rev. 100, 1223–1252.

8 Makio, H., Kashiwa, N. and Fujita, T. (2002) FI catalysts: a new family of high performance catalysts for olefin polymerization. Adv. Synth. Catal. 344, 477–493.

9 Gromada, J., Carpentier, J.-F. and Mortreux, A. (2004) Group 3 metal catalysts for ethylene and α-olefin polymerization 248, 397–410.

10 Wang, F. and Chen, C. (2019) A continuing legend: the Brookhart-type α-diimine nickel and palladium catalysts, Royal Society of Chemistry 10, 2354–2369.

11 Ittel, S. D., Johnson, L. K. and Brookhart, M. (2000) Late-Metal Catalysts for Ethylene Homo- and Copolymerization. Chem. Rev. 100, 1169–1204.

12 Johnson, L. K., Killian, C. M. and Brookhart, M. (1995) New Pd(II)- and Ni(II)-Based Catalysts for Polymerization of Ethylene and α-Olefins. J. Am. Chem. Soc. 117, 6414–6415.

13 Rix, F. C. and Brookhart, M. (1995) Energetics of Migratory Insertion Reactions in Pd(II) Acyl Ethylene, Alkyl Ethylene, and Alkyl Carbonyl Complexes. J. Am. Chem. Soc. 117, 1137–1138.

14 Guo, L., Dai, S., Sui, X. and Chen, C. (2015) Palladium and Nickel Catalyzed Chain Walking Olefin Polymerization and Copolymerization. ACS Catalysis 6, 428–441.

15 Chen, Y., Wang, L., Yu, H., Zhao, Y., Sun, R., Jing, G., Huang, J., Khalid, H., Abbasi, N. M. and Akram, M. (2015) Synthesis and application of polyethylene-based functionalized hyperbranched polymers, Elsevier Ltd 45, 23–43.

16 Tempel, D. J., Johnson, L. K., Huff, R. L., White, P. S. and Brookhart, M. (2000) Mechanistic Studies of Pd(II)−α-Diimine-Catalyzed Olefin Polymerizations 1 122, 6686–6700.

17 Mecking, S., Johnson, L. K., Wang, L. and Brookhart, M. (1998) Mechanistic Studies of the Palladium-Catalyzed Copolymerization of Ethylene and α-Olefins with Methyl Acrylate 120, 888–899.

18 Guo, L., Liu, W. and Chen, C. (2017) Late transition metal catalyzed α-olefin polymerization and copolymerization with polar monomers, Royal Society of Chemistry 1, 2487–2494.
19 Chen, C. (2018) Designing catalysts for olefin polymerization and copolymerization: beyond electronic and steric tuning, Springer US 2, 1–9.
20 Tan, C. and Chen, C. (2019) Emerging Palladium and Nickel Catalysts for Copolymerization of Olefins with Polar Monomers. Angew. Chem. Int. Ed. 58, 7192–7200.
21 Durand, J. and Milani, B. (2006) The role of nitrogen-donor ligands in the palladium-catalyzed polyketones synthesis 250, 542–560.
22 Rosar, V., Meduri, A., Montini, T., Fini, F., Carfagna, C., Fornasiero, P., Balducci, G., Zangrando, E. and Milani, B. (2014) Analogies and Differences in Palladium-Catalyzed CO/Styrene and Ethylene/Methyl Acrylate Copolymerization Reactions. ChemCatChem 6, 2403–2418.
23 Durand, J., Zangrando, E., Stener, M., Fronzoni, G., Carfagna, C., Binotti, B., Kamer, P. C. J., Müller, C., Caporali, M., van Leeuwen, P. W. N. M., et al. (2006) Long-Lived Palladium Catalysts for CO/Vinyl Arene Polyketones Synthesis: A Solution to Deactivation Problems. Chem. Eur. J. 12, 7639–7651.
24 Younkin, T. R., Connor, E. F., Henderson, J. I., Friedrich, S. K., Grubbs, R. H. and Bansleben, D. A. (2000) Neutral single-component nickel (II) polyolefin catalysts that tolerate heteroatoms. Science, American Association for the Advancement of Science 287, 460–462.
25 Deshmukh, S. S., Gaikwad, S. R., Gonnade, R. G., Pandole, S. P. and Chikkali, S. H. (2019) Pd-Iminocarboxylate Complexes and Their Behavior in Ethylene Polymerization. Chem. Asian J. 15, 398–405.
26 Nian, Y., Wang, J., Moriwaki, H., Soloshonok, V. A. and Liu, H. (2017) Analysis of crystallographic structures of Ni(ii) complexes of α-amino acid Schiff bases: elucidation of the substituent effect on stereochemical preferences 46, 4191–4198.
27 Kuchtanin, V. R., Kleščíková, L., Šoral, M., Fischer, R., Růžičková, Z., Rakovský, E., Moncoľ, J. and Segľa, P. (2016) Nickel(II) Schiff base complexes: Synthesis, characterization and catalytic activity in Kumadaâ€“Corriu cross-coupling reactions. Polyhedron, Elsevier Ltd 117, 90–96.
28 Jeslin Kanaga Inba, P., Annaraj, B., Thalamuthu, S. and Neelakantan, M. A. (2013) Cu(II), Ni(II), and Zn(II) Complexes of Salan-Type Ligand Containing Ester Groups: Synthesis, Characterization, Electrochemical Properties, and In Vitro Biological Activities. Bioinorganic Chemistry and Applications, Hindawi Publishing Corporation 2013, 439848–11.
29 Ding, L., Chu, Z., Chen, L., Lü, X., Yan, B., Song, J., Fan, D. and Bao, F. (2011) Pd-Salen and Pd-Salan complexes: Characterization and application in styrene polymerization. INOCHE, Elsevier B.V. 14, 573–577.
30 Bunda, S., Udvardy, A., Voronova, K. and Joó, F. (2018) Organic Solvent-Free, Pd(II)-Salan Complex-Catalyzed Synthesis of Biaryls via Suzuki-Miyaura Cross-Coupling in Water and Air. J Org Chem 83, 15486–15492.
31 Lihi, N., Bunda, S., Udvardy, A. and Joó, F. (2020) Coordination chemistry and catalytic applications of Pd(II)–, and Ni(II)–sulfosalan complexes in aqueous media. J. Inorg. Biochem., Elsevier 203, 110945.
32 Pessoa, J. O. C. and Correia, I. (2019) Salan vs. salen metal complexes in catalysis and medicinal applications: Virtues and pitfalls. Coordination Chemistry Reviews, Elsevier B.V. 388, 227–247.

33 Białek, M., Pochwała, M. and Spaleniak, G. (2014) Olefin polymerization and copolymerization by complexes bearing [ONNO]-Type salan ligands: Effect of ligand structure and metal type (titanium, zirconium, and vanadium). J. Polym. Sci. Part A: Polym. Chem., John Wiley & Sons, Ltd 52, 2111–2123.
34 Abu-Sarrah, A. S., Thewalt, U. and Rieger, B. (1999) Chiral palladium(II) complexes bearing tetradentate nitrogen ligands: synthesis, crystal structure and reactivity towards the polymerization of norbornene. Journal of Organometallic Chemistry 587, 58–66.
35 Xu, Y.-M., Li, K., Wang, Y., Deng, W. and Yao, Z.-J. (2017) Mononuclear Nickel(II) Complexes with Schiff Base Ligands: Synthesis, Characterization, and Catalytic Activity in Norbornene Polymerization. Polymers 9, 105–10.
36 Pintauer, T. and Matyjaszewski, K. (2009) Structural and Mechanistic Aspects of Copper Catalyzed Atom Transfer Radical Polymerization. In Metal Catalysts in Olefin Polymerization (Guan, Z., ed.), pp 221–251, Springer Berlin Heidelberg, Berlin, Heidelberg.
37 Xiong, H., Li, L., Liu, E., Cheng, J. and Zhang, G. (2017) A chiral multidentate salan-supported heterobimetallic catalyst for asymmetric Friedel-Crafts reaction. INOCHE, Elsevier B.V. 84, 24–27.
38 Benson, E. E., Kubiak, C. P., Sathrum, A. J. and Smieja, J. M. (2009) Electrocatalytic and homogeneous approaches to conversion of CO 2to liquid fuels. Chem. Soc. Rev. 38, 89–99.
39 Francke, R., Schille, B. and Roemelt, M. (2018) Homogeneously Catalyzed Electroreduction of Carbon Dioxide—Methods, Mechanisms, and Catalysts. Chem. Rev., American Chemical Society 118, 4631–4701.
40 Zhang, F., Zhang, H. and Liu, Z. (2019) Recent advances in electrochemical reduction of CO2. Current Opinion in Green and Sustainable Chemistry, Elsevier B.V. 16, 77–84.
41 Zhang, S., Fan, Q., Xia, R. and Meyer, T. J. (2020) CO_2 Reduction: From Homogeneous to Heterogeneous Electrocatalysis. Acc. Chem. Res. 53, 255–264.
42 Lü, F., Bao, H., Mi, Y., Liu, Y., Sun, J., Peng, X., Qiu, Y., Zhuo, L., Liu, X. and Luo, J. (2020) Electrochemical CO_2 reduction: From nanoclusters to single atom catalysts. Sustainable Energy Fuels, The Royal Society of Chemistry 4, 1012–1028.
43 Kibria, M. G., Edwards, J. P., Gabardo, C. M., Dinh, C. T., Seifitokaldani, A., Sinton, D. and Sargent, E. H. (2019) Electrochemical CO_2 Reduction into Chemical Feedstocks: From Mechanistic Electrocatalysis Models to System Design. Adv Mater, John Wiley & Sons, Ltd 31, e1807166.
44 Mi-Young, L., Tae, P. K., Wonhee, L., Hyungseob, L., Youngkook, K. and Seoktae, K. (2019) Current achievements and the future direction of electrochemical CO2 reduction: A short review. Critical Reviews in Environmental Science and Technology, Taylor & Francis 0, 1–47.
45 Louis, H., Udochukwu Akakuru, O., Monday, P. and Oluwatomisin Funmilayo, O. (2019) A review on the state-of-the-art advances for CO2 electro-chemical reduction using metal complex molecular catalysts. Eclética Química 44, 11–39.
46 Lim, R. J., Xie, M., Sk, M. A., Lee, J.-M., Fisher, A., Wang, X. and Lim, K. H. (2014) A review on the electrochemical reduction of CO2 in fuel cells, metal electrodes and molecular catalysts. Catalysis Today, Elsevier B.V. 233, 169–180.
47 Wang, J.-W., Zhong, D.-C. and Lu, T.-B. (2018) Artificial photosynthesis: Catalytic water oxidation and CO2 reduction by dinuclear non-noble-metal molecular catalysts. Coordination Chemistry Reviews, Elsevier B.V. 377, 225–236.

48 Khalil, M., Gunlazuardi, J., Ivandini, T. A. and Umar, A. (2019) Photocatalytic conversion of CO2 using earth-abundant catalysts_ A review on mechanism and catalytic performance. Renewable and Sustainable Energy Reviews, Elsevier Ltd 113, 109246.

49 Yaashikaa, P. R., Kumar, P. S., Varjani, S. J. and Saravanan, A. (2019) A review on photochemical, biochemical and electrochemical transformation of CO2 into value-added products. Journal of CO2 Utilization, Elsevier 33, 131–147.

50 Gamba, I. (2018) Biomimetic Approach to CO 2Reduction. Bioinorganic Chemistry and Applications 2018, 1–14.

51 Appel, A. M., Bercaw, J. E., Bocarsly, A. B., Dobbek, H., DuBois, D. L., Dupuis, M., Ferry, J. G., Fujita, E., Hille, R., Kenis, P. J. A., et al. (2013) Frontiers, Opportunities, and Challenges in Biochemical and Chemical Catalysis of CO 2Fixation. Chem. Rev. 113, 6621–6658.

52 Fogeron, T., Todorova, T. K., Porcher, J.-P., Gomez-Mingot, M., Chamoreau, L.-M., Mellot-Draznieks, C., Li, Y. and Fontecave, M. (2018) A Bioinspired Nickel(bis-dithiolene) Complex as a Homogeneous Catalyst for Carbon Dioxide Electroreduction. ACS Catalysis 8, 2030–2038.

53 Feng, C., Minh, A. C. and Zhao, Q. (2021) Synthesis and structural analysis of two cyclam derivatives. Journal of Molecular Structure, Elsevier B.V. 1224, 128842.

54 Gracia, L. L., Luci, L., Bruschi, C., Sambri, L., Weis, P., Fuhr, O. and Bizzarri, C. (2020) New Photosensitizers Based on Heteroleptic Cu IComplexes and CO 2Photocatalytic Reduction with [Ni II(cyclam)]Cl 2. Chem. Eur. J. 26, 9929–9937.

55 Jiang, C., Nichols, A. W., Walzer, J. F. and ORCID: 0000-0002-5182-1138, C. W. M. (2019) Electrochemical CO2 Reduction in a Continuous Non-Aqueous Flow Cell with [Ni(cyclam)]2. Inorg. Chem., American Chemical Society 1–10.

56 Mash, B. L., Raghavan, A. and Ren, T. (2018) Ni IIComplexes of C-Substituted Cyclam as Efficient Catalysts for Reduction of CO 2to CO (Sala, X., and Llobet, A., eds.) 2019, 2065–2070.

57 Behnke, S. L., Manesis, A. C. and Shafaat, H. S. (2018) Spectroelectrochemical investigations of nickel cyclam indicate different reaction mechanisms for electrocatalytic CO 2and H +reduction, Royal Society of Chemistry 47, 15206–15216.

58 Wu, Y., Rudshteyn, B., Zhanaidarova, A., Froehlich, J. D., Ding, W., Kubiak, C. P. and Batista, V. S. (2017) Electrode-Ligand Interactions Dramatically Enhance CO_2 Conversion to CO by the [Ni(cyclam)]$(PF_6)_2$ Catalyst. ACS Catalysis 7, 5282–5288.

59 Cook, T. D., Tyler, S. F., McGuire, C. M., Zeller, M., Fanwick, P. E., Evans, D. H., Peters, D. G. and Ren, T. (2017) Nickel Complexes of C-Substituted Cyclams and Their Activity for CO 2and H +Reduction. ACS Omega 2, 3966–3976.

60 Froehlich, J. D. and Kubiak, C. P. (2015) The Homogeneous Reduction of CO_2 by $[Ni(cyclam)]^+$: Increased Catalytic Rates with the Addition of a CO Scavenger. J. Am. Chem. Soc. 137, 3565–3573.

61 Froehlich, J. D. and Kubiak, C. P. (2012) Homogeneous CO 2Reduction by Ni(cyclam) at a Glassy Carbon Electrode. Inorg. Chem. 51, 3932–3934.

62 Saravanakumar, D., Song, J., Jung, N., Jirimali, H. and Shin, W. (2012) Reduction of CO2 to CO at Low Overpotential in Neutral Aqueous Solution by a Ni(cyclam) Complex Attached to Poly(allylamine). ChemSusChem 5, 634–636.

63 Beley, M., Collin, J. P., Ruppert, R. and Sauvage, J. P. (1984) Nickel(II)-cyclam: an extremely selective electrocatalyst for reduction of CO2 in water. J. Chem. Soc., Chem. Commun., The Royal Society of Chemistry 1315–1316.

64 Beley, M., Collin, J. P., Ruppert, R. and Sauvage, J. P. (1986) Electrocatalytic reduction of carbon dioxide by nickel cyclam2 in water: study of the factors affecting the efficiency and the selectivity of the process. J. Am. Chem. Soc. 108, 7461–7467.

65 Song, J., Klein, E. L., Neese, F. and Ye, S. (2014) The Mechanism of Homogeneous CO 2Reduction by Ni(cyclam): Product Selectivity, Concerted Proton–Electron Transfer and C–O Bond Cleavage. Inorg. Chem. 53, 7500–7507.

66 Liu, Q., Wu, L., Jackstell, R. and Beller, M. (2015) Using carbon dioxide as a building block in organic synthesis, Nature Publishing Group 6, 1–15.

67 Neves Gomes, Das, C., Jacquet, O., Villiers, C., Thuéry, P., Ephritikhine, M. and Cantat, T. (2011) A Diagonal Approach to Chemical Recycling of Carbon Dioxide: Organocatalytic Transformation for the Reductive Functionalization of CO2. Angew. Chem. Int. Ed. 51, 187–190.

68 Cokoja, M., Bruckmeier, C., Rieger, B., Herrmann, W. A. and Kühn, F. E. (2011) Transformation of carbon dioxide with homogeneous transition-metal catalysts: A molecular solution to a global challenge? Angew. Chem. Int. Ed. 50, 8510–8537.

69 Williams, C. M., Johnson, J. B. and Rovis, T. (2008) Nickel-Catalyzed Reductive Carboxylation of Styrenes Using CO 2 130, 14936–14937.

70 Lejkowski, M. L., Lindner, R., Kageyama, T., Bódizs, G. É., Plessow, P. N., Müller, I. B., Schäfer, A., Rominger, F., Hofmann, P., Futter, C., et al. (2012) The First Catalytic Synthesis of an Acrylate from CO2 and an Alkene—A Rational Approach. Chem. Eur. J., John Wiley & Sons, Ltd 18, 14017–14025.

71 Hendriksen, C., Pidko, E. A., Yang, G., Schäffner, B. and Vogt, D. (2014) Catalytic Formation of Acrylate from Carbon Dioxide and Ethene. Chem. Eur. J., John Wiley & Sons, Ltd 20, 12037–12040.

72 Huguet, N., Jevtovikj, I., Gordillo, A., Lejkowski, M. L., Lindner, R., Bru, M., Khalimon, A. Y., Rominger, F., Schunk, S. A., Hofmann, P., et al. (2014) Nickel-Catalyzed Direct Carboxylation of Olefins with CO2: One-Pot Synthesis of α,β-Unsaturated Carboxylic Acid Salts. Chem. Eur. J., John Wiley & Sons, Ltd 20, 16858–16862.

73 Manzini, S., Cadu, A., Schmidt, A.-C., Huguet, N., Trapp, O., Paciello, R. and Schaub, T. (2017) Enhanced Activity and Recyclability of Palladium Complexes in the Catalytic Synthesis of Sodium Acrylate from Carbon Dioxide and Ethylene. ChemCatChem, John Wiley & Sons, Ltd 9, 2269–2274.

74 Stieber, S. C. E., Huguet, N., Kageyama, T., Jevtovikj, I., Ariyananda, P., Gordillo, A., Schunk, S. A., Rominger, F., Hofmann, P. and Limbach, M. (2015) Acrylate formation from CO2 and ethylene: catalysis with palladium and mechanistic insight. Chem. Commun., The Royal Society of Chemistry 51, 10907–10909.

75 Manzini, S., Huguet, N., Trapp, O., Paciello, R. A. and Schaub, T. (2017) Synthesis of acrylates from olefins and CO2 using sodium alkoxides as bases. Catalysis Today 281, 379–386.

76 Sureshbabu, V. V. and Narendra, N. (2011) Protection Reactions. Amino Acids, Peptides and Proteins in Organic Chemistry, pp 1–97, Wiley-VCH Verlag GmbH & Co. KGaA, Weinheim, Germany.

77 El-Faham, A. and Albericio, F. (2011) Peptide coupling reagents, more than a letter soup. Chem. Rev. 111, 6557–6602.

78 Isidro-Llobet, A., Álvarez, M. and Albericio, F. (2009) Amino Acid-Protecting Groups. Chem. Rev. 109, 2455–2504.

79 Montalbetti, C. A. G. N. and Falque, V. (2005) Amide bond formation and peptide coupling. Tetrahedron 61, 10827–10852.
80 Valeur, E. and Bradley, M. (2009) Amide bond formation: beyond the myth of coupling reagents. Chem. Soc. Rev. 38, 606–631.
81 Höck, S., Marti, R., Riedl, R. and Simeunovic, M. (2010) Thermal Cleavage of the Fmoc Protection Group 64, 200–202.
82 Al-Warhi, T. I., Al-Hazimi, H. M. A. and El-Faham, A. (2012) Recent development in peptide coupling reagents. Journal of Saudi Chemical Society, King Saud University 16, 97–116.
83 Joullie, M. M. and Lassen, K. M. (2010) Evolution of amide bond formation. Arkivoc 2010, 189–250.
84 Kitteringham, E., McKeon, A. M., O'Dowd, P., Devocelle, M., Murphy, B. M. and Griffith, D. M. (2020) Synthesis and characterisation of a novel mono functionalisable Pt(IV) oxaliplatin-type complex and its peptide conjugate. Inorganica Chimica Acta, Elsevier 505, 119492.
85 Metzler-Nolte, N. and Guo, Z. (2016) Themed Issue on "Metallodrugs: Activation, Targeting, and Delivery," Royal Society of Chemistry 45, 12965–12965.
86 Soldevila-Barreda, J. J. and Sadler, P. J. (2015) Approaches to the design of catalytic metallodrugs. Current Opinion in Chemical Biology, Elsevier Ltd 25, 172–183.
87 Bradford, S. S. and Cowan, J. A. (2014) From Traditional Drug Design to Catalytic Metallodrugs: A Brief History of the Use of Metals in Medicine. Metallodrugs 1, 1–14.
88 Mjos, K. D. and Orvig, C. (2014) Metallodrugs in medicinal inorganic chemistry. Chem. Rev. 114, 4540–4563.
89 Sigel, H. and Martin, R. B. (1982) Coordinating properties of the amide bond. Stability and structure of metal ion complexes of peptides and related ligands. Chem. Rev., ACS Publications 82, 385–426.
90 Sóvágó, I. and Ősz, K. (2006) Metal ion selectivity of oligopeptides, The Royal Society of Chemistry 3841–3854.
91 Murphy, J. M., Powell, B. A. and Brumaghim, J. L. (2020) Stability constants of bio-relevant, redox-active metals with amino acids: The challenges of weakly binding ligands. Coordination Chemistry Reviews 412, 213253–21.
92 Kozlowski, H., Bal, W., Dyba, M. and Kowalik-Jankowska, T. (1999) Specific structure-stability relations in metallopeptides. Coordination Chemistry Reviews 184, 319–346.
93 El-Sherif, A. A. (2012) Stoichiometry and Research,"The Importance of Quantity in Biomedicine.""Coordination Chemistry of Palladium (II) Ternary Complexes with Relevant ….
94 Jószai, V., Nagy, Z., Ősz, K., Sanna, D., Di Natale, G., La Mendola, D., Pappalardo, G., Rizzarelli, E. and Sóvágó, I. (2006) Transition metal complexes of terminally protected peptides containing histidyl residues. J. Inorg. Biochem. 100, 1399–1409.
95 Livingstone, S. E. and Nolan, J. D. (1968) Metal Chelates of Biologically Important Compounds. I. Complexes of DL-Ethionine and S-Methyl-L-cysteine. Inorg. Chem. 7, 1447–1451.
96 Chandrasekharan, M., Udupa, M. R. and Aravamudan, G. (1973) Cysteine complexes of palladium(II) and platinum(II). Inorganica Chimica Acta 7, 88–90.
97 PETTIT, L. D., reviews, M. B. C. C.1985. Complex formation between palladium (II) and amino acids, peptides and related ligands. Elsevier

.

98 McAuliffe, C. A. (1967) The infrared spectra of palladium(II) and platinum(II) complexes of (±)-methionine. J. Chem. Soc. A 0, 641–642.
99 Ágoston, C. G., Jankowska, T. K. and Sóvágó, I. (1999) Potentiometric and NMR studies on palladium (II) complexes of oligoglycines and related ligands with non-co-ordinating side chains, Royal Society of Chemistry 3295–3302.
100 Wilson, E. W., Jr and Martin, R. B. (1970) Circular dichroism of palladium (II) complexes of amino acids and peptides. Inorg. Chem., Inorganic Chemistry 9, 528–532.
101 Maiti, B. K., Govil, N., Kundu, T. and Moura, J. J. G. (2020) Designed Metal-ATCUN Derivatives: Redox- and Non-redox-Based Applications Relevant for Chemistry, Biology, and Medicine. ISCIENCE, Elsevier Inc. 23, 101792.
102 Perinelli, M., Guerrini, R., Albanese, V., Marchetti, N., Bellotti, D., Gentili, S., Tegoni, M. and Remelli, M. (2020) Cu(II) coordination to His-containing linear peptides and related branched ones_ Equalities and diversities. J. Inorg. Biochem., Elsevier 205, 110980.
103 Gonzalez, P., Bossak, K., Stefaniak, E., Hureau, C., Raibaut, L., Bal, W. and Faller, P. (2018) N-Terminal Cu-Binding Motifs (Xxx-Zzz-His, Xxx-His) and Their Derivatives: Chemistry, Biology and Medicinal Applications. Chem. Eur. J. 24, 8029–8041.
104 Peana, M., Gumienna-Kontecka, E., Piras, F., Ostrowska, M., Piasta, K., Krzywoszynska, K., Medici, S. and Zoroddu, M. A. (2020) Exploring the Specificity of Rationally Designed Peptides Reconstituted from the Cell-Free Extract of Deinococcus radiodurans toward Mn(II) and Cu(II). Inorg. Chem. 59, 4661–4684.
105 Vicatos, G. M., Jackson, G. E., Hammouda, A. N., Bonomo, R. P. and Valora, G. (2019) Potentiometric and spectroscopic studies of the complex formation between copper(II) and Gly-Leu-Phe or Sar-Leu-Phe tripeptides. Polyhedron, Elsevier Ltd 170, 553–563.
106 Gavrish, S. P., Lampeka, Y. D., Babak, M. V. and Arion, V. B. (2018) Palladium Complexes of N,N'-Bis(2-aminoethyl)oxamide (H2L): Structural (PdIIL, PdII2L2, and PdIVLCl2), Electrochemical, Dynamic 1H NMR, and Cytotoxicity Studies. Inorg. Chem. 57, 1288–1297.
107 Gonzalez, P., Vileno, B., Bossak, K., Khoury, El, Y., Hellwig, P., Bal, W., Hureau, C. and Faller, P. (2017) Cu(II) Binding to the Peptide Ala-His-His, a Chimera of the Canonical Cu(II)-Binding Motifs Xxx-His and Xxx-Zzz-His. Inorg. Chem. 56, 14870–14879.
108 Park, G. Y., Lee, J. Y., Himes, R. A., Thomas, G. S., Blackburn, N. J. and Karlin, K. D. (2014) Copper-peptide complex structure and reactivity when found in conserved His-X(aa)-His sequences. J. Am. Chem. Soc. 136, 12532–12535.
109 Sóvágó, I., Kállay, C. and Várnagy, K. (2012) Peptides as complexing agents: Factors influencing the structure and thermodynamic stability of peptide complexes 256, 2225–2233.
110 Griffith, D. M., Bíró, L., Platts, J. A., Müller-Bunz, H., Farkas, E. and Buglyó, P. (2012) Synthesis and solution behaviour of stable mono-, di-and trinuclear Pd(II) complexes of 2,5-pyridinedihydroxamic acid: X-ray crystal structure of a novel Pd(II) hydroxamato complex. Inorganica Chimica Acta 380, 291–300.
111 Gábor Ágoston, C., Miskolczy, Z., Nagy, Z. and Sóvágó, I. (2003) The effect of ring size of fused chelates on the stability constants and spectroscopic properties of nickel(II) and palladium(II) complexes of peptides. Polyhedron 22, 2607–2615.

112 Wuts, P. G. M. and Greene, T. W. (2006) Greene's Protective Groups in Organic Synthesis, Wiley.
113 Bajusz, S., Medzihradszky, K., Kisfaludy, L., Low, M., Paulay, Z., Lang, M. T. and Szporny, L. (1968) Total synthesis of human corticotropin. Hungary, Richter, Gedeon, Vegyeszeti Gyar R. T.
114 Masignani, V., Scarlato, V., Scarselli, M., Galeotti, C. and Mora, M. (2001, January 18) Antigenic determinants of antigenic proteins of Neisseria meningitidis and their diagnostic, prophylactic and therapeutic use. World Intellectual Property Organization, Chiron S.p.A.
115 Chekalin, S. V., Golovlev, V. V., Kozlov, A. A., Letokhov, V. S., Matveets, Y. A. and Yartsev, A. P. (1988) Femtosecond laser photoionization mass spectrometry of molecules on surfaces. Springer Ser. Chem. Phys. 48, 414.
116 Ananda, K. and Suresh Babu, V. V. (2001) Deprotonation of hydrochloride salts of amino acid esters and peptide esters using commercial zinc dust. J Pept Res, John Wiley & Sons, Ltd 57, 223–226.
117 Sultane, P. R., Mete, T. B. and Bhat, R. G. (2015) A convenient protocol for the deprotection of N-benzyloxycarbonyl (Cbz) and benzyl ester groups. Tetrahedron Letters, Elsevier Ltd 56, 2067–2070.
118 Kuipers, B. J. H. and Gruppen, H. (2007) Prediction of molar extinction coefficients of proteins and peptides using UV absorption of the constituent amino acids at 214 nm to enable quantitative reverse phase high-performance liquid chromatography-mass spectrometry analysis. J Agric Food Chem 55, 5445–5451.
119 Gill, S. C. and Hippel, von, P. H. (1989) Calculation of protein extinction coefficients from amino acid sequence data. Analytical Biochemistry 182, 319–326.
120 Zhang, L., Lin, Y.-J., Li, Z.-H. and Jin, G.-X. (2015) Rational Design of Polynuclear Organometallic Assemblies from a Simple Heteromultifunctional Ligand. J. Am. Chem. Soc. 137, 13670–13678.
121 Chen, S., Vasquez, L., Noll, B. C. and Rakowski DuBois, M. (1997) Synthesis and Characterization of Mononuclear Indoline Complexes. Studies of σ and π Bonding Modes. Organometallics, American Chemical Society 16, 1757–1764.
122 Sundberg, R. J. (2010) Electrophilic Substitution Reactions of Indoles. In Heterocyclic Scaffolds II: 2nd ed., pp 47–115, Springer Berlin Heidelberg, Berlin, Heidelberg.
123 Singh, M. P., Saleem, F., Pal, R. S. and Singh, A. K. (2017) Palladacycles having normal and spiro chelate rings designed from bi- and tridentate ligands with an indole core: structure, synthesis and applications as catalysts. New J. Chem. 41, 11342–11352.
124 Kaminskaia, N. V., Ullmann, G. M., Fulton, D. B. and Kostic, N. M. (2000) Spectroscopic, kinetic, and mechanistic study of a new mode of coordination of indole derivatives to platinum(II) and palladium(II) ions in complexes. Inorg. Chem. 39, 5004–5013.
125 Hay, R. W. and Pujari, M. P. (1986) The palladium (II) promoted hydrolysis of methyl, ethyl and isopropyl glycylglycylglycinate. Inorganica Chimica Acta 123, 47–51.
126 Hay, R. W. and Pujari, M. P. (1984) The palladium(II)-promoted hydrolysis of methyl and isopropyl glycylglycinate. J. Chem. Soc., Dalton Trans. 1083–4.
127 Ozsváth, A., Farkas, E., Diószegi, R. and Buglyó, P. (2019) Versatility and trends in the interaction between Pd(ii) and peptide hydroxamic acids. New J. Chem., Royal Society of Chemistry 43, 8239–8249.

128 Martin, R. B. and Pitner, T. P. (1971) Inversion and proton exchange at asymmetric nitrogen centers in palladium (II) complexes 93, 4400–4405.
129 Pitner, T. P., Wilson, E. W. and Martin, R. B. (1972) Properties of palladium(II) complexes of peptides and histidine in basic solutions. Inorg. Chem. 11, 738–742.
130 Alexander, M. D. and Spillert, C. A. (1970) A Monodentate Ethylenediamine Complex of Cobalt(III). Inorg. Chem. 9, 2344–2346.
131 Severin, K., Bergs, R. and Beck, W. (1998) Bioorganometallic Chemistry-Transition Metal Complexes with α-Amino Acids and Peptides. Angew. Chem. Int. Ed. 37, 1634–1654.
132 Carvalho, M. A., Souza, B. C., Paiva, R. E. F., Bergamini, F. R. G., Gomes, A. F., Gozzo, F. C., Lustri, W. R., Formiga, A. L. B., Rigatto, G. and Corbi, P. P. (2012) Synthesis, spectroscopic characterization, DFT studies, and initial antibacterial assays in vitroof a new palladium(II) complex with tryptophan 65, 1700–1711.
133 Carvalho, M. A., Shishido, S. M., Souza, B. C., de Paiva, R. E. F., Gomes, A. F., Gozzo, F. C., Formiga, A. L. B. and Corbi, P. P. (2014) A new platinum complex with tryptophan: synthesis, structural characterization, DFT studies and biological assays in vitro over human tumorigenic cells. Spectrochim Acta A Mol Biomol Spectrosc 122, 209–215.
134 Lisa D Vasquez, B. C. N. A. M. R. D. (1998) Mononuclear Indoline Complexes. 2. Synthesis, Structure, and Reactivity of [(Cymene)Ru(η1-N-indoline)(CH3CN)2](OTf)2. Organometallics 17, 1–6.
135 Farkas, E. and Sóvágó, I. (2016) Metal complexes of amino acids and peptides. Amino Acids, Peptides and Proteins, Royal Society of Chemistry 41, 100.
136 Monger, L. J., Runarsdottir, G. R. and Suman, S. G. (2020) Directed coordination study of [Pd(en)(H2O)2]2+ with hetero-tripeptides containing C-terminus methyl esters employing NMR spectroscopy. J Biol Inorg Chem, Springer Berlin Heidelberg 25, 811–825.
137 Gutz, I. G. R. CurTiPot.
138 Armarego, W. L. F., Chai, C. and Chai, C. L. L. (2003) Purification of Laboratory Chemicals, Butterworth-Heinemann.
139 Li, J. and Sha, Y. (2008) A Convenient Synthesis of Amino Acid Methyl Esters, MDPI AG 13, 1111–1119.
140 Rúnarsdóttir, G. R. (2016) Synthesis and investigation of reactivity of alkylated tripeptides with metal ions. University of Iceland Masters Thesis.
141 OTERA, J. (1993) Transesterification. Chem. Rev. 93, 1449–1470.
142 Schreiner, B. and Beck, W. (2010) Coordination of the Ester Group - Hydrido-Rhodium(III) and Iridium(III) Complexes of Orthometallated Diphenylmethylene Glycine Esters [1]. Z. anorg. allg. Chem. 636, 499–505.
143 Nakamoto, K. (1970) Infrared spectra of inorganic and coordination compounds, Wiley-Interscience.
144 Zhu, L. and Kostić, N. (1992) Toward artificial metallopeptidases: mechanisms by which platinum (II) and palladium (II) complexes promote selective, fast hydrolysis of unactivated amide bonds in … 31, 3994–4001.
145 Bontchev, P. R., Boneva, M., Arnaudov, M. and Nefedov, V. I. (1984) Palladium(II) complexes of hydrazides of aspartic and glutamic acids. Inorganica Chimica Acta 81, 75–81.
146 Schreiner, B., Robl, C., Wagner-Schuh, B. and Beck, W. (2010) Metal complexes of biologically important ligands, CLXXIV [1]. Palladium(II) and platinum(II) complexes with schiff bases from 2-(Diphenylphosphino)benzaldehyde and a-

amino acid esters. Zeitschrift fur Naturforschung - Section B Journal of Chemical Sciences 65, 503–510.
147 Kozłowski, H. (1978) Spectroscopic and magnetic resonance studies on Ni (II), Cu (II) and Pd (II) complexes with Gly-Leu-Tyr and Tyr-Gly-Gly tripeptides. Inorganica Chimica Acta 31, 135–140.
148 Neese, F. (2012) The ORCA program system. WIREs Computational Molecular Science 2, 73–78.
149 Neese, F. (2018) Software update: the ORCA program system, version 4.0. WIREs Computational Molecular Science 8, e1327.
150 Shi, G., Dang, Y., Pan, T., Liu, X., Liu, H., Li, S., Zhang, L., Zhao, H., Li, S., Han, J., et al. (2016) Unexpectedly Enhanced Solubility of Aromatic Amino Acids and Peptides in an Aqueous Solution of Divalent Transition-Metal Cations. Phys. Rev. Lett. 117, 339–6.
151 Adamo, C. and Barone, V. (1999) Toward reliable density functional methods without adjustable parameters: The PBE0 model. The Journal of Chemical Physics 110, 6158–6170.
152 Perdew, J. P., Ernzerhof, M. and Burke, K. (1996) Rationale for mixing exact exchange with density functional approximations. The Journal of Chemical Physics, American Institute of Physics 105, 9982–9985.
153 Grimme, S., Antony, J., Ehrlich, S. and Krieg, H. (2010) A consistent and accurate ab initio parametrization of density functional dispersion correction (DFT-D) for the 94 elements H-Pu. The Journal of Chemical Physics 132, 154104.
154 Grimme, S., Ehrlich, S. and Goerigk, L. (2011) Effect of the damping function in dispersion corrected density functional theory. J. Comput. Chem. 32, 1456–1465.
155 Weigend, F. and Ahlrichs, R. (2005) Balanced basis sets of split valence, triple zeta valence and quadruple zeta valence quality for H to Rn: Design and assessment of accuracy. Phys. Chem. Chem. Phys., The Royal Society of Chemistry 7, 3297–3305.
156 Neese, F., Wennmohs, F., Hansen, A. and Becker, U. (2009) Efficient, approximate and parallel Hartree–Fock and hybrid DFT calculations. A “chain-of-spheres” algorithm for the Hartree–Fock exchange. Moving Frontiers in Quantum Chemistry: 356, 98–109.
157 Izsák, R. and Neese, F. (2011) An overlap fitted chain of spheres exchange method. The Journal of Chemical Physics 135, 144105.
158 Weigend, F. (2006) Accurate Coulomb-fitting basis sets for H to Rn. Phys. Chem. Chem. Phys., The Royal Society of Chemistry 8, 1057–1065.
159 Barone, V. and Cossi, M. (1998) Quantum Calculation of Molecular Energies and Energy Gradients in Solution by a Conductor Solvent Model. The Journal of Physical Chemistry A, American Chemical Society 102, 1995–2001.
160 York, D. M. and Karplus, M. (1999) A Smooth Solvation Potential Based on the Conductor-Like Screening Model. The Journal of Physical Chemistry A, American Chemical Society 103, 11060–11079.
161 Garcia-Ratés, M. and Neese, F. (2019) Effect of the Solute Cavity on the Solvation Energy and its Derivatives within the Framework of the Gaussian Charge Scheme. J. Comput. Chem., John Wiley & Sons, Ltd 41, 922–939.
162 Bykov, D., Petrenko, T., Izsák, R., Kossmann, S., Becker, U., Valeev, E. and Neese, F. (2015) Efficient implementation of the analytic second derivatives of Hartree–Fock and hybrid DFT energies: a detailed analysis of different approximations. Molecular Physics, Taylor & Francis 113, 1961–1977.

163 Garcia-Ratés, M. and Neese, F. (2019) Efficient implementation of the analytical second derivatives of hartree–fock and hybrid DFT energies within the framework of the conductor-like polarizable continuum model. J. Comput. Chem., John Wiley & Sons, Ltd 40, 1816–1828.
164 Jensen, F. (2014) Segmented Contracted Basis Sets Optimized for Nuclear Magnetic Shielding. J. Chem. Theory Comput. 11, 132–138.
165 Carretero, J. C. and Arrayás, R. G. Dichloro Bis(acetonitrile) Palladium.
166 Nakao, Y., Uyama, O. and Nakahara, A. (1974) Selective Activation of Methylene or Methine Groups in Nickel(Ii) Complexes of Tripeptides Composed of Glycine and/or Dl-Alpha-Alanine. Journal of Inorganic and Nuclear Chemistry 36, 685–688.
167 Lepetit, C., Vabre, B., Canac, Y., Alikhani, M. E. and Zargarian, D. (2018) Pentacoordinated, square pyramidal cationic PCP Ni(II) pincer complexes: ELF and QTAIM topological analyses of nickel–triflate interactions. Theoretical Chemistry Accounts, Springer Berlin Heidelberg 137, 1–22.
168 Scanlon, L. G., Tsao, Y. Y., Toman, K., Cummings, S. C. and Meek, D. W. (1982) Synthesis and characterization of square-pyramidal nickel(II) and cobalt(II) complexes with a linear tetradentate diphosphinediamine ligand. Crystal structures of [NiCl(3,3,3-N2P2)]PF6 and [CoCl(3,3,3-N2P2)]BF4.0.8H2O (3,3,3-N2P2 = a linear tetradentate diphosphinediamine). Inorg. Chem., American Chemical Society 21, 2707–2712.
169 Mathur, R. and Martin, R. B. (1965) Effects of charge and nickel ion on proton chemical shifts of glycyl peptides. J. Phys. Chem. 69, 668–671.
170 Sakurai, T., Nakao, Y. and Nakahara, A. (1980) 13C-NMR spectra of Ni(II) complexes of tripeptides and dipeptide-Schiff bases. Journal of Inorganic and Nuclear Chemistry 42, 1673–1675.
171 Dixon, N. E., Lawrance, G. A., Lay, P. A., Sargeson, A. M. and Taube, H. (1990) Trifluoromethanesulfonates and Trifluoromethanesulfonato-O Complexes 70–76.
172 Thomas, R. R., Sen, A., Beck, W. and Leidl, R. (1990) Acetonitrile Complexes of Selected Transition Metal Cations 63–67.
173 Howells, R. D. and Mc Cown, J. D. (2002) Trifluoromethanesulfonic acid and derivatives. Chem. Rev. 77, 69–92.
174 Gramstad, T. and Haszeldine, R. N. (1957) 806. Perfluoroalkyl derivatives of sulphur. Part VII. Alkyl trifluoromethanesulphonates as alkylating agents, trifluoromethanesulphonic anhydride as a promoter for esterification, and some reactions of trifluoromethanesulphonic acid. J. Chem. Soc. 4069–11.
175 Núñez Magro, A. A., Robb, L. M., Pogorzelec, P. J., Slawin, A. M. Z., Eastham, G. R. and Cole-Hamilton, D. J. (2010) Highly selective formation of unsaturated esters or cascade reactions to α,ω-diesters by the methoxycarbonylation of alkynes catalysed by palladium complexes of 1,2-bis(ditertbutylphosphinomethyl)benzene. Chem. Sci. 1, 723–730.
176 Suleiman, R., Tijani, J. and Ali, El, B. (2010) Palladium(II)-catalyzed catalytic aminocarbonylation and alkoxycarbonylation of terminal alkynes: Regioselectivity controlled by the nucleophiles. Applied Organometallic Chemistry 24, 38–46.
177 Katafuchi, Y., Fujihara, T., Iwai, T., Terao, J. and Tsuji, Y. (2011) Palladium-catalyzed hydroesterification of alkynes employing aryl formates without the use of external carbon monoxide. Adv. Synth. Catal. 353, 475–482.
178 Dong, K., Sang, R., Liu, J., Razzaq, R., Franke, R., Jackstell, R. and Beller, M. (2017) Palladium-Catalyzed Carbonylation of sec- and tert-Alcohols. Angew. Chem. Int. Ed., John Wiley & Sons, Ltd 56, 6203–6207.

179 Sang, R., Schneider, C., Razzaq, R., Neumann, H., Jackstell, R. and Beller, M. (2020) Palladium-catalyzed carbonylations of highly substituted olefins using CO-surrogates. Org. Chem. Front., Royal Society of Chemistry 7, 3681–3685.
180 Burhardt, M. N., Ahlburg, A. and Skrydstrup, T. (2014) Palladium-Catalyzed Thiocarbonylation of Aryl, Vinyl, and Benzyl Bromides. J. Org. Chem. 79, 11830–11840.
181 Takacs, J. M. and Jiang, X. T. (2003) The Wacker reaction and related alkene oxidation reactions 7, 369–396.

Appendix

*Appendix Table 1. ^1H NMR data of **1-3** in DMSO-d_6*

Chemical Shift (ppm)	1	2	3	Chemical Shift (ppm)	1	2	3
N—H $_{\text{Trp-In 3}}$	—	—	10.86	α-C_{Ala}	4.31	4.31	4.34
N—H $_{\text{Gly}}$	8.34	8.39	8.32	α-C_{Gly}	3.84	3.83	3.83
N—H $_{\text{Ala}}$	8.16	8.24	8.12	α-$C_{\text{Trp/Asp}}$	3.52	2.49 2.36	3.51
C—H $_{\text{Trp-In 7}}$	—	—	7.56	$OCH_{3\ \text{Gly}}$	3.62	3.63	3.63
C—H $_{\text{Trp-In 4}}$	—	—	7.33	β-$C_{\text{Trp/Asp}}$	2.37 2.35	3.64	3.10 2.78
C—H $_{\text{Trp-In 2}}$	—	—	7.18	$OC(CH_3)_{3\ \text{Asp}}$	1.38	1.39	—
C—H $_{\text{Trp-In 5}}$	—	—	7.06	β-C_{Ala}	1.23	1.21	1.16
C—H $_{\text{Trp-In 6}}$	—	—	6.97				

*Appendix Table 2. ^1H NMR data of **1-3** in D_2O*

Chemical Shift (ppm)	1	2	3	Chemical Shift (ppm)	1	2	3
C—C $_{\text{Trp-In 7}}$	—	—	7.66	α-C_{Gly}	4.02	4.06	3.77
C—H $_{\text{Trp-In 4}}$	—	—	7.53	α-$C_{\text{Trp/Asp}}$	3.75	2.77	4.01
C—H $_{\text{Trp-In 2}}$	—	—	7.31	$OCH_{3\ \text{Gly}}$	3.75	3.80	3.76
C—H $_{\text{Trp-In 5}}$	—	—	7.28	β-$C_{\text{Trp/Asp}}$	2.71	3.82	3.26
C—H $_{\text{Trp-In 6}}$	—	—	7.19	$OC(CH_3)_{3\ \text{Asp}}$	1.43	1.49	—
α-C_{Ala}	4.39	4.40	4.28	β-C_{Ala}	1.43	1.44	1.23

*Appendix Table 3. ^{13}C NMR data of **1-3** in DMSO-d_6*

Chemical Shift (ppm)	1	2	3	Chemical Shift (ppm)	1	2	3
$C{=}O_{Trp/Asp}$	172.82	172.99	173.84	C—H $_{Trp\text{-}In\ 5}$	—	—	111.28
$C{=}O_{Ala}$	172.61	172.73	172.68	C=C $_{Trp\text{-}In\ 1}$	—	—	110.22
γ-$C{=}O_{Asp}$	170.45	170.17	—	$OC(CH_3)_{3\ Asp}$	79.97	80.41	—
$C{=}O_{Gly}$	170.11	169.4	170.12	$OCH_{3\ Gly}$	51.68	51.67	52.69
C=C $_{Trp\text{-}In\ 4}$	—	—	136.20	α-$C_{Trp/Asp}$	51.51	39.15	54.91
C=C $_{Trp\text{-}In\ 9}$	—	—	127.39	α-C_{Ala}	47.78	47.85	47.52
C—H $_{Trp\text{-}In\ 2}$	—	—	123.94	α-C_{Gly}	40.48	40.48	40.48
C—H $_{Trp\text{-}In\ 6}$	—	—	120.84	β-$C_{Trp/Asp}$	40.24	51.52	30.42
C—H $_{Trp\text{-}In\ 8}$	—	—	118.46	$OC(CH_3)_{3\ Asp}$	27.75	27.61	—
C—H $_{Trp\text{-}In\ 7}$	—	—	118.19	β-C_{Ala}	18.50	18.18	18.64

*Appendix Table 4. Summary of infrared data for **1-4***

Frequency (cm^{-1})	**1**	**2**	**3**	**4**
ν(N—H_2)	3370	3375*	3370*	3356*
ν(N—H)	3314	3304	3297	3288
ν(C=O)				
OtBu	1725	1743	—	—
OMe	1759*	1757*	1749	1749
Amide I	1670	1659	1655	1660
ν(C=C)				
Aromatic	—	—	1673*	—
ν(N—H)				
Amide II	1546	1541	1517	1539
ν(C—O)				
OtBu	1250	1254	—	—
OMe	1213	1212	1213	1216
ν(O—C)				
OtBu	1155	1155	—	—

*Appendix Table 5 Comparative values for ν(C=O) vibrational modes observed versus DFT calculated for **1-3**. The Δ values show the systematic error of the calculated DFT values.*

Complex	ν(C=O) O^{t}Bu	ν(C=O) OMe	ν(C=O) Amide I	ν(C=O) Amide I
1 Obs	1725	1759	1670	1670
DFT	1758	1793	1745	1728
Δ	*33*	*34*	*75*	*58*
2 Obs	1743	1757	1659	1659
DFT	1757	1787	1740	1730
Δ	*14*	*30*	*81*	*71*
3 Obs	—	1749	1655	1655
DFT	—	1792	1747	1713
Δ	—	*43*	*92*	*58*

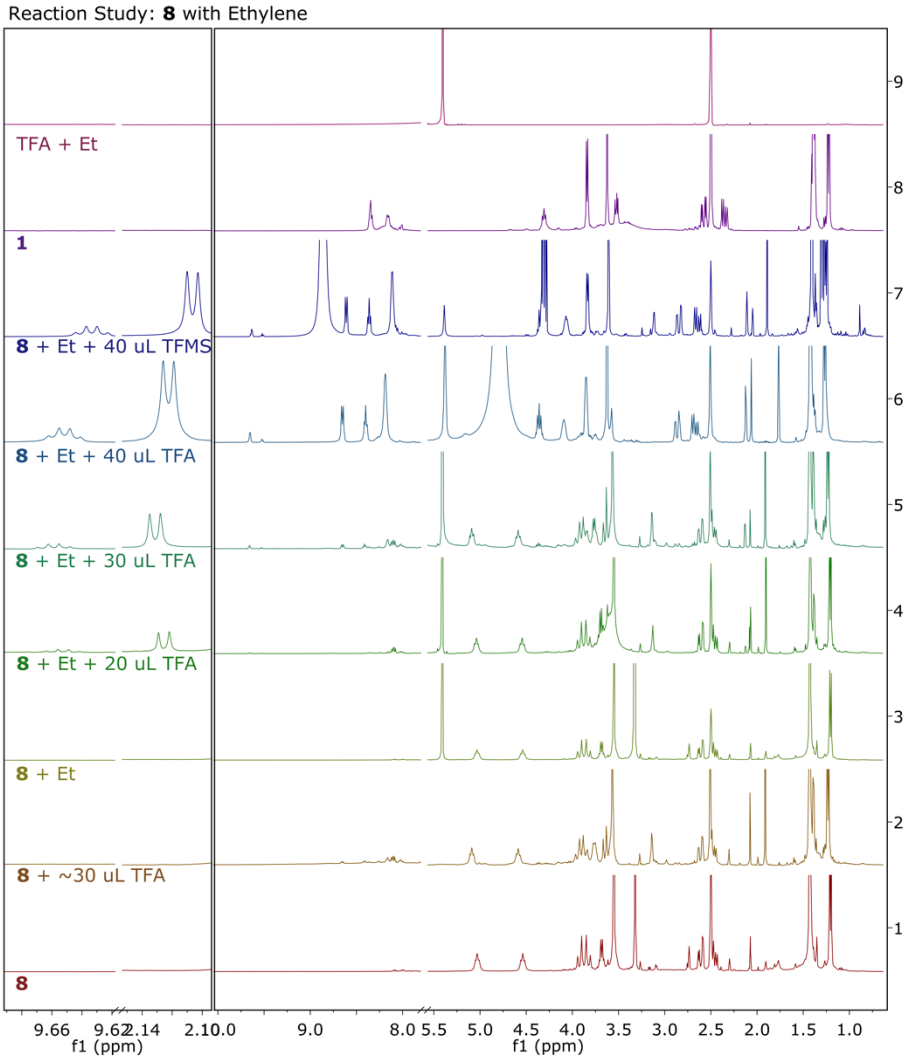

*Appendix Figure 1. Stacked ^{1}H NMR spectra of **8** (1) with addition of: (2) 30 µL TFA, (3) Ethylene, (4) 20 µL TFA and Ethylene, (5) 30 µL TFA and Ethylene, (6) 40 µL TFA and Ethylene, (7) 40 µL TFMS and Ethylene, (8) Ligand 1, (9) Blank with Ethylene and TFA*

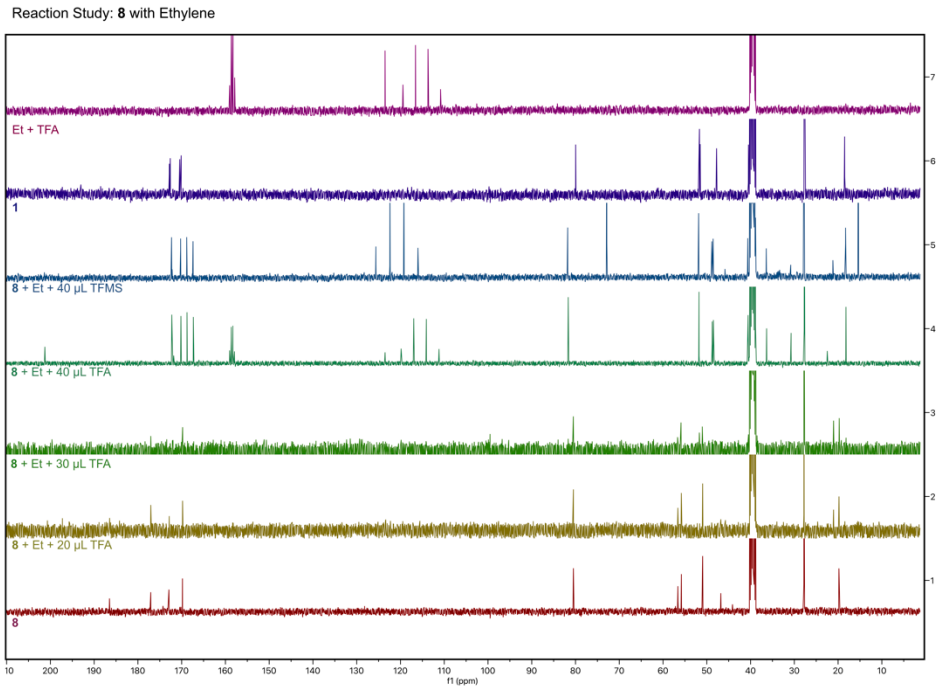

Appendix Figure 2. Stacked ^{13}C NMR **8** (1) with addition of: (2) 20 µL TFA and Ethylene, (3) 30 µL TFA and Ethylene, (4) 40 µL TFA and Ethylene, (5) 40 µL TFMS and Ethylene, (6) Ligand 1, (7) Blank with Ethylene and TFA

Article 1

JBIC Journal of Biological Inorganic Chemistry (2020) 25:811–825
https://doi.org/10.1007/s00775-020-01804-0

ORIGINAL PAPER

Directed coordination study of $[Pd(en)(H_2O)_2]^{2+}$ with hetero-tripeptides containing C-terminus methyl esters employing NMR spectroscopy

Lindsey J. Monger[1] · Gerdur R. Runarsdottir[1] · Sigridur G. Suman[1]

Received: 27 April 2020 / Accepted: 2 July 2020 / Published online: 16 July 2020

Abstract

Alkylation of the C-terminus acids in small peptides allows direction to amine and amide coordination, while changing the peptide composition to form tetradentate $\kappa^4[n,5,5]$, where $n = 5$-, 6-, 7-, or 8-membered ring coordination geometries, can be achieved. The alkylated tripeptide ligands, TrpAlaGly(OMe), β-Asp(OtBu)AlaGly(OMe), Asp(OtBu)AlaGly(OMe), and the fully methylated GSH, γ-Glu(OMe)Cys(SMe)Gly(OMe), were synthesized and their coordination properties to $[Pd(en)(H_2O)_2]^{2+}$ were studied. pH-dependent coordination was analyzed by NMR spectroscopy and the coordination to the alkylated tripeptides at selected pH values inferred from their NMR spectra. If selective coordination of amine/amide donors results in metal complexation, allowing for flexible and adjustable ligand frameworks, then this strategy could potentially be extended to other metal ions and peptide system.

Graphic abstract

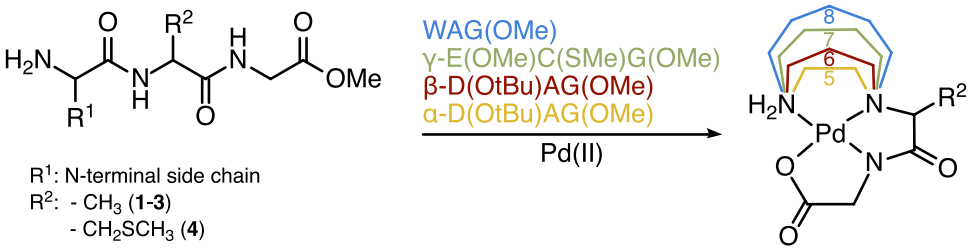

Keywords GSH · Pd(II) · NMR · Potentiometry · Tripeptide · AspAlaGly · β-AspAlaGly · TrpAlaGly

Abbreviations

Ala	Alanine
Asp	Aspartic acid
Cys	Cysteine
En	Ethylene diamine
Fmoc	Fluorenylmethoxycarbonyl
Glu	Glutamic acid
Gly	Glycine
GSH	Glutathione
GSMe	*S*-Methylated glutathione
Trp	Tryptophan
Z	Benzyl carbamate

Electronic supplementary material The online version of this article (https://doi.org/10.1007/s00775-020-01804-0) contains supplementary material, which is available to authorized users.

✉ Sigridur G. Suman
sgsuman@hi.is

[1] Science Institute, University of Iceland, Dunhagi 3, 107 Reykjavik, Iceland

Introduction

The complexation of biological peptides with various transition metal ions has been studied for many decades, specifically in the context of metallodrugs and metal toxicity [1–4]. In general, when complexed, peptides form stable 5-membered ring chelates through the amino, amide backbone, or the carboxylate moiety [5]. Some amino acids have

side-chain groups that are capable of additional coordination, allowing for a variety of geometries [6–15].

The formation of metal amide bonds requires the presence of a primary ligating group, and for simple oligopeptides, once amine coordination takes place, the amide coordination is facilitated [5, 14–16]. Pd(II) ions have a high affinity for nitrogen and soft sulfur donor atoms found in various organic ligands [17–22]. One characteristic feature found in the complexation of palladium(II) and small peptides is the ability of the metal ion to induce deprotonation of the amides [23, 24]. In the absence of coordinating anions, like chloride, the chelation of amides to the palladium ion is complete at pH values below 2, forming planar complexes with remarkable thermodynamic stability [23]. For tripeptides, typical chelation takes place via amine, amide, and carboxylate donor groups to form $\kappa^4(NH_2, N, N, O)$ tetradentate complexes [10].

Glutathione (GSH) is an omnipresent biologically active tripeptide and serves many functions in the body [25]. One distinct function of the GSH tripeptide is metal ion transport, and this functionality is due to the fact that GSH has eight different possible binding sites for metals and its conformational flexibility [26–29]. Soft metal ions like palladium are known to coordinate through the thiolate, a soft base, whereas transition metal ions can also coordinate through the amide functions [25, 30, 31]. In aqueous solutions, this coordination is pH-dependent, since it requires deprotonation of the amide donors.

An unusual characteristic of glutathione is that it is an *iso*-peptide, where the glutamic acid residue forms a γ-peptide bond through its side-chain, which increases the distance from the N-terminus amine to the adjacent amide and thiol moieties. This allows both the N-terminus amine and the thiol to act as an anchoring site for the metal ion [14, 32]. Glutathione is well studied in its native state [25, 33–37] as well as the glutathione thioether derivative [38–40]. When GSH is reacted with K_4PdCl_2 in aqueous solution, $[Pd(GSH)Cl]\cdot 3H_2O$ is formed which then dimerizes to form a chloride bridged species of the $M_2X_2L_2$ type, where Pd(II) is coordinated through the thiol sulfur and amide group on the glycyl residue at a pH of 7–10, forming a five membered ring [26]. When reacted with Ni(II), glutathione yielded a $Ni(HL)\cdot 2H_2O$ complex, which was reported to have octahedral geometry with the water molecules coordinated, one axial and one equatorial, and glutathione forming κ^4[5,7,8] tetradentate coordination [41].

The *iso*-peptide structure of GSH and its function as a metal ion transport brings up an interesting research question; whether it is possible, through pH manipulations and protection of the carboxylate and thiol moieties, to direct chelation of modified GSH. If selective coordination to amine/amide donors results in metal coordination of a κ^4[7,5,5] tetradentate coordination; and if this strategy could potentially be extended to other metal ions and peptide systems. The thiol/thioether side-chain of GSH imparts challenges for future bioinspired applications and, therefore, this work was extended by exchanging the cysteinyl residue for alanyl residue, and the glutamyl residue was exchanged for aspartic acid which has carboxylic acid side-chain that could be coupled to form either the *iso*- or C-terminus coupled peptide. In this way, the formation of either κ^4[6,5,5] or κ^4[5,5,5] membered ring tetradentate coordination geometries can be achieved, allowing for a flexible, adjustable ligand framework for potential bioinspired catalyst design [42]. A similar approach has been employed featuring histidine on the C-terminus of di- and tripeptides with κ^4[5,5,6] type coordination [8, 43].

To this effect, the novel alkylated tripeptides TrpAlaGly(OMe), **1**, β-Asp(O^{t}Bu)AlaGly(OMe), **2**, Asp(O^{t}Bu)AlaGly(OMe), **3**, and the fully methylated GSH, γ-Glu(OMe)Cys(SMe)Gly(OMe), **4** were synthesized (Fig. 1). Using the aa-AlaGly(OMe) framework allowed distinctive NMR resonances for the alanyl and glycyl residues to be identified and interpreted, while avoiding hydrophobicity introduced by larger side chains. Alkylation of the C-terminus both increases non-aqueous solubility and directs coordination to the N-donors. Additionally, a weaker ester donor group potentially serves as a non-rigid donor

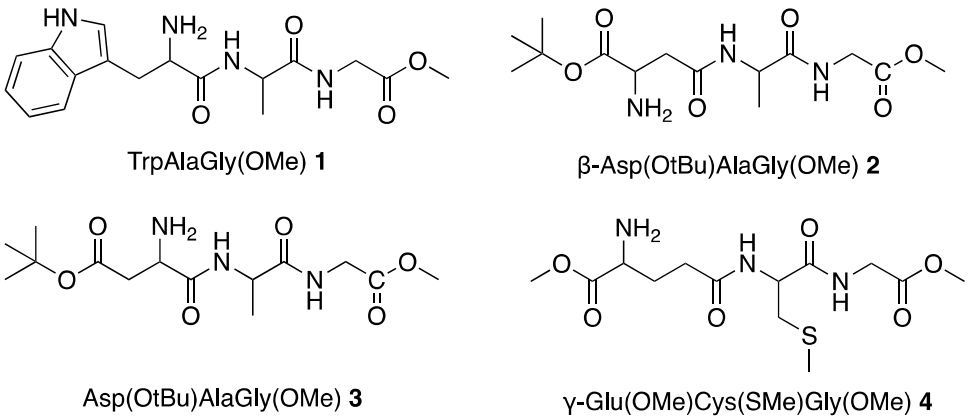

Fig. 1 The tripeptides synthesized and used in Pd-binding studies

offering an open coordination site at the metal center for application such as bioinspired catalysis [42]. Tryptophan was selected due to its five possible coordination sites; in addition to the primary amino and carbonyl functional groups of the acid, indole complexation has been reported through the secondary amine, [44] the C2 carbon, [45, 46] and the C3 carbon [47]. The amino acids β-Asp(O^{t}Bu) and Asp(O^{t}Bu) both have five different coordination sites possible, the amine, two amide groups, and the two esters. The *iso*-peptide, **2**, and the C-terminus coupled **3** allow for the possibility of a direct comparison of chemical reactivities based on the five versus six-membered chelates in future studies. TrpAlaGly(OMe), **1**, was chosen as a sulfur-free alternative for coordination to form chelates larger than six. Currently, it was of interest to see the coordination behavior of these ligands and confirm the different chelate ring sizes which could be verified where the ring size is increased at the N-terminus rather than at the C-terminus [8, 41, 43].

The coordination properties of tripeptides **1–4** to $[Pd(en)(H_2O)_2]^{2+}$ were studied in water. $[Pd(en)(H_2O)_2]^{2+}$ was selected to prevent dimerization of the metal ion [48], and study the initial formation of the Pd complex. pH-dependent coordination was analyzed by NMR spectroscopy and the coordination to the alkylated tripeptides at selected pH values inferred from their NMR spectra and reported literature. The molecular ions of the complexes formed were identified in mass spectra.

Materials and methods

Instrumentation

The NMR spectra were measured at ambient temperature. ^{1}H, COSY, and ^{13}C nuclear magnetic resonance spectra were recorded on a Bruker Avance 400 MHz spectrometer at 400 and 101 MHz, respectively. Solvents used were D_2O, DCl, and NaOD. Infrared spectra were recorded on a Nicolet Avatar 360 FT-IR (E.S.P.) spectrophotometer using KBr pellets. Mass spectra were recorded on a micrOTOF-Q spectrometer, equipped with E-spray atmospheric pressure ionization chamber (ESI). All pH measurements were performed at 298 K with Mettler Toledo pH and conductivity meter using certified buffer solutions of pH 4.01, 7.00, and 10.01.

Solvents and reagents used were purchased from Sigma-Aldrich and used without further purification unless otherwise stated. Alanylglycine, Fmoc-Asp(O^{t}Bu)-OH, Fmoc-Asp(OH)-O^{t}Bu, Z-Trp, and EDC-Cl use in peptide coupling were purchased from Bachem. Solvents used were distilled under nitrogen and dried using standard methods [49]. Thiol methylation of GSH was performed with modification of a published procedure [50]. Alanylglycine esterification was completed by reacting it with trimethylchlorosilane [51] and **4** was isolated as the hydrochloride salt. $[Pd(en)Cl_2]$ [52] and $[Pd(en)(H_2O)_2](NO_3)_2$ [53, 54] were prepared according to the published procedures.

pH titrations

The pH potentiometric titrations were carried out in 15 mL samples using four different metal-to-ligand ratios (0:1, 1:1, 2:1, 4:1). During titration, argon was bubbled through the samples to prevent oxygen and carbon dioxide and to prevent aggregation of the samples. The concentration of the ligand was fixed at ~ 3.2×10^{-3} M and the metal concentration adjusted to fit desired ratios. The ionic strength of the samples was adjusted with KCl to 0.2 M in a 60-fold excess to suppress complex formation due to competitive binding of the Cl^-. The titrations were carried out at constant temperature (298 K). The use of acid to lower the pH before titration was omitted, because the *t*-butyl ester is subject to acid catalyzed hydrolysis. The analytes were titrated with standardized potassium hydroxide and 30–40 data points were obtained for each titration curve. The apparent equilibrium constants were evaluated from the titration data (Table 1) as defined by Eqs. 1 and 2, using the evaluation function on the Excel sheet CurTiPot, developed by Prof. Gutz [55], where M, L, and H represent $[Pd(en)(H_2O)_2]^{2+}$ ion, the ligand, and protons, respectively:

$$pM + qL = rH \rightleftharpoons MpLqHr, \tag{1}$$

$$\beta_{pqr} = \frac{M_pL_qH_r}{[M]^q[L]^q[H]^r}. \tag{2}$$

NMR experimental procedure

The experiments were performed in D_2O. A stock solution of the ligand (0.020 M) and a stock solution of the Pd(II) (0.040 M) complex were mixed in a 1:1 ratio, for a final concentration of 5.0×10^{-3}. The ionic concentration was increased to 0.100 M with KCl and the pH adjusted with NaOD. Stock solutions were prepared fresh daily. The

Table 1 Protonation values of the Pd(II) complexes of tripeptide ligands

	1	2	3	4
Ligand				
pK_{a1} (amine)	9.25	8.79	8.56	8.21
Ligand + M				
pK_{a1} (amide)	7.65	7.33	7.42	–
pK_{a2} (amide)	7.65	7.33	7.42	–

reaction mixture was monitored over a 48 h period using NMR spectroscopy. The results were analyzed using ^{1}H and COSY NMR techniques.

General procedure for compound characterization by MS

The $[Pd(en)(H_2O)_2]^{2+}$ complex was dissolved in water, the ligand added in 1:1 ratio, and the pH increased to 10–11 with 0.1 M NaOH. The solution was allowed to stand for 1 h, then the water distilled off under reduced pressure, and the residue washed with ether to remove free ethylenediamine. The complex was extracted from the residue with MeOH. The methanol solution was diluted for ESI–MS spectra. Complexes with ligands **1**–**3** were obtained in the negative scan mode, and complexes with **4** in the positive scan mode. The complex molecular peaks were simulated to compare with found peaks. The spectra are shown in SI Information Figs. 10–19.

Synthesis

Coupling procedure

Coupling reactions were executed by adding N-protected amino acids to HOBt in a 1:1 molar equivalent and stirring in chloroform at 0 °C. Once the solution cooled, EDC-HCl (1.1 mol eq) was added and stirred for 30 min. AlaGly(OMe)-HCl (1 mol eq) was added, followed by dropwise addition of triethylamine (1.05 mol eq). The solution was stirred under slight N_2 flow at ambient temperature for 24 h. Product was washed with water and dried with $MgSO_4$ and the $CHCl_3$ removed in vacuo. The product was then washed with ether and dried in a vacuum desiccator to obtain clean product.

Z-TrpAlaGly(OCH_3) [56] 1a

Coupling reaction was executed using coupling procedure. Reaction was ran with 50 mL of $CHCl_3$. Z-Trp (1.153 g, 3.407 mmol), HOBt (0.460 g, 3.407 mmol), EDC-HCl (0.719 g, 3.748 mmol), ala-gly(OMe)-HCl (0.670 g, 3.407 mmol), and triethylamine (0.50 mL, 3.578 mmol). The product was purified by washing with water (3 × 20 mL), drying with MgSO4, and then removing the chloroform under reduced pressure. The yield was 1.607 g (98.1%). ^{1}H NMR (400 MHz, $CDCl_3$) δ 8.42 (s, 1H, NH_{indole}), 7.61 (d, J = 7.9 Hz, 1H, $H_{indole\text{-}C5}$), 7.32 (p, J = 3.9, 2.9 Hz, 6H, Ar_{CBZ}), 7.29 (d, J = 8.1 Hz, 2H, $H_{indole\text{-}C8}$), 7.20–7.12 (t, J = 7.5 Hz, 1H, $H_{indole\text{-}C7}$), 7.07 (t, J = 7.5 Hz, 1H, $H_{indole\text{-}C6}$), 7.03–6.99 (m, 1H, $H_{indole\text{-}C2}$), 6.77 (d, J = 5.6 Hz, 1H, NH_{Gly}), 6.61 (s, 1H, NH_{Ala}), 5.78–5.71 (m, 1H, NH_{Asp}), 5.16–5.03 (m, 2H, $CH_{2\text{-}CBZ}$), 4.56 (d, J = 6.9 Hz, 1H, α-H_{Asp}), 4.46 (q, J = 7.2 Hz, 1H, α-H_{Ala}), 3.85 (dd, J = 18.1, 5.6 Hz, 1H, α-H_{Gly}), 3.77–3.64 (m, 1H, α-H_{Gly}), 3.68 (s, 3H, $ROCH_{3\ Gly}$), 3.24 (qd, J = 14.6, 6.4 Hz, 2H, β-H_{Trp}), 1.20 (d, J = 7.0 Hz, 3H, β-H_{Ala}). ^{13}C NMR (101 MHz, $CDCl_3$) δ 172.27 (C=O_{Ala}), 171.62 (C=O_{Trp}), 170.31 (C=O_{Gly}), 156.39 (CO_{CBZ}), 136.34 ($C9_{indole}$), 136.23 (Ar_{CBZ}), 128.69 (Ar_{CBZ}), 128.63 (Ar_{CBZ}), 128.38 (Ar_{CBZ}), 128.26 (Ar_{CBZ}), 127.39 ($C4_{indole}$), 123.65 ($C2_{indole}$), 122.38 ($C7_{indole}$), 119.87 ($C6_{indole}$), 118.86 ($C5_{indole}$), 111.43 ($C3_{indole}$), 110.09 ($C8_{indole}$), 100.11 (Ar_{CBZ}), 77.48, 77.16, 76.84 ($CDCl_3$), 67.31 (CH_{2CBZ}), 55.92 (α-C_{Trp}), 52.43 ($OCH_{3\ Gly}$), 48.92 (α-C_{Ala}), 41.18 (α-C_{Gly}), 28.67 (β-C_{Trp}), and 18.01 (β-C_{Ala}).

Fmoc-β-Asp($OC(CH_3)_3$)AlaGly(OCH_3) 2a

Coupling reaction was executed using coupling procedure. Fmoc-Asp-O^{t}Bu (2.783 g, 6.764 mmol), (HOBt) (0.914 g, 6.764), EDC-HCl (1.426 g, 7.440 mmol), ala-gly(OMe)-HCl (3) (1.330 g, 6.764) and TEA (0.99 mL, 7.102 mmol). The yield was 3.682 g (98.3%). ^{1}H NMR (400 MHz, $CDCl_3$) δ 7.77 (d, *J* = 7.5 Hz, 2H, Ar_{Fmoc}), 7.63 (d, *J* = 7.6 Hz, 2H, Ar_{Fmoc}), 7.41 (t, *J* = 7.5 Hz, 2H, Ar_{Fmoc}), 7.37–7.31 (m, 2H, Ar_{Fmoc}), 7.11 (d, *J* = 5.7 Hz, 1H, NH_{Gly}), 6.61 (d, *J* = 7.5 Hz, 1H, NH_{Ala}), 6.20 (d, *J* = 8.3 Hz, 1H, NH_{Asp}), 4.67 (h, *J* = 7.3 Hz, 1H, α-H_{Ala}), 4.54 (dt, *J* = 9.1, 4.7 Hz, 1H, α-H_{Asp}), 4.36 (q, *J* = 10.4, 9.1 Hz, 2H, CH_{2Fmoc}), 4.23 (t, *J* = 7.2 Hz, 1H, CH_{Fmoc}), 4.18–3.97 (m, 2H, α-H_{Gly}), 3.71 (s, 3H, $ROCH_{3\ Gly}$), 2.99–2.76 (m, 2H, β-H_{Asp}), 1.49 (s, 9H, $RO(CH_3)_{3Asp}$), 1.42 (d, *J* = 7.0 Hz, 3H, β-H_{Ala}). ^{13}C NMR (101 MHz, $CDCl_3$) δ 172.56 (γ-C=O_{Asp}), 170.43 (C=O_{Ala}), 170.16 (C=O_{Asp}), 169.96 (C=O_{Gly}), 156.36 (C=O_{Fmoc}), 143.99 (Ar_{Fmoc}), 141.37 (Ar_{Fmoc}), 127.80 (Ar_{Fmoc}), 127.19 (Ar_{Fmoc}), 125.33 (Ar_{Fmoc}), 120.05 (Ar_{Fmoc}), 82.51 ($ROC(CH_3)_{3Asp}$), 67.31 (CH_{2Fmoc}), 52.48 (OCH_{3Gly}), 51.53 (α-C_{Ala}), 48.83 (α-C_{Asp}), 47.26 (CH_{Fmoc}), 41.23 (α-C_{Gly}), 38.31 (β-C_{Asp}), 28.06 ($OC(CH_3)_{3Asp}$), 18.60 (β-C_{Ala}). IR (KBr, cm^{-1}) 3300 (s, N–H, N–H_2), 1744 (s, C=O–OCH_3), 1730 (sh, C=O–$OC(CH_3)_3$), 1693 (s, Amide I), 1539 (s, Amide II), 1249 (sh, C=O–$OC(CH_3)_3$), 1220 (s, C=O–$OC(CH_3)_3$), and 1158 (s, C=O–OCH_3). MS (ESI/Positive) M ($C_{29}H_{35}N_3O_8$) = 553.6120, M/Z found(calc) = 576.2318(576.2316) [M + Na^+].

Fmoc-Asp($OC(CH_3)_3$)AlaGly(OCH_3) 3a

Coupling reaction was executed using coupling procedure. Reactant amounts are as follows. Fmoc-Asp(O^{t}Bu)-OH (1.406 g, 3.418 mmol), HoBt (0.462 g, 3.418 mmol), EDC-HCl (0.462 g, 3.418 mmol), ala-gly(OMe)-HCl (0.672 g, 3.418 mmol), TEA (0.5 mL, 3.588 mmol). The yield was 1.807 g (95.3%). ^{1}H NMR (400 MHz, $CDCl_3$) δ 7.85–7.69 (m, 2H), 7.66–7.51 (m, 2H), 7.40 (td, J = 7.6,

1.1 Hz, 2H), 7.31 (td, J = 7.5, 1.2 Hz, 2H), 6.89 (s, 2H), 5.88 (d, J = 8.3 Hz, 1H), 4.51 (p, J = 7.0 Hz, 1H), 4.43 (d, J = 7.0 Hz, 1H), 4.22 (t, J = 6.9 Hz, 1H), 4.12–3.89 (m, 2H), 3.72 (s, 3H), 2.94–2.66 (m, 2H), 1.52–1.32 (m, 11H). ^{13}C NMR (101 MHz, $CDCl_3$) δ 172.09 (γ-C=O_{Asp}), 171.24 (C=O_{Ala}), 170.75 (C=O_{Asp}), 170.20 (C=O_{Gly}), 143.83 (C=O_{Fmoc}), 143.76 (Ar_{Fmoc}), 141.45 (Ar_{Fmoc}), 127.94 (Ar_{Fmoc}), 127.24 (Ar_{Fmoc}), 125.15 (Ar_{Fmoc}), 120.18 (Ar_{Fmoc}), 82.30 (ROC$(CH_3)_{3Asp}$), 67.48 (CH_{2Fmoc}), 52.47 (OCH_{3Gly}), 51.50 (α-C_{Ala}), 49.20 (α-C_{Asp}), 47.24 (CH_{Fmoc}), 41.28 (α-C_{Gly}), 37.53 (β-C_{Asp}), 28.17 (OC$(CH_3)_{3Asp}$), 17.73 (β-C_{Ala}). IR (KBr, cm^{-1}) 3307 (s, N–H, N–H_2), 1754 (sh, C=O–OCH_3), 1732 (s, C=O–OC$(CH_3)_3$), 1654 (s, Amide I), 1533 (s, Amide II), 1246 (sh, C=O-OC$(CH_3)_3$), 1216 (s, C=O–OC$(CH_3)_3$), and 1153 (s, C=O–OCH_3). MS (ESI/Positive) M ($C_{29}H_{35}N_3O_8$) = 553.6120, M/Z found(calc) = 576.2316(576.2313) [M + Na^+].

TrpAlaGly(OCH_3) 1

The protecting group Z was removed by adding Z-TrpAlaGly(OMe) (1.515 g, 3.255 mmol) and 150 mg 10% catalyst loaded Pd/C together and evacuating the flask, backfilling with argon. Dry methanol (~ 20 mL) was syringed in. A balloon filled with H_2, attached to a needle, was inserted into the top of the septum, and the N_2 was flushed out of the flask and replaced with H_2 [57]. (Care must be taken because Pd/C is pyrophoric and can cause organic solvents to ignite when air is present.) The reaction mixture was stirred overnight with the H_2 balloon attached. When finished, the H_2 is flushed out by argon and the product is filtered through Celite on a fritted filter and washed with an additional 20 mL of methanol. Methanol was removed under reduced pressure with slight heat. Yield was 0.912 g (85%) ^{1}H NMR (400 MHz, $CDCl_3$) δ 8.30 (s, 1H, NH_{indole}), 7.69 (d, J = 7.8 Hz, 1H, NH_{Ala}), 7.65 (dd, J = 7.9, 1.0 Hz, 1H, $H_{indole\text{-}C5}$), 7.36 (dt, J = 8.1, 1.0 Hz, 1H, $H_{indole\text{-}C8}$), 7.20 (ddd, J = 8.2, 7.0, 1.2 Hz, 1H, $H_{indole\text{-}C7}$), 7.11 (ddd, J = 8.0, 7.0, 1.1 Hz, 1H, $H_{indole\text{-}C6}$), 7.07 (d, J = 2.4 Hz, 1H, $H_{indole\text{-}C2}$), 6.99 (t, J = 5.4 Hz, 1H, NH_{Gly}), 4.51 (p, J = 7.2 Hz, 1H, α-H_{Ala}), 4.07–3.91 (m, 2H, α-H_{Gly}), 3.78–3.73 (m, 1H, α-H_{Asp}), 3.73 (s, 1H, ROC$H_{3\ Gly}$), 3.35 (ddd, J = 14.5, 4.4, 0.9 Hz, 1H, β-H_{Trp}), 2.97 (dd, J = 14.5, 8.6 Hz, 1H, β-H_{Trp}), 1.72–1.65 (m, 2H, NH_{2Trp}), 1.31 (d, J = 7.0 Hz, 3H, β-H_{Ala}). ^{13}C NMR (101 MHz, $CDCl_3$) δ 175.44 (C=O_{Trp}), 172.66 (C=O_{Ala}), 170.35 (C=O_{Gly}), 136.53 ($C9_{indole}$), 127.56 ($C4_{indole}$), 123.29 ($C2_{indole}$), 122.45 ($C7_{indole}$), 119.79 ($C6_{indole}$), 119.03 ($C5_{indole}$), 111.51 ($C3_{indole}$), 111.42 ($C8_{indole}$), 55.45(α-C_{Trp}), 52.48 (ROC$H_{3\ Gly}$), 48.51 (α-C_{Ala}), 41.28 (α-C_{Gly}), 30.67 (β-C_{Trp}), 17.36 (β-C_{Ala}). IR (KBr, cm^{-1}) 3389 (sh, N–H, N–H_2), 3296 (b, N–H, N–H_2), 3056 (m, aromatic C–H stretch), 1749 (s, C=O–OCH_3), 1655 (s, Amide I), 1517 (s, Amide II), 1213 (s, C=O–OCH_3), 745 (s, aromatic C–H bend). UV–Vis($CHCl_3$), ε_{281} = 6114 L/mol cm. Specific rotation $[\alpha]_D = -18.76°$ (2.5 mg/100 mL, DMSO). MS (ESI/Positive) MW ($C_{17}H_{22}N_4O_4$) = 346.164, M/Z found(calc) = 347.1714(347.1709) [M + H^+]. CHN: ($C_{17}H_{22}N_4O_4$) found(calc) %, C: 58.78(58.95), H: 6.38(6.40), N: 15.91(16.17).

β-Asp(OC$(CH_3)_3$)AlaGly(OCH_3) 2

The protecting group Fmoc was removed by stirring Fmoc-β-Asp(O^{t}Bu)AlaGly(OMe) (3.778 g, 6.764 mmol) (2a) in 10 mL of DMF at 110 °C for 40 min [58]. Methanol was added to the DMF and was washed with 3 × 10 mL hexane. The DMF was removed in vacuo and the product purified with flash chromatography. Yield for this reaction was 2.120 g (94%) and after purification 1.296 g. ^{1}H NMR (400 MHz, $CDCl_3$) δ 8.20 (d, J = 6.3 Hz,1H, NH_{Ala}),8.03(d,J = 7.2 Hz,1H, NH_{Gly}),4.63(q,J = 7.2 Hz,1H, α-H_{Ala}), 4.38 (d, J = 6.9 Hz, 1H, α-H_{Asp}), 4.05 (qd, J = 17.6, 5.5 Hz, 2H, α-H_{Gly}), 3.75 (d, J = 5.7 Hz, 3H, ROC$H_{3\ Gly}$), 3.26 (ddd, J = 72.9, 17.2, 4.4 Hz, 2H, β-H_{Asp}), 1.51 (s, 9H, RO$(CH_3)_3$), 1.47 (d, J = 7.1 Hz, 3H, β-H_{Ala}). ^{13}C NMR (101 MHz, $CDCl_3$) δ 172.86 (γ-C=O_{Asp}), 171.90 (C=O_{Ala}), 170.60 (C=O_{Asp}), 170.49 (C=O_{Gly}), 82.83 (ROC$(CH_3)_{3Asp}$), 52.46 (OCH_{3Gly}), 51.68 (α-C_{Asp}), 49.12 (α-C_{Ala}), 41.20 (α-C_{Gly}), 38.51 (β-C_{Asp}), 28.05 (OC$(CH_3)_{3Asp}$), 17.76 (β-C_{Ala}). IR (KBr, cm^{-1}) 3385 (b, N–H, N–H_2), 3307 (b, N–H, N–H_2), 1743 (sh, C=O–OCH_3), 1728 (s, C=O–OC$(CH_3)_3$), 1653 (s, Amide I), 1541 (s, Amide II), 1254 (s, C=O–OC$(CH_3)_3$), 1210 (s, C=O–OC$(CH_3)_3$), 1155 (s, C=O–OCH_3). UV–Vis($CHCl_3$), ε_{258} = 1638.3 L/mol cm. Specific rotation $[\alpha]_D = -353.1°$ (2.5 g/100 mL, DMSO). MS (ESI/Positive) M ($C_{14}H_{25}N_3O_6$) = 331.368, M/Z found(calc) = 354.1633(354.1636) [M + Na^+]. CHN: ($C_{14}H_{25}N_3O_6$) found(calc) %, C: 50.28(50.75), H: 7.11(7.60), N: 13.86(12.68).

Asp(OC$(CH_3)_3$)AlaGly(OCH_3) 3

The protecting group Fmoc was removed using the same as procedure used above. Fmoc-Asp(O^{t}Bu)AlaGly(OMe) (2.453 g, 4.443 mmol) (**3a**). The yield was 82%. ^{1}H NMR (400 MHz, $CDCl_3$) δ 8.39–8.29 (d, J = 6.7 Hz, 1H, NH_{Ala}), 7.87 (t, J = 5.9 Hz, 1H, NH_{Gly}), 7.26 ($CDCl_3$), 4.58 (p, J = 7.0 Hz, 1H, α-H_{Ala}), 4.50 (d, J = 6.2 Hz, 1H, α-H_{Asp}), 3.98 (qd, J = 17.8, 5.6 Hz, 2H, α-H_{Gly}), 3.71 (s, 3H, ROC$H_{3\ Gly}$), 3.11 (t, J = 6.6 Hz, 2H, β-H_{Asp}), 1.42 (d, J = 4.1 Hz, 13H, RO$(CH_3)_3$ Asp, β-H_{Ala}). ^{13}C NMR (101 MHz, $CDCl_3$) δ 172.75 (γ-C=O_{Asp}), 170.77 (C=O_{Ala}), 170.24 (C=O_{Asp}), 168.44 (C=O_{Gly}), 82.93 (ROC$(CH_3)_{3\ Asp}$), 52.30 ($OCH_{3\ Gly}$), 50.23 (α-C_{Asp}), 49.95 (α-C_{Ala}), 41.04 (α-C_{Gly}), 36.23 (β-C_{Asp}), 28.00 (OC$(CH_3)_{3\ Asp}$), 17.59 (β-C_{Ala}). IR (KBr, cm^{-1}) 3360 (b, N–H, N–H_2), 3235 (b, N–H, N–H_2), 1755 (sh, C=O–OCH_3),

1728 (s, C=O–OC(CH_3)$_3$), 1670 (s, Amide I), 1545 (s, Amide II), 1249 (s, C=O–OC(CH_3)$_3$), 1214 (s, C=O–OC(CH_3)$_3$), and 1158 (s, C=O–OCH_3). UV–Vis($CHCl_3$), ε_{286} = 157.97 L/mol cm. Specific rotation [α] = − 1.4°(2.5 g/100 mL, DMSO). MS (ESI/Positive) M ($C_{14}H_{25}N_3O_6$) = 331.368, M/Z found(calc) = 332.1816(332.1816) [M + H^+]. CHN ($C_{14}H_{25}N_3O_6$)·1/2 H2O found(calc) %, C: 49.60(49.40), H: 7.58(7.70), N: 12.31(12.35).

γ-Glu(OMe)Cys(SMe)Gly(OMe) 4

The methyl esterification of GSH(SMe) was completed by adding GSH(SMe) (0.520 mg, 1.620 mmol) to distilled MeOH (20 mL) along with trimethylchlorosilane (0.825 mL, 6.510 mmol) [51]. This mixture was stirred under N2 for 24 h. An additional 0.825 mL of Me_3SiCl was added and the reaction stirred for another 24 h. The solvent was removed in vacuo, and the product stirred in diethylether. The ether was decanted off, resulting in isolation of a white hydroscopic powder as the hydrochloride salt of **4**. The yield was 0.514 g (82%). ^{1}H NMR (400 MHz, D_2O) δ 4.52 (dd, J = 8.7, 5.3 Hz, 1H, α-H_{Cys}), 4.13 (t, J = 6.7 Hz, 1H, α-H_{Glu}), 3.98 (d, J = 1.5 Hz, 2H, α-H_{Gly}), 3.79 (s, 3H, $ROCH_{3\ Glu}$), 3.69 (s, 3H, $ROCH_{3\ Gly}$), 2.99–2.91 (m, 1H, β-H_{Cys}), 2.80 (dd, J = 14.1, 8.7 Hz, 1H, β-H_{Cys}), 2.62–2.45 (m, 2H, β-H_{Glu}), 2.27–2.12 (m, 2H, γ-H_{Glu}), 2.08 (s, 3H, $RSCH_{3\ Cys}$). ^{13}C NMR (101 MHz, D_2O) δ 174.15 (δ-C=O_{Glu}), 173.06 (C=O_{Gly}), 171.76 (C=O_{Cys}), 170.14 (C=O_{Glu}), 53.65 (OCH_{3Glu}), 52.79 (OCH_{3Gly}), 52.62 (α-C_{Gly}), 52.16 (α-C_{Cys}), 41.20 (α-C_{Glu}), 34.87 (β-C_{Cys}), 30.65 (SCH_3), 25.26 (β-C_{Glu}), 14.63 (γ-C=O_{Glu}). IR (KBr, cm^{-1}): 3396(ms), 3257(ms) (N–H, R_2–NH), 3059 (ms, N–H, R–NH_3^+), 1748 (s, C=O–OCH_3), and 1645 (s, Amide I). UV–Vis(H_2O), ε_{258} = 30.8 L/mol cm. Specific rotation $[\alpha]_D$ = − 209.75° (2.5 g/100 mL, DMSO). MS (ESI/Positive): M ($C_{13}H_{24}N_3O_6S$) = 349.40, M/Z found (calc.) = 350.1380(350.1370) [M + H^+].

Results and discussion

The synthesis and characterization of three new tripeptide ligands (Fig. 1, **1**–**3**) is reported here. Although the parent tripeptides have been identified as fragments in protein digestion, [59–61] the ligands **1**–**3** were not synthesized previously. The thioether of glutathione is reported [62] and has been studied, [38–40] while the product of complete methylation is reported here for the first time (Fig. 1, **4**).

Synthesis

The synthesis of the tripeptides was achieved using solution phase peptide synthesis. Solution phase synthesis has many benefits for short peptide synthesis, including larger scale synthesis and less consumption of materials [63–65]. Either Z- or Fmoc-protecting groups were used in coupling reactions (Scheme 1), based on availability and cost of the protected amino acid.

The choice to use both the methyl ester and *t*-butyl ester on **2** and **3** presented itself with a variety of challenges in the synthesis. The *t*-butyl ester was selected as a commercially available protection on the Fmoc-protected aspartic acid, and the methyl ester protection was chosen over the *t*-butyl or ethyl because of facile completion of the esterification reaction for the methyl ester with quantitative yields. The reaction scheme is shown in Scheme 1. Dipeptide AlaGly was alkylated to AlaGly(OMe), and coupled with Z-(**1**) or Fmoc-protected α- or β-Asp(O^{t}Bu)(OH) (**2**,**3**) starting material in a coupling reaction that was optimized for facile work-up.

Esterification reactions to produce *t*-butyl or ethyl esters required long reaction times, and resulted in incomplete esterification and loss of yields. Challenges presented themselves in the selection of a deprotection method for the Fmoc or Z and work-up procedures to obtain pure compounds. Methyl ester hydrolysis is catalyzed by basic conditions above a pH of 10, whereas *t*-butyl esters are catalytically hydrolyzed in acidic conditions below a pH of 2, and is very sensitive to heating [66]. Complications arose during work-up due to the common solubilities of the product and side products, making separation difficult, this was solved through selection of solvent and base for the reaction.

Standard Fmoc cleavage procedures in basic medium could not be employed. Attempted deprotection of Fmoc-Asp(O^{t}Bu)AlaGly(OMe) and Fmoc-β-Asp(O^{t}Bu) AlaGly(OMe) using standard basic conditions resulted in the formation of aspartimide. DMF solvent mediated Fmoc cleavage worked well, although residual DMF content likely contributed to very hygroscopic behavior of the crude compounds. Dry, well-behaved, analytically pure compounds were isolated after washing them thoroughly with dry solvent after flash chromatography.

Attempts to precipitate out the HCl salt of **2** and **3** produced the partially hydrolyzed *t*-butyl ester species. Dry reaction conditions under inert air were used to precipitate the products using a HCl/Et_2O solution. Synthesis and purification of **1**, (Scheme 1) were straightforward using standard methods when employing the Z amine protecting group. After isolation and purification, **1**–**3** were stored under nitrogen in the freezer.

Two possible synthetic routes were explored to achieve complete alkylation of GSH to form **4** (Scheme 2). S-alkylated GSH, (GSMe) is commercially available, while fully methylated glutathione is not. For the desired experimental quantity, GSH was used as a starting material and both carboxylate esters and the thiol were alkylated to form the methyl esters of glutathione. In Route 1, esterification is followed by thiol methylation. Complete alkylation using

Scheme 1 Synthesis scheme for ligands **1**–**3**

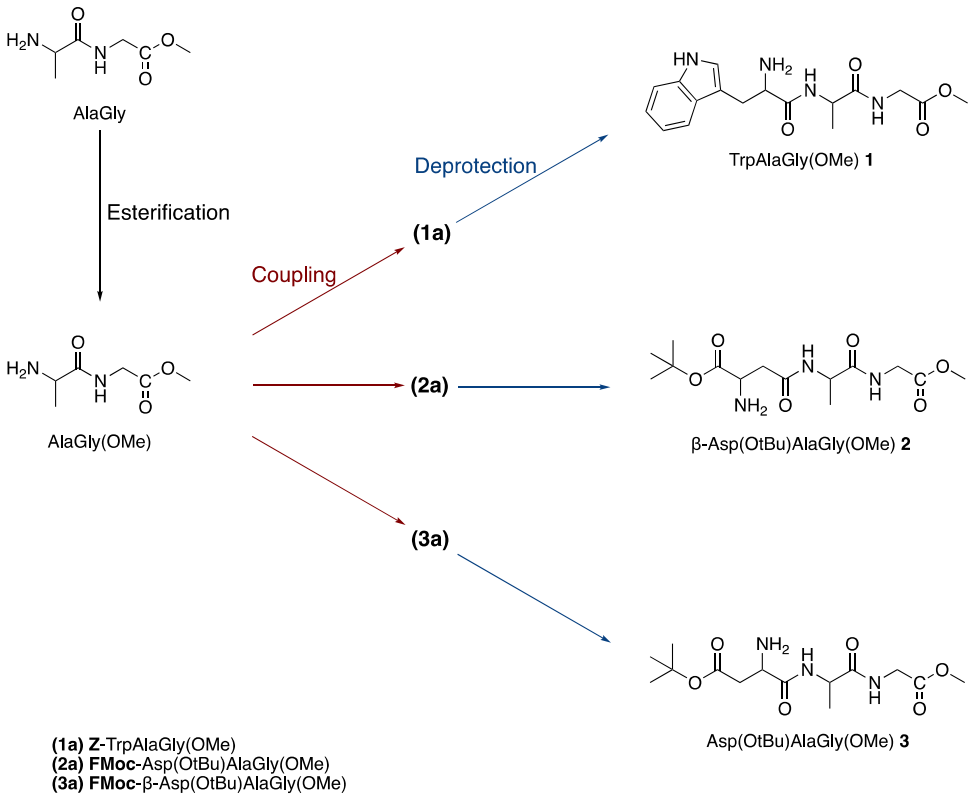

Scheme 2 Synthesis scheme for ligand **4**

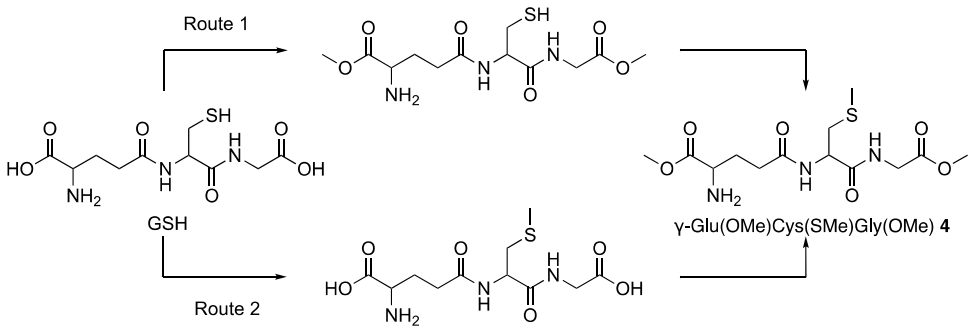

Route 1 proved unsuitable, since the basic aqueous conditions employed caused hydrolysis of the methyl esters. In the second approach, (Route 2) the thioether is formed first, followed by the esterification reaction. These successive reactions showed complete alkylation forming the hydrochloride salt of **4**.

All tripeptides were fully characterized using ^{1}H, ^{13}C, COSY, and HSQC, NMR spectroscopy, as well as ESI–MS, IR, UV–Vis, and elemental analysis. MS, ^{1}H, and ^{13}C are provided in the supplementary information (Figures SI 6A-9C).

Binding motifs and coordination geometries were investigated for compounds **1**–**4** in water with the metal ion $[Pd(en)(H_2O)_2]^{2+}$ employing ^{1}H-NMR spectroscopy and potentiometric titrations.

Potentiometric studies

Determination of the pK_a of ligands using pH titrations

Ligands **1**–**4** contain methyl esters on the C-terminus of the tripeptides. With the *t*-butyl esters protecting the side-chain of the aspartic acid residue on **2** and **3**, and the cysteinyl of **4** transformed into a thioether, only the amine deprotonation needs to be determined. The experimentally determined pK_a values are listed in Table 1. The pH titration curves are shown in SI information Figure SI 1. Conventionally, acid would be added to the mixture to ensure that the entire pH range is covered. However, this was

not possible here due to the acid hydrolytic sensitivity of the *t*-butylester. As a consequence, the titrations begin in the mid-pH range. Amino acid titrations normally need to cover the full pH value range to determine the pK_a of the carboxylate, which is observed below a pH of 3 [67]. However, in compounds **1**–**4**, this moiety has been converted to an ester, which should not affect the collection of data.

Ligand **1** has an amine and two amide groups as well as an indole amine group. By itself, ligand **1** shows amine deprotonation at a pH of 9.25. The reported pK_a of free tryptophan is 9.34 [67]. Again for **2**, the amine group is the only measurable pK_a; this was found to be 8.78. For **3,** the experimentally determined pK_a was 8.56, where the pK_a for aspartic acid is 9.66 [67]. Compound **2** amine being further away from the peptide bond experiences less effects than **3**. For compound **4,** two deprotonations seem to occur, one at 8.26 and another at 9.95. The pK_a value at 8.26 may correspond to deprotonation of the partially hydrolyzed thioether, where the pK_a for the thiol on GSH is 8.75 [67]. The second pK_a found is the amine deprotonation, where, for GSH, this value is 9.65. These differences in the pK_a values of the amino acid and the corresponding peptides are due to peptide bond formation.

Titrations of the ligands with $[Pd(en)(H_2O)_2]^{2+}$

Titrations of **1**–**4** with $[Pd(en)(H_2O)_2]^{2+}$ were performed in three different ligand-to-metal ratios. The titration curves are shown in Figure SI 1 along with the ligand titrations. As $[Pd(en)(H_2O)_2]^{2+}$ is added to the ligand solution, there is a drop in pH due to the Lewis acid nature of Pd(II). When more ligand is added, the shift to lower pH values is diluted for 2:1 ratio of ligand-to-metal and insignificant at a 4:1 ratio. This observation suggests that the plots for a 2:1 ratio are a combination of the free ligand and the 1:1 ratio titration. This pattern is also observed in the 4:1 titration data. It is clear from the plots that the en successfully inhibits the formation of bis type complexes, even with the addition of excess ligand. Therefore, it is sufficient to study the species present in the 1:1 ratio to identify all of the metal coordinated species in the mixtures. As before, the initial pH was not adjusted with the addition of acid, preventing observation of amine deprotonation, and allowing only the observation of amide deprotonation. The amide deprotonation takes place at significantly lower pH upon coordination, in the range of 7.33 to 7.65, as the Pd(II) coordination drives the deprotonation at a lower pH. No discernible deprotonation could be identified for solution **4** with $[Pd(en)(H_2O)_2]^{2+}$

pH-dependent NMR studies

pH-dependent NMR studies were performed in D_2O. A stock solution of the ligands (**1**–**4**) (0.020 M) and a stock solution of the Pd(II) (0.040 M) complex were mixed in a 1:1 ratio, for final concentrations of 5.0×10^{-3} M. The ionic concentration was increased to 0.100 M with KCl and the pH adjusted with NaOD. The reaction mixture was monitored over a 48-h period using NMR spectroscopy.

pH-dependent coordination of $[Pd(en)(H_2O)_2](NO_3)_2$ with 1

The initial pD of the mixture of $[Pd(en)(H_2O)_2]^{2+}$ and **1** resulted in a pD value of 4.76. This resulted in the formation of two metal complex isomers, in approximately a 1:1 ratio (Fig. 2). One of the isomers shows a large downfield shift for the α-C protons on the tryptophan residue, indicating primary amine coordination, followed by amide chelation, as indicated by the shift of the β-C*H* on the alanine residue. Furthermore, the en group is still present, as seen by the presence of its bound singlet at 2.71 ppm, leading to proposed structure **Pd-1A**. The second isomer present at this pH has a mono-coordinated ethylenediamine.

In a mono-coordinated ethylenediamine, the methylene protons are no longer equivalent, and they split to form three resonances [68]. For the second isomer, the multiplet at 2.50 ppm integrates to two protons corresponding to the distant CH_2 group of en. The multiplets at 2.14 ppm and 2.30 ppm integrate to one H each and represent the two non-equivalent protons closer to the Pd ion.

Evidence for indole amine coordination is seen in the doubling of all resonances for the entire indole moiety, with downfield shifts ~ 0.10 ppm. The indole coordination appears to be accompanied by both amides coordinating as seen by the shift in the α, and β-C protons for the tryptophan, alanine, and glycine residues. The corresponding coordination geometry is shown for **Pd-1B**, where an eight-membered ring has formed between the indole amine and the alanine amide, which then continues to the glycine amide, replacing one of the ethylenediamine donors to form a tridentate species. As the pD is increased to 6.52, this second isomer, **Pd-1B**, is the only species present in the NMR spectrum.

Increasing the pD to 7.92 results in complete dissociation of en as evidenced by appearance of free en signals at 2.77, leading to likely carboxylate ligation and suggests **Pd-1C** as the best model for this pH. The disappearance of the methyl ester signal (3.78 ppm) and the parallel appearance of MeOD at 3.37 ppm confirms ~ 75% methyl ester hydrolysis. Palladium catalyzed hydrolysis of methyl

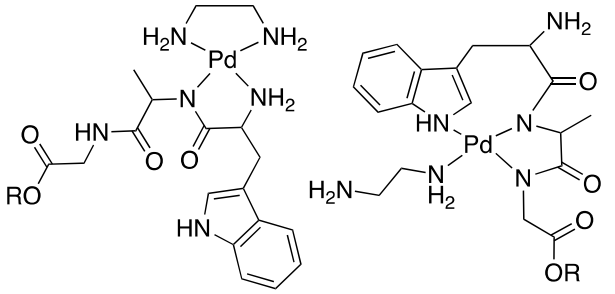

Pd-1A

Pd-1B

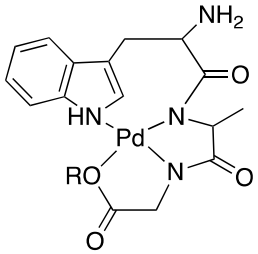

Pd-1C

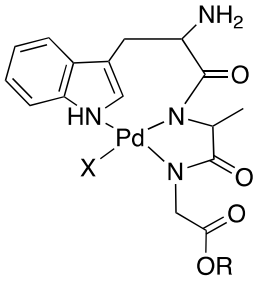

Pd-1D

pD	Species present		% Ester Hydrolysis	
			R (OMe)	R′ (O^{t}Bu)
4.76	A ~50%	B ~50%	~10	~
6.52	B ~100%	~	~19	~
7.92	C ~100%	~	~75	~
11.54	C ~75%	D ~25%	100	~

Fig. 2 Possible coordination geometries of **1** (5 mmol L^{-1}) with $[Pd(en)(H_2O)_2]^{2+}$ (5 mmol L^{-1}) (c_{KCl} = 100 mmol L^{-1}) over the pD range of 4.75–11.54, with hydrolysis values present after 1 h

esters for alanylglycine is known to occur at a pH of 4–5 [69, 70]; however, base catalyzed hydrolysis of methyl esters tends to start at pH values greater than 10 [66], indicating observed ester hydrolysis is Pd(II) catalyzed.

At pD of 11.54, the methyl ester is completely hydrolyzed and a new minor species appears (**Pd-1D**), as indicated by a shift in the methylene group of glycine. This new species is tentatively a hydrolyzed Pd(II), i.e., containing [71] a coordinated hydroxo group rather than the carboxylate group. At basic pH values, the fourth coordination site in Pd(II) peptides complexes has been reported as occupied by hydroxide ions [23] [72, 73].

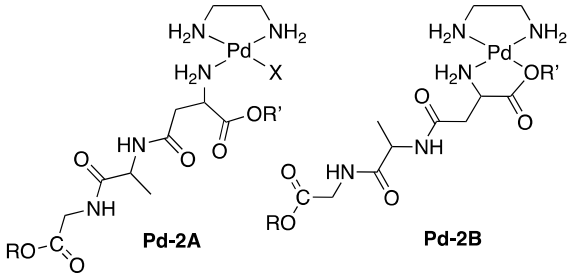

Pd-2A

Pd-2B

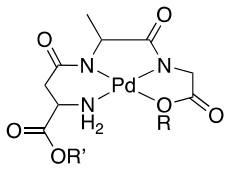

Pd-2C

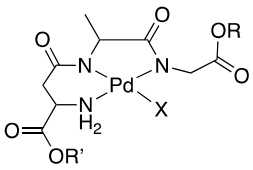

Pd-2D

pD	Species present		% Ester Hydrolysis	
			R (OMe)	R′ (O^{t}Bu)
5.01	A ~100%	~	~10	~8
6.93	B ~100%	~	~20	~20
9.21	C ~100%	~	~65	~35
11.06	C ~70%	D ~30%	100	~70

Fig. 3 Possible coordination geometries of 2 (5 mmol L^{-1}) with $[Pd(en)(H_2O)_2]^{2+}$ (5 mmol L^{-1}) (c_{KCl} = 100 mmol L^{-1}) over the pD range of 5.01–11.06, with hydrolysis values present after 1 h

pH-dependent coordination of $[Pd(en)(H_2O)_2](NO_3)_2$ with 2

Initial pD of the $[Pd(en)(H_2O)_2]^{2+}$ and **2** solution was 5.01. Observed coordination geometry of **2** and $[Pd(en)(H_2O)_2]^{2+}$ is shown in Fig. 3. Complexation was seen immediately by the downfield shift of the α-C Asp protons as well as the β-C Asp protons and the broadening and doubling of the en methylene protons of the $[Pd(en)]^{2+}$, due to the *trans* effect. This suggests a monodentate binding geometry as as seen in **Pd-2A**. However, some methyl ester hydrolysis (10%) and *t*-butyl hydrolysis (< 8%) are also occurring. No evidence of bidentate coordination of the peptide was observed at this pH.

At pD of 6.93, an upfield shift of the Asp α-C*H* and hydrolysis of the Asp *t*-butyl ester was observed, as indicated by the appearance of a *t*-butanol signal. Two species appear to be present, both with the coordination geometry **Pd-2B**; the majority (> 80%) showing probable $\kappa^2(NH_2, O^tBu)$ binding and the other (< 20%) showing $\kappa^2(NH_2, O–)$ binding due to *t*-butyl ester hydrolysis. Hydrolysis of the methyl ester reaches ~ 20% as indicated by the growing MeOH signal. Negligible change was associated with the

chemical shifts of Ala and Gly moieties. No evidence of amide chelation was present.

As many as four isomers were present at a pD of 9.61 due to varying degrees of hydrolysis of the methyl and *t*-butyl ester. The coordination geometry of all of the isomers is represented by **Pd-2C**. This assignment is deduced by dissociation of en and a concomitant shift of the Ala and Gly protons signaling amide binding, suggesting a $\kappa^4(NH_2, N, N, O)$ coordination geometry. Methyl and *t*-butyl ester hydrolysis was estimated to be ~ 65%/35% respectively, where the *t*-butyl ester hydrolysis was likely Pd-catalyzed, induced by the proximity of the ester to the Pd-NH_2 group.

At highly basic conditions of pD at 11.20, complete hydrolysis of the methyl ester was observed, and *t*-butyl ester hydrolysis was ~ 70%, while the major species maintained the coordination geometry shown as **Pd-2C**. Another minor species was observed via the shift of the Gly methylene protons suggesting dissociation of the Gly carboxylate from the metal. This species exhibits probable formation of a Pd-hydroxo species, as suggested by coordination geometry **Pd-2D**.

pH-dependent coordination of $[Pd(en)(H_2O)_2](NO_3)_2$ with 3

A mixture of $[Pd(en)(H_2O)_2]^{2+}$ with **3** at a pD of 3.77 did not result in complexation judged by the fact that the resonances from the $[Pd(en)(H_2O)_2]^{2+}$ complex remained intact. The amine protons shifted by 0.04 ppm, due to the change in pH, but all other resonances remain unchanged. The overall integration for ethylene diamine was low, due to precipitation of $[Pd(en)(H_2O)_2]^{2+}$ from solution. This precipitation is consistent with reports stating that amine coordination to the $[Pd(en)]^{2+}$ fragment does not take place until a pH of 4 due to competitive binding to Cl^- [23].

At a pD of 4.71, the formation of a new species, **Pd-3A** (Fig. 4), was observed. The tripeptide formed a tridentate species with Pd(II) that has a mono-coordinated ethylenediamine occupying the fourth coordination site. Evidence for this structure was seen in a significant shift of α- and β-C protons of the three amino acid residues, along with the doubling and broadening of the ethylene diamine resonance at 2.77 ppm. Free tripeptide **3** was still present amounting to about ~ 50% based on integrations. Convergence of the NMR resonances at pD of 7.34 evidenced coordination geometry **Pd-3A** becomes the major species. At this pD, the methyl ester starts hydrolyzing, and after 8 h, about 35% of the ester has been hydrolyzed.

After raising the pD to 11.20, the formation of tetradentate species **Pd-3B** is evidenced by the upfield shift of the α-C protons for glycine by 0.3 ppm and the complete dissociation of coordinated ethylene diamine, which was observed as free en at 2.78 ppm. At this pD, the methyl ester was completely hydrolyzed, and the *t*-butyl ester was ~ 30% hydrolyzed after 8 h.

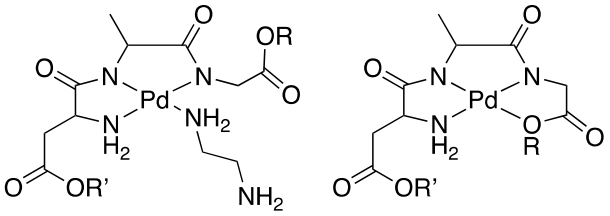

pD	Species present		% Ester Hydrolysis	
			R (OMe)	R' (O^tBu)
3.77	**3** ~100%	~	~0	~0
4.71	A ~55%	**3** ~45%	~12	~5
7.34	A ~100%	~	~35	~5
11.20	B ~100%	~	100	~30

Fig. 4 Possible coordination geometries of **3** (5 mmol L^{-1}) with $[Pd(en)(H_2O)_2]^{2+}$ (5 mmol L^{-1}) (c_{KCl} = 100 mmol L^{-1}) over the pD range of 3.75–11.25 with hydrolysis values present after 1 h

pH-dependent coordination of $[Pd(en)(H_2O)_2](NO_3)_2$ with 4

The reaction of $[Pd(en)(H_2O)_2]^{2+}$ with **4** at a pD of 2.30, observed via NMR, formed a species that appears to have κ^2(S,N) coordination (**Pd-4A,** Fig. 5). Initially, glutathione was bound to the metal through the thioether, as seen in the downfield S-methyl shift from 2.18 to 2.46 ppm, as time progresses, the thioether hydrolyzes resulting in the formation of MeOD. This hydrolysis started at ~ 5%, and after 48 h, had increased to ~ 72%. The en remains coordinated but shifts due to *trans* effects from 2.71 to 2.85 ppm, and this shift is accompanied by broadening of the signal. The evidence for cysteinyl amide coordination was seen in the downfield shift of the α-C*H* by 0.38 ppm, as well as the downfield shift of the β-C protons.

As the pD was raised to 3.06, **Pd-4A** only achieves ~ 50% formation, and mono-coordinated complex **Pd-4B** accounts for the other 50% speciation. Support for the formation of this species is the upfield shift in the α-C Glu residue to 3.8 ppm and the downfield shift of the Glu β- and γ-methylene protons. This coordination was also supported by the en resonance at 2.72 ppm. Here, the fourth coordination could be stabilized by a chloride ion, a water molecule, or possibly by the formation of a dimer. The thioether is hydrolyzed by approx. 55% after 1 h. Although challenging

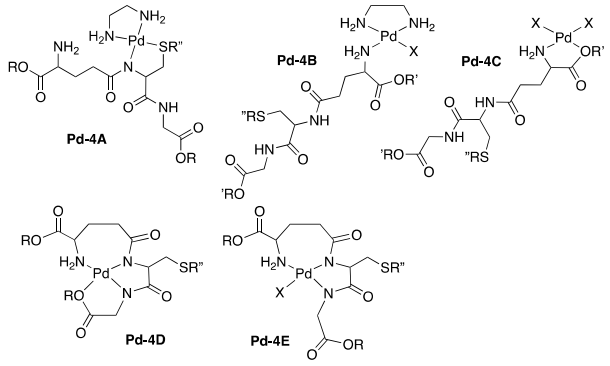

pD	Species present			% Ester/Thioether Hydrolysis	
				R (OMe)	R″ (SMe)
2.30	A ~ 100%	~	~	~ 0	~ 30
3.06	A ~ 50%	B ~ 50%	~	~ 0	~ 55
7.70	C ~ 90	B ~ 10	~	~ 21	~ 0
8.70	C ~ 80	D ~ 20	~	~ 80	~ 0
11.30	C ~ 30	D ~ 30	E ~ 30	100	~ 0

Fig. 5 Possible coordination geometries of **4** (5 mmol L^{-1}) with $[Pd(en)(H_2O)_2]^{2+}$ (5 mmol L^{-1}) (c_{KCl} = 100 mmol L^{-1}) over the pD range of 2.30–11.30 with hydrolysis values present after 1 h

to integrate accurately, the esters appear intact at pH values lower than 3.60.

At a pD of 7.70, the **Pd-4A** species was no longer present. The en group shifts to 2.78 ppm, signifying dissociation from the metal center. The slight upfield shift of the methyl ester protons of the Glu residue from 3.89 to 3.83 ppm signifies chelation to the Glu carboxylate, forming a five-membered chelate with the coordination geometry **Pd-4C**. Methyl ester hydrolysis was quantified at 21% after 1 h forming methanol. The thioether remains intact.

Pd-4C was still the major species at a pD value of 8.70, but a new minor species with tetradentate $\kappa^4(NH_2,N,N,O)$ was formed, as represented by **Pd-4D**. This observation was supported by a quadruplet observed at 4.19 ppm corresponding to Cys α-C, and by a Glu α-C protons triplet at 4.55 ppm. Further coordination was evidenced an upfield shift of the Glu β- (0.15 ppm), and γ- (0.25 ppm) methylene protons.

Once the basic pD of 11.30 is reached, the formation of a third species was observed; the probable Pd-hydroxo species (**Pd-4E**). At these basic conditions, the methyl esters were fully hydrolyzed, while the thioether remains intact.

Mass spectra of Pd(II) complexes with 1–4

The complexes were not amenable to isolation from aqueous solutions because of the multiple species present in solution and separation of products proved a serious challenge. As identification of the species present, mass spectra were obtained. The results summarized in Table 2 and SI Figs. 10–19 show the found and simulated spectra for the complexes. pH of 10.5 was chosen, assuming that molecular peaks of the expected complexes could be identified in the mass spectrum. At high pH, it is expected to see the carboxylate of the C-terminus amino acid as the fourth donor to Pd(II) or alternatively, either Cl^- or OH^- from the solution mixture.

The methyl ester hydrolysis is rapid and only ligand **1** showed peaks with the methyl ester intact. The t-butyl ester was observed in spectra of **2** and **3**. Ligand **4** confirmed an intact thioether.

The complexes predicted by NMR did show their molecular ion peaks in the mass spectrum. Ligands **1** and **3** showed the presence of ethylene diamine in minor peaks that could be caused by incomplete removal of free ethylene diamine during sample preparation.

Discussion

Coordination of $[Pd(en)(H_2O)_2]^{2+}$ with **1** through the indole nitrogen led to an unusual eight-membered chelate. Predictions could be made for 5-, 7-, or 8-membered chelates with **1**, although 8-membered chelates are rare [74]. Formation

Table 2 Summary of expected and found molecular ion peaks in the mass spectra of **1**–**4** with $[Pd(en)(H_2O)_2]^{2+}$ at pH of ~ 10.5

Ligand	Species expected by NMR			Species found by MS		
1	**Pd-1C** *major*	**Pd-1D** *minor*	–	**Pd-1C** *major*	**Pd-1D** *minor*	**Pd-1B**[1] *minor*
2	**Pd-2C** *major*	**Pd-2D** *minor*	–	**Pd-2C** *major*	**Pd-2D** *minor*	–
3	**Pd-3B** *major*	–	–	**Pd-3B** *major*	**Pd-3A**[2] *minor*	–
4	**Pd-4C** *One third*	**Pd-4D** *One third*	**Pd-4E** *One third*	**Pd-4C/E** *major*	**Pd-4D** *minor*	–

1 hydrolyzed methyl ester, *2* with and without ester hydrolysis

of an initial 5-membered ring via the amine and the Ala amide was observed at the lowest pH (Fig. 2, **Pd-1A**). Five membered chelate coordination of Trp with the $[Pd(en)]^{2+}$ fragment has been reported, from the indole C3 to the carboxyl O [47], as well as Pd(II) and Pt(II) bis-tryptophan complexes, in which coordination proceeds through the amine N and carboxyl O [75, 76].

The indole C2 proton is the most acidic proton and is most likely to leave when interacting with a Lewis acid [45]. C2-indole coordination together with Ala amide would lead to a less-strained 7-membered ring. Palladacycles with indoles have been reported, where the Pd(II) center is sigma bonded to the C2 carbon and the indole nitrogen is functionalized to form a 6-membered chelate with the palladium [46]. One more possibility is an 8-membered ring with the indole nitrogen and the nearest amide. Examples of h^1 coordination of Ru(II) with indole nitrogen show that it is not deprotonated [44] in such coordination, and is in that way comparable to amine coordination. The pK_a of the indole proton in $[(cymene)Ru(h^1\text{-indoline})(CH_3CN)_2]^{2+}$ was determined to be 5.2 or much lower than for free indole [77]. An NMR spectrum of **1** and Pd(II) mixed with two equivalences of base in DMSO-d_6 confirmed the loss of the amide resonances, but the N1 proton was still present. The C2 proton was located in the NMR spectrum of **1** with $[Pd(en)(H_2O)_2]^{2+}$ leading to the conclusion that **1** formed an 8-membered chelate with Pd^{2+} at all pH values, albeit a minor species at pH of 4.7. The k^4[8,5,5] coordination is dominant in the mixture at high pH, as well. An interesting result here is that the indole nitrogen is a strong donor for the Pd(II) center competing efficiently with the normally dominating amine donor group in peptide coordination.

Ligands **2** and **3** were expected to form, respectively, six- and five-membered chelates with the amine and the nearest amide. This was achieved but in an unpredictable manner. At moderate pH values, **2** preferred a 5-membered chelate with the amine and the side-chain ester carbonyl oxygen (Fig. 3, **Pd-2B**) promoting ester hydrolysis. This coordination type (N,O) is well known for simple amino acids [78]. Ligand **3** shows significantly less Pd^{2+} promoted *t*-butyl ester hydrolysis and formed a conventional 5-membered chelate. This chelation begins with the amine and continues through both amides, immediately rearranging the en ligand from bidentate to a mono-coordinated mode. The en was completely dissociated by a pD of 11.20, at which point the free carboxylate coordinates to form k^4[5,5,5] chelate. Ligand **3** shows multiple isomers that represent various forms of hydrolyzed ester combinations. Ligand **2** coordination is more strongly pH driven, where the **Pd-2B** coordination prevails until a pH of 7.33 (Table 1), at which point the amides are deprotonated and the en dissociates completely, leading to tetradentate k^4[6,5,5] complexation of **2** with Pd^{2+}. No mono-coordinated en was observed with **2**. The importance of the five-membered chelate over the six-membered chelate is only overcome at high pH where the amides are deprotonated regardless.

Considering both carboxylates and the thiol were alkylated, ligand **4** showed coordination preferences that were highly pH-dependent. At low pH, the amine/thioether coordination prevails (Fig. 5, **Pd-4A**) forming five-membered κ^2(S,N) chelate, promoting Pd-catalyzed thioether hydrolysis. This hydrolysis is analogous with the *t*-butyl ester coordination and subsequent hydrolysis seen for **2**. The thiol group on GSH normally has strong influence on GSH coordination chemistry [35, 38, 39, 53]; however, by forming the thioether, this reactivity was curbed at neutral and high pH values by preventing formation of the 5-membered κ^2(S,N) ring normally favored for GSH complexation. Both being *iso*-peptides, ligands **2** and **4** show similar coordination preferences at neutral and high pH values, where coordination starts at the amine, but the chelation to the carboxylate (Fig. 5, **Pd-4C**) is preferable to either 6- (**2**) or 7- (**4**) membered chelate formation with the nearest amide. Only at high pH values for **4** does chelation proceed through the amides and the formation of the k^4[7,5,5] chelate was observed.

Methyl ester hydrolysis (Fig. 6) significantly impacts coordination preferences of **1**–**4** at high pH where the free carboxylate competes to displace ethylenediamine and complete tetradentate coordination around the Pd^{2+} ion. At neutral pH, methyl ester hydrolysis was more prominent for **1** compared to the other ligands (Fig. 6). The methyl ester hydrolysis for **2** and **3** was comparable, while the *t*-butyl ester for **2** experienced significantly more Pd(II) catalyzed hydrolysis [17, 18] driven by the coordination preference of **2** to form a 5-membered ring at a pH lower than the pK_a of the ligand (Table 1; Fig. 5).

Conclusions

Three new alkylated tripeptides **1**–**3** were synthesized and characterized fully using solution phase synthesis in high yields. A synthetic route to fully alkylate GSH, **4**, is reported as well. The four tripeptides were explored as ligands for Pd(II) in water at different pH using ethylenediamine complex $[Pd(en)(H_2O)_2]^{2+}$ to explore stepwise coordination and draw out differences in ligand properties.

The ligands **1**–**4** formed coordination geometries as $k^4[n,5,5]$ ($n = 8,7,6,5$) chelates. **1** and **3** formed k^4[8,5,5] and k^4[5,5,5], respectively, at low pH values and this chelation dominated at all pH values explored. The observed coordination appears driven by different viewpoints; Where **1** forms a strong bond as a neutral donor to Pd(II) through the side-chain indole nitrogen and the nearest amide, while **3** forms a traditional 5-membered chelate

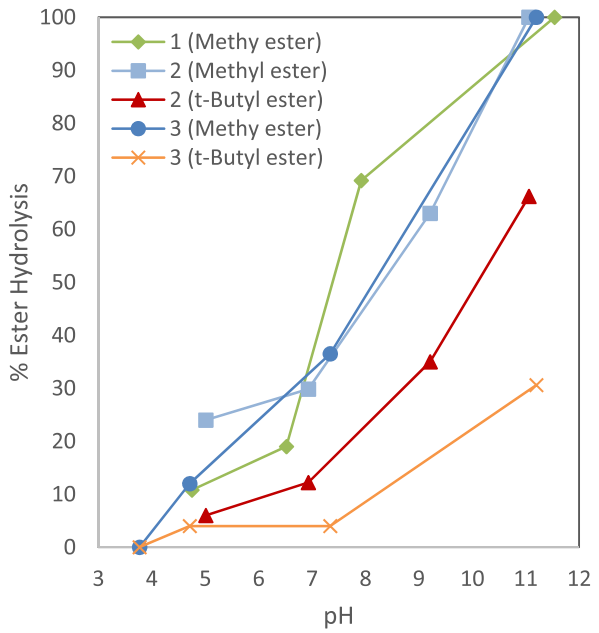

Fig. 6 Percent ester hydrolysis as a function of pH

with N-terminus amine and the nearest amide. Compounds **2** and **4** chose the N-terminus amine with an ester to form five-membered chelates preferably to the respective 6- and 7-membered chelates of the N-terminus amine and the nearest amide. These five membered chelates dominated the coordination until the pH was sufficiently high to deprotonate the amides, suggesting that 5-membered chelate stability is more important than the amine/amide coordination even for a soft ion such as Pd(II).

The tripeptides chosen exhibited their maximum expected chelating ring sizes at the N-terminus and confirmed that it is possible to form complexes with $k^4[n,5,5]$ ($n = 8,7,6,5$) chelates that may be employed to adjust ligand frameworks for bioinspired catalyst design in future work. The molecular ions of the complexes were found and matched with their simulated isotope patterns in the ESI MS of the complexes.

The esters showed significant hydrolysis that was both pH-dependent and Pd(II) catalyzed. The Pd(II) catalyzed hydrolysis was significant for **2** and **4**, where the coordinated carboxylate esters and thioether hydrolyzed at lower pH than the free functional groups. Despite the ester hydrolysis, the study successfully drew out interesting differences in the coordination of these ligands and directed coordination geometries using pH manipulations were successfully carried out. The 8-membered chelate with **1** was unexpected as well as the differences in chelation amenability of **2** and **3**. Ligand **4** was expected to show $k^4[7,5,5]$ coordination when fully alkylated and this was successfully achieved, but only at highly alkaline conditions. The variety in coordination behavior of **4** observed agrees with the notion that the GSH amine and thiol moieties may be its most important donor groups.

Acknowledgements Financial support by The Icelandic Centre of Research (Rannis) grant nr 152323 is gratefully acknowledged. SGS and GRR thank COST Action CM1105 for STSM Grant and Prof. Etelka Farkas for hosting the STMS at the early stages of this project. Dr Sigridur Jonsdottir is thanked for assistance with the collection of mass spectrometry data.

Compliance with ethical standards

Conflict of interest The authors declare that they have no conflict of interest.

References

1. Soldevila-Barreda JJ, Sadler PJ (2015) Approaches to the design of catalytic metallodrugs. Curr Opin Chem Biol 25:172–183. https://doi.org/10.1016/j.cbpa.2015.01.024
2. Metzler-Nolte N, Guo Z (2016) Themed Issue on "metallodrugs: activation, targeting, and delivery". Dalton Trans 45(33):12965–12965. https://doi.org/10.1039/C6DT90135B
3. Bradford SS, Cowan JA (2014) From traditional drug design to catalytic metallodrugs: a brief history of the use of metals in medicine. Metallodrugs 1:10–23
4. Mjos KD, Orvig C (2014) Metallodrugs in medicinal inorganic chemistry. Chem Rev 114:4540–4563
5. Sigel H, Martin RB (1982) Coordinating properties of the amide bond. Stability and structure of metal ion complexes of peptides and related ligands. Chem Rev 82(4):385–426
6. Sóvágó I, Kállay C, Várnagy K (2012) Peptides as complexing agents: factors influencing the structure and thermodynamic stability of peptide complexes. Coord Chem Rev 256(19):2225–2233. https://doi.org/10.1016/j.ccr.2012.02.026
7. Griffith DM, Bíró L, Platts JA, Müller-Bunz H, Farkas E, Buglyó P (2012) Synthesis and solution behaviour of stable mono-, di- and trinuclear Pd(II) complexes of 2,5-pyridinedihydroxamic acid: X-ray crystal structure of a novel Pd(II) hydroxamato complex. Inorg Chim Acta 380(1):291–300. https://doi.org/10.1016/j.ica.2011.09.050
8. Perinelli M, Guerrini R, Albanese V, Marchetti N, Bellotti D, Gentili S, Tegoni M, Remelli M (2020) Cu(II) coordination to His-containing linear peptides and related branched ones: Equalities and diversities. J Inorg Biochem 205:110980. https://doi.org/10.1016/j.jinorgbio.2019.110980
9. Peana M, Gumienna-Kontecka E, Piras F, Ostrowska M, Piasta K, Krzywoszynska K, Medici S, Zoroddu MA (2020) Exploring the specificity of rationally designed peptides reconstituted from the cell-free extract of deinococcus radiodurans toward Mn(II) and Cu(II). Inorg Chem. https://doi.org/10.1021/acs.inorgchem.9b03737
10. Vicatos GM, Jackson GE, Hammouda AN, Bonomo RP, Valora G (2019) Potentiometric and spectroscopic studies of the complex formation between copper(II) and Gly-Leu-Phe or Sar-Leu-Phe tripeptides. Polyhedron 170:553–563. https://doi.org/10.1016/j.poly.2019.06.011
11. Gavrish SP, Lampeka YD, Babak MV, Arion VB (2018) Palladium complexes of *N*, *N*′-Bis(2-aminoethyl)oxamide (H2L): structural (PdIIL, PdII2L2, and PdIVLCl2), electrochemical, dynamic 1H NMR, and cytotoxicity studies. Inorg Chem 57(3):1288–1297. https://doi.org/10.1021/acs.inorgchem.7b02732

12. Gonzalez P, Vileno B, Bossak K, El Khoury Y, Hellwig P, Bal W, Hureau C, Faller P (2017) Cu(II) binding to the peptide Ala-His-His, a chimera of the canonical Cu(II)-binding motifs Xxx-His and Xxx-Zzz-His. Inorg Chem 56(24):14870–14879. https://doi.org/10.1021/acs.inorgchem.7b01996
13. Park GY, Lee JY, Himes RA, Thomas GS, Blackburn NJ, Karlin KD (2014) Copper-peptide complex structure and reactivity when found in conserved His-Xaa-His sequences. J Am Chem Soc 136(36):12532–12535. https://doi.org/10.1021/ja505098v
14. Sóvágó I, Ősz K (2006) Metal ion selectivity of oligopeptides. Dalton Trans 32:3841–3854. https://doi.org/10.1039/B607515K
15. Kozlowski H, Bal W, Dyba M, Kowalik-Jankowska T (1999) Specific structure-stability relations in metallopeptides. Coord Chem Rev 184(1):319–346. https://doi.org/10.1016/S0010-8545(98)00261-6
16. Murphy JM, Powell BA, Brumaghim JL (2020) Stability constants of bio-relevant, redox-active metals with amino acids: the challenges of weakly binding ligands. Coord Chem Rev 412:213253. https://doi.org/10.1016/j.ccr.2020.213253
17. El-Sherif AA (2012) Coordination chemistry of palladium(II) ternary complexes with relevant biomolecules. In: Innocenti A (ed) Stoichiometry and research: the importance of quantity in biomedicine. InTech, intechopen.com, Rijeka, pp 79–120
18. Jószai V, Nagy Z, Ősz K, Sanna D, Di Natale G, La Mendola D, Pappalardo G, Rizzarelli E, Sóvágó I (2006) Transition metal complexes of terminally protected peptides containing histidyl residues. J Inorg Biochem 100(8):1399–1409. https://doi.org/10.1016/j.jinorgbio.2006.04.003
19. Livingstone SE, Nolan JD (1968) Metal chelates of biologically important compounds. I. Complexes of DL-ethionine and *S*-methyl-L-cysteine. Inorg Chem 7(7):1447–1451
20. Chandrasekharan M (1973) Cysteine complexes of palladium (II) and platinum (II). Inorg Chim Acta 7(1):88–90. https://doi.org/10.1016/S0020-1693(00)94785-6
21. Pettit LD, Bezer M (1985) Complex formation between palladium(II) and amino acids, peptides and related ligands. Coord Chem Rev 61:97–114. https://doi.org/10.1016/0010-8545(85)80003-5
22. McAuliffe CA (1967) The infrared spectra of palladium(II) and platinum(II) complexes of (±)-methionine. J Chem Soc A Inorg Phys Theor. https://doi.org/10.1039/J19670000641
23. Ágoston CG, Jankowska TK, Sóvágó I (1999) Potentiometric and NMR studies on palladium (II) complexes of oligoglycines and related ligands with non-co-ordinating side chains. J Chem Soc Dalton Trans 18:3295–3302
24. Wilson EW, Martin RB (1970) Circular dichroism of palladium(II) complexes of amino acids and peptides. Inorg Chem 9(3):528–532. https://doi.org/10.1021/ic50085a019
25. Krężel A, Bal W (1999) Coordination chemistry of glutathione. Acta Biochim Pol 46(3):567–580
26. Chow ST, McAuliffe CA, Sayle BJ (1975) Metal complexes of amino acids and derivatives—IX: reactions of the tripeptide, glutathione, with divalent cobalt, nickel, copper and palladium salts. J Inorg Nucl 37(2):451–454. https://doi.org/10.1016/0022-1902(75)80354-x
27. Bresson C, Spezia R, Solari PL, Jankowski CK, Den Auwer C (2015) XAS examination of glutathione–cobalt complexes in solution. J Inorg Biochem 142:126–131. https://doi.org/10.1016/j.jinorgbio.2014.10.006
28. Mah V, Jalilehvand F (2012) Lead(II) complex formation with glutathione. Inorg Chem 51(11):1–14. https://doi.org/10.1021/ic300496t
29. Shoeib T, Sharp BL (2013) Monomeric cisplatin complexes with glutathione: coordination modes and binding affinities. Inorg Chim Acta 405:258–264. https://doi.org/10.1016/j.ica.2013.06.006
30. Jószai V, Sóvágó I (2011) Palladium(II) complexes of oligopeptides containing aspartyl and glutamyl residues. Polyhedron 30(12):2114–2120. https://doi.org/10.1016/j.poly.2011.05.032
31. Shimazaki Y, Yamauchi O (2012) Group-10 metal complexes of biological molecules and related ligands: structural and functional properties. Chem Biodivers 9(9):1635–1658. https://doi.org/10.1002/cbdv.201100446
32. Lihi N, Lukács M, Szűcs D, Várnagy K, Sóvágó I (2017) Nickel(II), zinc(II) and cadmium(II) complexes of peptides containing separate aspartyl and cysteinyl residues. Polyhedron 133:364–373. https://doi.org/10.1016/j.poly.2017.05.044
33. Picquart M, Grajcar L, Baron MH, Abedinzadeh Z (1999) Vibrational spectroscopic study of glutathione complexation in aqueous solutions. Biospectroscopy 5(6):328–337. https://doi.org/10.1002/(SICI)1520-6343(1999)5:6<328:AID-BSPY2>3.0.CO;2-J
34. Mukhtiar M, Jan SU, Khan MF, Ullah N, Hussain A, Rehman SU, Qureshi MM (2018) Palladium glutathione, *N*-acetylcysteine, D-penicillamine conjugation chemistry. Pak J Pharm Sci 31(1):213–219
35. Mirzahosseini A, Somlyay M, Noszál B (2015) The comprehensive acid–base characterization of glutathione. Chem Phys Lett 622:50–56. https://doi.org/10.1016/j.cplett.2015.01.020
36. Singh G, Dogra SD, Kaur S, Tripathi SK, Prakash S, Rai B, Saini GSS (2015) Structure and vibrations of glutathione studied by vibrational spectroscopy and density functional theory. Spectrochim Acta Part A Mol Biomol Spectrosc 149:505–515. https://doi.org/10.1016/j.saa.2015.04.062
37. Rubino FM (2015) Toxicity of glutathione-binding metals: a review of targets and mechanisms. Toxics 3(1):20–62. https://doi.org/10.3390/toxics3010020
38. Lemma K, Elmroth S, Elding L (2002) Substitution reactions of [Pt(dien)Cl]+, [Pt(dien)(GSMe)]2+, cis- [PtCl2(NH3)2] and cis-[Pt(NH3)2(GSMe)2]2+ (GSMe = *S*-methylglutathione) with some sulfur-bonding chemoprotective agents. J Chem Soc Dalton Trans 10(7):1281–1286
39. Teuben JM, i Zubiri MR, Reedijk J (2000) Glutathione readily replaces the thioether on platinum in the reaction with [Pt(dien)(GSMe)]2+ (GSMe = S-methylated glutathione); a model study for cisplatin–protein interactions. J Chem Soc Dalton Trans. https://doi.org/10.1039/A908135F
40. Zabel R, Weber G (2016) Comparative study of the oxidation behavior of sulfur-containing amino acids and glutathione by electrochemistry-mass spectrometry in the presence and absence of cisplatin. Anal Bioanal Chem 408(4):1237–1247. https://doi.org/10.1007/s00216-015-9233-x
41. Foulds G (1998) Nickel 1987–1989. Coord Chem Rev 169(1):3–127. https://doi.org/10.1016/S0010-8545(98)00003-4
42. Ward TR (2019) ACS central science virtual issue on bioinspired catalysis. ACS Central Sci 5(11):1732–1735. https://doi.org/10.1021/acscentsci.9b01045
43. Gonzalez P, Bossak K, Stefaniak E, Hureau C, Raibaut L, Bal W, Faller P (2018) N-terminal Cu-binding motifs (Xxx-Zzz-His, Xxx-His) and their derivatives: chemistry, biology and medicinal applications. Chem Eur J 24(32):8029–8041. https://doi.org/10.1002/chem.201705398
44. Chen S, Vasquez L, Noll BC, Rakowski DuBois M (1997) Synthesis and characterization of mononuclear indoline complexes. Studies of σ and π bonding modes. Organometallics 16(8):1757–1764. https://doi.org/10.1021/om960744e
45. Sundberg R (2010) Electrophilic substitution reactions of indoles. Top Heterocycl Chem. https://doi.org/10.1007/7081_2010_52
46. Singh MP, Saleem F, Pal RS, Singh AK (2017) Palladacycles having normal and spiro chelate rings designed from bi- and tridentate ligands with an indole core: structure, synthesis and applications as catalysts. N J Chem 41(19):11342–11352. https://doi.org/10.1039/c7nj02116j

47. Kaminskaia NV, Ullmann GM, Fulton DB, Kostic NM (2000) Spectroscopic, kinetic, and mechanistic study of a new mode of coordination of indole derivatives to platinum(II) and palladium(II) ions in complexes. Inorg Chem 39(22):5004–5013. https://doi.org/10.1021/ic000254l
48. Zhang L, Lin Y-J, Li Z-H, Jin G-X (2015) Rational design of polynuclear organometallic assemblies from a simple heteromultifunctional ligand. J Am Chem Soc 137(42):13670–13678. https://doi.org/10.1021/jacs.5b08826
49. Armarego WLF (2017) Purification of laboratory chemicals, 8th edn. Butterworth-Heinemann, Oxford. https://doi.org/10.1016/B978-0-12-805457-4.50008-2
50. Azizi N, Khajeh Amiri A, Bolourtchian M, Saidi MR (2009) A green and highly efficient alkylation of thiols in water. J Iran Chem Soc 6(4):749–753. https://doi.org/10.1007/BF03246165
51. Li J, Sha Y (2008) A convenient synthesis of amino acid methyl esters. Molecules. https://doi.org/10.3390/molecules13051111
52. Mccormick BJ, Jaynes EN, Kaplan RI, Clark HC, Ruddick JD (1972) Dichloro(ethylenediamine)palladium(II) and (2,2′-Bipyridine)dichloropalladium (II). Inorg Synth 13:216–218
53. Siebert AFM, Sheldrick WS (1997) pH-Dependent competition between N, S and N, N′ chelation in the reaction of [Pt(en)(H2O)2]2+ (en = H2NCH2CH2NH2) with methionine-containing di- and tri-peptides. J Chem Soc Dalton Trans 3:385–394. https://doi.org/10.1039/A604689D
54. Lim MC, Bruce Martin R (1976) The nature of cis amine Pd(II) and antitumor cis amine Pt(II) complexes in aqueous solutions. J Inorg Nucl Chem 38(10):1911–1914. https://doi.org/10.1016/0022-1902(76)80121-2
55. Gutz IGR CurTiPot – pH and acid–base titration curves, 4.2 edn. http://www.iq.usp.br/gutz/Curtipot_.html
56. Sakina K, Kawazura K, Morihara K (1988) Enzymatic synthesis of delta sleep-inducing peptide. Int J Pept Protein Res 31(2):245–252. https://doi.org/10.1111/j.1399-3011.1988.tb00030.x
57. Sultane PR, Mete TB, Bhat RG (2015) A convenient protocol for the deprotection of *N*-benzyloxycarbonyl (Cbz) and benzyl ester groups. Tetrahedron Lett 56(16):2067–2070. https://doi.org/10.1016/j.tetlet.2015.02.131
58. Höck S, Marti R, Riedl R, Simeunovic M (2010) Thermal cleavage of the Fmoc protection group. CHIMIA Int J Chem 64(3):200–202. https://doi.org/10.2533/chimia.2010.200
59. Bajusz S, Medzihradszky K, Kisfaludy L, Low M, Paulay Z, Lang MT, Szporny L (1968) Total synthesis of human corticotropin. Hungary Patent HU155254
60. Masignani V, Scarlato V, Scarselli M, Galeotti C, Mora M (2001) Antigenic meningococcal peptides Italy patent WO 01/04316 A2
61. Chekalin SV, Golovlev VV, Kozlov AA, Matveets YA, Yartsev AP, Letokhov VS (1988) Femtosecond laser photoionization mass spectrometry of tryptophan-containing proteins. J Phys Chem 92(24):6855–6858. https://doi.org/10.1021/j100335a001
62. Kermack WO, Matheson NA (1957) The synthesis of some analogues of glutathione. Biochem J 65(1):45–48. https://doi.org/10.1042/bj0650045
63. El-Faham A, Albericio F (2011) Peptide coupling reagents, more than a letter soup. Chem Rev 111(11):6557–6602. https://doi.org/10.1021/cr100048w
64. Montalbetti CAGN, Falque V (2005) Amide bond formation and peptide coupling. Tetrahedron 61(46):10827–10852. https://doi.org/10.1016/j.tet.2005.08.031
65. Joullié MM, Lassen KM (2010) Evolution of amide bond formation. ARKIVOC viii:189–250
66. Wuts PGM, Greene TW (2006) Green's protective groups in organic synthesis. Green's protective groups in organic synthesis, 4th edn. John Wiley & Son, Inc, Hoboken
67. Lide DR (2004) CRC handbook chemistry and physics, 85th edn. CRC Press, Boca Raton
68. Alexander MD, Spillert CA (1970) Monodentate ethylenediamine complex of cobalt(III). Inorg Chem 9(10):2344–2346. https://doi.org/10.1021/ic50092a028
69. Hay RW, Pujari MP (1986) The palladium (II) promoted hydrolysis of methyl, ethyl and isopropyl glycylglycylglycinate. Inorg Chim Acta 123(1):47–51
70. Hay RW, Pujari MP (1986) The palladium (II) promoted hydrolysis of methyl, ethyl and isopropyl glycylglycylglycinate. Inorg Chim Acta 123(1):47–51
71. Ozsváth A, Farkas E, Diószegi R, Buglyó P (2019) Versatility and trends in the interaction between Pd(II) and peptide hydroxamic acids. N J Chem 43:8239–8250
72. Martin RB, Pitner TP (1971) Inversion and proton exchange at asymmetric nitrogen centers in palladium (II) complexes. J Am Chem Soc 93(18):4400–4405
73. Pitner TP, Wilson EW, Martin RB (1972) Properties of Palladium8II) complexes of peptides and histidine in basic solutions. Inorg Chem 11(4):738–742
74. Haas K, Ponikwar W, Nöth H, Beck W (1998) Facile synthesis of cyclic tetrapeptides from nonactivated peptide esters on metal centers. Angew Chem Int Ed 37(8):1086–1089. https://doi.org/10.1002/(SICI)1521-3773(19980504)37:8<1086:AID-ANIE1086>3.0.CO;2-V
75. Carvalho MA, Souza BC, Paiva REF, Bergamini FRG, Gomes AF, Gozzo FC, Lustri WR, Formiga ALB, Rigatto G, Corbi PP (2012) Synthesis, spectroscopic characterization, DFT studies, and initial antibacterial assays in vitro of a new palladium(II) complex with tryptophan. J Coord Chem 65(10):1700–1711. https://doi.org/10.1080/00958972.2012.679660
76. Carvalho MA, Shishido SM, Souza BC, de Paiva REF, Gomes AF, Gozzo FC, Formiga ALB, Corbi PP (2014) A new platinum complex with tryptophan: synthesis, structural characterization, DFT studies and biological assays in vitro over human tumorigenic cells. Spectrochim Acta Part A Mol Biomol Spectrosc 122:209–215. https://doi.org/10.1016/j.saa.2013.11.044
77. Vasquez LD, Noll BC, Rakowski DuBois M (1998) Mononuclear indoline complexes. 2. Synthesis, structure, and reactivity of [(Cymene)Ru(η1-N-indoline)(CH3CN)2](OTf)2. Organometallics 17(5):976–981. https://doi.org/10.1021/om970968c
78. Farkas E, Sóvágó I (2017) Metal complexes of amino acids and peptides. In: Amino acids, peptides and proteins, vol 41. R SocChem, pp 100–151. https://doi.org/10.1039/9781782626619-00100

SI Figure 1

Titration data for 1-4 with L to M ratios of 1:0 (light blue), 1:1 (magenta), 2:1 (blue) and 4:1 (teal)

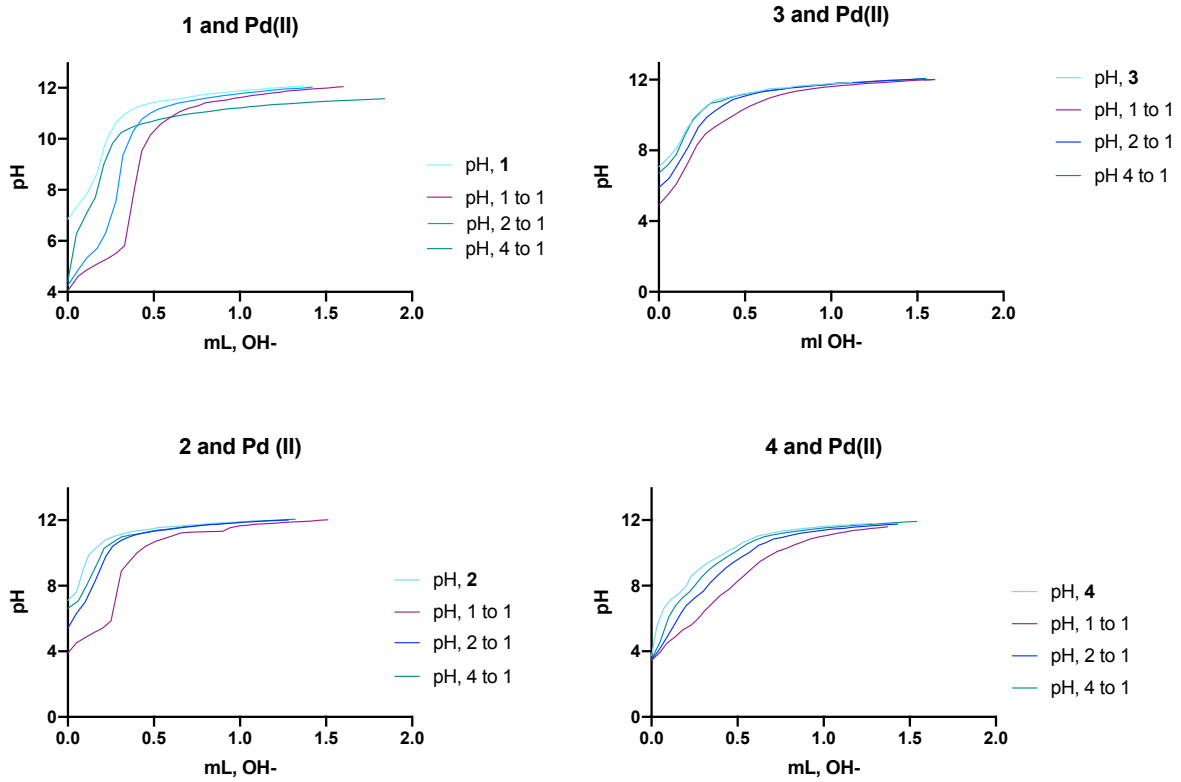

SI Figure 2

Stacked NMR spectra for **1** at t=1h at different pH values.

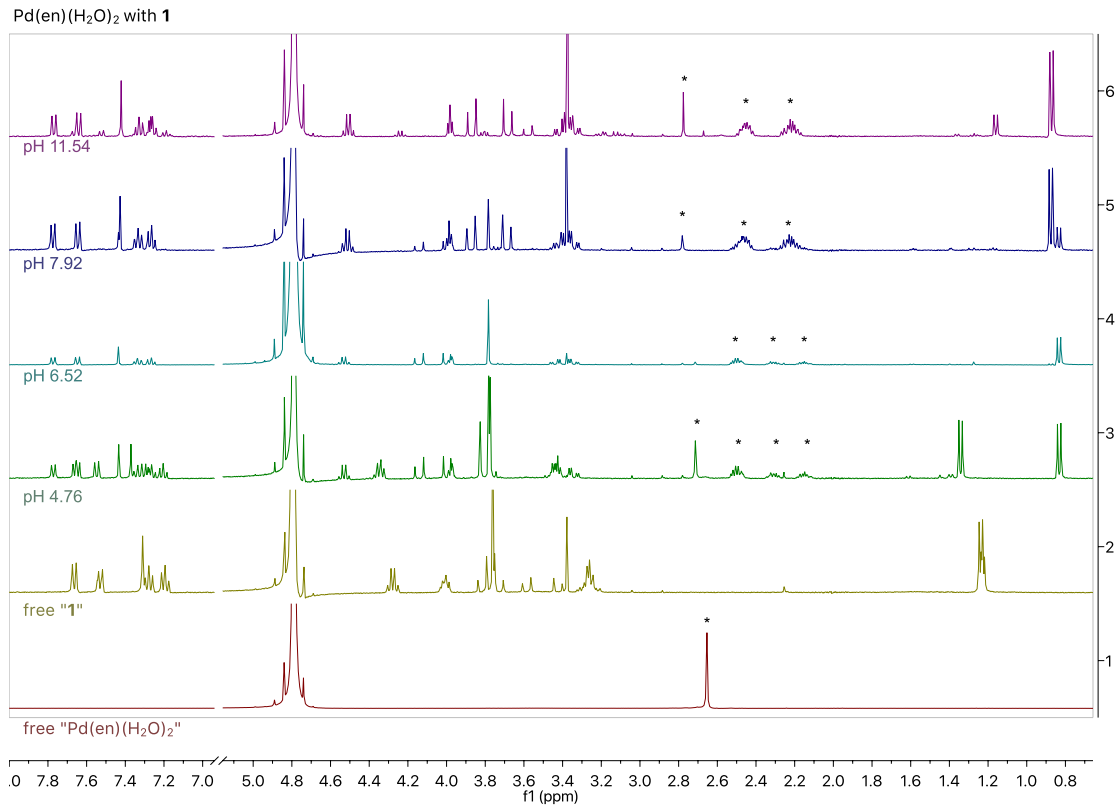

SI Figure 3

Stacked NMR spectra for **2** at t=1h at different pH values.

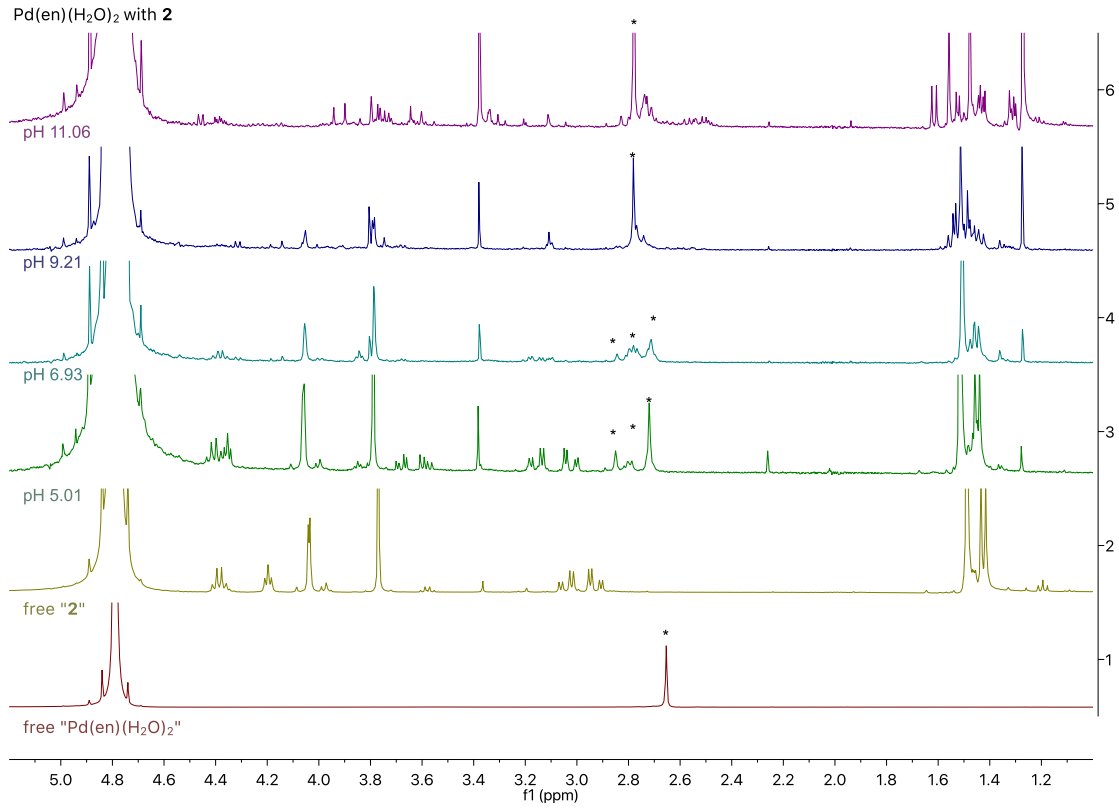

SI Figure 4

Stacked NMR spectra for **3** at t=1h at different pH values.

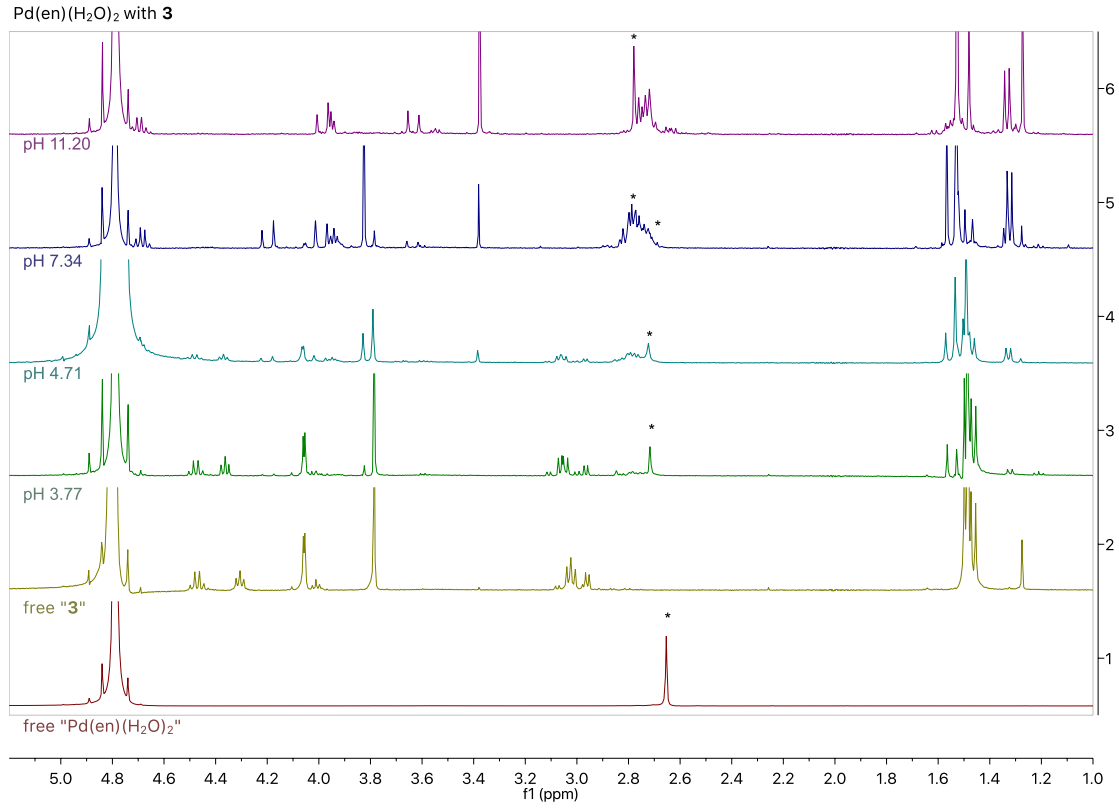

SI Figure 5

Stacked NMR spectra for **4** at t=1h at different pH values.

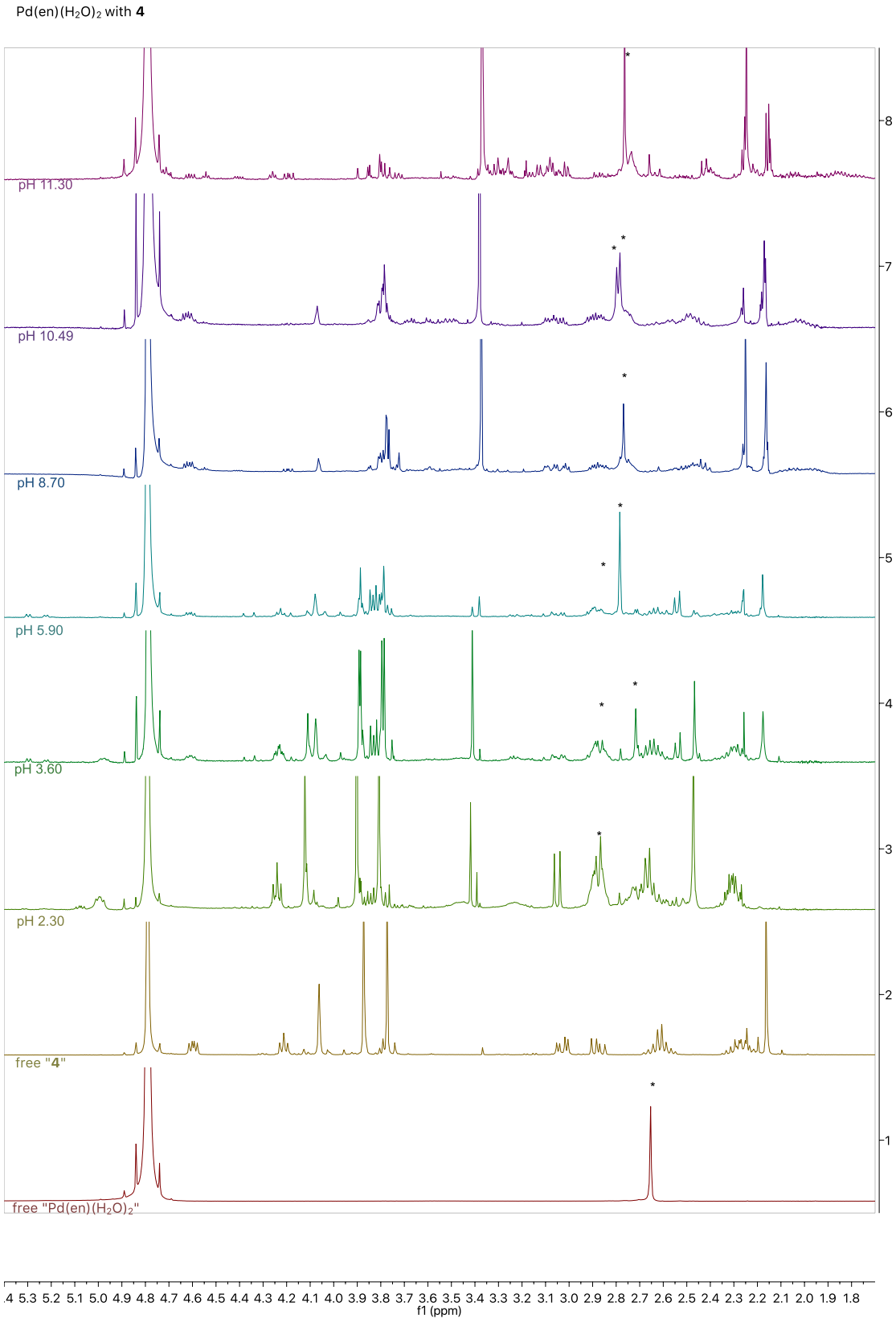

SI Figure 6A

^{1}H NMR spectra for **1**

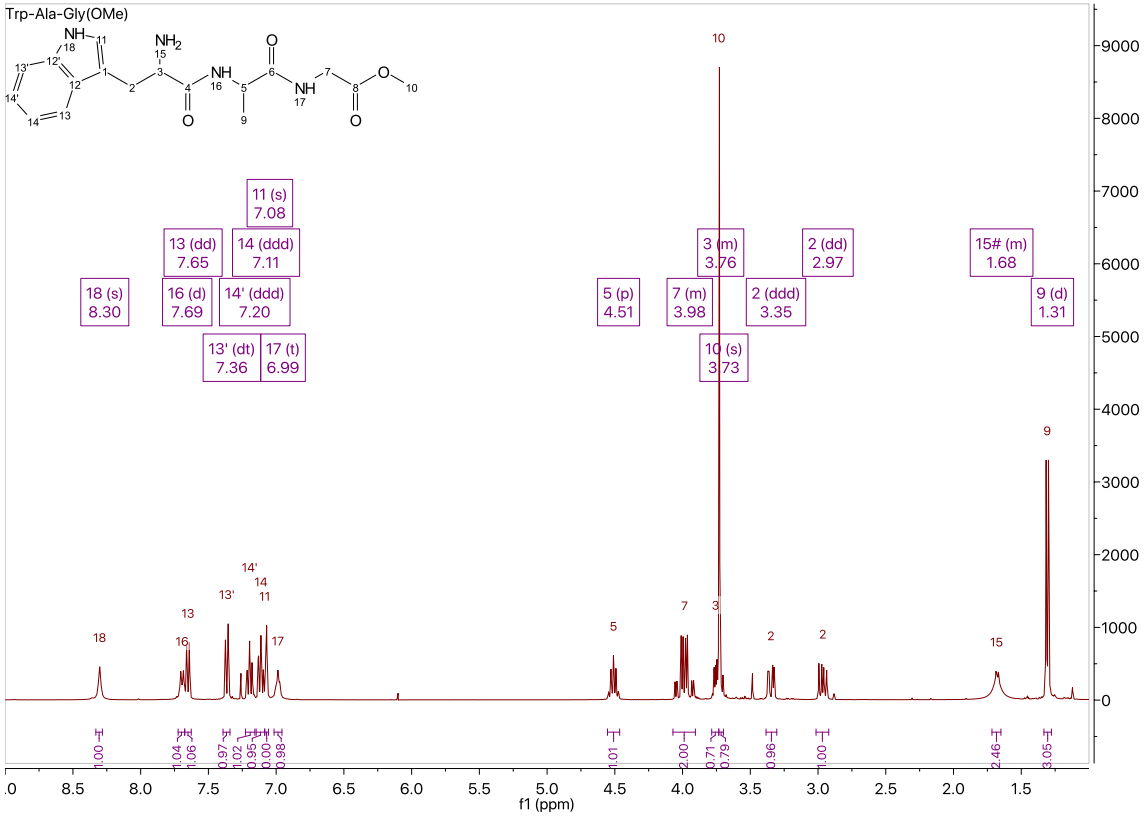

SI Figure 6B

^{13}C NMR spectra for **1**

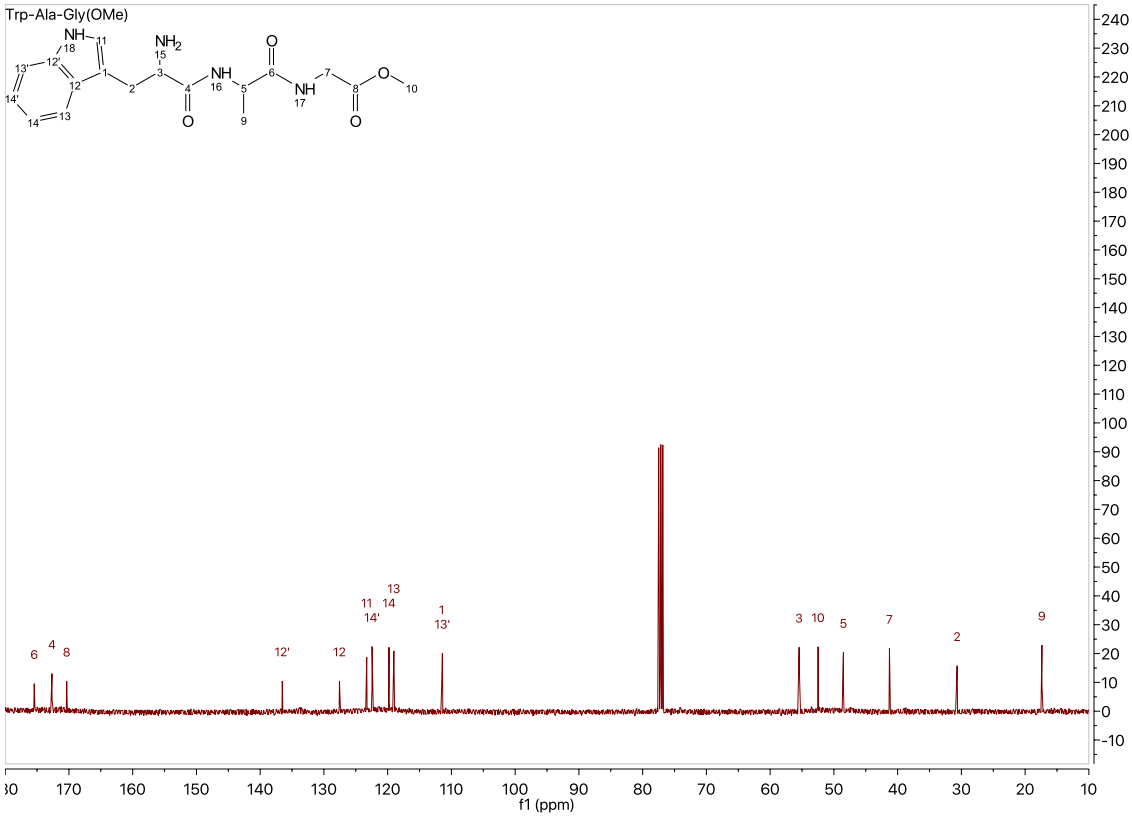

SI Figure 6C
MS scan for **1**

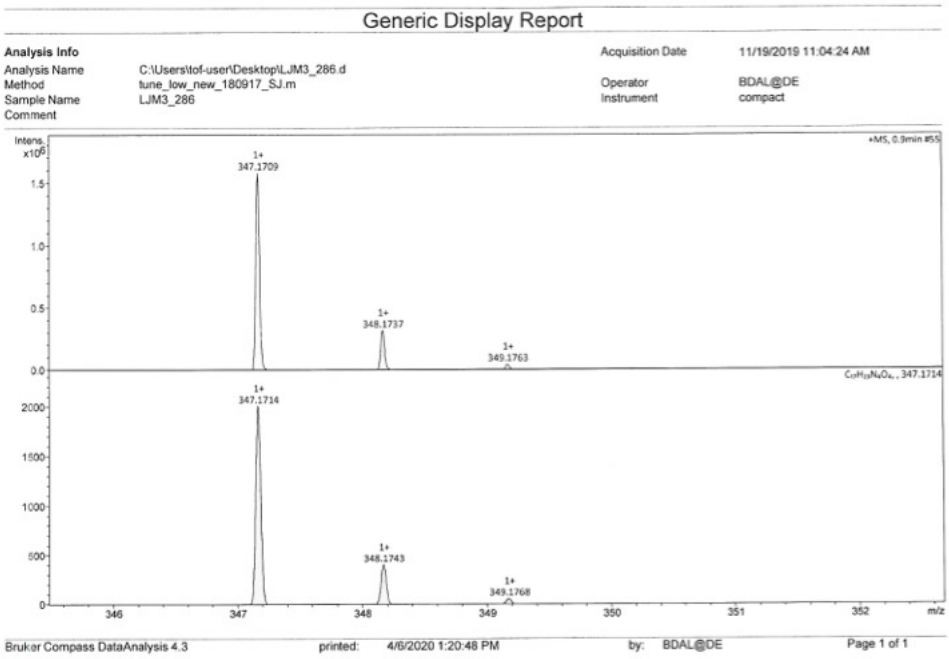

SI

SI Figure 7A
^{1}H NMR spectra for **2**

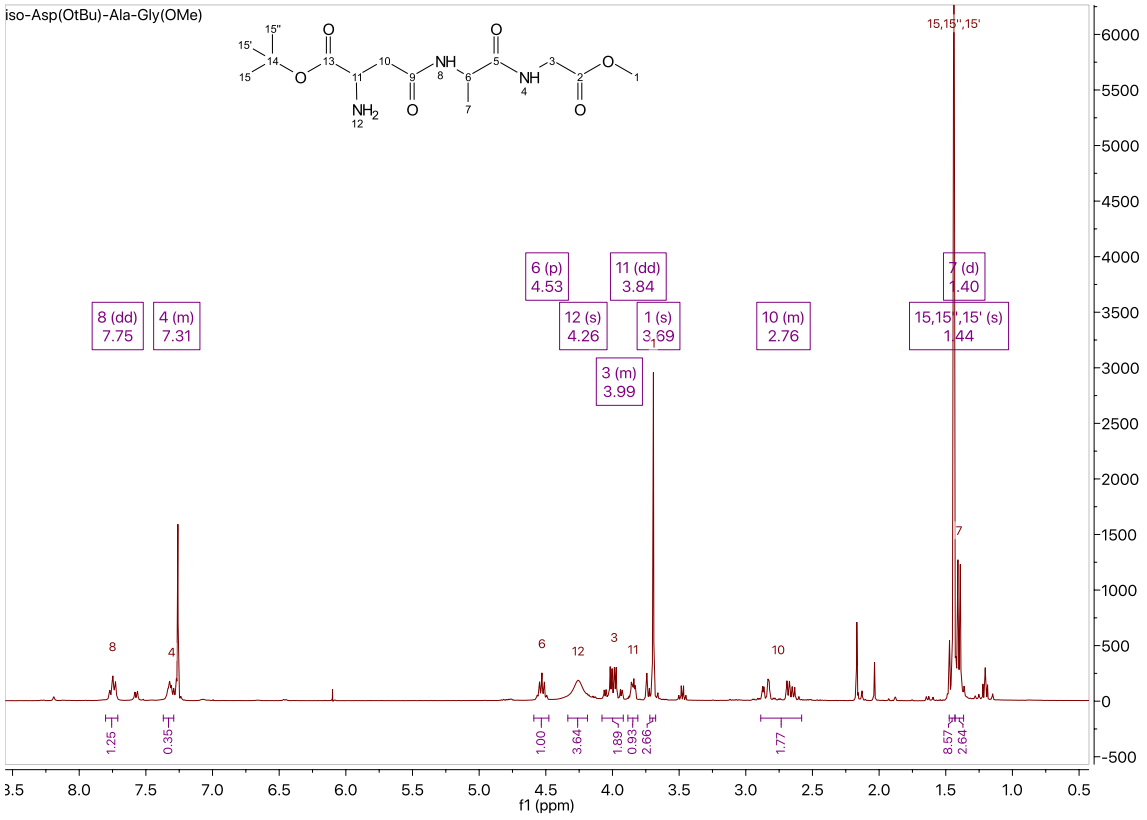

SI Figure 7B

^{13}C NMR spectra for **2**

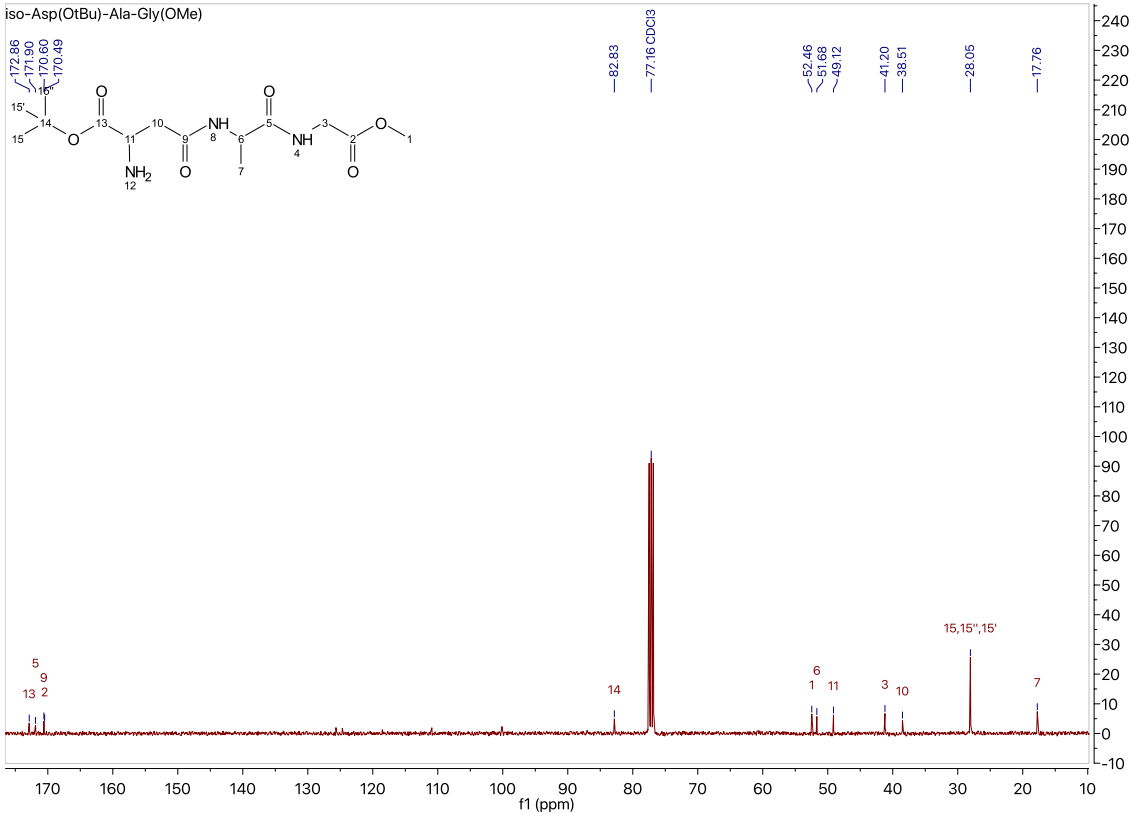

SI Figure 7C

MS scan for **2**

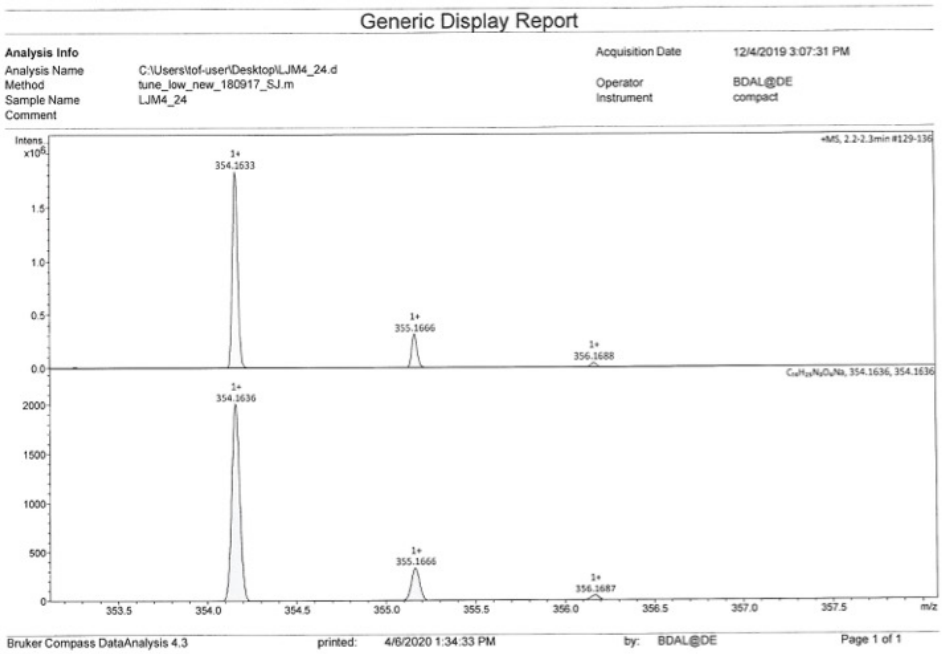

Figure 8A

^{13}C NMR spectra for **3**

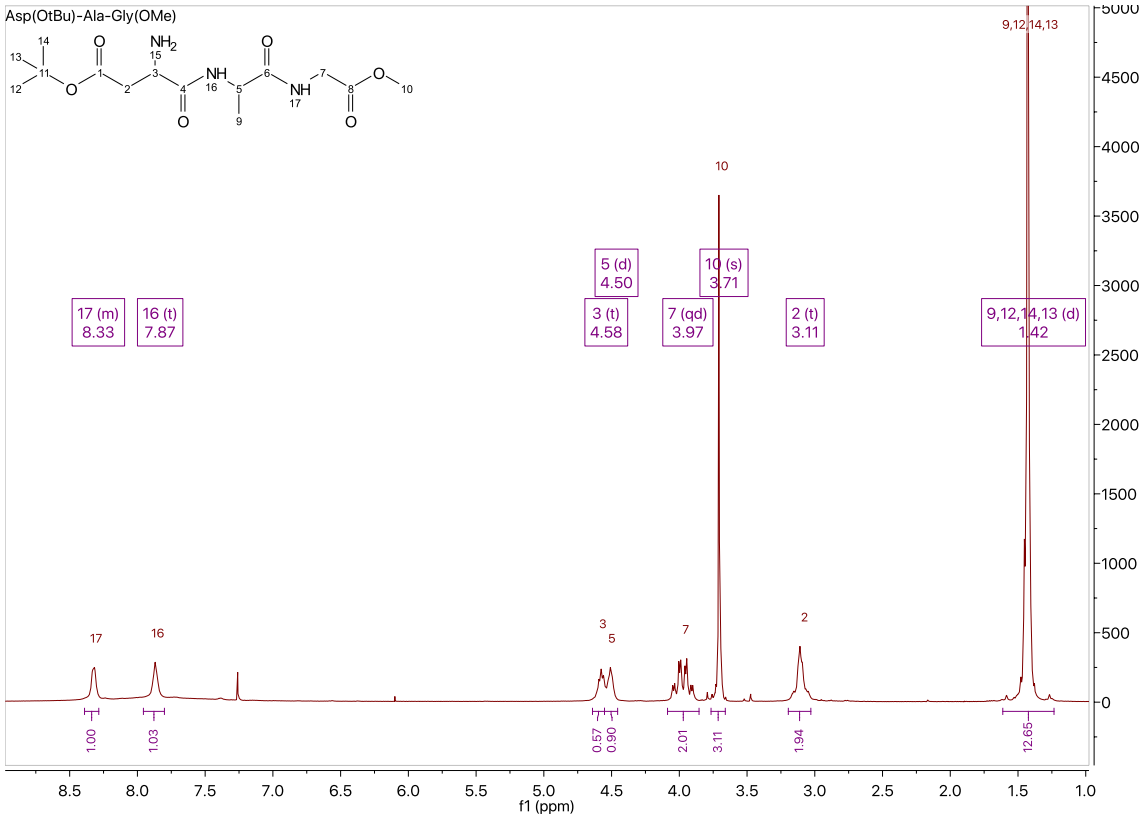

SI Figure 8B

^{13}C NMR spectra for **3**

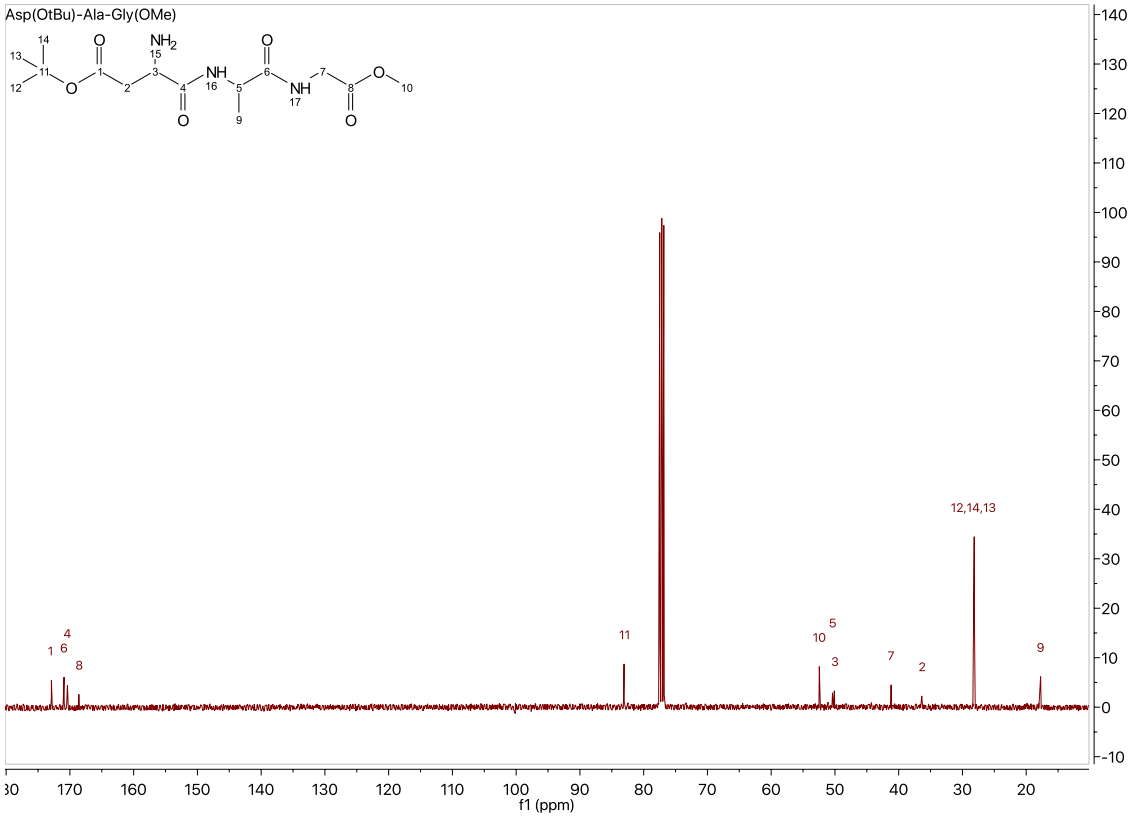

SI Figure 8C
MS scan for **3**

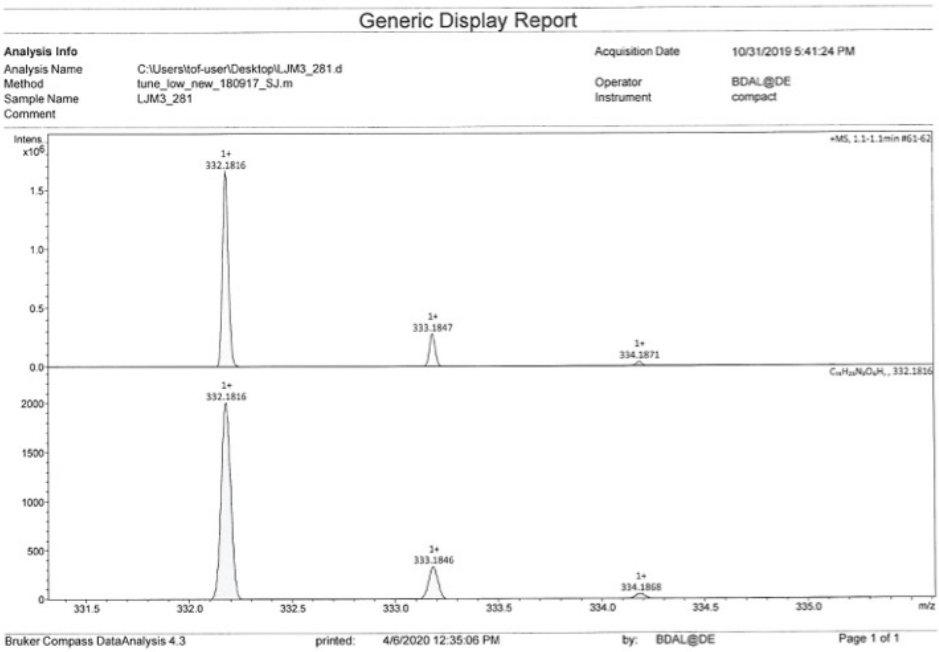

SI Figure 9A
^{1}H NMR spectra for **4**

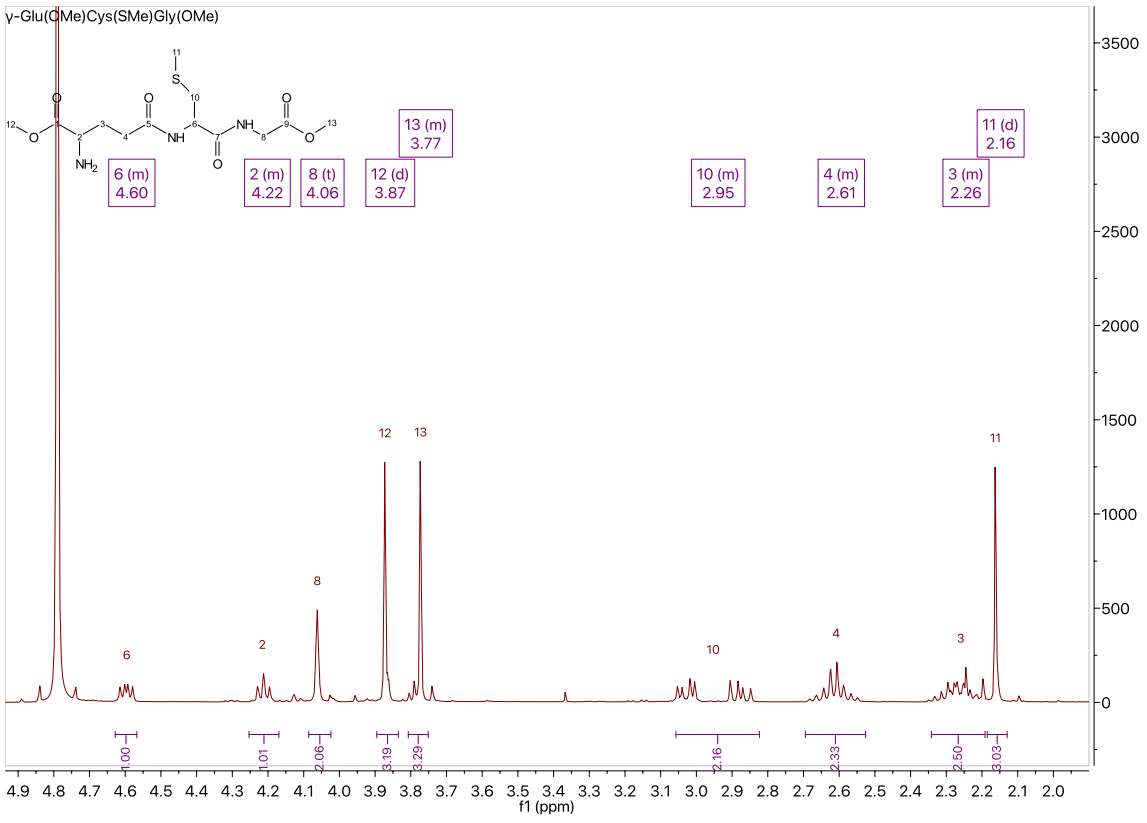

SI Figure 9B

^{13}C NMR spectra for **4**

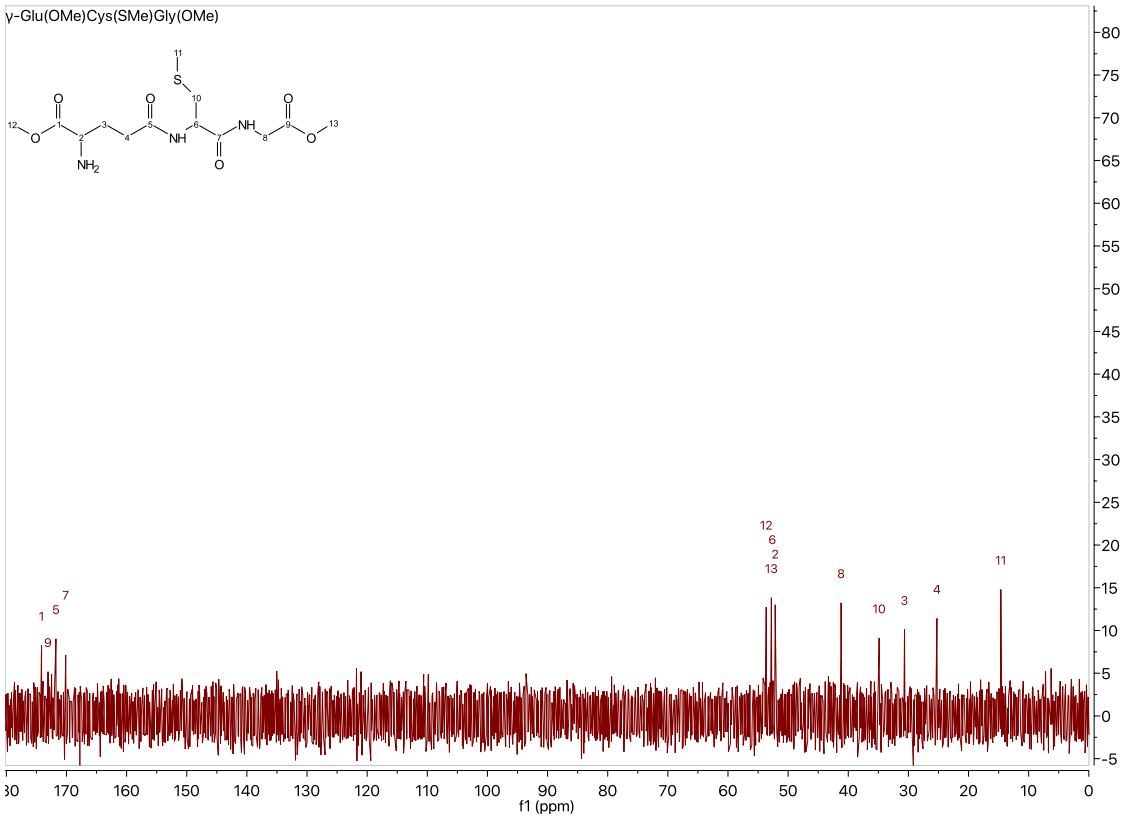

SI Figure 9C

MS scan for **4**

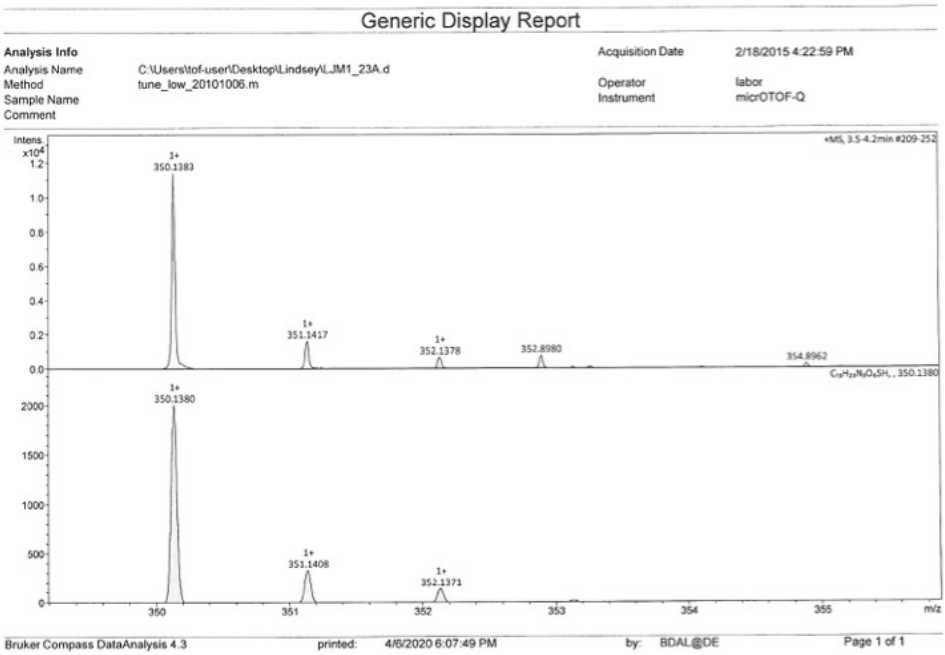

Article 2

Synthesis, Characterization, and reaction studies of novel Palladium tripeptide complexes.

Abstract

Pd(II) complexes with the tripeptides, α-Asp(OR)AlaGly(OR), β-Asp(OR)AlaGly(OR), and TrpAlaGly(OR) (R = H or alkyl) were synthesized and characterized. The ligands form tri and tetradentate complexes with Pd(II). Ligand exchange reactions of the tridentate complexes showed that sufficiently labile ligands may be removed to form the tetradentate coordination mode. The complex coordination geometry was studied using DFT calculations and reactivity with small molecules such as ethylene, acids, formate, and episulfide was investigated. The complexes adopt a square planar geometry with the tetradentae ligands and are rather inert towards ethylene coordination. They decompose in acid and under acidic condition and in the presence of ethylene, acetaldehyde was formed. The Pd(II) is a soft Lewis acid and thiophilic and the complex abstracts sulfur from the episulfide at apparent modest catalytic rates. With formate the metal dissociates from the ligand and reduces to Pd(0).

Introduction

Metallopeptide complexes are widely reported in the literature; Studies of these complexes primaraly relate to metalodrugs and metal toxixicity. However, related classes of ligands, like schiff base and cyclam derivatives are explored for their catalytic activation of small molecules. These ligand system are similar in their amino-oxygen chelate coordination. In metal complexes the amino-amide backbone forms stable 5-membered rings for α-amino acids. When studying the coordination of amino acids or di- and tripeptides, complexation forms through the carboxylic acid, in addition to the N-donor groups. This coordination effectively closes coordination for palladium, which has strong favorability towards square planer coordination geometry. One strategy is to form a weakly coordinated chelate to function as an "on-off" switch. Modification of the carboxcylic acid to form as ester, should act in such a manner.

One problem encountered with this strategy is the ability of palladium to catalyze ester

hydrolysis. In order to avoid this undesirable reaction, non-aqueous conditions must be employed.

In previous work we described the synthesis of three new tripeptide ligands (Figure 1) and investigated the effects of pH on their coordination to $Pd(en)(H_2O)^{2+}$. This work outlines the synthesis, characterization, and reactivity studies of three new tetradentate Pd(II) complexes.

Results and Discussion

Synthesis

The synthetic effort focused on the synthesis of a neutral complex with Pd(II) to maximize organosolubility in reactions of the complex with various small molecules. Several different synthetic routes were attempted to achieve this. Initial experiments used the ligand *α*-Asp(OtBu)AlaGly(OMe) (**1**) (Figure 1) because it is the most economic for synthetic optimization and its protecting group acid/base sensitivity renders the method to form its complexes reproducible for less sensitive ligands. A summary of the synthetic routes employed to synthesize neutral tripeptide complexes is shown in Figure 2.

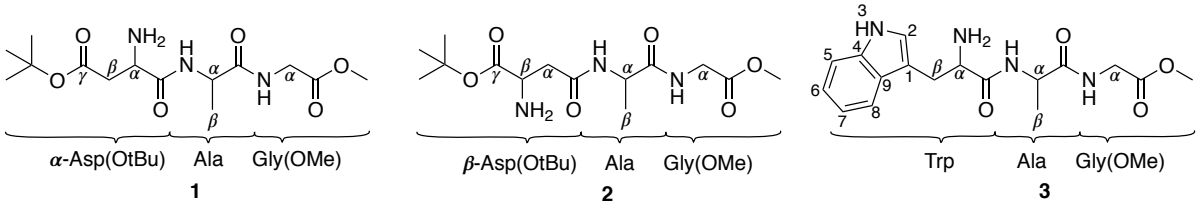

Figure 1. Tripeptide ligands used in synthesis

*Aqueous Synthesis of **4**.* Starting with an aqueous synthesis strategy, K_2PdCl_4 was dissolved in water, then added to an aqueous solution of the ligand. Coordination for this reaction is highly dependent on pH[1], where the degree of hydrolysis depends on reaction time. Using this strategy, the pH was adjusted to ~6.5 which results in the formation of two isomers, one major and one minor. The major product is the charged species K[Pd{Asp(OtBu)AlaGly(OMe)}Cl] (**4**). The composition of **4** was confirmed by mass spectrometry along with the presence of the Pd_2L_2Cl dimer. The coordination of **4** is κ^3-NH_2,N,N. Support for this coordination mode was determined by spectroscopic data.

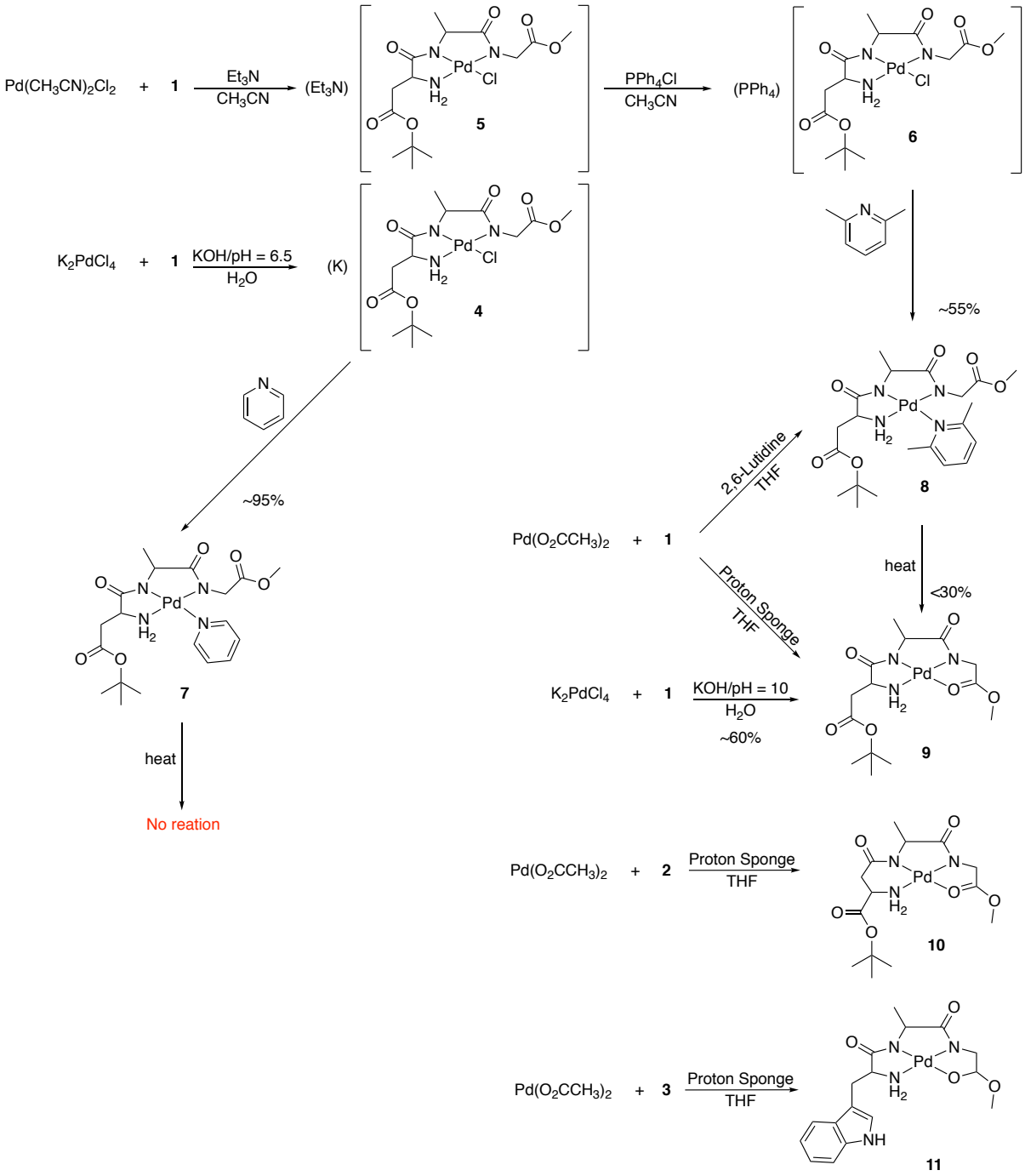

*Figure 2. Attempted synthetic routes to form charged (**4-6**) and neutral (**7-11**) Pd(II) complexes.*

However, complex **4** can be synthesized with improved control in a non-aqueous environment. *Synthesis of Tridentate Pd complexes, **5-6**.* Using $Pd(CH_3CN)_2Cl_2$ as the starting complex, and substituting KOH for two molar equivalents of triethylamine results in the complex (Et_3N)[Pd{Asp(OtBu)AlaGly(OMe)}Cl], **5**. This product composition was also confirmed by mass spectrometry. The NMR resonances for the ligand of these two different salts are

identical, whereas the latter has an organic cation, which can be tracked in the NMR spectra. Excess Et_3N^+ proved difficult to remove, but this was resolved by switching Et_3N^+ out for PPh_4^+. The cation exchange produced complex **6**, which had no noticeable effect on the shifts of the ligand resonances in the NMR however, this led to loss of yield and some decomposition. After the cation exchange, integration of the PPh_4^+ was ~1 mol equivalence, confirming **4-6** are mono-anionic. Although Et_3N^+ was able to form the mono-ionic complex, separation form the organic salts proved difficult.

*Ligand Exchange Reactions on Tridentate Coordinated Pd to form 7 and **8**.* In order to form the neutral complex, and increase organosolubility, attempts to exchange or remove the chloride were explored. To that effect, pyridine (py) was added to the potassium salt **4** and the results monitored with NMR (Table 1, **7**). The spectrum shows new peaks in the 7-8 ppm region indicating coordination of py. Integrating these peaks showed the chloride was successfully replaced by the pyridine. When the py complex **7** was heated at 110 ºC overnight, the py remained coordinated. In a second reaction, 2,6-lutidine (Lu) was added to **4** and the reaction monitored by NMR. Upon lutidine addition, integration of its peaks in the NMR showed incorporation of about 0.5-0.6 mol eq of lutidine or incomplete replacement of the chloride. Lutidine is a weaker nucleophile and is stericly more hindered than py, which explains why incorporation of the lutidine was less than pyridine.

A neutral palladium complex with coordinated lutidine was synthesized directly using $Pd(OAc)_2$ and 2 equivalence of 2,6-lutidine in dry THF (Figure 2, **8**). Upon heating **8** overnight at 110˚C, tracking this reaction via NMR, a minor species started to form. NMR integration suggests the new species is less than 30 % mol. Table 1 highlights the changes to the resonances in the NMR. Formation of free Lu was also observed, confirming that lutidine's labile coordination may be controlled with heat. This reaction was able to form the desired tetradentate complex Pd{Asp(OtBu)AlaGly(OMe)} (**9**).

*Aqueous Synthesis of **9**.* The aqueous synthesis strategy also afforded the neutral palladium complex **9**. This was accomplished by adding an aqueous solution of K_2PdCl_4 to an aqueous solution of the ligand, adjusting the pH to 10 and then immediately removing the solvent. The NMR for this species matches the product formed by heating **8,** which aided in the identification of this product. Here again the use of aqueous medium proved difficult to reproduce effectively for complex synthesis.

*Synthesis of Neutral Complexes **9-11**.* A novel non-aqueous strategy for the formation of **9** was developed. The ligand, along with "Proton Sponge" was dissolved in dry THF, $Pd(OAc)_2$ was

added to the solution and the reaction stirred under Ar. The proton sponge is a non-nucleophilic base which allows the last coordination site on the Pd(II) to remain open for the C-terminal ester to bind. The coordination of this complex is κ^4-NH_2,N,N,=O. Composition of **9** was confirmed by mass spectrometry as well as elemental analysis. This method established the synthesis of neutral palladium tripeptide complexes with C-terminus methyl esters, and was then applied to other ligands in the series (Figure 2, **10** and **11**).

The tripeptide *β*-Asp(OtBu)AlaGly(OMe) (**2**) is an *iso*-peptide, meaning that it forms the peptide bond through the side chain carboxylic acid. When coordinated to a metal center via the N-terminal amine and the nearest amide, the peptide forms a 6-membered chelate. In aqueous medium at neutral pH this system presents a competing coordination to the side chain carbonyl forming the 5-membered chelate instead of the κ^3-NH_2,N,N amide backbone[1]. The κ^4-NH_2,N,N,O chelated complex could be formed in basic aqueous conditions at a pH value of ~9. However, Pd(II) catalyzed hydrolysis at this pH value led to tert-butyl and methyl ester hydrolysis of up to 35% and 65%, compared to ligand **1**, which respectively only reached 5% and 35% hydrolysis at pH 7.3. Considering that data, aqueous synthesis using **2** was not a viable option, while using Proton Sponge as a base in dry THF yields the κ^4-NH_2,N,N,=O species, Pd{*β*-Asp(OtBu)AlaGly(OMe)} (**10**) in good yield. The composition of complex **10** was confirmed by mass spectrometry and elemental analysis.

Aqueous coordination studies of the tripeptide TrpAlaGly(OMe) (**3**) with to $Pd(en)(H_2O)^{2+}$ revealed that the tryptophan indole participates in coordination [1]. This conclusion was based on the downfield shift of the indole moiety by ~0.11 ppm, whereas the shift associated with the Trp *α*-C protons was relatively small. The NMR study revealed that at low pH the NH_2 would coordinate as expected and chelation would continue to the Ala amide. However, as the pH was increased to ~8 the κ^4-NH_{indole},N,N,O isomer was detected, forming an 8 membered ring. This study also showed that the methyl ester is hydrolyzed up to 75% under these conditions. Utilizing this information, **3** was complexed to $Pd(OAc)_2$ in THF with Proton Sponge acting as base. This yields the isomer κ^4-NH_2,N,N,=O (Figure 2, **11**). This complex was fully characterized using elemental analysis and NMR, IR, and mass spectrometry.

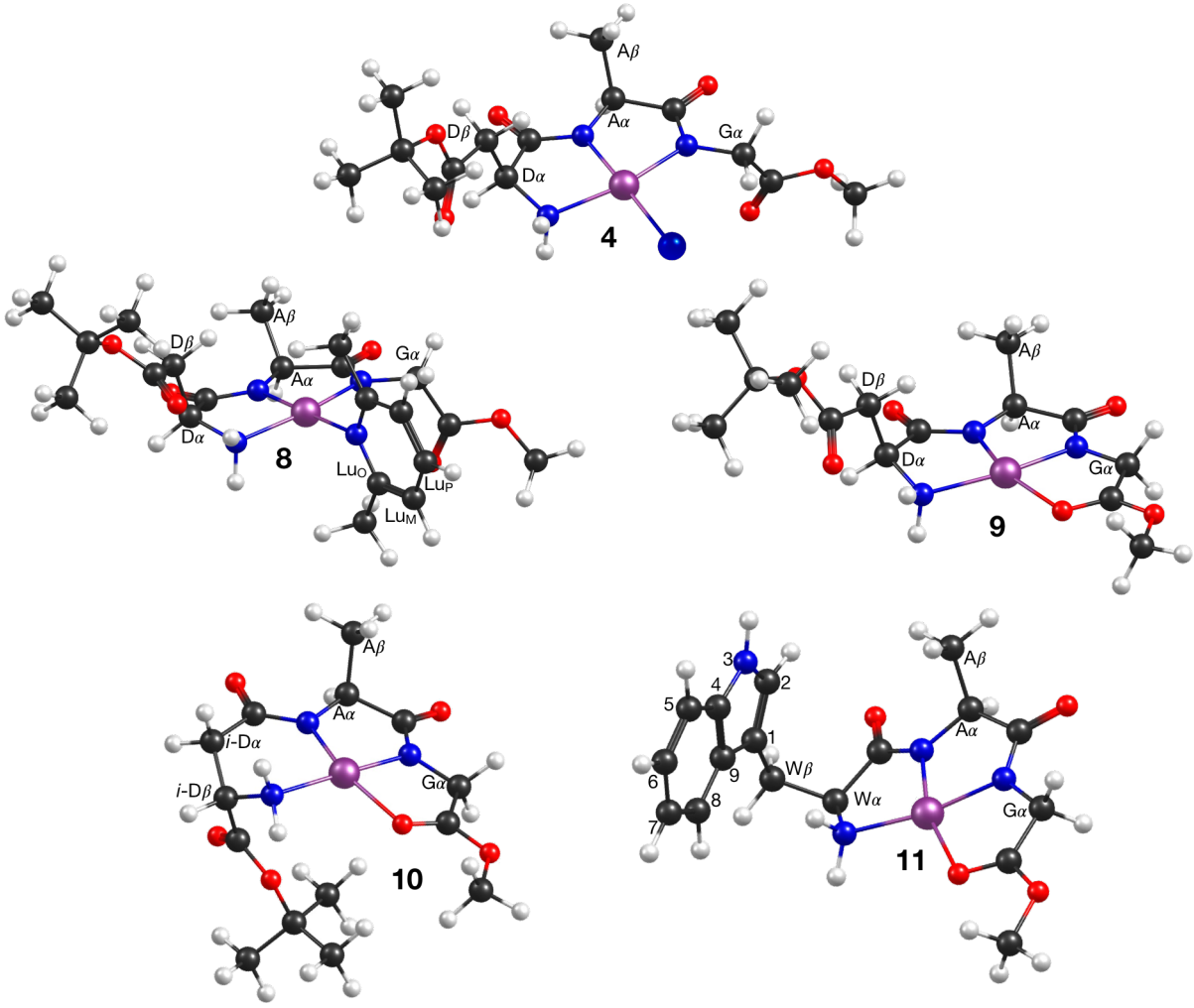

*Figure 3 DFT optimized structures of complexes **4**, **8-11**.*

Characterization

Complexes **4-11** were characterized via NMR and IR spectroscopy, with quantum chemical calculations at the DFT level used to aid the spectral interpretation. In order to correctly assign coordination geometries, similarities and differences in the complex NMR chemical shifts, and shifts in infrared frequencies of major bands were examined. Observed values were compared to calculated chemical shifts and vibrational frequencies of the DFT-optimized structural models.

DFT calculations with a continuum solvation model were employed to determine the lowest energy structures in solution for complexes **4-11** which can be seen in Figure 3. Several different conformational possibilities were explored computationally. As the Pd(II) complexes are preferably square planar NH_2,N,N coordination was expected and the lowest energy DFT-

calculated conformers agreed. Due to the conformational flexibility of the tripeptide ligand, a number of conformers for each complex are available (primarily due different orientations of the Asp or Trp sidechains) but only the lowest energy conformer was considered in the calculations of spectroscopic properties.

^{1}H NMR Analysis.

General expected behavior. The coordinated amine/amide backbone is a commonality of **4**-**11**; this coordination was established in the proton NMR (Table 1) by the appearance of amino protons as two triplets between ~5.0 and 3.8 ppm, while the amide protons, located ~8.40 – 8.10 ppm disappear. Generally, the α-C protons shift upfield whereas Ala α-C protons tend to shift the most and have the largest shifting range. This behavior is expected considering the Asp amide is trans to the fourth coordination sphere, and thus the magnetic environment of these protons changes more significantly.

NMR of coordinated ligands in complexes 4-11. In the ^{1}H NMR spectrum for **4**, the resonances generally shift upfield the most compared to ligand **1**, presumably owing to the fact that this is the only negatively charged species in the series, and the chloride's π-donation to palladium effectively increases shielding around the ligand. Coordination of pyridine to **4** resulted in downfield shifts of the amine, Asp and Ala α-C protons (Table 1, **7**), which is explained by pyridine π-back-bonding, resulting metal deshielding. However, the Gly α-C and methyl ester protons shifted further upfield, one explanation for this is π-interactions with the pyridine. Heating **7** overnight at 110 °C did not show any observable changes in the NMR. The complex with coordinated Lu (**8**) has slightly different spectroscopic behaviors compared to **7**. Notably, a large upfield shift of the NH_2 protons (0.20 and 0.23 ppm). In **8** the Gly protons experience the largest shielding effects of the series, appearing with a large coupling constant of ~ 96Hz with resonances at 3.14, and 2.91 ppm. This is further evidence of π-interaction between the lutidine and the glycine moiety. Upon heating **8** overnight at 110 °C a new species is observed, where the Lu is is no longer coordinated. This new species matches the spectra of **9**.

*Table 1. Summary of NMR data from synthetic experiments to form neutral Pd(II) complexes with α-Asp(OtBu)AlaGly(OMe) (**1**), β-Asp(OtBu)AlaGly(OMe) (**2**), and TrpAlaGly(OMe) (**3**) where **4** is the species K[Pd(**1**)Cl, **7** = Pd(**1**)Py, **8** = Pd(**1**)Lu, **9** = Pd(**1**), 10 = Pd(**2**), 11 = Pd(**3**). *Represents the minor species.*

Frequency (ppm)	**4**	**7**	**8**	**8** + Δ*	**9**	**10**	**11**	**1**	**2**	**3**
N—H $_{Trp\text{-}In\ 3}$	—	—	—	—	—	—	10.90	—	—	10.86
Py *Ortho*	—	8.73	—	—	—	—	—	—	—	—
Py/Lu *Meta*	—	7.57	7.33	7.02	—	—	—	—	—	—
Py/Lu *Para*	—	7.99	7.78	7.54	—	—	—	—	—	—
N—H $_{Gly}$	—	—	—	—	—	—	—	8.34	8.39	8.32
N—H $_{Ala}$	—	—	—	—	—	—	—	8.16	8.24	8.12
C—H $_{Trp\text{-}In\ 7}$	—	—	—	—	—	—	7.55	—	—	7.56
C—H $_{Trp\text{-}In\ 4}$	—	—	—	—	—	—	7.37	—	—	7.33
C—H $_{Trp\text{-}In\ 2}$	—	—	—	—	—	—	7.27	—	—	7.18
C—H $_{Trp\text{-}In\ 5}$	—	—	—	—	—	—	7.09	—	—	7.06
C—H $_{Trp\text{-}In\ 6}$	—	—	—	—	—	—	6.99	—	—	6.97
N—H_2	4.20 3.86	4.96 4.38	4.76 4.15	5.03 4.54	5.04 4.55	4.63 4.48	4.96 4.24	—	—	—
α-C_{Ala}	3.54	3.66	3.66	3.68	3.68	3.89	3.78	4.31	4.31	4.34
α-C_{Gly}	3.64	3.52	3.14 2.91	3.86	3.87	3.62	3.96	3.84	3.83	3.83
α-$C_{Trp/Asp}$	3.40	3.44	3.54	3.53	3.52	2.33	3.40	3.52	2.49 2.36	3.51
OCH_3 $_{Gly}$	3.50	3.34	3.34	3.55	3.55	3.55	3.55	3.62	3.63	3.63
Lu CH_3	—	—	3.18	2.41	—	—	—	—	—	—
β-$C_{Trp/Asp}$	2.45 2.35	2.61 2.40	2.57 2.41	2.63 2.46	2.61 2.45	3.18	3.28 2.87	2.37 2.35	3.64	3.10 2.78
$OC(CH_3)_3$ $_{Asp}$	1.40	1.40	1.41	1.42	1.42	1.44	—	1.38	1.39	—
β-C_{Ala}	1.15	1.23	1.23	1.20	1.20	1.08	1.24	1.23	1.21	1.16

Support for the coordination mode of **9** was established in part by examining the ^{1}H NMR. The appearance of the NH_2 protons at 4.76 and 5.03 ppm establish amine coordination. The Asp α-C proton appears at about the same resonances as in **1.** However, the Ala *α*-C protons experiences a large upfield shift, supporting Asp amide coordination. The Gly protons only shift by 0.03 ppm compared to **1**, but the Gly coupling pattern changes from a doublet to a quadruplet, signifying Ala amide coordination. The small change in resonances is explained with carbonyl oxygen coordination. Carbonyl is a *π*-acceptor ligand, deshielding the metal. An

argument for a coordinated carboxylate ester oxygen is not supported given the small change in the methyl ester chemical shift.

The NMR spectrum of **10** was poorly resolved owing to the lability of the 6 membered ring. However, important information regarding coordination geometry can still be gleaned from the 2-D coupling patterns and discernible resonance positions. Elevated temperature NMR experiments (330K) were performed to improve the spectral resolution. Coordination of the amine is evidenced by the NH_2 resonances at 4.63 and 4.48 ppm. Side chain methylene protons of the N-terminal amino acid (Asp or Trp) are a characteristic feature of the ligands **1**-**3**. These protons are distereotopic and, when recorded in DMSO-*d6*, appear as a doublet of quadruplets, because they are in different magnetic environments with different vicinal coupling. For **4**-**9** these protons are outside a chelate ring and show similar coupling constants as the ligands. However, **10** encloses the methylene protons in a 6-membered ring and they become an apparent quadruplet (see Figure 3). Additionally, a large upfield shift of the α-C protons for Asp (0.46 ppm), Ala (0.42 ppm), and Gly (0.21 ppm), confirms the amine/amide backbone chelation.

In **11**, the appearance of the NH_2 protons at 4.96 and 4.24 ppm confirms N-terminus amine coordination, whereas the indole resonances are relatively unchanged suggesting N-terminal amine coordination rather than via the indole amine. Respective shifts in the Ala (Δ0.56 ppm) and Trp (Δ0.11 ppm) α-C protons shift downfield, are in agreement with **9**-**10**.

^{13}C NMR Analysis.

The ^{13}C NMR spectrum collected for the ligands (**1**-**3**) and complexes (**4**, **8**-**11)** can be seen in Table 2. Assignments for the carbon spectrum were aided by the 2-D NMR technique HSQC, which reveals ^{13}C and ^{1}H coupling. As expected, all of the α-carbons shifted downfield, while the Ala α-carbons undergo the largest downfield shifts and have the broadest range.

The most significant and difficult assignments for ^{13}C belonged to the carbonyl carbons. In order to confidently assign these signals, DFT calculations were used to elucidate coordination modes and to calculate the ^{13}C chemical shifts. These calculations are based on the optimized

*Table 2. Assigned ^{13}C NMR resonance for ligands **1-3** and complexes **4,8-11**. *(Lutidine resonances can be found in experimental section)*

Frequency (ppm)	4	8*	9	10	11	1	2	3
$C{=}O_{Trp/Asp}$	170.14	169.93	169.79	170.75	172.93	172.82	172.99	173.84
$C{=}O_{Ala}$	185.17	185.45	177.03	176.26	178.24	172.61	172.73	172.68
γ-$C{=}O_{Asp}$	175.91	175.9	172.89	172.58	—	170.45	170.17	—
$C{=}O_{Gly}$	172.34	171.71	186.47	?	186.55	170.11	169.4	170.12
$C{=}C$ Trp-In 4	—	—	—	—	136.37	—	—	136.20
$C{=}C$ Trp-In 9	—	—	—	—	127.11	—	—	127.39
C—H Trp-In 2	—	—	—	—	123.33	—	—	123.94
C—H Trp-In 6	—	—	—	—	121.11	—	—	120.84
C—H Trp-In 8	—	—	—	—	118.44	—	—	118.46
C—H Trp-In 7	—	—	—	—	118.24	—	—	118.19
C—H Trp-In 5	—	—	—	—	111.41	—	—	111.28
$C{=}C$ Trp-In 1	—	—	—	—	109.47	—	—	110.22
$O\underline{C}(CH_3)_3$ Asp	79.93	80.14	80.47	82.32	—	79.97	80.41	—
OCH_3 Gly	50.52	50.79	50.96	50.92	50.93	51.68	51.67	52.69
α-$C_{Trp/Asp}$	56.55	56.50	55.81	40.16	59.58	51.51	39.15	54.91
α-C_{Ala}	57.05	57.13	56.60	58.87	56.50	47.78	47.85	47.52
α-C_{Gly}	46.49	45.84	46.79	44.73	46.86	40.48	40.48	40.48
β-$C_{Trp/Asp}$	39.86	39.73	39.94	54.7	29.93	40.24	51.52	30.42
$OC(\underline{C}H_3)_3$ Asp	27.79	27.79	27.79	27.58	—	27.75	27.61	—
β-C_{Ala}	19.43	19.78	19.80	20.64	19.92	18.50	18.18	18.64

geometries found in Figure 3. Table 3 shows a comparison of observed and calculated carbonyl ^{13}C chemical shifts, which are adjusted for systematic differences in shielding values. For **4** and **8** there is decent agreement between the observed and calculated values for Gly and Asp esters, and Asp amides however, the Ala amide shows stronger deshielding then calculations suggest. Coordination of the ester carbonyl ($C{=}O_{Gly}$), seen in **9** and **11**, is accompanied by a large downfield shift from ~170 (**1**-**3**) to ~186 ppm which is consistent with reported values[2]. Due to the lability of **10**, this peak was not observed, even in the high temperature NMR experiment.

*Table 3. Assigned ^{13}C NMR resonance for complexes **4,8-11** compared to calculate values.*

Frequency (ppm)	**4** (obs)	**4** (calc)	**8** (obs)	**8** (calc)	**9** (obs)	**9** (calc)	**10** (obs)	**10** (calc)	**11** (obs)	**11** (calc)
$C{=}O_{Trp/Asp}$	170.14	170.82	169.93	171.07	169.79	171.39	170.75	165.3	172.93	169.9
$C{=}O_{Ala}$	185.17	181.86	185.45	182.5	177.03	177.63	176.26	176.5	178.24	177.11
γ-$C{=}O_{Asp}$	175.91	171.72	175.9	174.71	172.89	172.31	172.58	172.4	—	—
$C{=}O_{Gly}$	172.34	171.34	171.71	173.3	186.47	186.23	?	187.8	186.55	185.82

Infrared Data Analysis.

Infrared spectroscopic data was collected for ligands **1-3** and complexes **4**, **8-11** and is detailed in Table 4. Vibrational modes for the ligands and complexes were assigned with the aide of DFT calculations, based on relative value sets. Comparative values for observed and calculated carbonyl stretching bands for **9-11** are presented in Table 5.

For **4**, **8-11**, the low energy shift of the symmetric and asymmetric stretching modes for NH_2 to ~3250 - 3100 cm^{-1}, at energies typical of coordinated N_{amino}[3], confirm amine coordination. Whereas low energy shifts of the Amide I band by 50-100 cm^{-1}, which combine with the Amide II band, support amine/amide backbone chelation. Additionally, the palladium to nitrogen vibrational energies appear consistent with reported values [3-6].

*Table 4. Summary of infrared data from synthetic experiments to form Pd(II) complexes **4, 8-11** with ligands **1-3**. *Denotes shoulder absorption.*

Frequency (cm^{-1})	**4**	**8**	**9**	**10**	**11**	**1**	**2**	**3**
ν(N—H_2)	3234	3223	3245	3239	3286	3370	3375*	3370*
ν(N—H)	3138	3100	3129	3121	3235	3314	3304	3297
ν(C=O)								
OtBu	1723	1732	1729	1732	—	1725	1743	—
OMe	1748*	1750*	1541	1551	1554	1759*	1757*	1749
Amide I	1585 1570	1604 1582	1608 1584	1590 1567	1598 1569	1670	1659	1655
ν(C=C)								
Aromatic	—	—	—	—	1668	—	—	1673*
ν(N—H)								
Amide II	—	—	—	—	—	1546	1541	1517
ν(C—O)								
OtBu	1254	1250	1253	1258	—	1250	1254	—
OMe	1210	1210	1205	1207	1207	1213	1212	1213
ν(O—C)								
OtBu	1148	1147	1145	1155	—	1155	1155	—
ν(M—N)	573 548	568 548	573 548	573 533	568 534	—	—	—

*Table 5. Comparative values for ν(C=O) vibrational modes observed verses DFT calculated for **4**, **8-11** and ligands **1-3**. The Δ values show the systematic error of the calculated DFT values.*

Complex	ν(C=O) OtBu	ν(C=O) OMe	ν(C=O) Amide I	ν(C=O) Amide I
4 Obs	1723	1748	1585	1570
DFT	1767	1782	1659	1639
Δ	*44*	*34*	*74*	*69*
8 Obs	1732	1750	1604	1582
DFT	1749	1790	1664	1642
Δ	*17*	*40*	*60*	*60*
9 Obs	1729	1541	1608	1584
DFT	1757	1677	1666	1652
Δ	*28*	*136*	*58*	*68*
10 Obs	1732	1551	1590	1567
DFT	1784	1674	1653	1653
Δ	*52*	*123*	*63*	*86*
11 Obs	—	1554	1598	1569
DFT	—	1652	1677	1662
Δ	—	*98*	*79*	*93*
1 Obs	1725	1759	1670	1670
DFT	1758	1793	1745	1728
Δ	*33*	*34*	*75*	*58*
2 Obs	1743	1757	1659	1659
DFT	1757	1787	1740	1730
Δ	*14*	*30*	*81*	*71*
3 Obs	—	1749	1655	1655
DFT	—	1792	1747	1713
Δ	—	*43*	*92*	*58*

For **4** and **8** the methyl ester carbonyl band is still present and ~1750 cm^{-1}, indicating that the carbonyl is uncoordinated. Lutidine coordination is confirmed for **8** with the appearance of an aromatic ν(C=C) band at 1471 cm^{-1} (free Lu 1481 cm^{-1}) and by the shift of the out-of-plane CH band to higher frequency (787 cm^{-1}) compared to that of the free ligand (770 cm^{-1}) [3]. Unfortunately, Pd-Cl vibrations appear at far-IR frequencies and are not observable. Compared to **4** and **8**, the spectrum for **9** has a strong distinct band at 1541 cm^{-1}. Palladium complexes with similar ester coordination have been synthesized and report a large shift of the ester carbonyl stretching frequency to lower energies [7] upon coordination. This indicates that the methyl ester carbonyl oxygen is coordinated to Pd, resulting in a lower energy shift of ~200 cm^{-1}. This assignment is supported by the calculated relative vibrational frequencies for this

complex; A similar band is present in the spectra collected for **10** and **11**, suggesting **9-11** have methyl ester carbonyl coordination. In addition the methyl ester ν(C--O) for **9-11** appears to have the same low energy shift of ~ 7 cm^{-1}.

Reaction studies

Ethylene

To examine whether these complexes were good candidates for the catalysis, ethylene reactivity studies were performed and monitored with NMR spectroscopy. The general procedure was to dissolve the complexes in DMSO-*d6* and record the spectrum, bubble ethylene directly into the NMR tube and record the spectra again. The addition of ethylene produced a peak at 5.14 ppm, since this is where the signal for free ethylene in DMSO-*d6* should be, it was concluded there was no reaction. It was surmised that the addition of an *α*-proton was needed in order to see reaction chemistry.

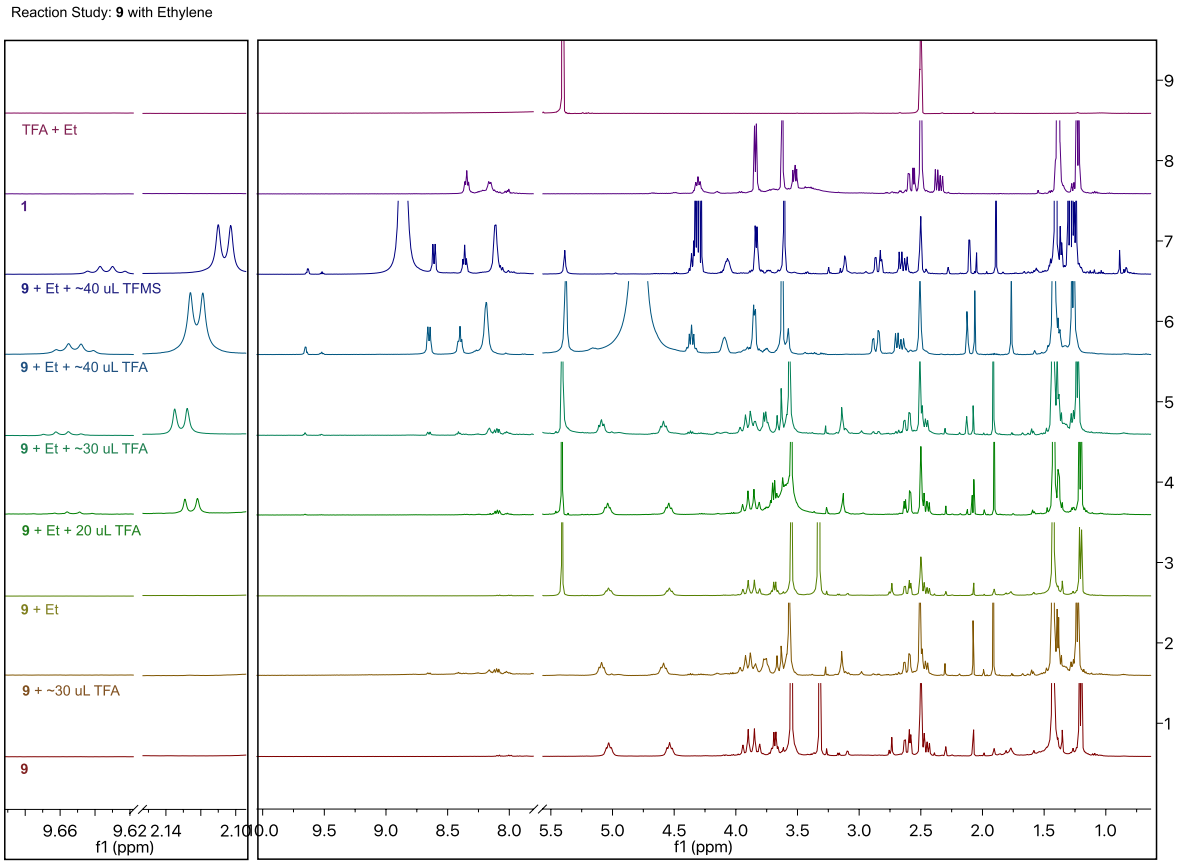

*Figure 4. Stacked ^{1}H NMR spectra of 9 (1) with addition of: (2) 30uL TFA, (3) Ethylene, (4) 20 uL TFA and Ethylene, (5) 30 uL TFA and Ethylene, (6) 40 uL TFA and Ethylene, (7) 40 uL TFMS and Ethylene, (8) Ligand **1**, (9) Blank with Ethylene and TFA*

Trifluoroacetic acid (TFA) and Triflic acid (TFMS) were selected because one is a weak acid, and the other a strong acid; Neiter TFA or TFMS have interfering proton resonances. Portions ranging from ~10 to 20-fold excess of TFA or TFMS were added the spectra were recorded again. These spectra are depicted in Figure 4.

Procedure: Complex **9** (10.1 mg, 0.023 mmol) was dissolved in 650 μL of DMSO-d6, the NMR recorded, then ethylene was bubbled in for 1 min, and the NMR recorded again. (Figure 4-4) TFA (~20 μL, 0.128 mmol; ~30 μL, 0.192 mmol; ~40 μL (0.256 mmol) was added to the NMR tube and the spectrum recorded again. There were also some solvent impurities and residual proton sponge present.

Results: After ethylene addition a singlet at 5.41 ppm representing free ethylene appeared however, no coordinated ethylene was observed and there were no changes to the spectrum of the complex. With the addition of ~20 μL TFA to the sample, a few noticeable differences were observed (Figure 4-3). Small proton sponge impurities capture the acidic proton, and the resonance shifts from 2.74 to 3.13 ppm; This had little effect on the reaction chemistry since a 10 - 20-fold excess of TFA was added. A new doublet formed at 2.13 ppm that couples to a quadruplet at 9.66 ppm in a 3:1 ratio. If the doublet represents 3 protons then this compound is < 5 % of the complex; This is accompanied by the loss of the H_2O residue signal at 3.33 ppm.

Increasing the amount of TFA to ~30 μL results in more changes to the recorded spectra (Figure 4-5). Three resonances form downfield at 8.65(d), 8.40(t), and 8.19(s) ppm, which couple with small resonances at 4.38(t), 3.86(m) and 4.10(m), respectively. These are the amino/amide protons and are presumably formed by dissociation of the Pd(II) from the ligand. Again, the doublet at 2.13 ppm which couples to the quadruplet at 9.66 ppm in a 3:1 ratio, representing ~10 % proportional to the complex.

When ~40 μL TFA was added to the sample, the spectrum changes significantly, as seen in Figure 4-6. All of the signals shift downfield and Ala and Gly α-C protons couple with the signals at ~8.20 – 8.65 ppm; These resonances suggest the complete demetalation and protonation of the N functional groups in the presence of acidic protons. The resonances at 2.13 and 9.66 ppm increase proportionally with the quantity of TFA and now integrate to ~15 - 20 %. Comparing this spectra with the free ligand **1**, there is little overlap in signal

positioning, this may likely be a function of pH.

The reverse order of reagent addition was performed, where TFA (~30 μL) was added (Figure 4-2), a spectrum recorded, then ethylene was bubbled in and these spectra were compared. With just TFA addition, the Ala α-C protons shift downfield by ~0.10 ppm. However, the doublet at 2.13 ppm, coupled with the triplet at 9.66 ppm, appears only after both TFA and ethylene are present. These resonances are formed by the oxidation of ethylene to form acetaldehyde (Scheme 1). This reaction is catalyzed by Pd(II) after dissociation of the ligand. A blank spectrum of TFA and ethylene in DMSO (Figure 4-9) confirmed that this is not a spontaneous reaction. The spectra produced a singlet at 5.41 ppm (free ethylene) and a broad doublet at 7.03 ppm, which could be related to trace H_2O interactions with TFA.

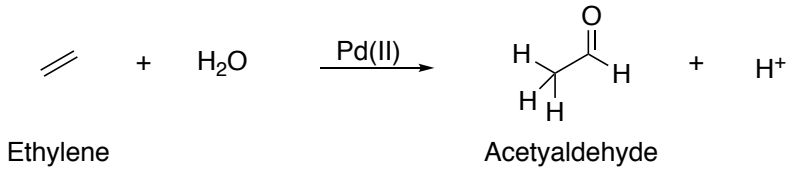

Scheme 1. Oxidation of ethylene to form acetaldehyde catalyzed by Pd(II)

Triflic acid (TFMS) was substituted for trifluoroacetic acid in order determine if a different proton source produces the same product. Unlike TFA, TFMS is non-coordinating.

Procedure: For this experiment, an NMR tube was charged with **9** (10.0 mg, 0.023 mmol) and ethylene was bubbled in, then TFMS was added (~40 uL, 0.443 mmol), and the sample was collected (Figure 4-7).

Results: Comparing the ^{1}H NMR of spectra 6 and 7 in Figure 4, many of the same signals are present, including the downfield protons on the N-functional groups; Indicating excess of TFMS also results in demetalation. Two new resonances are formed in this reaction, a triplet at 1.29 ppm integrating to ~8 protons and a quadruplet at 4.30 ppm, integrating to ~5.5 protons. This product is most likely ethyl trifluoromethanesulfonate (Scheme 2), which is known to form from triflic acid in the presents of ethylene[8,9]. The NMR had some Pd black precipitate after three days but was still a yellow solution.

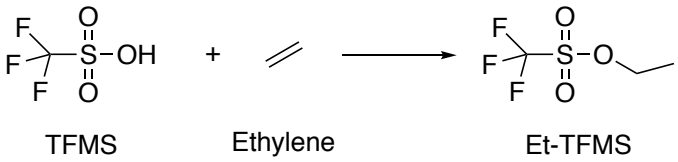

Scheme 2. Spontaneous reaction between trifluoromethanesulfonate and ethylene to form ethyl trifluoromethanesulfonate

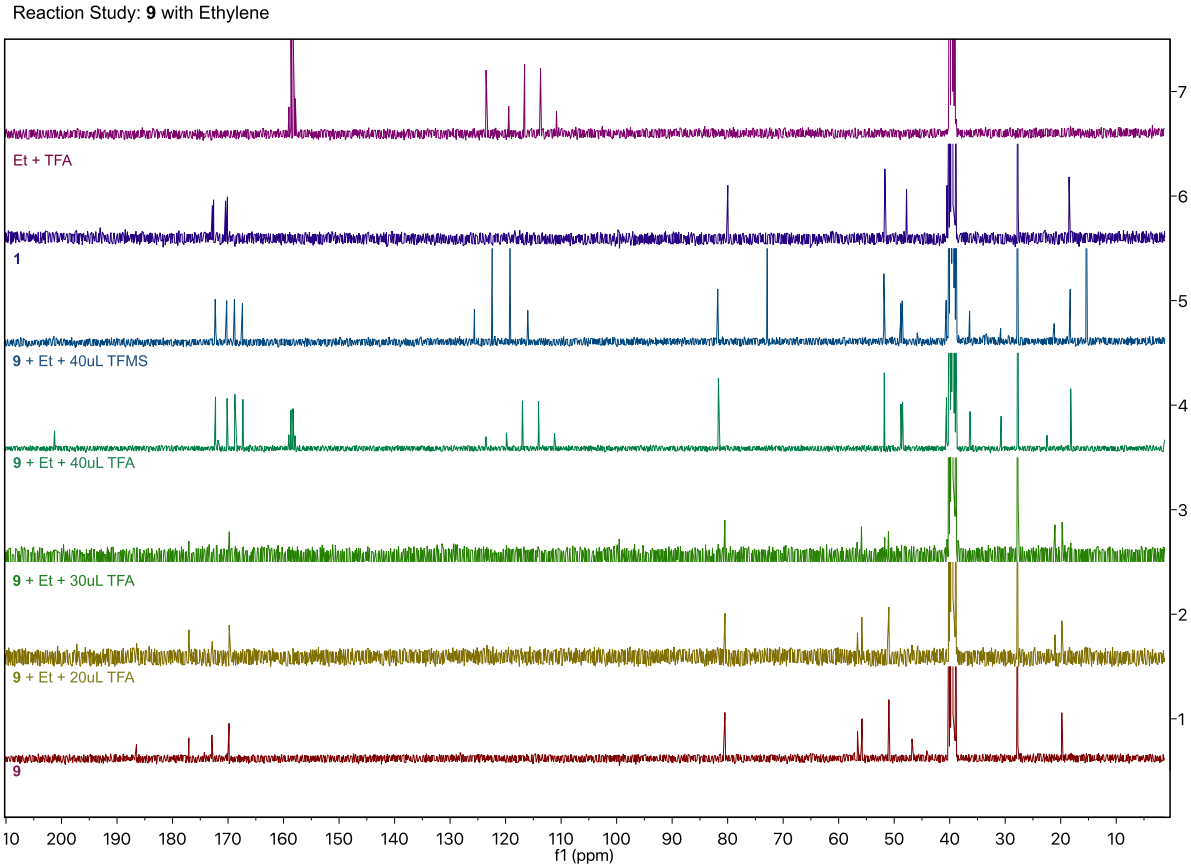

Figure 5. Stacked 13C NMR 9 (1) with addition of: (2) 20 uL TFA and Ethylene, (3) 30 uL TFA and Ethylene, (4) 40 uL TFA and Ethylene, (5) 40 uL TFMS and Ethylene, (6) Ligand 1, (7) Blank with Ethylene and TFA.

Examining the ^{13}C NMR for this experiment reveals the addition of 20-30μL TFA, does not result in changes to the signals of **9** (See Figure 5). Although ~10 to 15-fold TFA excess was added, the signature quadruplets at ~158 and ~115 ppm are not present in the spectrum. This could be related to the volatility of this reagent and the length of ^{13}C experiments. When more TFA (40 uL) or TFMS (40 uL) is added, the ^{13}C signals are affected significantly. This supports the findings that demetalation has occurred. Table 6 list the signals formed with the addition of TFMS, along with the observed signals for **9** and **1**. Conformation of Et-TFMS formation is see in the corresponding ^{13}C signals at 15.67 and 73.08, respectively. The formation of an

aldehyde signal at 201.25 ppm and the appearance of a peak at 31.10 supports the assertion that acetaldehyde is formed.

*The TFA experiment was also carried out on complex **10**.*

Procedure: An NMR tube was charged with **10** (9.7 mg, 0.022 mmol) and a spectrum recorded, then TFA (~ 20 uL, 0.128 mmol) was added and the spectrum recorded; Ethylene was bubbled in, and the NMR recorded again.

Results: With the addition of TFA the spectrum changes dramatically. Again, the three downfield resonances are formed at 8.49(d), 8.24(t), and 8.20(d) ppm which couple to 4.37(t), 3.84(d) and 4.17(m) indicate that for part of the sample N amine/amide protonation and demetallation has occurred. The Asp β-C protons shift from 2.34(q) to 2.76(d) and couple with the Asp α-C protons at 3.44(t) ppm (shifted from 3.18 ppm); This proton couples with NH_2 at 5.01 and 4.73 ppm, indicating that the amine is still coordinated in some of the sample. After ethylene addition the resonance at 2.13(d) and 9.66(q) ppm appear in a 3:1 ratio, where if the doublet represents 3 protons, then this compound is ~10% of the complex. The ^{13}C for this experiment is not very telling due to the lability of the complex.

Methyl formate

Carbonylation reactions are typically performed using CO in conjunction with various monomers, including olefins and alcohols under high pressure to yield various carboxylic acid derivatives. In order to avoid the use of carbon monoxide as C1-feedstock, which not only is toxic and difficult to transport, but also requires a reactor set-up, CO-surrogates can be used. Chief among these CO alternative are formic acid derivatives. [10]

In order to examine whether these complexes are candidates for carbonylation reactions, first activation of methyl formate was investigated. A stock solution of methyl formate (0.100 mM) in DMF was added to 40 mg of sample in a 1.1 : 1 ratio. However, upon mixing, the formation and precipitation of Pd black occurred immediately.

Sulfur reagents

The reactivity of **9** and **10** toward catalytic sulfur atom transfer reaction was also investigated. These studies were performed and monitored with NMR spectroscopy. Samples were prepared

aerobically by mixing together thiirane and DMSO-*d6* in a screw cap NMR tube. Initial ^{1}H NMR spectrum were recorded at ambient temperature and pressure to obtain a blank spectrum. A pre-weighed amount of solid catalyst was added to the NMR tube and ^{1}H NMR spectrum was recorded. The progress of the reaction was monitored over the course of hour or days to determine conversion of thiirane to alkene. Controlled reactions under the same conditions but omitting the catalyst, showed no identifiable alkene formation over commensurate time periods as the catalytic runs.

Catalytic study of 9 (3 mol %) with cyclohexene sulfide

Procedure: Cyclohexene sulfide (47 microL, 0.3833 mmol) was added to DMSO-d_6 (0.6 ml) in screw-cap NMR tube and ^{1}H NMR was recorded (blank). Complex **9** (5 mg, 0.0115 mmol) was added to NMR tube and ^{1}H NMR spectrum for recorded instantly.

Results: Complex **9** showed quick conversion of cyclohexene sulfide to cyclohexene (Scheme 1) reaching up to 20%, then leveling out after ~30%. Deactivation of the catalyst occurs after ~30 hours. Figure 6 outlines the percent conversion as a function of time.

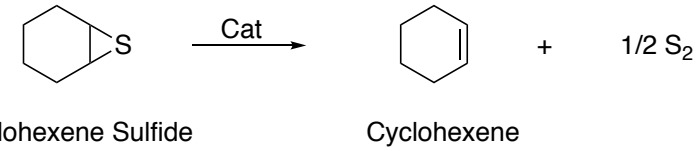

Scheme 3. Catalytic conversion of cyclohexene sulfide to cyclohexene

*Catalytic study of **10** (3 mol %) with cyclohexene sulfide*

Procedure: Cyclohexene sulfide (47 microL, 0.3833 mmol) was added to DMSO-d_6 (0.6 ml) in screw-cap NMR tube and ^{1}H NMR was recorded (blank). Complex **10** (5 mg, 0.0115 mmol) was added to NMR tube and ^{1}H NMR spectrum for recorded instantly.

*Results:*Complex **10** showed much higher conversion of cyclohexene sulfide to cyclohexene, with conversion reaching > 50% after 24 hours before deactivation.

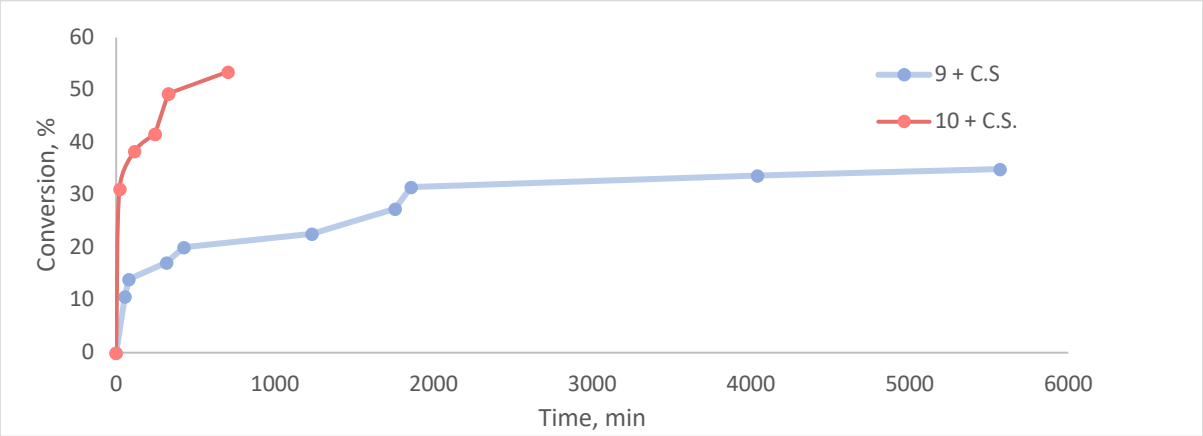

Figure 6. Percent catalytic conversion of cyclohexene sulfide to cyclohexene with complexes 9 and 10, monitored via ^{1}H NMR.

Approximately 1 mg of Pd{WAG(OMe)} was dissolved in 1.5 mL of solvent (DMF, CH_3CN, DMSO) and 0.200 mL of propylene sulfide or 0.100 mL of cyclohexane sulfide was added to the solution. The vials were capped and allowed to sit overnight. If solid precipitate formed it was separated via centrifuge and UV-Vis spectroscopy of the solutions was taken.

In DMF complex **11** exhibits absorbance bands at 281, 290, 314(sh), 338(sh) and 458(sh) nm; The addition of cyclohexene sulfide and propylene sulfide did not result in formation of a precipitate. With the addition of cyclohexene sulfide, a hypsochromic shift from 458 to 390 nm was observed this was accompanied by a merger of the shoulder bands at 314 and 338 nm to 328 nm. When propylene sulfide was added to complex **11** in DMF a strong absorption band at 330 nm arises. This is also accompanied by the hypsochromic shift of 458 nm to a shoulder band around 375 nm.

The complex did not fully dissolve in acetonitrile and the solubility of **11** was determined to be about 1.5 mg in 20 ml of CH_3CN. Due to the low solubility of **11** in acetonitrile, the addition of propylene sulfide and cyclohexane sulfide turned the solution cloudy immediately. In acetonitrile **11** has absorbance bands at 281, 290, 314(sh), 338(sh, and 458(sh) nm), mirroring the bands in DMF. After the addition of propylene sulfide, the absorbances at 314 and 338 nm converge into a shoulder peak at 326 nm, and there is a hypsochromic shift from 458 to 392 nm. This same hypsochromic shift can be seen in the cyclohexene sulfide solution, however the excess cyclohexene sulfide masks the spectra under 360 nm.

The reaction of **11** with cyclohexene sulfide in DMSO resulted in the same hypsochromic shift

at around 400 nm and the shoulder band at 327 nm, as seen in the DMF and acetonitrile. The addition of propylene sulfide resulted in a clear solution with a white precipitate which is a result of demetalation.

Discussion

Combining spectroscopic data from ^{1}H and ^{13}C NMR, infrared, and mass spectroscopy, along with elemental analysis, the coordination geometry of five distinct complexes was elucidated.

It was soundly established that complexes **4**-**11** have coordinated amine/amide backbone coordination and that the 4th coordination dramatically effected the spectroscopy of the complex.

Complexes **4**-**6** were mono-anionic with coordinated chloride in the 4th coordination. This resulted in the proton signals displaying large shielding effects from the charged metal ion. However, this effect was muted in the ^{13}C NMR. Complexes formed with pyridine (**7**) and lutidine (**8**) exhibited π-interaction with the glycine moiety, resulting in upfield displacements in the ^{1}H and ^{13}C spectra.

The most difficult assignment was the methyl ester carbonyl coordination for **9**-**11**. Establishing this coordination started with the collection of the mass spectroscopy data, which gave the $M+Na^{+}$ species with error less than 2.0 ppm. The methyl esters in **9**-**11** experiences the same degree of shielding in the ^{1}H NMR, and in the ^{13}C NMR the methyl carbon has similar shifts between **1**-**3** and **9**-**11** suggesting similar coordination for these three complexes. The carbonyl carbon has a distinct downfield shift to ~187 ppm for **9** and **11**, which was confirmed by DFT calculations. The carbonyl carbon for **10** was not detected, because of lability, but the comparative data of this common moiety indicate that it too has carbonyl coordination.

For ligand **3** there are distinct differences in the coordination behavior in non-aqueous versus aqueous synthesis, where it was established that the indole amine competitively coordinated with metal instead of the N-terminal amine.

The reactivity studies of **9** and **10** with ethylene show activation of the ethylene group only with the addition of a proton source. The ethylene is oxidized to form the acetaldehyde. This is a well-known mechanism, the Wacker Process (WP), with industrial applications. In the WP olefins are converted to aldehydes via catalytic oxidation. The olefin is first coordinated to a metal center (usually a Pd(II) salt), followed by and external attack by an oxidizing agent, then

proton transfer, and finally dissociation. These reactions were stoichiometric when first studied because of decomposition of $PdCl_2$ to Pd(0), but the addition of $CuCl_2$ to oxidize Pd(0) gave way for a bi-cyclic catalytic reaction with the overall reaction equation seen in Scheme 3.

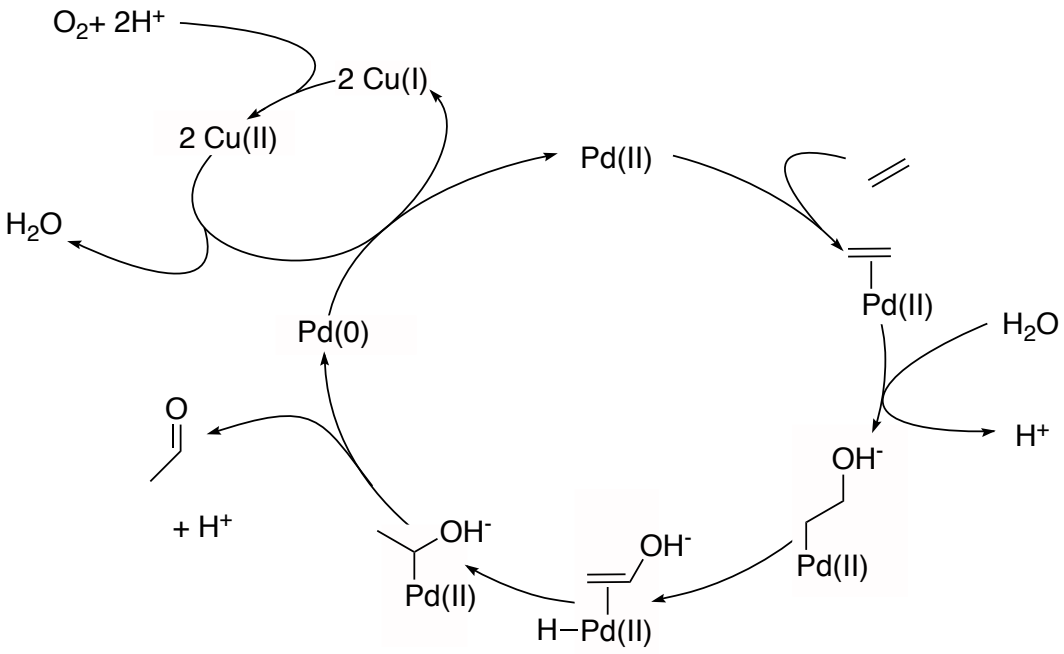

Scheme 4. Catalytic cycle for the palladium catalyzed oxidation of alkenes to aldehydes.

In the reaction studies carried out in this work, the acid causes demetalation after ~10-fold excess acid added. As more acid is added, the degree of demetalation increases, and the amount of converted acetaldehyde also increases. It is unclear if the formation of acetaldehyde is limited by the amount of acidic protons or oxidizing agent, namely water.

Conclusion

The development of a non-aqueous synthesis strategy, using a non-nucleophilic base was instrumental in the formation of neutral tetra-dentate palladium complexes with κ^4-NH_2,N,N,=O coordination. The development of this class of complexes was meant to achieve maximum organosolubility, in order to carry out reactions in non-coordinating solvents. Despite **9** and **10** having multiple functional groups including the methyl and tert-butyl esters and **11** with an indole, these complexes are relatively insoluble. These complexes were most soluble in DMSO and DMF but were also slightly soluble in acetonitrile and alcohols. However, they were insoluble in most organic solvents. As a consequence, characterization

and reaction studies were carried out in coordinating solvents. The use of this synthetic strategy offers the possibility to facilitate coordination of esters carbonyl oxygen to metals.

Complex **9** exhibited a mild ability to convert ethylene to acetaldehyde, but it is unclear if this is due solely to Pd(II), as the ligand was demetalated in parallel with this reaction proceeding.

Both **9** and **10** are able to catalytically transfer sulfur atom however, **10** outperforms **9** in TOF before deactivation.

Experimental

Instrumentation

Infrared spectra were recorded on a Nicolet Avatar 360 FT-IR (E.S.P.) spectrophotometer using KBr pellets. ^{1}H, COSY, and ^{13}C nuclear magnetic resonance spectra were recorded at ambient temperature on a Bruker Avance 400 MHz spectrometer at 400 and 101 MHz, respectively. Solvents used were D_2O, DMSO-d_6, and $CDCl_3$. Mass spectra were recorded on a micrOTOF-Q spectrometer, equipped with E-spray atmospheric pressure ionization chamber (ESI).

Reagents used were purchased from Sigma Aldrich and used without further purification unless otherwise stated. Alanylglycine, Fmoc-Asp(OtBu)-OH, Fmoc-Asp(OH)-OtBu, Z-Trp, and EDC-Cl use in peptide coupling were purchased from Bachem. Solvents were purchased from Sigma Aldrich and were distilled under nitrogen and dried using standard methods[11]. Alanylglycine esterification was completed by reacting it with trimethylchlorosilane[12], [$Pd(CH_3CN)Cl_2$] was prepared according to the published procedures.

Quantum chemical calculations

Calculations were performed with a development version ORCA program[13,14]. The density functional theory based protocol consisted of the PBE0-D3BJ functional[15-17] (including the D3 dispersion correction by Grimme and coworkers [18,19] and the triple-zeta basis set def2-TZVP[20]. The RIJCOSX[21,22] approximation was used to calculate Coulomb and Exchange integrals, using the def2/J auxiliary basis set by Weigend et al. and the GridX5 (ORCA keyword) grid was used. Tighter grids for the exchange-correlation terms were also used (Grid5, FinalGrid6 keywords in ORCA). The CPCM solvation model using a Gaussian pointcharge scheme and a

scaled vdW surface was used to incorporate solvation effects. Vibrational frequencies were calculated analytically, as implemented in ORCA. ^{13}C NMR shieldings were calculated using the same level of theory, except the pcSseg-2 basis sets were utilized on carbon and hydrogen atoms. The calculated shieldings were converted into chemical shifts by calculating the shielding difference with respect to tetramethylsilane at the same level of theory. Chemical shifts were shifted by -15 ppm due to a systematic overestimation.

Ligand synthesis

The ligands were synthesized following published procedure. [1] Coupling reactions were executed by adding EDC-HCl (1.1 mol eq) to a solution with 1:1 molar equivalent of N-protected amino acid and HOBt in chloroform (0º C). AlaGly(OMe)-HCl (1 mol eq) was added, followed by addition of triethylamine (1.05 mol eq). The solution was stirred under slight N_2 flow at ambient temperature for 24 h. Product was washed with water and dried with $MgSO_4$ and the $CHCl_3$ removed in vacuo. The Fmoc-protection group was removed [23] by stirring the tripeptide in DMF at 110º C for 1 hour. Methanol was added to the DMF and then washed with hexane. Solvent was removed in vacuo and purified with flash chromatography. The CBZ-protection group was removed[24] by catalytic hydrolysis with H_2 using 10% Pd/C in dry MeOH. Product was collected by filtering through celite and removing the solvent in vacuo.

Complex synthesis

K[Pd{***α***-Asp(OtBu)AlaGly(OMe)}Cl] (**4**): K_2PdCl_4 (0.040 g, 0.136 mmol) and **1** (0.050 g, 0.136 mmol) were dissolved in H_2O (5 mL) and KOH was added until pH=6.5. Solution was stirred overnight under N_2. The H_2O was removed in vacuo and the product was isolated by dissolving in EtOH and filtering. ^1H NMR (400 MHz, DMSO-d_6) δ 4.20 (dd, 1H, NH_{Asp}), 3.84 (d, 1H, NH_{Asp}), 3.69 – 3.57 (m, 2H, α-H_{Gly}), 3.56 – 3.51 (m, 1H, α-H_{Ala}), 3.50 (s, 3H, -OCH_3 $_{Gly}$), 3.43 – 3.36 (m, 1H, α-H_{Asp}), 2.50 (DMSO), 2.48 – 2.42 (m, 1H, β-H_{Asp}), 2.35 – 2.29 (m, 1H, β-H_{Asp}), 1.40 (s, 9H, -$O(CH_3)_3$ $_{Asp}$), 1.15 (d, 3H, β-H_{Ala}). IR (KBr) cm^{-1}: 3315, 3234 (b, ν(N—H)), 1723 (s, ν(C=O)), 1585 (s, ν(C=O)), 1570 (s, ν(C—N)), 1254 (s, ν(C—O)), 1210 (s, ν(C—O)), 1148 (s, ν(C—O)). UVVis (H_2O): ε_x MS (ESI/Negative) MW: ($C_{14}H_{23}N_3O_6PdCl$) = 471.2230, M/Z found(calc) = 472.0311(472.0313) [M^-].

(Et_3N)[Pd{***α***-Asp(OtBu)AGly(OMe)}Cl] (**5**): $Pd(CH_3CN)_2Cl_2$ (0.076 g, 0.297 mmol) and **1**

(0.097 g, 0.297 mmol) were dissolved in dry THF (~20 mL) and triethylamine (0.08 mL, 0.585 mmol) was added. The reaction was stirred overnight under Ar. Solution was filtered through celite and removed in vacuo. Excess yield due to Et_3NCl salt. ^1H NMR (400 MHz, DMSO-d_6) δ 4.21 (dd, 1H, NH_{Asp}), 3.85 (t, 1H, NH_{Asp}), 3.69 – 3.56 (m, 2H, α-H_{Gly}), 3.56 – 3.51 (m, 1H, α-H_{Ala}), 3.50 (s, 3H, -$OCH_{3\ Gly}$), 3.40 (d, 1H, α-H_{Asp}), 3.08 (q, 14H, -$CH_{2\ TEA}$), 2.50 (DMSO), 2.44 (d, 1H, β-H_{Asp}), 2.33 (dd, 1H, β-H_{Asp}), 1.40 (s, 9H, -$O(CH_3)_{3\ Asp}$), 1.23 – 1.13 (m, 24H, -$O(CH_3)_{3\ Asp}$,-$CH_{3\ TEA}$). IR (KBr) cm^{-1}: 3313, 3215 (b, ν(N—H)), 1750 (s, ν(C=O)), 1724 (s, ν(C=O)), 1601 (s, ν(C=O)), 1583 (s, ν(C—N)), 1250 (s, ν(C—O)), 1210 (s, ν(C—O)), 1148 (s, ν(C—O)).

(PPh_4)[Pd{***α***-Asp(OtBu)AlaGly(OMe)}Cl] (**6**): PPh_4Cl (0.128 g, 0.293 mmol) and **1b** (0.220 g, 0.586 mmol) were dissolved in dry THF. The resulting precipitate was filtered. ^1H NMR (400 MHz, Chloroform-*d*) δ 7.98 – 7.91 (m, 4H, PPh_{para}), 7.81 (td, 8H, PPh_{meta}), 7.69 – 7.60 (m, 8H, PPh_{ortho}), 7.26(CDCl3), 4.01 – 3.85 (q, 2H, α-H_{Gly}), 3.96 (m, 1H, α-H_{Ala}), 3.64 (d, 1H, α-H_{Asp}), 3.58 (s, 3H, -$OCH_{3\ Gly}$), 2.82 (d, 1H, β-H_{Asp}), 2.50 (dd, 1H, β-H_{Asp}), 1.42 (s, 9H, -$O(CH_3)_{3\ Asp}$), 1.35 (d, 3H, β-H_{Ala}). IR (KBr) cm^{-1}: 3314, 3215 (b, ν(N—H)), 1750 (s, ν(C=O)), 1724 (s, ν(C=O)), 1601 (s, ν(C=O)), 1583 (s, ν(C—N)), 1250 (s, ν(C—O)), 1194 (s, ν(C—O)), 1138 (s, ν(C—O))

Pd{D(OtBu)AG(OMe)}(Lu) (**8**)**: 1** (0.097 g, 0.293 mmol) and 2,6-lutidine (0.064 mL, 0.585 mmol) were dissolved in THF (20 mL). $Pd(OAc)_2$ (0.066 g, 0.293 mmol) was added and the reaction stirred under Ar overnight. The solution was filtered, the volume reduced in vacuo and precipitated out and washed with Et_2O. ^1H NMR (400 MHz, DMSO-d_6) δ 7.78 (t, 1H, Lu_{para}), 7.33 (dd, 2H, Lu_{meta}), 4.76 (dd, 1H, NH_{Asp}), 4.15 (t, 1H, NH_{Asp}), 3.71 – 3.60 (m, 1H, α-H_{Ala}), 3.54 (q, 1H, α-H_{Asp}), 3.34 (s, 3H, -$OCH_{3\ Gly}$), 3.18 (s, 6H, Lu_{CH3}), 3.14 (d, 1H, α-H_{Gly}), 2.91 (d, 1H, α-H_{Gly}), 2.57 (dd, 1H, β-H_{Asp}), 2.50 (DMSO), 2.45 – 2.34 (m, 1H, β-H_{Asp}), 1.41 (s, 9H, -$O(CH_3)_{3\ Asp}$), 1.23(m, 3H, β-H_{Ala}). ^{13}C NMR (101 MHz, DMSO) δ 185.45 ($C{=}O_{Asp}$), 175.90 ($C{=}O_{Ala}$), 171.70 ($C{=}O_{Gly}$), 169.93 (γ-$C{=}O_{Asp}$), 160.12 (Lu_{ortho}), 159.69 (Lu_{ortho}), 139.08 (Lu_{para}), 122.72 (Lu_{meta}), 122.60 (Lu_{meta}), 80.14 (-O**C**$(CH_3)_{3\ Asp}$), 57.13 ($OCH_{3\ Gly}$), 56.50 (α-C_{Asp}), 50.79 (α-C_{Ala}), 45.84 (α-C_{Gly}), 39.73 (β-C_{Asp}), 39.52(DMSO), 27.79 ((-OC(**C**$H_3)_{3\ Asp}$), 25.86 (Lu_{CH3}), 25.77 (Lu_{CH3}), 19.78 (β-C_{Ala}). IR (KBr) cm^{-1}: 3303, 3223 (b, ν(N—H)), 1750 (s, ν(C=O)),1732 (s, ν(C=O)), 1604 (s, ν(C=O)), 1582 (s, ν(C—N)), 1250 (s, ν(C—O)), 1200 (s, ν(C—O)), 1147 (s, ν(C—O)). MS (ESI/Positive) MW: ($C_{21}H_{32}N_4O_6Pd$) = 542.9290, M/Z

found(calc) = 565.1254(565.1257) [M+Na^+]

Pd{***α***-Asp(OtBu)AlaGly(OMe)} (**9**): **1** (0.331 g, 1.000 mmol) and Proton Sponge (0.536 g, 2.500 mmol) were dissolved in THF (20 mL). $Pd(OAc)_2$ (0.224 g, 1.000 mmol) was added and the reaction stirred under Ar for 5 h. The solution was concentrated in vacuo and precipitated out with several additions of EtOAc and toluene. Product was recrystallize as a purple solid from acetonitrile and EtOAc (0.295 g, 67.7%) ^{1}H NMR (400 MHz, DMSO-d_6) δ 5.04 (t, 1H, NH_{Asp}), 4.55 (t, 1H, NH_{Asp}), 3.95 – 3.79 (m, 2H, α-H_{Gly}), 3.68 (q, 1H, α-H_{Ala}), 3.56 (s, 1H, α-H_{Asp}), 3.55 (s, 3H, -$OCH_{3\ Gly}$), 2.61 (dd, 1H, β-H_{Asp}), 2.50 (DMSO), 2.48 – 2.42 (m, 1H, β-H_{Asp}), 1.42 (s, 9H, -$O(CH_3)_{3\ Asp}$), 1.20 (d, 3H, β-H_{Ala}). ^{13}C NMR (101 MHz, DMSO) δ 177.03($C{=}O_{Asp}$), 172.89($C{=}O_{Ala}$), 169.79(γ-$C{=}O_{Asp}$), 99.49($C{=}O_{Gly}$), 80.47(-O**C**$(CH_3)_{3\ Asp}$), 56.59($OCH_{3\ Gly}$), 55.80(α-C_{Asp}), 50.93(α-C_{Ala}), 46.79(α-C_{Gly}), 39.94(β-C_{Asp}), 39.52(DMSO), 27.79(-OC(**C**$H_3)_{3\ Asp}$), 19.80(β-C_{Ala}). IR (KBr) cm^{-1}: 3313, 3245 (b, ν(N—H)), 1731 (s, ν(C=O)), 1588 (s, ν(C=O)), 1541 (s, ν(C—N)), 1253 (s, ν(C—O)), 1206 (s, ν(C—O)), 1145 (s, ν(C—O)). UVVis (CH_3CN): ε_x MS (ESI/Positive) MW: ($C_{14}H_{25}N_3O_6Pd$) = 435.7730, M/Z found(calc) = 458.0515(458.0520) [M+Na^+]. CHN ($C_{14}H_{23}N_3O_6Pd$) found(calc) %: C: 38.36(38.59), H: 5.25(5.32), N: 9.64(9.64)

Route 2: ***α***-D(OtBu)AG(OMe) (0.120 g, 0.362 mmol) dissolved in 10 ml H_2O was added to an aqueous solution of K_2PdCl_4 (0.146 g, 0.362 mmol) in 20 mL H_2O. The pH was increased to 10 with KOH and stir for 0.5 h. The water was removed, and the product was isolated by dissolving in acetonitrile and filtering. Presence of 4 was confirmed spectroscopically, but purification was unsuccessful.

Pd{***β***-Asp(OtBu)AlaGly(OMe)} (**10**): **2** (0.331 g, 1.000 mmol) and Proton Sponge (0.536 g, 2.500 mmol) were dissolved in THF (20 mL). $Pd(OAc)_2$ (0.224 g, 1.000 mmol) was added and the reaction stirred under Ar for 5 h. The solution was concentrated in vacuo and precipitated out with several additions of EtOAc and toluene. Product was recrystallize as a red-orange solid from acetonitrile and EtOAc (0.295 g, 67.7%) ^{1}H NMR (400 MHz, DMSO-d_6) δ 4.62 (m, 1H, NH_{Asp}), 4.48 (m, 1H, NH_{Asp}), 3.95 (m, 1H, α-H_{Ala}), 3.72 – 3.52 (m, 2H, α-H_{Gly}), 3.56 (s, 3H, -$OCH_{3\ Gly}$), 3.18 (s, 1H, α-H_{Asp}), 2.50 (DMSO), 2.44 – 2.22 (m, 2H, β-H_{Asp}), 1.44 (s, 9H, -$O(CH_3)_{3\ Asp}$), 1.08 (d, 3H, β-H_{Ala}). ^{13}C NMR (101 MHz, DMSO) δ 172.88($C{=}O_{Asp}$), 171.14($C{=}O_{Ala}$), 170.16 (γ-$C{=}O_{Asp}$), 99.49($C{=}O_{Gly}$), 82.32 (-O**C**$(CH_3)_{3\ Asp}$), 51.26 ($OCH_{3\ Gly}$), 54.70 (α-C_{Asp}), 59.14 (α-C_{Ala}), 46.20 (α-C_{Gly}), , 41.09 (β-C_{Asp}), 39.52(DMSO), 28.13 (-

OC($\mathbf{C}H_3$)$_{3\ Asp}$), 21.07 (β-C_{Ala}). IR (KBr) cm^{-1}: 3313, 3245 (b, ν(N—H)), 1731 (s, ν(C=O)), 1588 (s, ν(C=O)), 1541 (s, ν(C—N)), 1253 (s, ν(C—O)), 1206 (s,ν(C—O)), 1145 (s, ν(C—O)). UVVis (CH_3CN): ε_x MS (ESI/Positive) MW: ($C_{14}H_{25}N_3O_6Pd$) = 435.7730, M/Z found(calc) = 458.0515(458.0520) [M+Na^+]. CHN ($C_{14}H_{23}N_3O_6Pd$) C: 38.28(38.59), H: 5.24(5.32), N: 9.69(9.64)

Pd{TrpAlaGly(OMe)} **(11)** TrpAlaGly(OMe) (0.143 g, 0.413 mmol) and Proton Sponge (0.221 g, 1.032 mmol) were dissolved in THF (20 mL). $Pd(OAc)_2$ (0.093 g, 0.413 mmol) was added and the reaction stirred under Ar for 5 h. The solution was concentrated in vacuo and precipitated out with Et2O. The orange solid was collected and washed with portions of EtOAc and Et_2O. Hot CH_3CN was used to redissolve the product, product was filtered and concentrated in vacuo. (0.169 g, 90.0%). ^{1}H NMR (400 MHz, DMSO-d_6) δ 10.90 (d, 1H, NH_{indole}), 7.55 (d, 1H, $H_{indole\text{-}C7}$), 7.37 (d, 2H, $H_{indole\text{-}C4}$), 7.27 (d, 2H, $H_{indole\text{-}C2}$), 7.09 (ddd, 1H, $_{indole\text{-}C5}$), 6.99 (ddd, 1H, $H_{indole\text{-}C6}$), 4.96 (t, 1H, NH_{Trp}), 4.24 (t, 1H, NH_{Trp}), 3.96 (d, 1H, α-H_{Gly}), 3.83 (d, 1H, α-H_{Gly}), 3.82 – 3.75 (m, 2H, α-H_{Ala}), 3.55 (s, 4H, $ROCH_{3\ Gly}$), 3.40 (dt, 2H, α-H_{Trp}), 3.28 (dd, 1H, β-H_{Trp}), 2.87 (dd, 2H, β-H_{Trp}), 1.24 (d, 3H, β-H_{Ala}). ^{13}C NMR (101 MHz, DMSO) δ 178.24(C=O_{Trp}), 172.93(C=O_{Ala}), 136.37($C3_{indole}$), 127.11($C8_{indole}$), 123.99($C2_{indole}$), 121.10($C5_{indole}$), 118.44($C6_{indole}$), 118.24($C7_{indole}$), 111.41($C4_{indole}$), 109.47($C1_{indole}$), 67.00, 59.58, 56.50($OCH_{3\ Gly}$), 50.93(α-C_{Ala}), 46.86(α-C_{Gly}), 39.52(DMSO), 29.93(β-C_{Trp}), 19.92(β-C_{Ala}). IR (KBr) cm^{-1}: 3370, 3286, 3235(b, ν(N—H)), 1741(s, ν(C=O)), 1569(sh)(s, ν(C=O)), 1543(ν(C—N)), 1333, 1070, 1010(ν(C—N)), 1105(sh), 1025, 981(ν(C—N)), 1207 (ν(C—O)), 1178 (s, ν(C—O)). UVVis (CH_3CN): ε_x MS (ESI/Positive) MW: ($C_{17}H_{20}N_4O_4Pd$) = 450.7910, M/Z found(calc) = 437.0417(437.0419) [M+Na^+]. CHN ($C_{17}H_{20}N_4O_4Pd$) found(calc) %: C: 44.51(43.55), H: 4.73(4.73), N: 11.47(11.95)

References

1. L.J. Monger, G.R. Runarsdottir, S.G. Suman. “Directed coordination study of [Pd(en)(H2O)2]2+ with hetero-tripeptides containing C-terminus methyl esters employing NMR spectroscopy”. J Biol Inorg Chem. 8 ed. Springer Berlin Heidelberg, 2020. 25(5): 811–825. 10.1007/s00775-020-01804-0.
2. B. Schreiner, W. Beck. “Coordination of the Ester Group - Hydrido-Rhodium(III) and Iridium(III) Complexes of Orthometallated Diphenylmethylene Glycine Esters [1]”. Z. anorg. allg. Chem. 2010. 636(3-4): 499–505. 10.1002/zaac.200900474.

3. K. Nakamoto. “Infrared spectra of inorganic and coordination compounds”. Wiley-Interscience, 1970.
4. L. Zhu, N. Kostić. “Toward artificial metallopeptidases: mechanisms by which platinum (II) and palladium (II) complexes promote selective, fast hydrolysis of unactivated amide bonds in …”. 1992. 31: 3994–4001.
5. M.A. Carvalho, B.C. Souza, R.E.F. Paiva, F.R.G. Bergamini, A.F. Gomes, F.C. Gozzo, et al. “Synthesis, spectroscopic characterization, DFT studies, and initial antibacterial assays in vitroof a new palladium(II) complex with tryptophan”. 7 ed. 2012. 65(10): 1700–1711. 10.1080/00958972.2012.679660.
6. P.R. Bontchev, M. Boneva, M.A.I.C. acta, 1984. “Palladium (II) complexes of hydrazides of aspartic and glutamic acids”. Elsevier. 1984. 81: 75–81. 10.1016/S0020-1693(00)88738-1.
7. B. Schreiner, C. Robl, B. Wagner-Schuh, W. Beck. “Metal complexes of biologically important ligands, CLXXIV [1]. Palladium(II) and platinum(II) complexes with schiff bases from 2-(Diphenylphosphino)benzaldehyde and a-amino acid esters”. Zeitschrift fur Naturforschung - Section B Journal of Chemical Sciences. 2010. 65(4): 503–510. 10.1515/znb-2010-0411.
8. R.D. Howells, J.D. Mc Cown. “Trifluoromethanesulfonic acid and derivatives”. Chem. Rev. 2002. 77(1): 69–92. 10.1021/cr60305a005.
9. T. Gramstad, R.N. Haszeldine. “806. Perfluoroalkyl derivatives of sulphur. Part VII. Alkyl trifluoromethanesulphonates as alkylating agents, trifluoromethanesulphonic anhydride as a promoter for esterification, and some reactions of trifluoromethanesulphonic acid”. J. Chem. Soc. 1957. 4069–11. 10.1039/jr9570004069.
10. R. Sang, C. Schneider, R. Razzaq, H. Neumann, R. Jackstell, M. Beller. “Palladium-catalyzed carbonylations of highly substituted olefins using CO-surrogates”. Org. Chem. Front. Royal Society of Chemistry, 2020. 7(22): 3681–3685. 10.1039/D0QO01164A.
11. W.L.F. Armarego, C. Chai, C.L.L. Chai. Purification of Laboratory Chemicals. Butterworth-Heinemann, 2003.
12. J. Li, Y. Sha. “A Convenient Synthesis of Amino Acid Methyl Esters”. MDPI AG, 2008. 13(5): 1111–1119. 10.3390/molecules13051111.
13. F. Neese. “Software update: the ORCA program system, version 4.0”. WIREs Computational Molecular Science. 2018. 8(1): e1327. 10.1002/wcms.1327.
14. F. Neese. “The ORCA program system”. WIREs Computational Molecular Science. 2012. 2(1): 73–78. 10.1002/wcms.81.
15. C. Adamo, V. Barone. “Toward reliable density functional methods without adjustable parameters: The PBE0 model”. The Journal of Chemical Physics. 1999. 110(13): 6158–6170. 10.1063/1.478522.
16. J.P. Perdew, M. Ernzerhof, K. Burke. “Rationale for mixing exact exchange with density functional approximations”. The Journal of Chemical Physics. American Institute of Physics, 1996. 105(22): 9982–9985. 10.1063/1.472933.
17. G. Shi, Y. Dang, T. Pan, X. Liu, H. Liu, S. Li, et al. “Unexpectedly Enhanced Solubility of Aromatic Amino Acids and Peptides in an Aqueous Solution of Divalent Transition-Metal Cations”. Phys. Rev. Lett. 2016. 117(23): 339–6. 10.1103/PhysRevLett.117.238102.
18. S. Grimme, J. Antony, S. Ehrlich, H. Krieg. “A consistent and accurate ab initio parametrization of density functional dispersion correction (DFT-D) for the 94

elements H-Pu". The Journal of Chemical Physics. 2010. 132(15): 154104. 10.1063/1.3382344.
19. S. Grimme, S. Ehrlich, L. Goerigk. "Effect of the damping function in dispersion corrected density functional theory". J. Comput. Chem. 2011. 32(7): 1456–1465. 10.1002/jcc.21759.
20. F. Weigend, R. Ahlrichs. "Balanced basis sets of split valence, triple zeta valence and quadruple zeta valence quality for H to Rn: Design and assessment of accuracy". Phys. Chem. Chem. Phys. The Royal Society of Chemistry, 2005. 7(18): 3297–3305. 10.1039/b508541a.
21. F. Neese, F. Wennmohs, A. Hansen, U. Becker. "Efficient, approximate and parallel Hartree–Fock and hybrid DFT calculations. A 'chain-of-spheres' algorithm for the Hartree–Fock exchange". Moving Frontiers in Quantum Chemistry:. 2009. 356(1): 98–109.
22. R. Izsák, F. Neese. "An overlap fitted chain of spheres exchange method". The Journal of Chemical Physics. 2011. 135(14): 144105. 10.1063/1.3646921.
23. S. Höck, R. Marti, R. Riedl, M. Simeunovic. "Thermal Cleavage of the Fmoc Protection Group". 2010. 64(3): 200–202. 10.2533/chimia.2010.200.
24. P.R. Sultane, T.B. Mete, R.G. Bhat. "A convenient protocol for the deprotection of N-benzyloxycarbonyl (Cbz) and benzyl ester groups". Tetrahedron Letters. Elsevier Ltd, 2015. 56(16): 2067–2070. 10.1016/j.tetlet.2015.02.131.

Article 3

Synthesis, Characterization, and Electrochemistry of Ni(II) Tripeptide Complexes.

Lindsey J. Monger, Ragnar Bjrnsson, Sigridur G. Suman

Abstract

Ni(II) complexes with the ligands, α-Asp(OtBu)AlaGly(OMe), β-Asp(OtBu)AlaGly(Ome), and TrpAlaGly(OMe) were synthesized and characterized using infrared and $^{1}H,^{13}C$ NMR spectroscopy, mass spectra and microanalysis. The complex geometries were predicted using DFT calculations of their optimized geometry as distorted square planar complexes. The esters of these ligands proved highly pH sensitive and hydrolyze fully at moderately basic conditions. The electrochemistry of the complexes was run in water to reveal irreversible redox behavior of all three complexes.

Introduction

Metallopeptide complexes are widely reported in the literature; Studies of these complexes primaraly relate to metalodrugs and metal toxixicity[1-4]. However, Ni(II) complexes of related classes of ligands, including Schiff base and cyclam derivatives, have been explored for their catalytic activation of small molecules. These ligand systems are similar in their amino-oxygen chelate coordination. In metal complexes the amino-amide backbone forms stable 5-membered rings for α-amino acids. Complexation takes place through the N-donor groups primarally, however if there are not enough nitrogens, as is the case with amino acids, di-, and tripeptides, coordination can occur through the C-terminus carboxylate[5]. The resulting flat geometry and [5,5,5] ring coordination geometry effectively closes coordination for Ni(II), which strongly favors a square planar coordination geometry.

Looking to expand on previous works, the coordination chemistry of Ni(II) with three tripeptides was examined. The complexes were synthesized to form electron-rich Ni(II) centers that could serve for η^1-coordination of CO_2.

In previous work the synthesis of three alkylated tripeptide ligands (Figure 1) was described, and the effects of pH on their coordination to $[Pd(en)(H_2O)]^{2+}$ were investigated. This was followed by synthesis and characterization of new neutral tetradentate Pd(II) complexes and tridentate analogs. In this work the same ligands were employed to synthesize Ni(II) complexes who were expected to be more amenable to CO_2 axial coordination than the Pd(II) analogues.

Results and Discussion

Synthesis

Several combinations of Ni(II) salts, bases and solvent system were attempted for synthesis of Ni(II) complexes. The ligands chosen were shown to be susceptible to changes in pH when coordinating to the Pd(II) ions under aqueous conditions. The methyl ester is labile under basic conditions. Considering this, hydrolysis of the methyl ester at elevated pH values was expected in an aqueous synthesis.

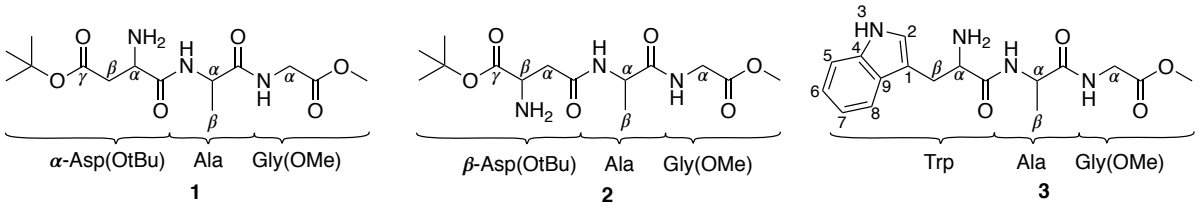

Figure 1. Tripeptide ligands used in synthesis

Using an aqueous synthesis strategy, *in situ* formation of $Ni(OH)_2$ was achieved by the addition of KOH and Ni(II) starting material. The ligands **1-3** were dissolved in H_2O and the preformed Ni(II) hydroxide and tripeptide solutions were added together; The pH was increased to 10 with KOH, and the mixture was allowed to stir between 0.5-2 h. The reaction mixture was filtered, the water removed, and the product isolated by dissolving in alcohol, filtering, then precipitating out with ether and washing. Several factors determined what product formed, including order of addition and the starting Ni(II) compound used.

Nickel Acetate as Starting Material

When using $Ni(CH_3CO_2)_2$ as starting material, the di-hydrolyzed species $[Ni\{\alpha\text{-AspAlaGly}\}]^{2-}$ was formed, which was confirmed by mass spectrometry. However, different preparations revealed different ^1H NMR spectra (Table 1). When the Ni(II) solution was added to the ligand (aq), the species generated in Table 1, **4a** is observed; But in a reversed addition procedure, the product listed in Table 1 (**4b**) is formed. In both **4a** and **4b**, significant upfield shifts in the α-C protons which are centralized between 3.50-3.30 ppm were observed. This is a strong indication of coordination between nickel and the amine/amide nitrogens. C-terminus carboxylate coordination is well known in tripeptide coordination and the emergence of a quadruplet pattern with a large coupling constant (~20 Hz), from loss of free rotation for the Gly $\boldsymbol{\alpha}$-C protons, suggests carboxylate coordination for both **4a** and **4b**.

Applying the synthetic condition by adding the Ni(II) solution to ligand **2**, the dianionic complex $[Ni\{\beta\text{-AspAlaGly}\}]^{2-}$ (**5a**) is formed, along with a minor isomeric product (<5%).

*Table 1. Summary of NMR data in D_2O from synthetic experiments forming mono- and di-anionic Ni(II) complexes with α-Asp(OtBu)AlaGly(OMe) (**1**) and β-Asp(OtBu)AlaGly(OMe) (**2**), where **4a** and **4b** are $[Ni(\alpha\text{-AspAlaGly})]^{2-}$, **5a** is $[Ni(\beta\text{-AspAlaGly})]^{2-}$, **6** is K[Ni(α-Asp(OtBu)AlaGly)], and **7** is K[Ni(β-Asp(OtBu)AlaGly)]*

Frequency (ppm)	**4a**	**4b**	**5a**	**6**	**7**	**1**	**2**
$\alpha\text{-C}_{Ala}$	3.48	3.58	3.54	3.57	3.76	4.39	4.40
$\alpha\text{-C}_{Gly}$	3.50-3.30	3.55-3.38	3.57-3.40	3.63-3.31	3.65-3.21	4.02	4.06
$\alpha\text{-C}_{Asp}$	3.40	3.53	2.55 2.41	3.51	2.34 2.18	3.75	2.77
$OCH_{3\ Gly}$	—	—	—	—	—	3.75	3.80
$\beta\text{-C}_{Asp}$	2.47 2.32	2.71	3.50	2.61	3.57	2.71	3.82
$OC(CH_3)_{3\ Asp}$	—	—	—	1.65	1.60	1.43	1.49
$\beta\text{-C}_{Ala}$	1.14	1.19	1.22	1.23	1.19	1.43	1.44

Examining the difference between **4a** vs. **4b**, and **5a** vs. its minor isomer, it is unclear what these structural isomers are. As these are dianionic species in aqueous solution, the coordination preference is not obvious. The resonances which experience the largest change

are on the Asp α-C protons, which are closest to the carboxylate. These spectra were taken in D_2O which could mean pH-dependent resonance shifts. Less likely is the formation of a five-coordinate isomer with square pyramidal geometry. Figure 2 outlines possible isomers for the dianionic species **4a**, **4b** and **5a**. Due to the inconsistent behavior and difficulty in reproducing the synthesis of these dianionic species, other approaches were tested, and a method developed that consistently forms the monoanionic complexes.

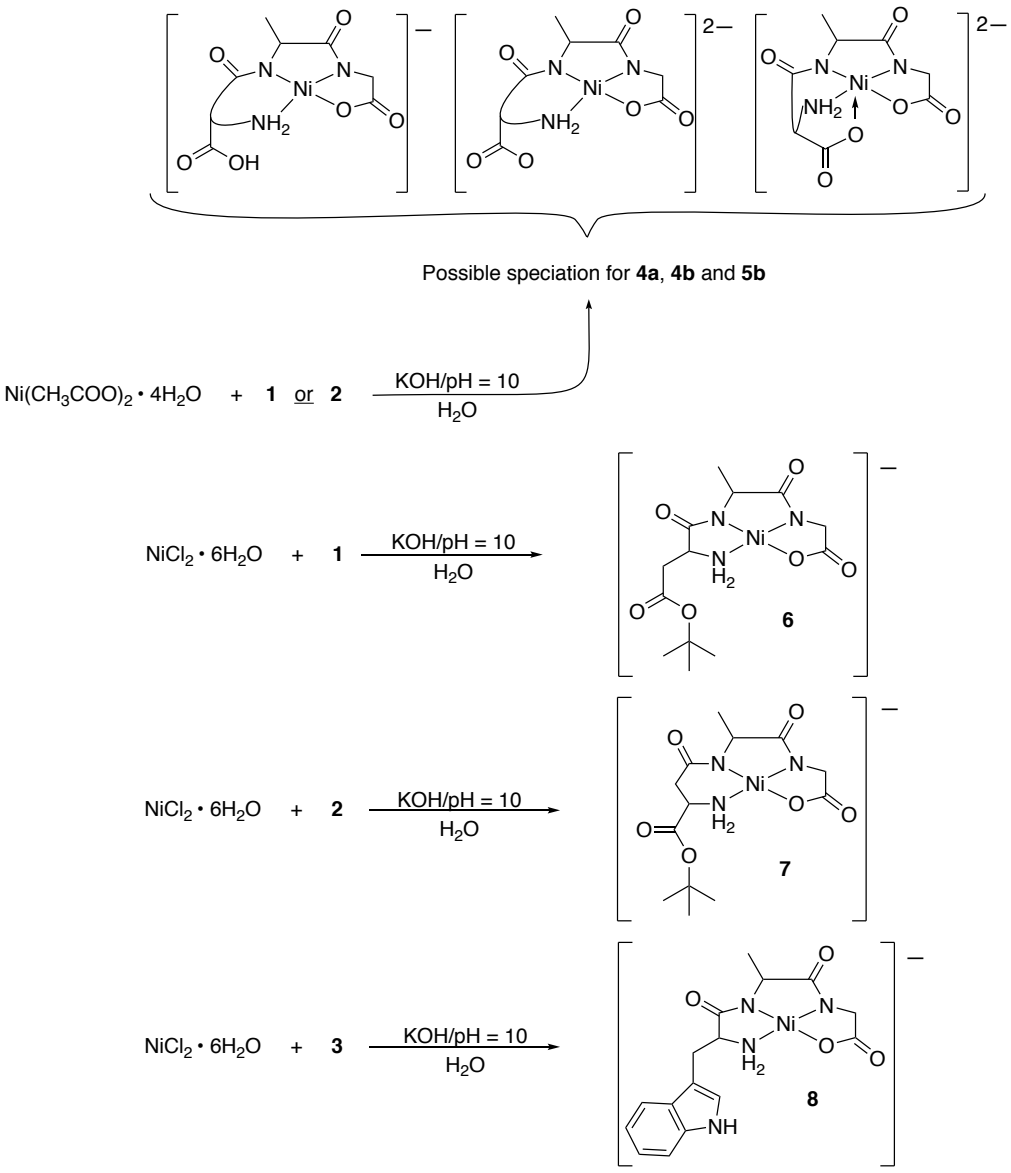

*Figure 2. Synthetic routes to form complexes **4-8** where **4a**, **4b** and **5a** are possible isomers for the dianionic complexes formed from **1** and **2**.*

Nickel Chloride as a Starting Material

With the same general procedure, but switching the metal starting material to $NiCl_2$, adding the

Ni(II) solution to the ligand solution resulted in hydrolysis of the methyl ester but preserved the *tert*-butyl ester, forming the mono-ionic species K[Ni{α-Asp(OtBu)AlaGly}](See Table 1, **6**). The synthetic method uses excess nickel where the $Ni(OH)_2$ formed is only slightly soluble leading to the ligand experiencing base concentration dependent on the rate of $Ni(OH)_2$ formation. The difference in behavior may be related to the differences in the aqueous dissociation constants for $NiCl_2$ versus $Ni(CH_3CO_2)_2$, where $NiCl_2$ dissociates faster and the $Ni(OH)_2$ precipitates rapidly with excess base, and the ligand can coordinate immediately. The ester hydrolysis at these conditions was minimal.

The monoanionic species also has a large upfield shift in the α-C protons, and a large coupling constant for the Gly protons, indicating κ^4-NH_2,N,N,O chelation. The aqueous synthesis using $NiCl_2$ was then applied to ligands **2** and **3** to form the K[Ni{β-Asp(OtBu)AlaGly}] (**7**) and K[Ni{α-TrpAlaGly}] (**8**) (Figure 2).

Attempts to form the neutral Ni-tripeptide complexes in non-aqueous conditions were unsuccessful. Various non-coordinating starting complexes were used including $Ni(F_3CSO_3)_2$ and $[Ni(CH_3CN)_6]^{2+}$ and several bases including "Proton Sponge", which proved successful for palladium.

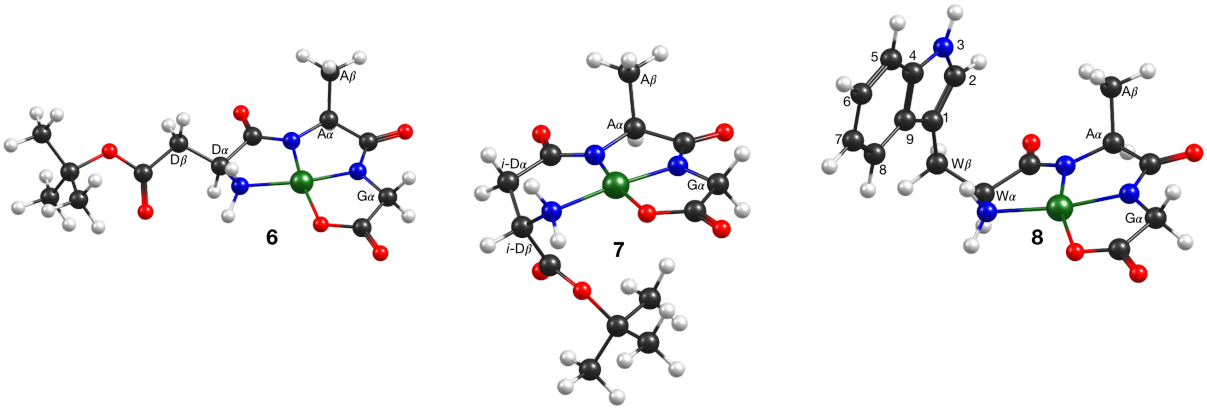

*Figure 3 DFT optimized structures of complexes **6-8**.*

Characterization

Complexes **4-8** were characterized via NMR and IR spectroscopy, with quantum chemical calculations at the DFT level used to aid the spectral interpretation. In order to correctly assign coordination geometries, similarities and differences in the complex NMR chemical shifts, and

shifts in infrared frequencies of major bands were examined. Observed values were compared to calculated chemical shifts and vibrational frequencies of the DFT-optimized structural models.

Structural Analysis: DFT Calculations

DFT calculations with a continuum solvation model were employed to determine the lowest energy structures in solution for complexes **4**-**8** which can be seen in Figure 3. Several different conformational possibilities were explored computationally. As the Ni(II) complexes are preferably square planar, NH_2,N,N coordination was expected and the lowest energy DFT-calculated conformers agreed. Due to the conformational flexibility of the tripeptide ligand, a number of conformers for each complex are available (primarily as a result of different orientations of the Asp or Trp sidechains) but only the lowest energy conformer was considered in the calculations of spectroscopic properties.

^{1}H NMR Analysis.

The coordinated amine/amide backbone is a commonality of **4**-**8**; this coordination is established in the proton NMR (Table 1(D_2O), & 2(DMSO)). Throughout the series there is large upfield shift to all the side chain protons. Which corresponds with previously established Ni(II) tripeptide complexes. As expected, the complexes are negatively charged and thus experience more shielding. The Ala α-C protons tend to shift the most and have the largest ppm range, which is expected considering the Asp amide is trans to the fourth coordination sphere, which is occupied by the carboxylate.

Examining the ^{1}H spectra for **6**-**8** in DMSO (Table 2), a better understanding of coordination geometries can be ascertained. The appearance of the NH_2 protons at ~3.60 - 2.20 ppm confirms amine coordination. The Gly α-C protons all shift a comparative value and appear as a quadruplet with coupling constant of ~20 Hz, suggesting carbonyl coordination. However, there is very little shift related to the tert butyl ester. This suggests **6**-**8** have the common κ^4-NH_2,N,N,O coordination modes.

Complex **8** exhibits a unique upfield shift on a coordinated amine proton at 2.20 ppm; This strong shielding effect, coupled with a downfield shift of the indole C2 proton, is likely related to strong H bounding.

*Table 2. Summary of NMR data in DMSO from synthetic experiments to form mono-anionic Ni(II) complexes with ligands **1-3**, where **6** is the species K[Ni(α-Asp(OtBu)AlaGly)], **7** = K[Ni(β-Asp(OtBu)AlaGly)], **8** = K[Ni(TrpAlaGly)]*

Frequency (ppm)	**6**	**7**	**8**	**1**	**2**	**3**
N—H $_{Trp\text{-}In\ 3}$	—	—	10.89	—	—	10.86
N—H $_{Gly}$	—	—	—	8.34	8.39	8.32
N—H $_{Ala}$	—	—	—	8.16	8.24	8.12
C—C $_{Trp\text{-}In\ 7}$	—	—	7.48	—	—	7.56
C—H $_{Trp\text{-}In\ 4}$	—	—	7.34	—	—	7.33
C—H $_{Trp\text{-}In\ 2}$	—	—	7.31	—	—	7.18
C—H $_{Trp\text{-}In\ 5}$	—	—	7.06	—	—	7.06
C—H $_{Trp\text{-}In\ 6}$	—	—	6.95	—	—	6.97
N—H_2	3.57 3.03	3.37 3.11	3.62 2.20	—	—	—
α-C_{Ala}	3.02	3.29	3.10	4.31	4.31	4.34
α-C_{Gly}	2.99	2.96	2.97	3.84	3.83	3.83
α-$C_{Trp/Asp}$	3.07	2.01 1.87	2.96	3.52	2.49 2.36	3.51
OCH_3 $_{Gly}$	—	—	—	3.62	3.63	3.63
β-$C_{Trp/Asp}$	2.39 2.21	2.90	2.96 2.72	2.37 2.35	3.64	3.10 2.78
$OC(CH_3)_3$ $_{Asp}$	1.41	1.39	—	1.38	1.39	—
β-C_{Ala}	1.00	0.94	1.00	1.23	1.21	1.16

^{13}C NMR Analysis.

The ^{13}C NMR spectrum collected for the ligands (**1-3**) and complexes **(6-8)** in DMSO-d6 can be seen in Table 3. Assignments for the carbon spectrum were aided by the 2-D NMR technique HSQC, which reveals ^{13}C and ^{1}H coupling. As expected, all of the *α*-carbons shifted downfield, while the Ala *α*-carbons undergo the largest downfield shifts and have the broadest range.

The most significant and difficult assignments for ^{13}C belonged to the carbonyl carbons. In order to confidently assign these signals, DFT calculations were used to elucidate coordination modes and to calculate the ^{13}C chemical shifts. These calculations were based on the optimized geometries found in Figure 3. The resonance shifts for complex **7** differ slightly from **6** and **9**. This is presumably related to the six-membered ring formed in this complex. As a result, the

Gly C=O signal for **7** only shifts downfield by ~ 1.5 ppm compared to 5.5 and 7.0 ppm seen in **6** and **8**, respectively.

*Table 3. Assigned ^{13}C NMR resonance for ligands **1-3** and complexes **6-8** in DMSO-d6.*

Frequency (ppm)	6	7	8	1	2	3
$C{=}O_{Trp/Asp}$	182.19	182.23	182.20	172.82	172.99	173.84
$C{=}O_{Ala}$	180.30	180.14	180.37	172.61	172.73	172.68
γ-$C{=}O_{Asp}$	170.17	170.61	—	170.45	170.17	—
$C{=}O_{Gly}$	175.71	171.02	177.09	170.11	169.40	170.12
C=C $_{Trp\text{-}In\ 4}$	—	—	136.29	—	—	136.20
C=C $_{Trp\text{-}In\ 9}$	—	—	127.39	—	—	127.39
C—H $_{Trp\text{-}In\ 2}$	—	—	123.87	—	—	123.94
C—H $_{Trp\text{-}In\ 6}$	—	—	120.91	—	—	120.84
C—H $_{Trp\text{-}In\ 8}$	—	—	118.38	—	—	118.46
C—H $_{Trp\text{-}In\ 7}$	—	—	118.23	—	—	118.19
C—H $_{Trp\text{-}In\ 5}$	—	—	111.28	—	—	111.28
C=C $_{Trp\text{-}In\ 1}$	—	—	110.06	—	—	110.22
$O\underline{C}(CH_3)_{3\ Asp}$	79.93	80.80	—	79.97	80.41	—
$OCH_{3\ Gly}$	—	—	—	51.68	51.67	52.69
α-$C_{Trp/Asp}$	54.53	39.01	57.83	51.51	39.15	54.91
α-C_{Ala}	56.42	58.32	56.39	47.78	47.85	47.52
α-C_{Gly}	48.31	48.66	48.40	40.48	40.48	40.48
β-$C_{Trp/Asp}$	39.02	52.79	28.86	40.24	51.52	30.42
$OC(\underline{C}H_3)_{3\ Asp}$	27.77	27.61	—	27.75	27.61	—
β-C_{Ala}	18.65	19.66	18.63	18.50	18.18	18.64

Infrared Data Analysis.

The infrared spectra were taken as KBr pellets and analyzed in the range of 4000 cm^{-1} to 400 cm^{-1}. Shifts of key bands upon coordination to the Ni(II) were monitored. Table 4 shows the positions found for these bands. Vibrational modes for the ligands and complexes were assigned with the aide of DFT calculations, based on relative value sets. Comparative values for observed and calculated carbonyl stretching bands for **4**-**8** are presented in Table 5.

For **4**-**8**, the low energy shift of the symmetric and asymmetric stretching modes for NH_2 to ~3400 - 3250 cm^{-1}, at energies typical Nickel coordinated N_{amino}[6], confirm amine coordination. Whereas low energy shifts of the Amide I band by 50-100 cm^{-1}, which combine with the Amide II band, support amine/amide backbone chelation. The ν(Ni—N) is observed at values consistent with literature values.

For **4a** and **5a** the *tert* butyl ester band does not shift to lower energy indicating hydrolysis to form an acid (~1730-1700 cm^{-1}), but rather shifts into the strong Amide I band. This is accompanied by a strong absorption at ~1400 cm^{-1}, which is characteristic of a carboxylate anion.

*Table 4. Summary of IR data from synthetic experiments to form Ni(II) complexes with **1-3** where *-denotes shoulder bands and †-denotes the hydrolyzed acid*

Frequency (cm^{-1})	**6**	**7**	**8**	**1**	**2**	**3**
ν(N—H_2)	3401	3396	3396	3370	3375*	3370*
ν(N—H)	3308	3257	3292	3314	3304	3297
ν(C=O)						
OtBu	1722	1729	—	1725	1743	—
OMe	1653*†	1656*†	1651*†	1759*	1757*	1749
Amide I	1597	1600 1562	1593	1670	1659	1655
ν(C=C)						
Aromatic	—	—	1675*	—	—	1673*
ν(N—H)						
Amide II	—	—	—	1546	1541	1517
ν(C—O)						
OtBu	1254	1257	—	1250	1254	—
OMe	1289	1282	1290	1213	1212	1213
ν(O—C)						
OtBu	1146	1155	—	1155	1155	—
ν(M—N)	466	470	469	—	—	—

The ν(C=O) for the C-terminus carbonyl (OMe) shift to a lower energy upon hydrolysis and coordination to frequencies of ~1650 cm^{-1}. This is consistent with calculated values shown in Table 5. All carbonyl stretching frequencies are in good agreement with the comparative shifts values calculated from the DFT optimized geometries shown in Figure 5.

*Table 5. Comparative values for ν(C=O) vibrational modes observed vs. calculated for **4-11** and ligands **1-3**. The **Δ** values show the observed deviation between observed and calculated vibrational frequencies. †-Denotes the hydrolyzed acid*

Complex	ν(C=O) OtBu	ν(C=O) OMe	ν(C=O) Amide I	ν(C=O) Amide I
4 Obs	1595†	1653†	1595	1595
DFT	1657	1681	1654	1652
Δ	*62*	*28*	*59*	*57*
5 Obs	1602†	1648†	1602	1560
DFT	1654	1683	1655	1612
Δ	*52*	*35*	*53*	*52*
6 Obs	1722	1653†	1597	1597
DFT	1766	1684	1664	1656
Δ	*44*	*31*	*67*	*59*
7 Obs	1729	1656†	1600	1562
DFT	1780	1687	1657	1622
Δ	*51*	*31*	*57*	*60*
8 Obs	—	1651†	1593	1593
DFT	—	1674	1661	1654
Δ	—	*23*	*68*	*61*
1 Obs	1725	1759	1670	1670
DFT	1758	1793	1745	1728
Δ	*33*	*34*	*75*	*58*
2 Obs	1743	1757	1659	1659
DFT	1757	1787	1740	1730
Δ	*14*	*30*	*81*	*71*
3 Obs	—	1749	1655	1655
DFT	—	1792	1747	1713
Δ	—	*43*	*92*	*58*

UV-visible Spectroscopy.

The electronic spectra for complexes **6-8** are shown in Figure 3. The spectra display the CT band at ~255 nm. Strong concentrations are needed to observe the *d-d* transitions(inlay). These transitions are at ~430-450 nm.

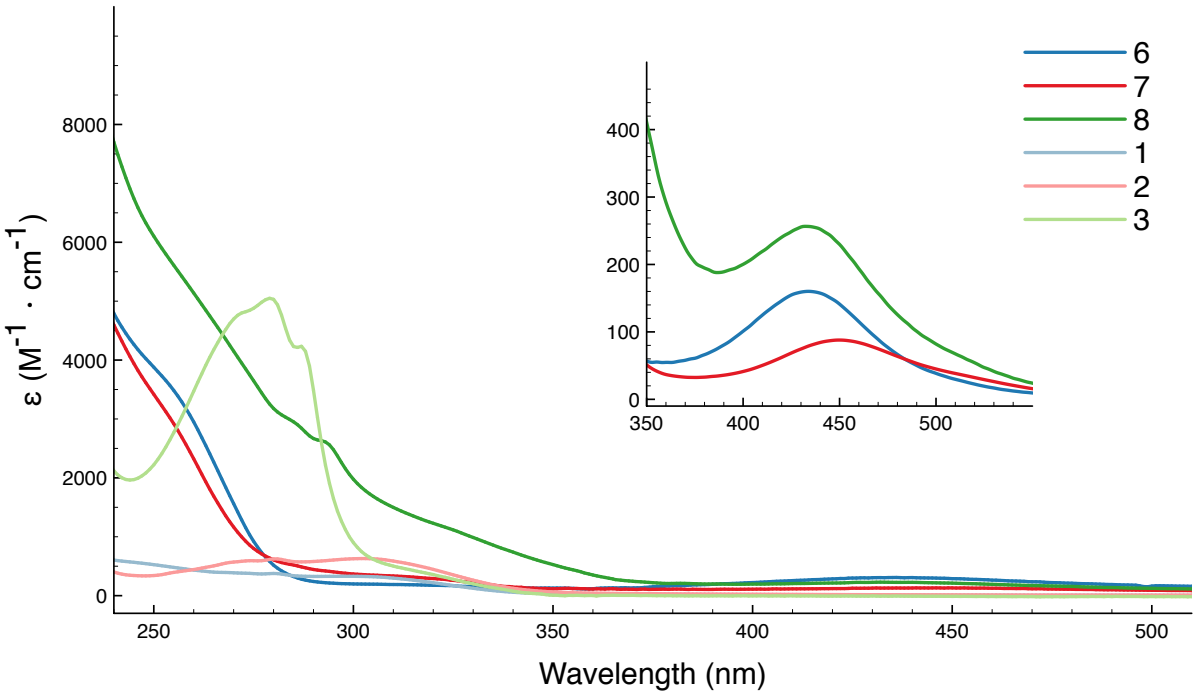

*Figure 3. UV-Vis spectrum of **6-8** and ligand **1-3** in H_2O taken at micromolar concentrations. Inlay is close up of spectra for **6-8** taken at millimolar with higher concentrations.*

Mass spectra. MS spectra were obtained using ESI-MS in the negative ion scan for anions and the positive ion scan for neutral or positive ions. The found ion peaks were simulated with expected isotope patterns to confirm the composition of the compound found compared to the expected composition. The isolated compounds showed an excellent match with less than 2 ppm variation in simulated vs found values.

Physical Properties

Cyclic Voltammetry. The electrochemistry of the complexes was explored in water. The cyclic voltammograms were run for 2 mM solutions of **4**, **5**, and **8** and 0.25 M in KNO_3 as supporting electrolyte. $Ag/AgCl_2$ was used as the reference electrode. The data are summarized in Table 6.

In general the redox behavior is irreversible. The ligands show strong irreversible reduction at values lower than -600 millivolts. The ligand **2** shows a single reduction wave at -616 mV while ligand **1** has two at -634 mV and at -940 mV. The data for ligand **3** was not obtained but complex **8** shows reduction similar to **4a** at -661 mV that is likely the ligand based reduction.

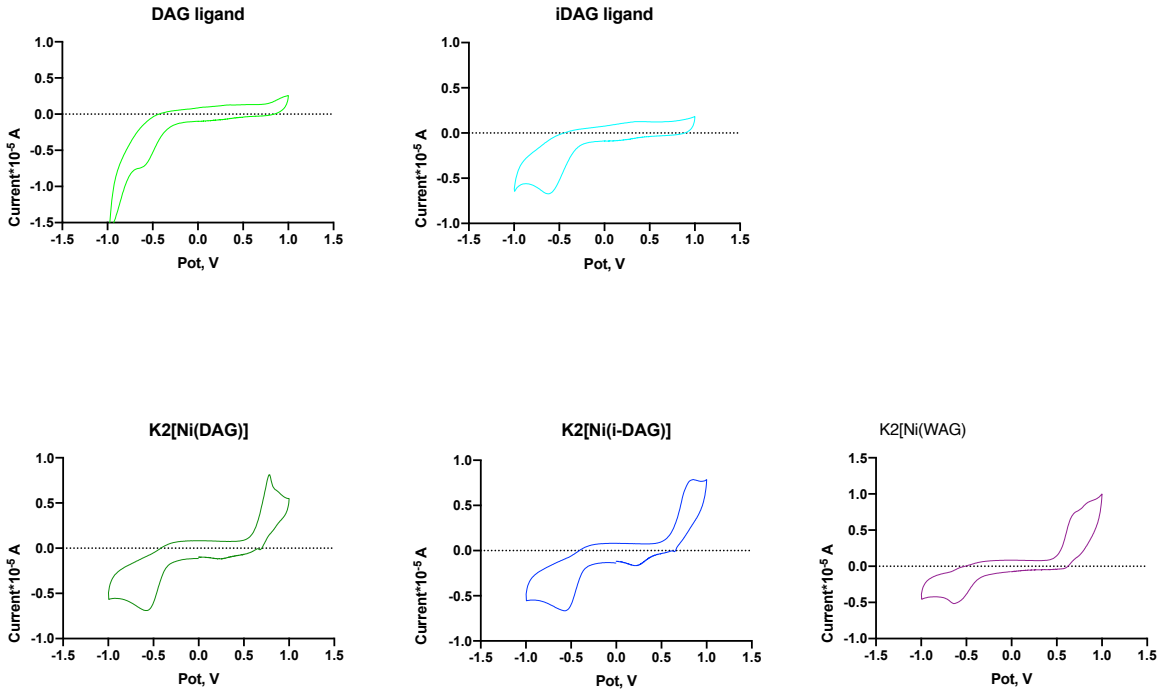

*Figure 4. Electrochemical CV traces of Ni(II) complexes **4**, **5**, and **8** and ligands **1-3** in water.*

Table 6. List of potentials and peak currents for Cyclic Voltammetry experiments in aqueous solution with 0.25 M KNO_3 vs. $Ag/AgCl_2$.

Complex	Potential (mV)	Peak current
4a	218	-0.118
	643	-0.0092
	794	0.787
	911	0.595
	-589	-0.689
5a	214	-0.166
	875	0.781
	607	-0.0046
	-571	-0.665
8	794	0.828
	929	0.927
	691	0.092
	-661	-0.504
1	-634	-0.742
	-940	-1.53
2	-616	-0.672

The complexes show irreversible oxidations. Traces of **4a** and **5a** are very similar except the **4a** shows two irreversible oxidations and **5a** only one. The **4a** oxidations were observed at 794 and 911 mV, and **5a** oxidation wave was observed at 875 mV. The **4a** and **5a** show irreversible metal-based reduction at 218 and 214 mV respectively. Complex **8** exhibits two oxidation waves at 794 and 929 mV, and a weak irreversible reduction at 691 mV that is presumed metal based.

Discussion

Combining spectroscopic data from ^{1}H and ^{13}C NMR, infrared, and mass spectroscopy, along with elemental analysis, the coordination geometry of three Nickel tripeptide complexes was elucidated. It was soundly established that complexes **4**-**8** have coordinated amine/amide backbone coordination and that the 4th coordination is occupied by the hydrolyzed carboxylate on the C-terminus.

Complexes **4a**, **4b** and **5a** were synthesized with $Ni(CH_3CO_2)_2$ starting complex and are di-anionic with κ^4-NH_2,N,N,O chelation; However, the complete characterization of the isomers was difficult to elucidate because of pH dependence. Changing the starting nickel complex to $NiCl_2$ resulted in mono-anionic complexes **6**-**8**. These too formed κ^4-NH_2,N,N,O chelated complexes.

For ligand **3** there are distinct differences in the coordination behavior in non-aqueous versus aqueous synthesis, where it was established that the indole amine competitively coordinated with metal instead of the N-terminal amine.

Various attempts to form the neutral Ni-tripeptide complexes in non-aqueous conditions, including the use of "Protons Sponge" (previously discovered useful in the synthesis of neutral palladium complexes) prove unsuccessful. These attempts resulted in multiple isomers forming broad resonances in the NMR spectral and only miniscule patterns in mass spectroscopy. Suspected reasoning for this is related to the strong Lewis acidity of Palladium(II) compared to Nickel(II), allowing complexation between Pd(II) and the ester carbonyl lone pair, whereas Ni(II) does not.

Conclusion

The synthesis of di- and mono- anionic complexes based on the tripeptides α-Asp(OtBu)AlaGly(OMe), β-Asp(OtBu)AlaGly(OMe), and TrpAlaGly(OMe) were carried out in aqueous solutions by *in situ* formation of $Ni(OH)_2$, where the product was dependent on the starting complex. Characterization of these complexes was aided by DFT calculations. These complexes are air stable and water soluble. Further CV studies may show these complexes useful for the electrochemical reduction of CO_2, by lowering the overpotential of CO_2 activation.

Experimental Synthesis

Instrumentation

Infrared spectra were recorded on a Nicolet Ava- tar 360 FT-IR (E.S.P.) spectrophotometer using KBr pellets. ^1H, COSY, and ^{13}C nuclear magnetic resonance spectra were recorded at ambient temperature on a Bruker Avance 400 MHz spectrometer at 400 and 101 MHz, respectively. Solvents used were D_2O, DMSO-d_6, and $CDCl_3$. Electronic spectra were obtained using either Varian Cary 100 Bio spectrophotometer or Perkin Elmer Lambda 25 UV/Vis spectrophotometer. Cyclic voltammetric measurements were recorded on EC Epsilon Eclipse™ Potentiostat/Galvanostat. Mass spectra were recorded on a micrOTOF-Q spectrometer, equipped with E-spray atmospheric pressure ionization chamber (ESI). Elemental Analyses were obtained from Midwest Microlab, IN, USA.

Reagents used were purchased from Sigma Aldrich and used without further purification unless otherwise stated. Alanylglycine, Fmoc-Asp(OtBu)-OH, Fmoc-Asp(OH)-OtBu, Z-Trp, and EDC-Cl use in peptide coupling were purchased from Bachem. Solvents were purchased from Sigma Aldrich and were distilled under nitrogen and dried using standard methods[7]. Alanylglycine esterification was completed by reacting it with trimethylchlorosilane[8],

Quantum chemical calculations

Calculations were performed with a development version of the ORCA program[9,10]. A density functional theory based protocol was used, consisting of the PBE0-D3BJ functional[11,12] (including the D3 dispersion correction by Grimme and coworkers [13,14] and the triple-zeta basis

set def2-TZVP[15]. The RIJCOSX[16,17] approximation was used to calculate Coulomb and Exchange integrals, using the def2/J auxiliary basis set by Weigend et al. The CPCM solvation model using a Gaussian pointcharge scheme and a scaled vdW surface was used to incorporate solvation effects. Vibrational frequencies were calculated analytically, as implemented in ORCA. ^{13}C NMR shieldings were calculated using the same level of theory, except the pcSseg-2 basis sets were utilized on carbon and hydrogen atoms. The calculated shieldings were converted into chemical shifts by calculating the shielding difference with respect to tetramethylsilane at the same level of theory. Chemical shifts were shifted by -15 ppm due to a systematic overestimation.

Ligand synthesis

The ligands were synthesized following published procedure. [18] Coupling reactions were executed by adding EDC-HCl (1.1 mol eq) to a solution with 1:1 molar equivalent of N-protected amino acid and HOBt in chloroform (0º C). AlaGly(OMe)-HCl (1 mol eq) was added, followed by addition of triethylamine (1.05 mol eq). The solution was stirred under slight N_2 flow at ambient temperature for 24 h. Product was washed with water and dried with $MgSO_4$ and the $CHCl_3$ removed in vacuo. The Fmoc-protection group was removed [19] by stirring the tripeptide in DMF at 110º C for 1 hour. Methanol was added to the DMF and then washed with hexane. Solvent was removed in vacuo and purified with flash chromatography. The CBZ-protection group was removed[20] by catalytic hydrolysis with H_2 using 10% Pd/C in dry MeOH. Product was collected by filtering through celite and removing the solvent in vacuo.

Complex synthesis

$[Ni\{\boldsymbol{\alpha}\text{-AspAlaGly}\}]^{2-}$ (**4a**) $Ni(OAc)_2$-6H2O (xx g, xx mmol) and **1** (xx g, xx mmol) were dissolved in H_2O (5 mL) and KOH was added until pH=10. Solution was stirred for 0.5 h then the H_2O was removed in vacuo and the product was isolated by dissolving in iso-propyl alcohol and filtering. ^1H NMR (400 MHz, Deuterium Oxide) δ 3.48 (s, 1H, α-H_{Ala}), 3.40 (d, 1H, α-H_{Asp}), 3.50 – 3.30 (m, 2H, α-H_{Gly}), 2.47 (dd, 1H, β-H_{Asp}), 2.32 (dd, 1H, β-H_{Asp}), 1.14 (d, 4H, β-H_{Ala}). IR (KBr) cm^{-1}: 3397, 3274 (b, ν(N—H)), 1651 (sh, ν(C=O)), 1593 (s, ν(C=O)), 1397 (s, ν(C—O)), 460 (w, ν(Ni—N)) MS (ESI/Negative) MW: ($C_9H_{12}N_3O_6Ni^-$) = 316.9034, M/Z found(calc) = 316.0096(316.0085) [M^-].

[Ni{***β***-AspAlaGly}]$^{2-}$ (**5a**) $Ni(OAc)_2$-$6H_2O$ (0.250 g, 1.005 mmol) and KOH (0.085 g, 1.515 mmol) were dissolved and $Ni(OH)_2$ was formed in situ, **1** (0.179 g, 0.540 mmol) was dissolved in H_2O (5 mL) the the Ni(II) solution was added to the ligand and the pH was increased with 1 M KOH until a pH of 10 was achieved. Solution was stirred for 2 h then the H_2O was removed in vacuo. The product was redissolved in iso-propyl alcohol and filtered. Product was precipitated out using a combination of EtOH and EtOAc. (0.144 g, 65%) ^{1}H NMR (400 MHz, Deuterium Oxide) δ 3.89 – 3.73 (m, 1H, α-H_{Ala}), 3.69 (q, 1H, β-H_{Asp}), 3.66 – 3.39 (m, 2H, α-H_{Gly}), 2.55 (d, 1H, α-H_{Asp}), 2.41 (dd, 1H, , α-H_{Asp}), 1.42 (d, 3H, β-H_{Ala}). IR (KBr) cm^{-1}: 3404, 3272 (b, ν(N—H)), 1646 (sh, ν(C=O)), 1602 (s, ν(C=O)), 1561 (s, ν(C=O)), 1401 (s, ν(C—O)), 4657 (w, ν(Ni—N)) MS (ESI/Negative) MW: ($C_9H_{12}N_3O_6Ni^-$) = 316.9034, M/Z found(calc) = 316.0092(316.0085) [M$^-$].

K[Ni{***α***-Asp(OtBu)AlaGly}] (**6**) $NiCl_2$•$6H_2O$ (0.250 g, 1.052 mmol) and KOH (0.100 g, 0.889 mmol) were dissolved in 20mL H_2O, **1**-HCl (0.231 g, 0.628 mmol) was dissolved in H_2O (5 mL) the the Ni(II) solution was added to the ligand and the pH was increased with 1 M KOH until a pH of 10 was achieved. Solution was stirred for 2 h then the H_2O was removed in vacuo. The product was redissolved in iso-propyl alcohol. Product was precipitated out using a combination of EtOH and EtOAc . (0.203 g, 78%) ^{1}H NMR (400 MHz, DMSO-d_6) δ 3.57 (s, 1H, NH_{Asp}), 3.07 (d, 1H, α-H_{Asp}), 3.03 (s, 1H, NH_{Asp}), 3.02 (s, 1H, α-H_{Ala}), 2.99 (d, 2H, α-H_{Gly}), 2.50 (DMSO), 2.39 (dd, 1H,β-H_{Asp}), 2.21 (dd, 1H, β-H_{Asp}), 1.41 (s, 9H, -O(CH_3)$_{3\ Asp}$), 1.00 (d, 3H, β-H_{Ala}). ^{13}C NMR (101 MHz, DMSO) δ 182.19(C=O_{Asp}), 180.30(C=O_{Ala}), 175.71(C=O_{Gly}),170.17(γ-C=O_{Asp}), 79.93 (-O$C(CH_3)_{3\ Asp}$), 56.42 (α-C_{Ala}), 54.53 (α-C_{Asp}), 48.31 (α-C_{Gly}), 39.52(DMSO), 39.02 (β-C_{Asp}), 27.77 (-O$C(CH_3)_{3\ Asp}$), 18.65 (β-C_{Ala}). IR (KBr) cm^{-1}: 3401, 3308 (b, ν(N—H)), 1722(s, ν(C=O)), 1642(sh, ν(C=O)), 1597(s, ν(C=O)), 1550(sh, ν(C=O)), 1254(s, ν(C—O)), 1289(s, ν(C—O)), 1146(s, ν(C—O)). 466(w, ν(Ni—N)). UV-Vis (H_2O): ε_x MS (ESI/Negative) ($C_{13}H_{20}N_3O_6Ni$) = 373.0114, M/Z found(calc) = 372.0716(372.0711) [M$^-$]. CHN ($C_{13}H_{20}N_3O_6Ni$)•H_2O found(calc) %: C: 36.97(36.30), H: 4.99(5.16), N: 9.89(9.77)

K[Ni{***β***-Asp(OtBu)AlaGly}] (**7**) $NiCl_2$•$6H_2O$ (0.500 g, 2.104 mmol) and KOH (0.200 g, 1.779 mmol) were dissolved in 20mL H_2O, **2**-HCl (0.367 g, 1.000 mmol) was dissolved in 10 mL of H_2O. While monitoring pH add the Ni(II) solution to the ligand solution and adjust the pH to10 with 1M KOH solution, maintained a pH of 10 and stir for 2 hours. Excess $Ni(OH)_2$ was filtered

off and the solvent removed in vacuo. The product was redissolved in iso-propyl alcohol. Product was precipitated out using a combination of EtOH and EtOAc. (0.168 g, 41%) ^{1}H NMR (400 MHz, DMSO-d_6) δ 3.37 (s, 7H, NH_{Asp}), 3.29 (q, 1H, α-H_{Ala}), 3.16 – 3.05 (m, 1H, NH_{Asp}), 2.96 (q, 2H, α-H_{Gly}), 2.94 – 2.85 (m, 1H, β-H_{Asp}), 2.01 (dd, 1H, α-H_{Asp}), 1.87 (dt, 1H, α-H_{Asp}), 1.39 (s, 10H, -O$(CH_3)_{3\ Asp}$), 0.94 (d, 3H, β-H_{Ala}).NMR (400 MHz, DMSO-d_6) δ 3.37 (s, 7H, H_2O), 3.29 (q, 1H, α-H_{Ala}), 3.16 – 3.05 (m, 2H, NH_{Asp}), 2.96 (s, 2H, α-H_{Gly}), 2.94 – 2.85 (m, 1H, α-H_{Asp}), 2.01 (dd, 1H, β-H_{Asp}), 1.87 (dt, 1H, β-H_{Asp}), 1.39 (s, 10H, -O$(CH_3)_{3\ Asp}$), 0.94 (d, 3H, β-H_{Ala}). ^{13}C NMR (101 MHz, DMSO) δ 182.23 (C=O_{Asp}), 180.14 (C=O_{Ala}), 171.02 (C=O_{Gly}), 170.61 (γ-C=O_{Asp}), 80.80 (-O$C(CH_3)_{3\ Asp}$), 58.32 (α-C_{Ala}), 52.79 (α-C_{Asp}), 48.66 (α-C_{Gly}), 39.52(DMSO), 39.01 (β-C_{Asp}), 27.61 (-O$C(CH_3)_{3\ Asp}$), 19.66 (β-C_{Ala}). IR (KBr) cm^{-1}: 3396, 3257(b, ν(N—H)), 1729(s, ν(C=O)), 1548(sh)(s, ν(C=O)), 1601(s, ν(C=O)), 1561(s, ν(C=O)), 1257(s, ν(C—O)), 1282(s, ν(C—O)), 1155(s, ν(C—O)), 470(w, ν(Ni—N)). UV-Vis (H_2O): ε_x MS (ESI/Negative) MW: ($C_{13}H_{20}N_3O_6Ni$) = 373.0114, M/Z found(calc) = 372.0713(372.0711) [M$^-$]. CHN ($C_{13}H_{20}N_3O_6Ni$)•H_2O found(calc) %: C: 35.91(36.30), H: 5.13(5.16), N: 9.63(9.77)

K[Ni{TrpAlaGly}] (**8**) $NiCl_2$•$6H_2O$ (0.0.3 g, 1.262 mmol) and KOH (0.150 g, 1.334 mmol) were dissolved in 20mL H_2O. **3** (0.346 g, 1.000 mmol) was dissolved in 10 mL of H_2O. While monitoring pH add the Ni(II) solution to the ligand solution and adjust the pH to10 with 1M KOH solution, maintained a pH of 10 and stir for 2 hours. Excess $Ni(OH)_2$ was filtered off and the solvent removed in vacuo. The product was redissolved in iso-propyl alcohol and filtered. Product was precipitated out using a combination of EtOH and EtOAc. (0.206 g, 48%) ^{1}H NMR (400 MHz, DMSO-d_6) δ 10.89 (d, 1H, NH_{indole}), 7.48 (d, 1H, $H_{indole\text{-}C7}$), 7.34 (dt, 1H, $H_{indole\text{-}C4}$), 7.31 (d, 1H, $H_{indole\text{-}C2}$), 7.06 (ddd, 1H, $H_{indole\text{-}C5}$), 6.95 (ddd, 1H, $H_{indole\text{-}C6}$), 3.65 – 3.56 (m, 1H, NH_{Trp}), 3.10 (q, 1H, α-H_{Ala}), 3.01 (d, 2H, β-H_{Trp}), 2.96 (d, 1H, β-H_{Trp}), 3.07 – 2.87 (m, 2H, α-H_{Gly}), 2.72 (dd, 1H, β-H_{Trp}), 2.20 (dd, 1H, NH_{Trp}), 1.00 (d, 3H, β-H_{Ala}). ^{13}C NMR (101 MHz, DMSO) δ 182.20 (C=O_{Trp}), 180.37 (C=O_{Ala}), 177.09 (C=O_{Gly}), 136.29 ($C3_{indole}$), 127.39 ($C8_{indole}$), 123.87 ($C2_{indole}$), 120.91 ($C5_{indole}$), 118.38 ($C6_{indole}$), 118.23 ($C7_{indole}$), 111.28 ($C4_{indole}$), 110.06 ($C1_{indole}$), 57.83 (α-C_{Trp}), 56.39 (α-C_{Ala}), 48.40 (α-C_{Gly}), 39.52(DMSO), 28.86 (β-C_{Trp}), 18.63 (β-C_{Ala}). IR (KBr) cm^{-1}: 3396, 3292,(b, ν(N—H)), 1647(sh)(s, ν(C=O)), 1593(s, ν(C=O)), 1290(s, ν(C—O)), 469(w, ν(Ni—N)). UV-Vis (H_2O): ε_x MS (ESI/Positive) MW: ($C_{16}H_{17}KN_4O_4Ni$) = 426.0240, M/Z found(calc) =

387.0610(387.0609) [M^-]. CHN ($C_{16}H_{18}N_4O_4Ni$)•H_2O found(calc) %: C: 43.56(43.07), H: 4.88(4.52), N: 12.49(12.54)

Acknowledgements: Funding for this project from The Icelandic Centre of Research (Rannís) grant nr. 152323 is gratefully acknowledged.

References

1. J.J. Soldevila-Barreda, P.J. Sadler. "Approaches to the design of catalytic metallodrugs". Current Opinion in Chemical Biology. Elsevier Ltd, 2015. 25: 172–183. 10.1016/j.cbpa.2015.01.024.
2. N. Metzler-Nolte, Z. Guo. "Themed Issue on 'Metallodrugs: Activation, Targeting, and Delivery'". Dalton Trans. Royal Society of Chemistry, 2016. 45(33): 12965–12965. 10.1039/C6DT90135B.
3. J.C. Joyner, J.A. Cowan. "Target-directed catalytic metallodrugs". Braz. J. Med. Biol. Res. 2013. 46(6): 465–485. 10.1590/1414-431X20133086.
4. K.D. Mjos, C. Orvig. "Metallodrugs in medicinal inorganic chemistry". Chem. Rev. 2014. 114(8): 4540–4563.
5. H. Sigel, R.B. Martin. "Coordinating properties of the amide bond. Stability and structure of metal ion complexes of peptides and related ligands". Chem. Rev. ACS Publications, 1982. 82(4): 385–426.
6. K. Nakamoto. "Infrared spectra of inorganic and coordination compounds". Wiley-Interscience, 1970.
7. W.L.F. Armarego, C. Chai, C.L.L. Chai. Purification of Laboratory Chemicals. Butterworth-Heinemann, 2003.
8. J. Li, Y. Sha. "A Convenient Synthesis of Amino Acid Methyl Esters". MDPI AG, 2008. 13(5): 1111–1119. 10.3390/molecules13051111.
9. F. Neese. "The ORCA program system". WIREs Computational Molecular Science. 2012. 2(1): 73–78. 10.1002/wcms.81.
10. F. Neese. "Software update: the ORCA program system, version 4.0". WIREs Computational Molecular Science. 2018. 8(1): e1327. 10.1002/wcms.1327.

11. C. Adamo, V. Barone. “Toward reliable density functional methods without adjustable parameters: The PBE0 model”. The Journal of Chemical Physics. 1999. 110(13): 6158–6170. 10.1063/1.478522.
12. J.P. Perdew, M. Ernzerhof, K. Burke. “Rationale for mixing exact exchange with density functional approximations”. The Journal of Chemical Physics. American Institute of Physics, 1996. 105(22): 9982–9985. 10.1063/1.472933.
13. S. Grimme, J. Antony, S. Ehrlich, H. Krieg. “A consistent and accurate ab initio parametrization of density functional dispersion correction (DFT-D) for the 94 elements H-Pu”. The Journal of Chemical Physics. 2010. 132(15): 154104. 10.1063/1.3382344.
14. S. Grimme, S. Ehrlich, L. Goerigk. “Effect of the damping function in dispersion corrected density functional theory”. J. Comput. Chem. 2011. 32(7): 1456–1465. 10.1002/jcc.21759.
15. F. Weigend, R. Ahlrichs. “Balanced basis sets of split valence, triple zeta valence and quadruple zeta valence quality for H to Rn: Design and assessment of accuracy”. Phys. Chem. Chem. Phys. The Royal Society of Chemistry, 2005. 7(18): 3297–3305. 10.1039/b508541a.
16. F. Neese, F. Wennmohs, A. Hansen, U. Becker. “Efficient, approximate and parallel Hartree–Fock and hybrid DFT calculations. A ‘chain-of-spheres’ algorithm for the Hartree–Fock exchange”. Moving Frontiers in Quantum Chemistry:. 2009. 356(1): 98–109.
17. R. Izsák, F. Neese. “An overlap fitted chain of spheres exchange method”. The Journal of Chemical Physics. 2011. 135(14): 144105. 10.1063/1.3646921.
18. L.J. Monger, G.R. Runarsdottir, S.G. Suman. “Directed coordination study of [Pd(en)(H2O)2]2+ with hetero-tripeptides containing C-terminus methyl esters employing NMR spectroscopy”. J Biol Inorg Chem. 8 ed. Springer Berlin Heidelberg, 2020. 25(5): 811–825. 10.1007/s00775-020-01804-0.
19. S. Höck, R. Marti, R. Riedl, M. Simeunovic. “Thermal Cleavage of the Fmoc Protection Group”. 2010. 64(3): 200–202. 10.2533/chimia.2010.200.
20. P.R. Sultane, T.B. Mete, R.G. Bhat. “A convenient protocol for the deprotection of N-benzyloxycarbonyl (Cbz) and benzyl ester groups”. Tetrahedron Letters. Elsevier Ltd, 2015. 56(16): 2067–2070. 10.1016/j.tetlet.2015.02.131.